Mathematical and numerical studies of models describing cell motility

Alessandro Cucchi

UNIVERSITÉ DE PARIS

École Doctorale de Sciences Mathématiques de Paris Centre - ED 386

Laboratoire MAP5, UMR CNRS 8145

THÈSE DE DOCTORAT EN MATHÉMATIQUES

Specialité : Mathématiques Appliquées

présentée par

Alessandro CUCCHI

Mathematical and numerical studies of models describing cell motility

---

Dirigée par

Nicolas MEUNIER

Présentée et soutenue publiquement le 6 juillet 2021 devant un jury composé de :

Mme. Christèle Etchegaray (CR - Université de Bordeaux)	**Invitée**
M. Antoine Mellet (Full Professor - University of Maryland)	**Examinateur**
M. Nicolas Meunier (PU - Université d'Evry Val d'Essonne)	**Directeur de Thèse**
M. Clair Poignard (DR - Université de Bordeaux)	**Examinateur**
M. Luigi Preziosi (Full Professor - Politecnico di Torino)	**Rapporteur**
Mme. Marcela Szopos (PU - Université de Paris)	**Examinatrice**
M. Nicolas Vauchelet (PU - Université Paris 13)	**Rapporteur**

Études mathématique et numérique de modèles décrivant la motilité cellulaire

Résumé. La motilité cellulaire est un phénomène complexe qui intervient dans de nombreux processus biologiques fondamentaux. En effet, elle est le résultat d'un grand nombre d'interactions faisant intervenir différentes échelles de temps et d'espace. Cette thèse est consacrée à l'étude de plusieurs modèles mathématiques décrivant la motilité cellulaire par reptation. Nous avons développé deux approches différentes de modélisation. Dans une première partie, nous considérons la cellule comme un domaine déformable qui se déplace grâce à sa dynamique interne. Nous étudions un modèle de champ de phase de type Canh-Hilliard couplé à une équation de réaction-diffusion et nous montrons que ce modèle converge formellement vers un problème à frontière libre de type Hele-Shaw avec tension surface qui inclut un terme de bord non standard déstabilisant et qui dépend de la vitesse du bord. Nous effectuons une analyse rigoureuse dans les cas 1D et 2D et nous montrons l'apparition de deux phénomènes : l'existence de solutions de type Traveling Wave et le phénomène d'Hystérésis. Ces phénomènes se produisent lorsque le terme déstabilisant du bord est suffisamment fort. Dans une deuxième partie, nous considérons la cellule comme une particule active et nous étudions les effets d'un environnement externe complexe sur le mouvement de la cellule. Nous étudions la compétition de trois quantités : la dynamique interne, l'action d'un signal qui attire la cellule et la présence d'obstacles fixes de forme circulaire. Nous observons numériquement l'existence d'une valeur de la vitesse que la cellule ne dépasse pas, même si l'intensité du signal augmente. Cette valeur seuil de la vitesse dépend du nombre d'obstacles. Nous pensons que ces modèles pourront permettre de mieux comprendre certains aspects de la motilité cellulaire puisqu'ils sont capables de décrire la polarisation et l'interaction avec l'environnement extérieur.

Mots clés : migration cellulaire, migration cellulaire conduite, equations aux dérivées partielles, problèmes à frontière libre, équations différentielles stochastiques, simulations numériques.

Mathematical and numerical studies of models describing cell motility

Abstract. Cell migration occurs in many fundamental biological processes and it is an highly complex phenomenon: it is the result of a great amount of intracellular interactions and it occurs through different scales in time and spaces. This Thesis is dedicated to the study of mathematical models describing cell migration by crawling. We developed two different modeling approaches. First, the cell is a moving domain with deformable shape moving thanks to its internal dynamics. We consider a phase field-model of Canh-Hilliard type coupled with a reaction-diffusion equation. We proved formally that this model converges to a Hele-Shaw type free-boundary problem with a surface tension and including an additional destabilizing boundary term depending on the boundary velocity. We conduce a rigorous analysis in the 1D and 2D case and we found the existence of two phenomena: the appearance of Traveling Wave like solution and of Hysteresis phenomenon. This occurs when the destabilizing boundary term is strong enough. Second, we consider the cell as a moving active particle and we study the effects of a complex external environment on the cell motion. We analyzed the competition of three quantities: the internal dynamics, the action of an attracting signal and the presence of fixed circular obstacles. We numerically observe the existence of a velocity value that the cell can not exceed even if signal intensity increases. The velocity threshold value depends on the number of obstacles. We believe that these models represent an important contribution for a better understanding of cell migration, since they are able to describe the polarization and the guidance of cell motion.

Key words: cell migration, guidance of cell migration, partial differential equations, free-boundary problems, stochastic differential equations, numerical simulations.

Études mathématique et numérique de modèles décrivant la motilité cellulaire

La cellule est définie comme l'unité de base de la vie. La cellule est composée d'un très grand nombre de molécules qui interagissent entre à travers des réactions chimiques et physiques. Il existe de nombreux types de cellules, et chaque type de cellule a un rôle particulier et des fonctions particulières dans le contexte biologique où la cellule vit. L'une des fonctions les plus importantes des cellules est leur capacité à se déplacer. Cette capacité est essentielle dans le processus de propagation des cellules tumorales, où les cellules malignes se déplacent et provoquent des métastases, ainsi que dans la réponse immunitaire, où les globules blancs patrouillent l'ensemble du corps. La migration cellulaire, qu'il s'agisse de cellules isolées ou de cellules se déplaçant collectivement, est donc fondamentale dans de nombreux domaines de la biologie. Le phénomène de migration cellulaire est le résultat de nombreuses interactions qui ont lieu à l'intérieur de la cellule et qui se produisent à différentes échelles de temps et d'espace. Pour cette raison, la migration cellulaire représente l'exemple le plus simple de système actif. Les cellules capables de migrer présentent un état de polarisation lorsqu'elles se déplacent dans une direction fixée, ce qui se traduit par le maintien d'une forme asymétrique pendant le mouvement. Le phénomène de polarisation est provoqué soit spontanément, soit en réponse à l'environnement externe où la cellule se déplace, et il est nécessaire pour conduire une migration efficace. Cette thèse est consacrée à l'étude de deux modèles mathématiques permettant de décrire la migration cellulaire individuelle. Nous considérons le cas particulier de la migration cellulaire par reptation, c'est-à-dire le cas où la cellule se déplace grâce à son contact avec un substrat adhésif. Le premier modèle est un modèle particulier à frontière libre qui décrit le mouvement de la cellule comme une conséquence directe de l'interaction active entre l'activité cellulaire interne et la membrane cellulaire. Le second modèle est un modèle stochastique décrivant le guidage du mouvement cellulaire par l'environnement externe à travers des stimuli chimiques et physiques. Nous pensons que ces modèles représentent une contribution importante à l'étude de la migration cellulaire car ils décrivent deux des aspects les plus importants de la migration cellulaire : la polarisation et le guidage du mouvement cellulaire.

Le Chapitre 2 est consacré à l'étude d'un modèle particulier de champ de phase pour décrire la migration cellulaire. Le modèle se traduit par un système non linéaire d'une équation parabolique dégénérative du quatrième ordre de type Cahn-Hilliard pour la fonction de champ de phase couplée à une équation de réaction-diffusion décrivant la dynamique cellulaire interne, soit

$$\begin{cases} \partial_t \rho + \operatorname{div}(\rho v) = 0 & \text{sur } \Omega,\ t > 0 \\ v = -\nabla \left[\gamma \left(-\varepsilon \Delta \rho + \frac{1}{\varepsilon} W'(\rho) \right) + \phi \right] & \text{sur } \Omega,\ t > 0 \\ \partial_t \phi - \varepsilon \Delta \phi = \frac{1}{\varepsilon} \left(\beta \rho - \phi \right) & \text{sur } \Omega,\ t > 0 \end{cases} \tag{1}$$

avec $\varepsilon > 0$, $\gamma > 0$, $\beta \geq 0$ et W a potentiel double-puits tel que $W(z) = 0$ si et seulement si $z \in \{0, 1\}$ et $W(z) > 0$ pour $z \neq 0,\ 1$. Dans cette partie, nous considérons $W(z) = z^2(1-z)^2$. Des

conditions de bord sur $\partial\Omega$ du type no-flux et des conditions initiales sont ajoutées pour compléter le système. Du point de vue de la modélisation, le système (1) est très simple. Nous utilisons seulement deux quantités pour décrire la cellule : la fonction de champ de phase ρ qui décrit tout ce qui vit à l'intérieur de la cellule (cytosquelette, solvant, moteurs moléculaires...), et la myosine II dont la concentration est indiquée par ϕ qui est un moteur moléculaire s'assemblant en mini filaments qui interagissent avec l'actine et se comportent comme agent réticulant actif pour générer des forces de contraction ou dilatation dans le réseau du cytosquelette. Les principales hypothèses conduisant à (1) sont les suivantes : (i) la vitesse de la cellule v est donnée par le flux interne local d'actine, (ii) la myosine II diffuse lentement dedans la celulle, (iii) les filaments d'actine subissent une polymérisation et une dépolymérisation uniformes à l'intérieur de la cellule, (iv) la pression osmotique impliquée dans le réseau des forces d'actine agit pour saturer l'instabilité linéaire provoquant la séparation de phase et pour lisser l'interface entre les régions riches en cytosol et les régions pauvres en cytosol. Les processus sous-jacents sont : la friction du cytosol sur le substrat ainsi que le caractère actif de la myosine II. Notre premier résultat concerne l'existence de solutions faibles du problème (1) dans le cas unidimensionnel. Dans ce contexte, nous considérons Ω comme un intervalle et, en considérant des conditions initiales ρ_{in} et ϕ_{in} avec des régularités spécifiques, nous montrons l'existence de solutions faibles $(\rho(x,t),\phi(x,t))$ pour $x \in \Omega$ et $t \in [0,T]$ avec $T < +\infty$. En particulier nous montrons la positivité de la solution faible ρ, c'est-à-dire pour toute condition initiale positive ρ_{in} on a que $\rho \geq 0$. En outre, elle satisfait la propriété de conservation de la masse $\int_\Omega \rho(x,t)\,\mathrm{d}x = \int_\Omega \rho_{in}(x)\,\mathrm{d}x$ pour tout $t > 0$. La preuve repose sur deux étapes. Premièrement, nous commençons par une procédure de régularisation de paramètre $\delta > 0$ pour étudier le caractère dégénéré de l'équation lorsque $\rho = 0$ et l'existence de solutions pour le problème régularisé est obtenue par un argument de point fixe sur la fonction ϕ. Ensuite, nous montrons l'existence de solutions faibles en passant à la limite pour $\delta \to 0$, et nous obtenons la formulation faible de (1). Cette dernière étape fait référence à des techniques classiques utilisées dans l'étude de l'équation de type "thin film". Notre deuxième résultat concerne la limite formelle d'interface pour $\varepsilon \ll 1$ du système (1) pour toute dimension. En supposant des propriétés de régularité sur le potentiel double-puits W, la solution $\rho^\varepsilon(x,t)$ du système (1) converge formellement en $\varepsilon \to 0$ vers $\rho^0(t) = \chi_{\Sigma(t)}$ où l'évolution de $\Sigma(t)$ est décrite par le problème de frontière libre de type Hele-Shaw suivant

$$\begin{cases} -\Delta q = 0 & \text{sur } \Sigma(t), \\ q = \gamma\kappa(t) + \beta F(V) & \text{en } \partial\Sigma(t), \\ V = -\nabla q \cdot \mathbf{n} & \text{en } \partial\Sigma(t). \end{cases} \tag{2}$$

où V est la vitesse normale du bord $\partial\Sigma(t)$, κ indique la courbure moyenne de $\partial\Sigma$ avec γ le paramètre de surface dépendant uniquement du potentiel double-puits W, et le terme $F(V)$ modélise les effets du potentiel actif ϕ^ε dans la limite où $\varepsilon \ll 1$, avec le paramètre β indiquant l'intensité de cet effet. La nouveauté du problème limite (2) est la fonction $F : \mathbb{R} \to \mathbb{R}$: nous prouvons que la fonction F est monotone décroissante en V. En conséquence, le terme actif $\beta F(V)$ donne au système un effet déstabilisant conduisant à des phénomènes instables tels que solutions de type ondes progressives et l'hystérésis qui seront analysés dans les Chapitres 3 et 4. En effet, nous pouvons réécrire la condition au bord dans (2) comme

$$q - \beta F(-\nabla q \cdot \mathbf{n}) = \gamma\kappa(t),$$

ce qui représente une condition (non linéaire) de type Robin avec le "mauvais" signe (qui pourrait conduire à des solutions multiples). Dans le Chapitre 2, nous analysons rigoureusement le problème limite (2) dans le cas unidimensionnel. Nous considérons $\Sigma(t)$ comme un intervalle de la forme $\Sigma(t) = (a(t), b(t))$ de longueur constante $\ell = |\Sigma(t)|$ (la propriété de préservation de la masse est vérifiée). Nous montrons qu'il existe une valeur critique $\gamma_c > 0$ (c'est-à-dire $\gamma_c = -\ell/2F'(0)$) telle que la propriété suivante est vérifiée. Si $\beta \leq \gamma_c$, alors la solution unique de (2) est la solution stationnaire $\Sigma(t) = (a(0), b(0))$. Si $\beta > \gamma_c$, alors il existe au moins deux solutions en plus de la solution stationnaire qui se déplacent avec une vitesse positive ou négative dépendant du potentiel

double-puits W et du paramètre β. Ce résultat prouve que, au moins dans le cas unidimensionel, le modèle limite (2) a une dynamique non triviale et présente des phénomènes instables lorsque β est assez grand. En effet, rien n'empêche une solution de changer de vitesse de manière discontinue (par exemple, une solution qui se déplace avec une vitesse positive pourrait s'arrêter soudainement). Ceci indique un processus instable dans lequel une petite variation dans le milieu peut faire qu'une cellule stationnaire commence soudainement à se déplacer, ou qu'une cellule en mouvement change de direction. De tels comportements sont précisément ce qui est observé dans les expériences de migration cellulaire.

Le Chapitre 3 est consacré à l'étude du problème limite (2) dans le cas bidimensionnel que nous réécrivons comme suit

$$\begin{cases} \Delta p = 0 & \text{sur } \Omega(t), \\ p + \beta f(V) = \gamma\kappa(t) & \text{en } \partial\Omega(t), \\ V = -\nabla p \cdot \mathbf{n} & \text{en } \partial\Omega(t), \\ \Omega(t=0) = \Omega_0. \end{cases} \tag{3}$$

Dans ce problème, le domaine $\Omega(t)$ représente l'espace occupé par la cellule au temps t dont la frontière $\partial\Omega(t)$ est inconnue et doit être déterminée avec la fonction inconnue p représentant la pression à l'intérieur de la cellule. La nouveauté du problème (3) est le terme $\beta f(V)$ où la fonction $f : \mathbb{R} \to \mathbb{R}$ est une fonction donnée avec les propriétés suivantes

(A1) f fonction assez régulière, croissante monotone et telle que $f(0) = 0$,
(A2) $\lim_{x\to+\infty} f(x) = 1$ et $\lim_{x\to-\infty} f(x) = -1$,
(A3) $f'(0) > 0$, $f''(0) = 0$ et $f'''(0) < 0$,
(A4) $f''(x) \leq 0\ \forall x > 0$ et $f''(x) \geq 0\ \forall x < 0$.

Un exemple type d'une fonction f satisfaisant les hypothèses précédentes est $f(x) = \tanh(x)$. Le problème à frontière libre (3) est plus compliqué que le problème de Hele-Shaw habituel (correspondant au cas où $\beta = 0$). En effet, la condition au bord s'écrit comme

$$p - \beta f(-\nabla p \cdot \mathbf{n}) = \gamma\kappa(t)$$

ce qui représente une condition au bord tu type Robin. En utilisant les hypothèses **(A1)** – **(A4)**, le terme $\beta f(V)$ représente un effet déstabilisant sur le système. D'un point de vue modélisation, le terme $-\beta f(V)$ peut être modélisé comme une force qui pousse contre la membrane de la cellule et qui génère les protrusions responsables du mouvement. Cette partie est consacrée à l'étude de la solution du problème (3) sous forme d'onde progressive dans le cas bidimensionnel. Le phénomène de polarisation (essentiel pour le mouvement d'un cellule) est mathématiquement décrit par l'existence de solutions du type ondes progressives. Ceci valide donc l'intérêt de ce modèle pour décrire la motilité cellulaire. Les solutions d'ondes progressives correspondent à un domaine de forme fixe se déplaçant par translation avec une vitesse constante dans une direction donnée, soit

$$\Omega(t) = \Omega_0 + ct\mathbf{u}, \tag{4}$$

pour une vitesse c et une direction de mouvement $\mathbf{u}$. Dans la suite, nous indiquerons par (Ω_0, c) une solution d'onde progressive de (3) si le domaine $\Omega(t)$ défini par (4) est une solution de (3). On remarque que ce problème est isotrope, et donc nous considérerons le cas precis où $\mathbf{u} = \mathbf{e}_x = (1, 0)$ et $c > 0$. Nous prouvons deux résultats importants. Premièrement, nous prouvons que pour tout $\gamma, \beta > 0$, il existe une famille à un paramètre $(\Omega_\lambda, c_\lambda)$ de solutions d'ondes progressives de (**??**) paramétrée par $\lambda \in (\gamma/\beta f'(0), \infty)$ telles que $c_\lambda > 0$, Ω_λ est un ensemble convexe représentant le graphe d'une fonction h telle que $h'(0) = 0$. Ce résultat relie la valeur du paramètre λ à une propriété géométrique de Ω_λ et prouve que chaque valeur de λ (suffisamment grande) donne une solution d'onde progressive différente. Dans le second résultat, notre objectif est de déterminer la valeur critique precise de $\beta > 0$ telle que, pour un volume fixe, des ondes progressives non triviales existent. Nous prouvons par un argument locale de bifurcation qu'une branche de solutions d'ondes

progressives avec une vitesse non nulle émerge de la solution triviale B_{R_0} (disque de rayon R_0) à $\beta = R_0/f'(0)$. En particulier, les solutions de bifurcation sont de la forme

$$\begin{cases} \beta(s) = \frac{R_0}{f'(0)} + \alpha s^2 + o(s^2), \\ c(s) = s + o(s), \end{cases}$$

où $\alpha > 0$ et s représente un petit paramètre. De plus, la bifurcation apparaît via une bifurcation de type Pitchfork. Ce résultat montre qu'au moins pour une certaine $\beta > R_0/f'(0)$, il existe une solution d'onde progressive se déplaçant dans n'importe quelle direction avec une vitesse positive. Cette valeur critique de β est cohérente avec celle que nous avons trouvée dans le cas unidimensionnel où $\ell/2$ indique la dimension du domaine. En conclusion, pour une valeur suffisamment grande du paramètre β, nous pouvons identifier deux comportements différents : un domaine symétrique avec une vitesse nulle ou un domaine asymétrique avec une vitesse non nulle. D'un point de vue biologique, cela signifie que si la force pousse suffisamment fort, une rupture de symétrie spontanée de la cellule se produit, entraînant la motilité cellulaire.

Le Chapitre 4 est consacré à l'étude du problème à frontière libre (3) avec f satisfaisant l'hypothèse **(A1)**–**(A3)**, et nous voulons étudier la question suivante : la connaissance de la forme de la cellule au temps t_0 (c'est-à-dire $\Omega(t_0)$) est-elle suffisante pour déterminer $p(t_0)$ et ainsi caractériser le comportement de $\Omega(t)$ pour $t \geq t_0$? Nous considérons ici le cas le plus simple où $\Omega(t_0) = B_{R_0}$ disque de rayon R_0. Pour répondre à cette question, nous observons que (3) implique en particulier que la fonction p résout le problème de Robin non linéaire au bord suivant

$$\begin{cases} \Delta p = 0 & \text{sur } B_{R_0}, \\ p + \beta f(-\nabla p \cdot \mathbf{n}) = \frac{\gamma}{R_0}, & \text{en } \partial B_{R_0}. \end{cases} \tag{5}$$

Par un argument local de bifurcation, nous prouvons que le système (5) peut avoir plus d'une solution pour certaines valeurs de β au moins. En particulier, nous prouvons qu'il existe un intervalle $I = (-\varepsilon, \varepsilon)$ et une branche de bifurcation de solutions $s \in I \mapsto (\beta(s), p(s))$ résolvant le problème (5) avec

$$p(s, x, y) = \frac{\gamma}{R_0} + \frac{x}{f'(0)} s + o(s), \quad \text{with} \quad \beta(0) = \frac{R_0}{f'(0)} > 0, \quad \beta'(0) = 0, \quad \beta''(0) > 0. \tag{6}$$

Ce résultat stipule que pour au moins certaines valeurs de $\beta > R_0/f'(0)$, il existe une branche de solutions au problème (5) apparaissant via une bifurcation de type Pitchfork. Puisque la vitesse normale de ∂B_{R_0} est définie par $V = -\nabla p \cdot \mathbf{n}$, nous avons que la branche $p = p(s)$ définit une branche de vitesses limites non nulles donnée par

$$V = -\frac{\mathbf{e}_x \cdot \mathbf{n}}{f'(0)} s + o(s),$$

ce qui correspond (en première approximation) à une solution d'onde progressive non stationnaire se déplaçant avec la vitesse $\frac{1}{f'(0)} s$ dans la direction $\mathbf{e}_x$. Ce résultat conduit à la réponse à la question précédente : si l'on ne nous donne que les informations sur le domaine au temps t_0, nous pouvons avoir plus d'une vitesse du bord non nulle et nous ne pouvons pas prédire le comportement futur de $\Omega(t)$. Un tel phénomène est appelé hystérésis, où le comportement futur dépend non seulement de la configuration à l'instant t mais aussi de son histoire. L'hystérésis dans le cas de la motilité cellulaire est en accord avec les observations expérimentales.

Comme nous l'avons expliqué, une capacité importante des cellules mobiles est de se polariser et de produire le mouvement par la création de protrusions. Ce processus est stimulé par les propriétés intrinsèques de la cellule mais aussi par l'environnement externe. Dans le Chapitre 5, nous voulons étudier l'effet de l'environnement externe sur la dynamique de la cellule. Dans ce but,

nous considérons la cellule comme une particule active et nous analysons la compétition de trois quantités : la dynamique active interne de la cellule, l'action d'un gradient spatial constant de signal d'attraction et la présence d'obstacles circulaires non mobiles. Nous considérons en particulier le modèle suivant. Soit $\vec{V}_t \in \mathbb{R}^2$ la vitesse de la cellule satisfaisant l'équation différentielle stochastique suivante

$$\mathrm{d}\vec{V}_t = \left[(1-h)\tanh(\alpha v_t)\vec{e}_{\theta_t} + h\tanh(\beta)\vec{e}_{\theta_g} - \lambda\vec{V}_t\right]\mathrm{d}t + \sigma\mathrm{d}\vec{W}_t \quad \text{pour } 0 < t \leq T. \tag{7}$$

Le paramètre $\alpha \geq 0$ représente la capacité de la cellule à créer des protrusions dans la direction du mouvement désignée par $\vec{e}_{\theta_t}$, et $\beta \geq 0$ répresente la capacité de la cellule à créer des protrusions dans la direction du signal d'attraction désignée par $\vec{e}_{\theta_s}$, avec $(\vec{W}_t)_{\geq 0}$ représentant un mouvement brownien standard bidimensionnel. Les paramètres positifs λ, σ représentent respectivement la durée de vie des protrusions et l'intensité du bruit. Nous analysons d'abord le cas unidimensionnel (sans obstacles). En étudiant la distribution stationnaire de $\vec{V}_t$ et en utilisant la méthode d'Euler-Maruyama pour les simulations numériques, nous révélons une transition entre un régime dominé par la dynamique interne et un autre dominé par le signal externe : si β est petit, alors la cellule ne suit pas toujours le signal et elle peut aller dans d'autres directions, mais si β est assez grand la cellule suit le signal. Nous analysons ensuite le cas bidimensionnel. Nous considérons un domaine quadratique de la forme $\Omega = [0,2]\times[0,2]$ et une seule particule de forme circulaire fixe (représentant la cellule) se déplaçant dans un environnement contenant une distribution uniforme d'obstacles circulaires fixes et un gradient constant du signal d'attraction. La vitesse de la cellule $\vec{V}_t$ est solution de (7) et nous utilisons un algorithme de contact particulier pour traiter l'interaction entre la cellule et les obstacles. Nous avons effectué des simulations numériques avec la méthode Euler-Maruyama pour étudier ces effects sur la dynamique de la cellule. Nous avons analysé trois cas : la dynamique d'une particule brownienne déversée ($\alpha = \beta = 0$ et $\lambda \neq 0$), l'effet d'une force constante dans la dynamique d'une particule brownienne frainée ($\alpha = 0$, $\beta \neq 0$, $\lambda \neq 0$ et la force unitaire constante $F = (2\times 2/5, 1.5\times 2/5)$), et la dynamique d'une particule active ($\alpha \neq 0$, $\beta \neq 0$, $\lambda \neq 0$ et la force constante $F = (2\times 2/5, 1.5\times 2/5)$). Nous avons obtenu des résultats intéressants pour ce dernier cas. Premièrement, la courbe du module de vitesse moyenne a un comportement non strictement monotone par rapport à β pour tout nombre d'obstacles. Ceci est dû à la présence des obstacles : lorsque l'intensité est suffisamment forte, la particule reste coincée entre les obstacles. Deuxièmement, les histogrammes bidimensionnels de vitesse sont concentrés non seulement dans la direction de la force F mais aussi dans d'autres régions. En effet, l'effet de la force est moins efficace puisque la particule ressent également sa propre dynamique interne. La trajectoire de la cellule reflète alors ces caractéristiques. Même si pour de grandes valeurs de β on reconnaît quelques directions de persistance en accord avec la direction de la force, la trajectoire est très perturbée à cause de la dynamique interne et la particule peut couvrir différentes directions.

Contents

Chapter 1

Introduction

The cell is defined as the basic unit of life. The cell is composed by a huge number of molecules interacting with each other through chemical and physical reactions. There exist many types of cells, and each type of cell has a particular role and particular functions in the biological context where it lives. For instance, some eukaryotes cells conduce the cellular division for reproducing, and the white blood cells (also called leukocytes) which composed the immune system protect the body from malignant invaders and diseases.

One of the most important functions of cells is their ability to move. This ability is essential in the process of spreading of tumor cells, where malignant cells move and cause metastasis, as well as in the immune response, where the white blood cells patrol the whole body. Cell migration, both of isolated cells and when moving collectively, is therefore of fundamental importance in many fields of biology. The phenomenon of cell migration is the result of many interactions taking place inside the cell and which occur at different time and space scales. For this reason, both individual and collective cell migration represent the simplest examples of an active system. Cells capable of migration show a polarization state when they move in a given direction, which translates in sustaining an asymmetric shape during the motion. This phenomenon, also called front-rear polarization, is caused either spontaneously or in response to external inputs and it is required for conducing efficient cell migration.

This Thesis is dedicated to the study of two mathematical models for describing the phenomenon of individual cell migration. There exist many migration modes, but we will focus on the particular case of cell migration by crawling, that is the case where the cell moves thanks to its contact with an adhesive substrate. The first model is a particular free-boundary model describing the cell motion as a direct consequence of the active interaction between the internal cellular activity and the cellular membrane. The second model is a stochastic model describing the guidance of cell motion by the external environment through chemical and physical stimuli. We believe that these models represent an important contribution in the study of cell migration since they describe two of the most important aspects of cell migration: the polarization and the guidance of cell motion.

This Chapter represents the Introduction of the Thesis. First, we present a general biological introduction of the mechanisms underlying the cell migration by crawling. Then, a general mathematical introduction for free-boundary problems where we will introduce important existing results which have been extensively used in the study of our models. A general outline of the Thesis can be found at the end of this Chapter.

1.1 General description of cell migration

This section is dedicated to a general introduction of the process of cell migration. We are aware that cell migration is a very complex phenomenon which is still the subject of active research in

the biological, physical and mathematical fields. Nevertheless, the purpose here is to furnish the basic biological and physical knowledge for understanding the principal aspects of cell migration.

We first describe the main biological components located inside the cell which are involved in the motion. Then, we introduce the particular process of motion by crawling which can be schematized into three main steps. Finally, we discuss some aspects of cellular guidance where we emphasize the role of particular phenomena such as internal polarization and stimulation from the external environment.

Cellular internal anatomy

The cell is composed of many biological components which have a specific purpose in regulating cell life. These components are enclosed within a membrane called the cellular membrane. This membrane is the outer covering and it is able to generate active interactions between the cell and the external environment. One of the principal components enclosed in the cellular membrane is the cytoskeleton, which represents the primary regulator of the physical and mechanical integrity of the cell. Indeed, the cytoskeleton helps the cell to maintain its shape and internal organization providing also mechanical support for motion. The cytoskeleton has three main functions: it spatially organizes what lies inside the cell, it connects the cell physically and biochemically to the external environment, and it generates coordinated internal forces that allow the cell to move and to change shape. These functions have an essential role in many fundamental cellular processes such as motility and division. A great amount of polymers lie in the cytoskeleton which interact with the cytoskeleton itself. They are organized into interconnected networks which resist to deformations and reorganize in response to interactions with external environment. Three different type of polymers have been identified: microtubules, intermediate filaments and actin filaments. We will see later that actin filaments represent the most important network of polymers in the regularization of cell motion. A schematic representation of these polymers is presented in Figure 1.1.

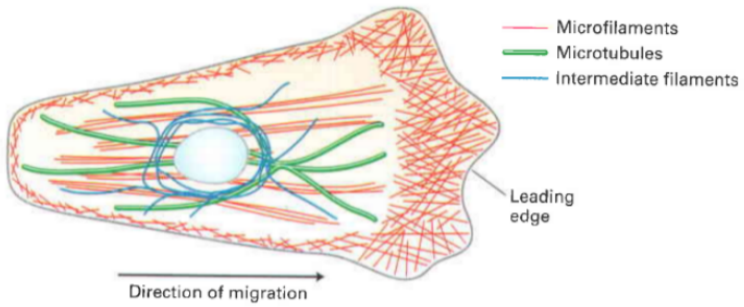

Figure 1.1 – A representation of the polymers composing the cytoskeleton. Microtubules in blue, intermediate filaments in green and actin microfilaments in red. The light blue spherical area in the center is the cell nucleus. The meading edge represents the cell membrane which separates the interior and the exterior of cell. Source: Lodish et al. [31].

Microtubules Microtubules are the stiffest within the polymers and they are polarized. Therefore, they can switch between a state of growing conduced by the polymerization and a state of shrinking conduced by the depolymerization.

Intermediate filaments Intermediate filaments are the least stiff polymers. They can be crosslinked to each others, they are not polarized and they cannot support directional movement of molecular motors. They contribute to the mechanical integrity of the cell nucleus.

Actin filaments Actin is a protein that can assemble into a filamentous structure giving rise to actin filaments. Actin filaments are endowed with a polar structure where the two different ends are referred as plus and as minus end. Actin filaments form an out-of-equilibrium system where the actin is added at the plus-end by a process called polymerization, and dissociates from the minus-end by a process called depolymerization. A schematic representation of these process is presented in Figure 1.2 on the left. It has been observed that polymerization takes place near the membrane of the cell, while depolymerization occurs away from the membrane towards of the cell body. The process of polymerization and depolymerization induces a movement directed towards the interior of the cell. This movement is called retrograde flow and it is directly involved in cell motion.

Actin filaments interact with other actin filaments through the action of two proteins called Arp2/3 and α-actin. Arp2/3 bundles the actin filaments in a network structure, while α-actin ties them in a parallel structure. This process results in the creation of a region with an high density of actin filaments called lamellipodium that is essential in the generation of motion. For a more detailed description of this dynamics we refer to the work of Small et al. [43]. Actin filaments interact also with another important protein: the Myosin-II protein, which belongs to the family of myosin proteins. The myosin molecules lie in the cytoskeleton and they assemble to form minifilaments which are more processive and interact with the actin filaments longer than a single myosin molecule. These minifilaments can create crosslinkers which bind to actin filaments. As explained by Joanny and Prost [28], the myosin proteins are able to "walk" on a single actin filaments and induce internal contractile stresses. A schematic representation of the action of myosin proteins on actin filaments is presented in Figure 1.2 on the right. Thanks to the binding property of myosin molecules, these stresses can be transmitted to the whole actin network so that the entire cytoskeleton can be contracted. This process leads to cell displacement. Together with Arp2/3 and α-actine proteins, myosin proteins contribute to the formation of a region of high density in actin filaments called actin cytoskeleton. Figure 1.3 shows a fluorescence micrograph highlighting the distribution of actin filaments and myosin-II proteins inside the cell.

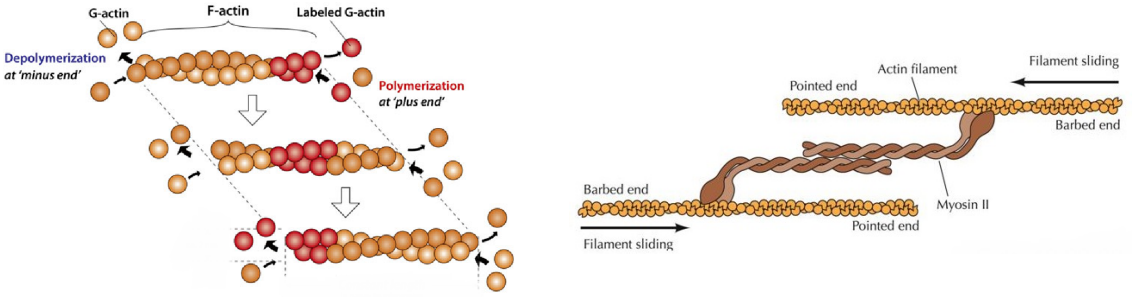

Figure 1.2 – On the left, schematized representation of the polymerization at the plus-end (on the right) and the depolymerization at the minus-end (on the left). This process generates a retrograde movement of actin monomers from the plus-end towards the minus-end. On the right, a schematic representation of the action of a minifilament of myosin (represented in light brow) on two actin filaments (represented in yellow). Source: Alberts et al. [1]

These polymers interact continuously with the cellular membrane which then participate actively in the mediation of the main functions of the cytoskeleton and in the process of cell migration.

Cellular membrane The cellular membrane separates the internal part from the external part of the cell so that it maintains the integrity of the cell. It works as a "communicator" between the internal activity of the cell and the external environment. For instance, the creation of elongations of the membrane called protrusions, which are essential in cell motion, are the results of this communication mediated by the membrane. As explained by Sense and Plastino [42], a feedback loop occurs: actin filaments generates a pushing force leading to deformations of the cell membrane

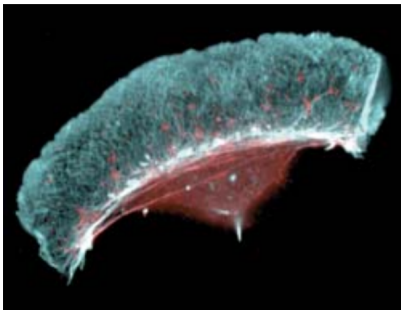

Figure 1.3 – Fluorescence micrograph of a keratinocyte cell. Actin filaments in blue are at the cell front, Myosin-II in red is at the cell rear. Both are also located in the white band crossing the cell. Source: Lodish et al. [31].

and creation of protrusions, and in turn the membrane acts on the growing actin filaments for controlling the direction of the protrusions and thus inducing the cell motion.

The biological interactions presented above constitute only a part of the dynamics that takes place inside the cytoskeleton. Many other interactions appear with other kinds of proteins in order to regulate polymerization and depolymerization as well as the dynamics of actin filaments. As presented in the work of Joanny and Prost [28] and Jürlicher et al. [29], the cytoskeleton is considered as an active system and it is described physically as an active gel. Indeed, it continuously consumes energy involved in processes of polymerization and depolymerization as well as in creation and transmission of contractile stress generated by myosin proteins. For more details on this theory of the hydrodynamic description of cytoskeleton as an active gel, we refer the reader to [28, 29] and the PhD thesis of Etchegaray [21].

The process of cell migration by crawling

The type of cell as well as the features of the external environment where it moves influence directly the type of migration and different migration modes have been identified. This Thesis is dedicated to the study of the particular case of cell migration by crawling, represetning the case where the motion is the result of an interaction between the cell and an adhesive substrate. Many studies have been conduced for identifying the main features of migration by crawling. In the experiments of Ananthakrishnan and Ehrlicher [4], three main steps have been determined as characterizing of this scenario. First, at the cell front elongations of the cell membrane called protrusions start growing in the direction of motion. Then, the protrusions elongate and adhere to the substrate, while the cell rear de-adheres from the substrate. Finally, contractile forces are generated between the cell and the substrate and the cell body is pulled forward to start the motion. Figure 1.5 shows a schematic representation of this process. In the following, we describe in more details each of the these steps.

Creation of protrusions In the works of Mogilner and Oster [35] and of Small et. al. [43], polymerization of actin filaments towards the cell membrane has been identified as the basic mechanism of the creation of protrusions. An actin filament is not a stiff bar that stops growing once it reaches the membrane but it is elastic and able to bend in response to loads. In turn, the cell membrane is an elastic membrane which can deform when a load is imposed. Then, the protrusions are generated thanks to the interaction between polymerization of actin filaments and the elasticity of the membrane. The thin layer composed by the protrusions that starts to protrude is an agglomeration of actin filaments called lamellipodium. Depending on the cell type and external conditions, the lamellipodium can vary in breadth from $\sim 1\,\mu m$ to $5\,\mu m$. Actin filaments localized

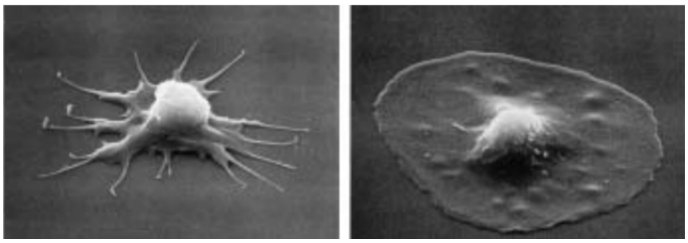

Figure 1.4 – Examples of creation of filopodia on the left and lamellipodium on the right. Changes in morphology result from the reorganization of the actin filaments linked to the cell membrane. Source: experimental figures from Lodish et al. [31].

in the lamellipodum can assemble into bundles generating two types of agglomeration: when they do not extend beyond the boundary of lamellipodium, they are called "microspikes", while when they extend they are called "filopodia". One of the main features of filopodia is that they are able to feel the external environment though some proteins localized at their tip which work as receptors. Thanks to this feature, the filopodia define the direction of the motion. Figure 1.4 shows examples of creation of lamellipodia and filipodia, arising from experiments.

Adhesion of the cell front and de-adhesion of the cell rear After elongating, the protrusions adhere to the substrate thanks to the action of particular adhesion molecules localized in the lamellipodium [30, 37]. The sites of attachment are local complexes created by some extramembrane proteins that link actin bundles in the lamellipodium with the substrate. As the protrusions adhere to the substrate, contractile forces at the cell front and traction forces at the cell rear are generated, and the cell rear starts to de-adhere from the substrate. The process of de-adhesion involves the disassembling of adhesion local complexes previously established.

Traction and contraction forces to pull the cell body forward Once the protrusion adhere to the substrate, traction forces and contraction force are generated respectively at the cell front and cell rear for pulling the cell body forward. These forces are largely generated by the action of the myosin proteins on the actin filaments localized in the lamellipodium. As explained in [30], these traction forces give rise to a retrograde flow on the actin filaments which goes in the opposite direction of the motion.

The phenomenon of Polarization

We have introduced in the previous sections some of the main properties of the active internal dynamics of a cell and we have seen how these are implicated in the process of cell migration by crawling. One of the most important abilities of a cell which has also an essential role in the generation of the motion is the Polarization. The Polarization or cell polarity appears as a morphological asymmetry state defining two distinct regions having precise functions. One region is the front of the cell, where polymerization of actin filaments takes places and creation of protrusions occurs inducing the direction of motion. The other region is the rear of the cell, where contractile forces are generated in order to pull the cell body forward. The creation and the maintenance of this asymmetry state is due to the actin retrograde flow. It has been observed that the Polarization is extremely important in cell migration and without this front-rear polarity a cell would be unable to conduce directed migration.

There exist different processes which can establish the cell polarity. In this section, we introduce two particular mechanisms which have been extensively used in this Thesis: the spontaneous Polarization, and the Polarization induced by cues in the external environment.

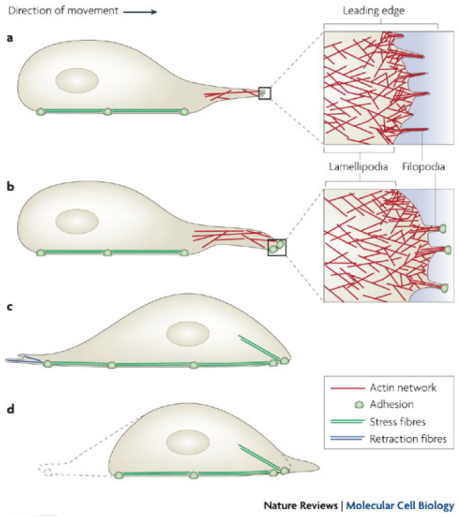

Figure 1.5 – The process of cell migration by crawling diveded into three steps: (a) the creation of protrusions, (b)-(c) the adhesion of the cell front and the de-hadesion of the cell rear, (d) contraction forces to pull the cell body forward. Source: Mattila and Lappalainen [34].

The spontaneous Polarization

A recent result showing a positive correlation between the spontaneous Polarization and the migration property in migrating cells is presented by Maiuri et al. [32]. They found a positive correlation between cell polarity and actin retrograde flow: the actin retrograde flows reinforces cell polarity by enhancing the asymmetry of polarity cues represented by molecules responsible for the generation of contractile stresses (an example of these molecules is the myosin proteins). This means that faster actin retrograde flow gives rise to more stable polarity state. They found that this positive correlation impacts on the long-term migration behavior of cells and results in a positive correlation between cell speed and cell persistence: faster cells migrate more straight than slower cells. Two experimental images of unpolarized and polarized cell and a schematic illustration of the distribution of polarity cue is presented in Figure 1.6.

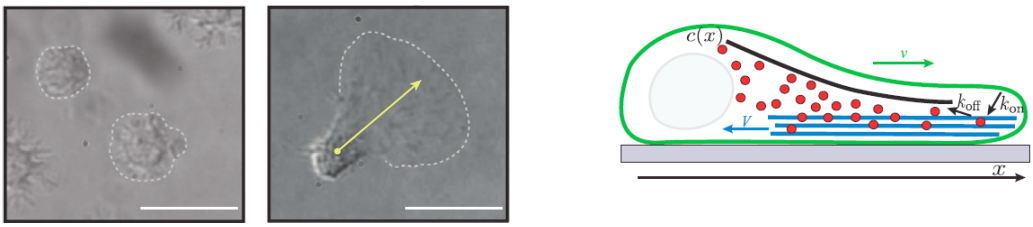

Figure 1.6 – On the left, images of cells in unpolarized state (on the left) with no lamelippodia, and in polarized state (on the right) with lamellipodia. On the right, schematic illustration of polarity cue distrubution (red dots with concentration profile $c(x)$) in a polarized cell moving with velcity v, with actin filaments in blue of velocity V and migration substrate in gray. Source: Maiuri et al. [32].

Polarization induced by the external environment

The external environment is able to guide the cell migration by the effect of local anisotropic features. Indeed, the presence of some molecular receptors localized at the protrusions tips stimulates

the inner Polarization of the cell which then leads to the regularization of protrusions activity and to directed motion. This process generates a symmetry breaking from an non-polarized state to a polarized one. The environment influences cell motion either chemically if some molecular specie attracts/repulses the cell, or mechanically through specific physical properties of the substrate or particular geometric configurations. This phenomenon is called Ratchetaxis and it has been studied by Caballero et al. [8].

When the external environment acts on cell motion chemically, on can speak of the Chemotaxis. The Chemotaxis has been studied by Wang [48] and it refers to the process of guidance of cell motion in the presence of an external gradient in the chemoattractant. Through its molecular receptors, the cell identifies the position of the chemoattractant, it starts polarizing and consequently creating protrusions in the direction of the highest concentration of the chemoattractant. An example of Chemotaxis is the response of the immune cells which feel the bacterium in the environment and start moving towards. Figure 1.7 shows an experiment of guidance of motion for a neutrophil cell in response to gradient of chemoattractant.

Further experiments showed that cell migration can be guided also by the presence of geometrical anysotropies in the environment. For instance, Caballero et al. [8] examined motile cells behaving in environments composed by a series of adhesive patches having asymmetric triangular shapes and separated by non-adherent gaps. The schematic illustration of this setting is presented in Figure 1.8. They found that this set-up causes creation of protrusions in specific directions. In particular, they observed that cells migrated mostly towards the direction defined by the pointed end in both short- (10 h) and long-term (days) experiments.

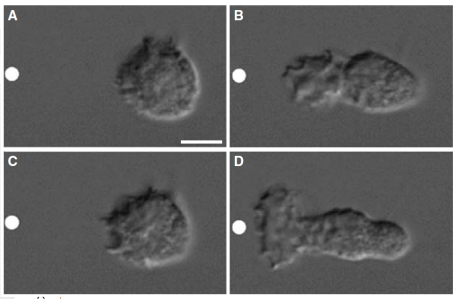

Figure 1.7 – Motion of a neutrophil cell induced by a gradient of chemoattractant. The cell starts polarizing and creating protrusions towards the white point representing the chemoattractant. Observations at (A) 5sec., (B) 30sec., (C) 81 sec., and (D) 129sec. of stimulation. Source: Wang [48].

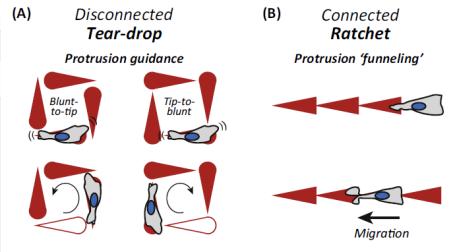

Figure 1.8 – Scheme of cell motion induced by adhesive ratchets. In (A) tear drop guiding cell motion in a clockwise or counter-clockwise direction. In (B) connected patches directing cell motion such that the lamellipodia funnel into the next triangular shape. Source: Caballero et al. [8].

1.2 Free-boundary problems for cell migration

This section is dedicated to a general introduction of free-boundary problems which have been extensively used in our work.

As we described previously, the process of cell migration by crawling can be schematized into three main steps: creation of protrusions at the cell front, adhesion of the protrusions and the deadhesion of the cell rear, and creation of contractile forces for pulling the cell body forward. These steps are the result of a complex interplay between the internal active dynamics and the deformation of the cell membrane. Sense and Plastino [42] showed that this interplay is governed by a feedback loop: the cell membrane is an active matter which regulates the dynamics of actin filaments, which in turn act actively on the mechanics of the cell membrane. This suggests that the cell membrane as well as its coupling between the active internal dynamics needs to be included in models describing cell migration.

In reality, the cell is a well-defined three-dimensional body with constant volume. A first modeling approximation is to consider the cell as a moving domain which is either of deformable shape or of fixed shape. Models which use the first approach are called free-boundary models. These are the most realistic models (for instance, the creation of protrusions occurs when the cell membrane changes its shape), but also much more complicated to analyze than those that use the second approach. Indeed, as we will explain later, the free-boundary problems are identified as partial differential equations defined on a unknown moving domain $\Omega(t)$ endowed with a deformable boundary where boundary conditions need to be imposed. Our aim in this section is to introduce some of the principal free-boundary problems that we have extensively used for the derivation of our free-boundary model.

A possible starting point for the study of free-boundary problem is the use of phase-field models and the study of their Sharp Interface Limit. As we will explain later, in the phase-field models the cell membrane is identified by an interface of width $\varepsilon > 0$ separating two zones called phases: one phase corresponding to the interior of the cell and the other phase to the exterior of the cell. This interface diffuses and moves according to a particular partial differential equation. The connection between phase-field models and free-boundary problems is the so called Sharp Interface Limit. This represents the study of the limiting behavior for $\varepsilon \to 0$ of the phase-fields models. This leads to obtain a limit problem which describes the evolution of a curve characterizing the boundary of a deformable domain $\Omega(t)$ whose interior represents one phase, that is the interior of the cell, and the exterior represents the other phase, that is the exterior of the cell.

This section is organized as follows. First, we introduce and describe two reference phase-field models which have been extensively used in the study of cell migration: the Allen-Cahn and the Cahn-Hilliard equations. Then, we present their respectively Sharp Interface Limit and we will show the cases where this leads to have a free-boundary problem as limiting problem with a specific section dedicated to the particular case of the Hele-Shaw free-boundary problem. This presentation of the arguments will be useful for a better understanding of the derivation of our free-boundary problem.

Allen-Cahn and Cahn-Hilliard equations

The diffusive interface is modeled by having a width of the order $\varepsilon > 0$ and it is identified by the so-called phase-field function $\rho^\varepsilon = \rho^\varepsilon(t, x)$ for $t > 0$ an $x \in \Omega$, where Ω is a bounded fixed domain representing the full space where ρ^ε evolves. One phase is identified by a value ρ_a and the other phase by another value ρ_b. The phase-field function has the property to be $\rho^\varepsilon \approx \rho_a$ in one phase, and $\rho^\varepsilon \approx \rho_b$ in the other phase. The interface is then identified by the sharp transition of ρ^ε between the two values ρ_a and ρ_b, that is the interface is localized where $|\nabla \rho^\varepsilon| = O(1/\varepsilon)$.

A first equation describing the evolution of ρ^ε is the Allen-Cahn equation which has been introduced by Allen and Cahn [3] for modeling the movement of grains on the interface of crystalline solids. Successively the equation has been used to model phenomena of isothermic phase separation and many other phenomena linked to material sciences. We refer to the introdiction of the PhD

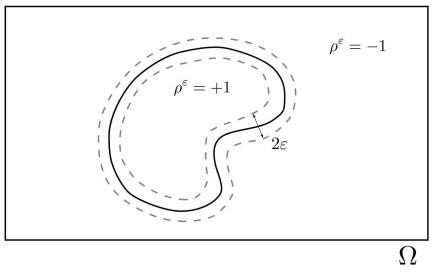

Figure 1.9 – Example of ρ^ε where the phases are $\rho_a = +1$ and $\rho_b = -1$. The space of width 2ε indicates the points in Ω where ρ^ε changes smootly between the two phases. The continous line indicates the points where ρ^ε assumes the value $(\rho_a + \rho_b)/2$.

thesis of Makki [33] and Saoud [41] for a complete literature. The equation writes as a second order parabolic partial differential equation

$$\partial_t \rho^\varepsilon = \Delta \rho^\varepsilon - \frac{1}{\varepsilon^2} W'(\rho^\varepsilon) \quad \text{on } \Omega,\ t > 0. \tag{1.1}$$

The function W is a double-well potential which is usually considered to be of polynomial type whose wells represent the two phases ρ_a and ρ_b and which satisfies,

$$\begin{cases} W'(z) = 0 \text{ if and only if } z \in \{\rho_a, \rho_b, (\rho_a + \rho_b)/2\}, \\ W'(z) < 0 \text{ for } z < \rho_a \text{ and } (\rho_a + \rho_b)/2 < z < \rho_b, \\ W'(z) > 0 \text{ for } \rho_a < z < (\rho_a + \rho_b)/2 \text{ and } z > \rho_b. \end{cases} \tag{1.2}$$

A typical choice which is used in the study of the Allen-Cahn equation is to consider the $\rho_a = -1$ and $\rho_b = +1$ and W of the form $W(z) = (1/4)(1 - z^2)^2$.

The Allen-Cahn equation (1.6) can be seen as an approximation of the dynamics of a moving interface separating the two phases ρ_a and ρ_b. In order to understand this idea, we consider the one-dimensional case. If we denote by $\bar{\rho}^\varepsilon$ the stationary solution of the one-dimensional form of the equation (1.1), the function $\bar{\rho}^\varepsilon$ satisfies $\varepsilon(\bar{\rho}^\varepsilon)'' = (1/\varepsilon)W'(\bar{\rho}^\varepsilon)$. By a changing of variables and energy conservation estimates, $\bar{\rho}^\varepsilon$ is of the form $\bar{\rho}^\varepsilon(x) = \tanh(x/(\varepsilon\sqrt{2}))$. It is clear in this case that ε represents the width of the interface separating the phase $\bar{\rho}^\varepsilon = -1$ and the phase $\bar{\rho}^\varepsilon = +1$.

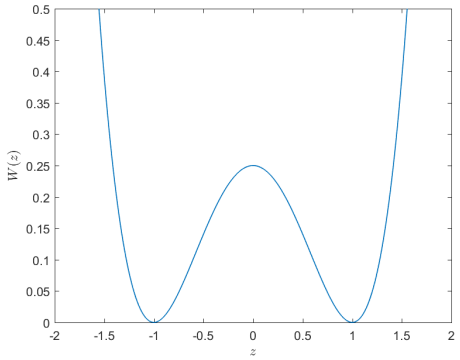

Figure 1.10 – Graph of a double-well potential of the form $W(z) = (1/4)(1 - z^2)^2$.

Theoretical studies of the Allen-Cahn equation in dimensions greater then 2 have been conduced. For a complete analysis we refer the reader the lecture notes of Chodosh [13] and to the references listed inside.

The Allen-Cahn equation is often interpreted as the gradient flow in the space $L^2(\Omega)$ of the so-called Ginzburg-Landau energy E defined as

$$E[\rho] := \int_\Omega \left(\frac{\varepsilon}{2} |\nabla \rho|^2 + \frac{1}{\varepsilon} W(\rho) \right) \mathrm{d}x. \tag{1.3}$$

The gradient flow formulation says that the solution of the Allen-Cahn equation is the function ρ which evolves by minimizing the free energy E. We refer to the note of Chodosh [13] and the references listed inside for the mathematical details.

An important feature of the Allen-Cahn equation is that it is not conservative, that is the variation of the total mass $\frac{\mathrm{d}}{\mathrm{d}t} \int_\Omega \rho^\varepsilon(t,x)\,\mathrm{d}x$ is not zero. For this reason, many phase-field models using the Allen-Cahn equation for describing conservative physical phenomena need an additional term to ensure the conservative property which usually takes the form of a non-local Lagrange multiplier. These kind of equations are known as the conservative Allen-Cahn equations and they assume the following form

$$\partial_t \rho^\varepsilon = \Delta \rho^\varepsilon - \frac{1}{\varepsilon^2} W'(\rho^\varepsilon) + \lambda_\varepsilon(t) \quad \text{on } \Omega,\ t > 0 \tag{1.4}$$

where $\lambda(t) := \frac{1}{|\Omega|} \int_\Omega \frac{1}{\varepsilon^2} W'(\rho^\varepsilon)\,\mathrm{d}x$ is the Lagrange multiplier which preserves the total mass. We refer the reader to the work of Bronsard and Stoth [7] for more details on this particular case.

Another important equation modeling phase separation is the Cahn-Hilliard equation which was first described by Cahn [9] and by Cahn and Hilliard [10]. The Cahn-Hilliard equation writes as a forth order differential equation

$$\partial_t \rho^\varepsilon = \operatorname{div}[M(\rho^\varepsilon) \nabla (\, W'(\rho^\varepsilon) - \varepsilon^2 \Delta \rho^\varepsilon\,)] \quad \text{on } \Omega,\ t > 0, \tag{1.5}$$

where $M = M(\rho^\varepsilon)$ is a non-negative function called "mobility" coefficient and W is a double-well potential satisfying the properties (1.2). A typical choice used in the analysis of the Cahn-Hilliard equation is to consider W of the form $W(z) = (1/4)(1-z^2)^2$. An important property of the Cahn-Hilliard equation is that it naturally preserves the total mass by imposing no-flux boundary conditions. For the details on the derivation of the equation (1.5), we refer to [9, 10] as well as to the work of Gurtin [25].

When the mobility function M is constant, the related equation is called the constant motility Cahn-Hilliard equation. It has been proved that solutions with constant mobility may not be bounded between -1 and $+1$ representing a nonphysical case. We refer to the work of Novick-Cohen [36] for more details. In the case where the mobility depends on ρ^ε and it is degenerative, that is non-stricly positive and assuming zero value at -1 and $+1$, the related equation is more physically meaningful, but much more difficult by a mathematical point of view (due indeed to the deneracy). Elliot and Garcke [20] consider a degenerative mobility of the form $M(z) = (1-z^2)$ and proved a local in time existence of solution and that solutions which initially take values in $[-1,1]$ will do so for all positive time.

Sharp Interface Limit of the Allen-Cahn and Cahn-Hilliard equations

The Sharp Interface Limit corresponds to the study of the limiting behavior for $\varepsilon \to 0$ of the phase-field models and it represents a connection between free-boundary problems and phase-field models. Indeed, the limit $\varepsilon \to 0$ leads to phase separation and the diffusive interface of width ε tends to a moving curve which evolves according to geometric laws. In the Sharp Interface Limit, the phase-field function ρ^ε is such that

$$\lim_{\varepsilon \to 0} \rho^\varepsilon(x,t) = \rho^0(x,t) = \begin{cases} \rho_a & \text{for } x \in \Omega(t), \\ \rho_b & \text{for } x \in \Omega \setminus \Omega(t), \end{cases}$$

where ρ_a, ρ_b are the two wells of the double-well potential W used in the phase-field equation, and the domains $\Omega(t) \subset \Omega$ and $\Omega \setminus \Omega(t) \subset \Omega$ indicate the moving domain of the phase of density ρ_a and the phase of density ρ_b, respectively.

A large amount of works have been done for studying the Sharp Interface Limit of the Allen-Cahn and the Cahn-Hilliard equations. Evans, Soner and Souganidis [23] proved rigorously that the mean curvature flow governs the asymptotic behavior of the solutions of the Allen-Cahn equation (1.1) for global time. They proved that in the limit for $\varepsilon \to 0$, the solution of (1.1) is such that $\rho^\varepsilon \to +1$ in a region and $\rho^\varepsilon \to -1$ in the complementary region and the interface $\Gamma(t)$ between these regions moves as a surface with normal velocity V_n satisfying

$$V_n = \kappa, \tag{1.6}$$

where κ indicates the mean curvature of $\Gamma(t)$.

As for the conservative Allen-Cahn equation (1.4), it was proved that for $\varepsilon \to 0$ the moving interface $\Gamma(t)$ evolves according to a non-local volume preserving mean curvature flow with normal velocity V_n satisfying

$$V_n = \kappa - \frac{1}{|\Gamma(t)|} \int_{\Gamma(t)} \kappa \, \mathrm{d}s, \tag{1.7}$$

where κ is the mean curvature of $\Gamma(t)$ and $|\Gamma(t)|$ its perimeter. This result has been proved rigorously by Bronsard and Stoth [7] for local time by considering radial solutions of (1.4) with a Neumann boundary condition. Successively Chen, Hilhorst and Logak [12] proved the rigorous limit for local time in the general case with a suitable choice of the initial data.

he Sharp Interface Limit of the Cahn-Hilliard equation (1.5) with constant mobility $M(\rho^\varepsilon) = 1$ was derived in a formal way by Pego [38]. By the use of matched asymptotic expansions, he formally proved that the equation approaches the Mullins-Sekerka problem. The Mullins-Sekerka problem describes the evolution of a surface $\Gamma(t)$ moving with normal velocity V_n satisfying

$$V_n = [\nabla u] \cdot \mathbf{n} \quad \text{on } \Gamma(t), \tag{1.8}$$

with $\mathbf{n}$ the unit outer normal vector of $\Gamma(t)$ and $[\,\cdot\,]$ represents the sum of the normal derivatives of u from each side of $\Gamma(t)$. The sign of V_n follows the convection that normal velocities of expanding surfaces are positive. The function u is the solution of the problem

$$\begin{cases} -\Delta u = 0 & \text{in } \Omega \setminus \Gamma(t), \\ u = \gamma\kappa & \text{on } \Gamma(t), \end{cases} \tag{1.9}$$

where the parameter $\gamma > 0$ is the surface tension depending only on W, κ is the mean curvature of $\Gamma(t)$ The sign of κ follows the convention that convex closed sets have positive curvature. The Mullins-Sekerka problem is also known as the two-phase Hele-Shaw problem where $\Gamma(t)$ is the separating suerface. This limit was proved rigorously by Alikakos, Bates and Chen [2] as long as the limit problem admits classical solutions locally in time. Successively, Stoth [44] show the rigorous convergence under the assumption of radially symmetry and boundness for the energy of the initial data.

A particular degenerate case of the Cahn-Hilliard equation have been studied by Glasner [24]. The author takes a double well-potential such that $W(\rho) = 0$ if and only if $\rho = 0$ and $\rho = \rho_b > 0$ and a mobility of the form $M(\rho^\varepsilon) = \rho^\varepsilon$. The degeneracy then occurs only at the phase $\rho^\varepsilon = 0$. He shows formally that as $\varepsilon \to 0$ the equation converges to the one-phase Hele-Shaw free-boundary problem

$$\begin{cases} -\Delta p = 0 & \text{in } \Omega_b(t), \\ p = \gamma\kappa & \text{on } \partial\Omega_b(t), \\ V_n = -\nabla p \cdot \mathbf{n} & \text{on } \partial\Omega_b(t). \end{cases} \tag{1.10}$$

The domain $\Omega_b(t)$ is the region occupied by the phase $\rho = \rho_b$, and its boundary $\partial\Omega_b(t)$ is the moving interface separating the phases $\rho = 0$ and $\rho = \rho_b$. This interface moves with boundary

velocity V_n. The function κ is the curvature of $\Omega_b(t)$ and the parameter $\gamma > 0$ represents the surface tension depending only on the double-well potential W.

We dedicate the next section to the Hele-Shaw free-boundary problem and to the statement od particular properties for this problem.

The Hele-Shaw problem

The limiting problems (1.8)-(1.9) and (2.63) are free-boundary problems known as the two-phases and the one-phase Hele-Shaw problem, respectively. After briefly introducing its physical derivation, we present some important analytic results of the Hele-Shaw problem which have been extensively used in the study of our model.

The Hele-Shaw problem arose from an experiment conduced by the engineer Henry Shelby Hele-Shaw in 1898. He studied the flow of an incompressible viscous fluid in a cell composed by two very closely separated horizontal plates. This cell is called the Hele-Shaw cell. The fluid is injected into (or suctioned from) the cell thought a point on one plate serving as source (or a sink). The fluid starts to expand during the injection, while it starts to shrink during the suction. The domain $\Omega(t) \in \mathbb{R}^2$ represents the moving region occupied by the fluid for $t \geq 0$, and $\mathbf{u} = \mathbf{u}(t, x) \in \mathbb{R}^2$ is the bulk velocity considered independent of the vertical dimension. The incompressibility conditions leads to

$$\operatorname{div}(\mathbf{u}) = 0 \quad \text{in } \Omega(t).$$

The fluid pressure is related to the bulk velocity by the Darcy's law writing

$$\mathbf{u} = -\nabla p \quad \text{in } \Omega(t),$$

where the negative sign represents the standard physics convention that fluids flow from regions of high pressure to regions of low pressure. The above equality usually contains physical parameters such as fluid viscosity and the distance between the plates. We consider here unitary parameters to simply the presentation. It follows that the fluid pressure satisfies the Laplace's equation

$$\Delta p = 0 \quad \text{in } \Omega(t).$$

A first boundary condition concerns the pressure and it is called the dynamic boundary condition. By neglecting the surface tension on the boundary, it can be written as

$$p = 0 \quad \text{on } \partial\Omega(t).$$

The motion of the boundary $\partial\Omega(t)$ is due to its normal boundary velocity V_n which satisfies the second boundary condition called the kinematic boundary condition. It writes as

$$V_n = \mathbf{u} \cdot \mathbf{n} \quad \text{on } \partial\Omega(t).$$

The Hele-Sahw problem with zero surface tension writes then as follows

$$\begin{cases} \Delta p = 0 & \text{in } \Omega(t), \\ p = 0 & \text{on } \partial\Omega(t), \\ V_n = -\nabla p \cdot \mathbf{n} & \text{on } \partial\Omega(t). \end{cases} \tag{1.11}$$

For a complete description of the physical derivation of the Hele-Shaw problem in two cases of injection and suction, we refer to the book of Gustafsson and Vasil'ev [27]

During the injection, and under particular smoothness hypothesis of the initial curve $\partial\Omega(0)$, the existence and the uniqueness locally in time of a solution to the problem (1.11) was first proved by Vinogradov and Kufarev [47], and then a simplified version was given by Gustafsson [26]. For this reason, the case of injection is usually defined as the "well-posed" Hele-Shaw problem. The case of suction represents the opposite situation where the viscous fluid shrinks it is instead identified as

the "ill-posed" Hele-Shaw problem. The ill-posedness reveals by the formation of instabilities on the boundary identified by formation of cups and long fingers. These instability phenomena have been studied by Richardson [39] for cups formation, and by Saffman and Taylor [40] for fingers formation.

Successively, some variations of the ill-posed case have been considered in order to "regularize" the Hele-Shaw problem. In particular, these variations concern additional physical effects on the boundary which lead to different boundary conditions for the fluid pressure. First, the introduction of the surface tension has been considered such that it acts on the boundary by penalizing points that have high curvature, that is points where the interface is very sharp. The related Hele-Shaw problem is written as

$$\begin{cases} \Delta p = 0 & \text{in } \Omega(t), \\ p = \gamma\kappa & \text{on } \partial\Omega(t), \\ V_n = -\nabla p \cdot \mathbf{n} & \text{on } \partial\Omega(t), \end{cases} \tag{1.12}$$

where $\gamma > 0$ is the surface tension and κ the curvature of the boundary $\partial\Omega(t)$. The regularizing effect of the surface tension has been showed by Tanveer [45] and by Vanden-Broeck [46] by highlighting that the surface tension is able to control the width of the fingers. The locally in time existence of solutions for this problem was proved by Chen [11] for an arbitrary smooth initial curve $\partial\Omega(0)$. He used a perturbation approach on the boundary velocity with the second derivative of the curvature with respect to the arc length and apriori estimates. In [11], it was proved as well the global in time existence in the case of initial data close enough to a circle.

A second case of regularizing procedure concerns a velocity-dependent boundary condition which penalizes points of high boundary velocities. This case is well known as the kinetic undercooling and it has been extensively analyzed by Dallaston and McCue [18, 19] (see also the PhD thesis of Dallaston [17]). The Hele-Shaw problem with surface tension and kinetic undercooling boundary conditions in then written as

$$\begin{cases} \Delta p = 0 & \text{in } \Omega(t), \\ p = \gamma\kappa + cV_n & \text{on } \partial\Omega(t), \\ V_n = -\nabla p \cdot \mathbf{n} & \text{on } \partial\Omega(t), \end{cases} \tag{1.13}$$

where $c > 0$ represents the undercooling parameter, and V_n is the boundary velocity which is considered positive when the domain advances. The authors in [18, 19] furnish also a numerical method for studying the effect of the kinetic undercooling and its interaction with the surface tension. They show numerically that in the case of an expanding domain, the undercooling has a stabilizing effect on the the boundary, that is it penalizes in terms of boundary velocity the points of high curvature. This means that the points of high curvature have a boundary velocity smaller then the one of those points of small curvature.

We introduce in the next section a brief introduction of existing work that used phase-field models and their sharp-interface limit in the context of cell migration. A wider explanation of this application on cell migration will be presented in the following Chapters of this Thesis.

Context of cell migration

Phase-field models are extensively used for modeling cell migration. Indeed, they allow to deal with the dynamics of the cellular membrane which represents the moving interface separating the interior of the cell (one phase) and the exterior of the cell (the other phase). In this context, the phase-field function ρ^ε has the property to be $\rho^\varepsilon \approx 1$ inside of the cell and $\rho^\varepsilon \approx 0$ outside the cell, and the cell membrane is identified by the transition of ρ^ε between these two values. The quantity $\int_\Omega \rho^\varepsilon(t,x)\,\mathrm{d}x$ represents the volume of the cell which has to be conserved during the evolution. For these reason, either the conservative Allen-Cahn equation or the Cahn-Hilliard equation are used

to describe the evolution of ρ^ε, where then the double-well potential is such that

$$W(z) = 0 \text{ if and only if } z \in \{0, 1\}. \tag{1.14}$$

We described previously that the cell migration is the result of a complex interplay between the dynamics of the cell membrane and the active internal dynamics. In order to take into account this important coupling, the phase-field models used to describe cell migration are usually coupled with partial differential equation describing the active internal dynamics such as actin polymerization and depolymerization, the retrograde flow and the interaction of the myosin proteins on the dynamics of actin filaments.

The analysis of the Sharp Interface Limit for these kind of coupled equations are then conduced to derive the asymptotic behavior of the moving interface. This leads to a limiting problem describing the evolution of a moving closed curve which represents the cell membrane. Because of the coupling, very often rigorous asymptotic results are complicated to obtain. For this reason, the starting point is to study a formal asymptotic analysis to derive the limiting problem as it was done for instance in the derivation of the Sharp Interface Limit for the Cahn-Hilliard equation.

An important two-dimansional phase-field model of crawling cell migration which uses the conservative Allan-Cahn equation is presented by Ziebert, Swaminathan and Aranson [49]. It consists of a system of a coupled system of a the phase-filed function ρ^ε of the type conservative Allen-Cahn equation and a vectorial parabolic equation for the orientation vector of the actin filaments polymerization. The system was then reformulated by Berlyand, Potomkin and Rybalko [5] for a more suitable form asymptotic analysis which then was conduced by the same authors in [6]. The formal derivation of the Sharp Interface Limit leads to a volume preserving mean curvature driven motion with an additional nonlinear term due to adhesion to the substrate and protrusion by the cytoskeleton.

In this Thesis we analyze a different type of 2D phase-field model with respect to the one presented in [6]. It consists of a coupled system between a degenerative Cahn-Hilliard type equation for the phase-field function and a convection-reaction-diffusion equation describing the evolution for the myosin proteins concentration interacting with the actin filaments. We will see that the formal Sharp Interface Limit results int a free-boundary problem of Hele-Shaw type with surface tension and an additional destabilizing velocity-dependent term on the boundary.

1.3 Structure of the Thesis

We present in this section a general overview of the studies and results presented in this Thesis. Beside the Introduction, this Thesis is composed of three chapters.

- The Chapter 2 is entitled **A Cahn-Hilliard model for cell motility** and it refers to the results presented in the article [15] which represents a first joint work with Mellet and Meunier. The aim of this part is to introduce a diffusive interface model for cell migration and study its asymptotic behavior. The model writes as a coupled system composed by a phase-field equation of degenerate Cahn-Hilliard type and a reaction-diffusion-equation for an active potential describing the internal dynamics of the cell. We prove the weak existence of solutions in the one-dimensional case and we derive formally the Sharp Interface Limit in any dimension. In the two-dimensional case, the Sharp Interface Limit leads to a Hele-Shaw free-boundary problem which includes the effect of surface tension and an additional destabilizing velocity-dependent term. We furnish analytic results of this problem in the one dimensional case. We prove in particular in this case existence of Traveling Wave like solution and Hysteresis phenomenon.

- The Chapter 3 is entitled **Traveling Waves in the 2D case** and it refers to the results presented in the preprint [16] representing a second joint work with Mellet and Meunier. The aim of this part is to study a particular free-boundary problem which arises as the sharp interface limit of the phase-field model presented in Chapter 2. In particular, we prove the existence of Traveling Wave solutions. We first show the (local) existence of Traveling Wave solutions via a bifurcation argument. Then, we present a constructive method which is able to "track" the Traveling Wave. For that, we show also a numerical method which is able to furnish the numerical form of the related Traveling Wave. For both methods, we obtain that Traveling Wave like solutions appear when the destabilizing term on the boundary condition of the free-boundary problem is strong enough.

- The Chapter 4 is entitled **Hysteresis in the 2D case** and it refers to an ongoing research representing a third joint work with Mellet and Meunier. The aim of this part is to study the phenomenon of Hysteresis in the two dimensional case for a simplified version of the free-boundary problem introduced in Chapter 3. We fix the time $t = t_0$ and we consider the problem defined on the fixed domain $\Omega(t = t_0)$ (we consider a disk). Via a local bifurcation argument, we show that if the destabilizing term is strong enough this problem has more than one solution. This means that if we are given only a picture of the cell at a given time t_0, we can not predict its future behavior. Such a phenomenon is called Hysteresis.

- The Chapter 5 is entitled **Cell migration in complex environment** and it refers to the results presented in the proceedings [14] in collaboration with Etchegaray, Meunier, Navoret and Sabbagh. The aim of this part is to consider the cell as a moving particle and to study its motion in the external environment in response to an attracting signal and topographical fixed obstacles. We enrich an existing 2D stochastic model for cell crawling to account for the the presence of a constant gradient in attracting signal and of fixed circular-shape obstacles. We consider two scenario. First, we studied only the interaction of the attracting signal and the presence of obstacles. Then, we introduced also the effect of the active internal dynamics. In both cases, we found numerically the existence of a velocity value depending on the number of obstacles that the cell cannot exceed, even if the force intensity increases.

Bibliography

[1] B. ALBERTS, A. JOHNSON, J. LEWIS, M. RAFF, K. ROBERTS, AND P. WALTER, *The self-assembly and dynamic structure of cytoskeletal filaments*, Garland Science, 2002.

[2] N. D. ALIKAKOS, P. W. BATES, AND X. CHEN, *Convergence of the Cahn-Hilliard equation to the Hele-Shaw model*, Arch. Rational Mech. Anal., 128 (1994), pp. 165–205.

[3] S. M. ALLEN AND J. W. CAHN, *A microscopic theory for antiphase boundary motion and its application to antiphase domain coarsening*, Acta Metall. Mater., 27 (1979), pp. 1085–1095.

[4] R. ANANTHAKRISHNAN AND A. EHRLICHER, *The forces behind cell movement*, Int J Biol Sci, 3 (2007), pp. 303–317.

[5] L. BERLYAND, M. POTOMKIN, AND V. RYBALKO, *Non-uniqueness in a nonlinear sharp interface model of cell motility*, arXiv preprint arXiv:1409.5925, (2014).

[6] ——, *Sharp interface limit in a phase field model of cell motility*, Netw. Heterog. Media, 12 (2017), pp. 551–590.

[7] L. BRONSARD AND B. STOTH, *Volume-Preserving Mean Curvature Flow as a limit of a nonlocal Ginzburg-Landau equation*, SIAM J. Math. Anal., 28 (1997), p. 769–807.

[8] D. CABALLERO, J. COMELLES, M. PIEL, R. VOITURIEZ, AND D. RIVELINE, *Ratchetaxis: Long-range directed cell migration by local cues*, Trends in Cell Biology, 25 (2015), pp. 815–827.

[9] J. W. CAHN, *On spinoidal decomposition*, Acta Metall., 9 (1961), pp. 796–801.

[10] J. W. CAHN AND J. HILLIARD, *Free energy of a nonuniform system. i. interfacoial free energy*, J. Chem. Phys., 28 (1958), pp. 258–267.

[11] X. CHEN, *The Hele-Shaw problem and area-preserving curve-shortening motions*, Arch. Ration. Mech. Anal., 123 (1993), pp. 117–151.

[12] X. CHEN, D. HILHORST, AND E. LOGAK, *Mass conservation Allen-Cahn equation and volume preserving Mean Curvature Flow*, Interfaces Free Bound., 12 (2010), pp. 527–549.

[13] O. CHODOSH, in Lecture notes on geometric features of the Allen-Cahn equation, 2019.

[14] A. CUCCHI, C. ETCHEGARAY, N. MEUNIER, L. NAVORET, AND L. SABBAGH, *Cell migration in complex environments: chemotaxis and topographical obstacles*, ESAIM: Proceedings and Surveys, 67 (2020), pp. 191–209.

[15] A. CUCCHI, A. MELLET, AND N. MEUNIER, *A Cahn-Hilliard model for cell motility*, SIAM J. Math. Anal., 52 (2020), pp. 3843–3880.

[16] A. CUCCHI, A. MELLET, AND N. MEUNIER, *Self polarization and traveling wave in a model for cell crawling migration.* preprint, 2021.

[17] M. C. DALLASTON, *Mathematical models of bubble evolution in a Hele-Shaw Cell*, PhD thesis, Queensland University of Technology, 2013.

[18] M. C. DALLASTON AND S. W. MCCUE, *Numerical solution to the Saffman-Taylor finger problem with kinetic undercooling regularisation*, ANZIAM J., 52 (2010), pp. 124–138.

[19] M. C. DALLASTON AND S. W. MCCUE, *Bubble extinction in Hele-Shaw flow with surface tension and kinetic undercooling regularization*, Nonlinearity, 26 (2013), pp. 1639–1665.

[20] C. M. ELLIOTT AND H. GARCKE, *On the Cahn-Hilliard equation with degenerate mobility*, SIAM J. Math. Anal, 27 (1996), pp. 404–423.

[21] C. ETCHEGARAY, *Modélisation mathématique et numérique de la migration cellulaire*, PhD thesis, Université Paris-Saclay (ComUE), 2016.

[22] C. ETCHEGARAY AND N. MEUNIER, *A stochastic model for protrusion activity*, ESAIM: Proceedings and Surveys, 62 (2018), pp. 56–67.

[23] L. C. EVANS, H. M. SONER, AND P. E. SOUGANIDIS, *Phase transitions and generalized motion by mean curvature*, Communications on Pure and Applied Mathematics, 45 (1992), pp. 1097–1123.

[24] K. GMASNER, *A diffusive interface approach to Hele-Shaw flow*, Nonlinearity, 16 (2002), pp. 49–66.

[25] M. E. GURTIN, *Generalized Ginzburg-Landau and Cahn-Hilliard equations based on a microforce balance*, Phys D: Nonlinear Phenomena, 62 (1996), pp. 178–192.

[26] B. GUSTAFSSON, *On a differential equation arising in a Hele-Shaw flow moving boundary problem*, Arkiv för matematik, 22 (1984), pp. 251–268.

[27] B. GUSTAFSSON AND A. VASIL'EV, *Conformal and potential analysis in Hele-Shaw cells*, Springer Science & Business Media, 2006.

[28] J. F. JOANNY AND J. PROST, *Active gels as a description of the actin-myosin cytoskeleton*, HFSP Journal, 3 (2009), pp. 94–104.

[29] F. JÜRLICHER, K. KRUSE, J. PROST, AND J.-F. JOANNY, *Active behavior of the Cytoskeleton*, Physics Reports, 449 (2007), pp. 3–28.

[30] Y. LI, P. BHIMALAPURAM, AND A. R. DINNER, *Model for how retrograde actin flow regulates adhesion traction stresses*, Journal of Physics: Condensed Matter, 22 (2010), p. 194113.

[31] H. LODISH, A. BERK, C. A. KAISER, M. KRIEGER, M. P. SCOTT, A. BRETSCHER, H. PLOEGH, P. MATSUDAIRA, ET AL., *Molecular cell biology*, Macmillan, 2008.

[32] P. MAIURI, J. RUPPRECHT, S. WIESER, AND ET AL., *Actin flows mediate a universal coupling between cell speed and cell persistence*, Cell, 463 (2015), pp. 374–386.

[33] A. MAKKI, *Étude de modèlles en sélparation de phase tenant compte d'effets d'anisotropie*, thesis, Université de Poitiers, 2016.

[34] P. K. MATTILA AND P. LAPPALAINEN, *Filopodia: molecular architecture and cellular functions*, Nature reviews Molecular cell biology, 9 (2008), pp. 446–454.

[35] A. MOGILNER AND G. OSTER, *The physics of lamellipodial protrusion*, European biophysics journal, 25 (1996), pp. 47–53.

[36] A. NOVICK-COHEN, *The Cahn–Hilliard equation: mathematical and modeling perspectives,*, Adv. Math. Sci. Appl., 8 (1998), p. 965–985.

[37] J. T. PARSONS, A. R. HORWITZ, AND M. A. SCHWARTZ, *Cell adhesion: integrating cytoskeletal dynamics and cellular tension*, Nature reviews Molecular cell biology, 11 (2010), pp. 633–643.

[38] R. L. PEGO, *Front migration in the nonlinear Cahn-Hilliard equation*, Proc. Roy. Soc. London Ser. A, 422 (1989), pp. 261–278.

[39] S. RICHARDSON, *On the classification of solutions to the zero-surface-tension model for Hele-Shaw free boundary flows*, Quarterly of Applied Mathematics, 55 (1997), pp. 313–319.

[40] P. G. SAFFMAN AND G. I. TAYLOR, *The penetration of a fluid into a porous medium or Hele-Shaw cell containing a more viscous liquid*, Proc. R. Soc. Lond. A 245, 245 (1958), pp. 312–329.

[41] W. SAOUD, *Study of a coupled Cahn-Hilliard/Allen-Cahn system in phase separation*, thesis, Université de Poitiers, 2018.

[42] P. SENS AND J. PLASTINO, *Membrane tension and cytoskeleton organization in cell motility*, J. Phys.: Condens. Matter, 27 (2015), p. 273103.

[43] J. V. SMALL, T. STRADAL, E. VIGNAL, AND K. ROTTNER, *The lamellipodium: where motility begins*, Trends in Cell Biology, 12 (2012), pp. 112–120.

[44] E. E. B. STOTH, *Convergence of the Cahn-Hilliard equation to the Mullins-Sekerka problem in spherical symmetry*, J. Differ. Equ., 125 (1996), pp. 154–183.

[45] S. TANVEER, *the effect of surface tension on the shape of a Hele-Shaw cell bubble*, Physics of Fluids, 29 (1986), pp. 3537–3548.

[46] J.-M. VANDEN-BROECK, *Fingers in a Hele–Shaw cell with surface tension*, The Physics of Fluids, 26 (1983), pp. 2033–2034.

[47] Y. P. VINOGRADOV AND P. KUFAREV, *On a problem of filtration*, Akad. Nauk SSSR Prikl. Mat. Meh, 12 (1948), pp. 181–198.

[48] F. WANG, *The signaling mechanisms underlying cell polarity and chemotaxis.*, Cold Spring Harbor perspectives in biology, 1 (2009), p. a002980.

[49] F. ZIEBERT, S. SWAMINATHAN, AND I. S. ARANSON, *Model for self-polarization and motility of keratocyte fragments*, J. R. Soc. Interface, 9 (2012), pp. 1084–1092.

Chapter 2

A Cahn-Hilliard model for cell motility

This Chapter refers to the article [17] in collaboration with Mellet and Meunier.

2.1 Introduction of the phase-field model and statement of the results

This Chapter is devoted to the analysis of the following system of equations, which we will introduce in Section 2.2 as a simple model for cell motility:

$$\begin{cases} \partial_t \rho = \operatorname{div}\left(\rho \nabla\left[\gamma\left(-\varepsilon\Delta\rho + \frac{1}{\varepsilon}W'(\rho)\right) + \phi\right]\right), \\ \partial_t \phi - \varepsilon\Delta\phi = \frac{1}{\varepsilon}\left(\beta\rho - \phi\right), \end{cases} \tag{2.1}$$

for $x \in \Omega \subset \mathbb{R}^n$, $t > 0$, with $\varepsilon > 0$, $\gamma > 0$, $\beta \geq 0$ and W a double-well potential satisfying

$$W(0) = W(1) = 0, \quad W(\rho) > 0 \text{ if } \rho \neq 0,\, 1 \tag{2.2}$$

(for instance $W(\rho) = \rho^2(1-\rho)^2$). This system will be supplemented by appropriate boundary conditions on $\partial\Omega$ and initial conditions. The system (2.1) involves a fourth order degenerate Cahn-Hilliard equation coupled to a second order diffusion equation. We make the following simple observations:

- When the potential ϕ is zero (for instance if $\beta = 0$ and $\phi(t=0) = 0$), then (2.1) is a classical Cahn-Hilliard equation with degenerate mobility, whose sharp interface limit (ε goes to zero) is the Hele-Shaw free boundary model with surface tension (or one-phase Mullins-Sekerka free boundary problem, see [23]). For this model it is well-known that the ball is a stable stationary solution.
- When the surface tension parameter γ is zero, System (2.1) is a repulsive Keller-Segel type system (although without diffusion in the ρ equation): the potential ϕ describes a chemorepulsion type of phenomenon (see [15]). When $\varepsilon \ll 1$, the dynamic is close to that of the porous medium equation $\partial_t \rho = \frac{1}{2}\beta\Delta\rho^2$ which does not have stationary solutions in $\mathbb{R}^n$ since the support of the solution will spread for all $t > 0$ (except possibly for an initial waiting time).

As we will explain below, these two competing mechanisms are what makes this model interesting in the context of cell motility. In particular it is well suited to describe the active character of the membrane of the cell and the formation of protrusions.

Our goal in this chapter is threefolds. First, we will prove the existence of non-negative solutions for the coupled system (2.1) in the one dimensional case. This is non trivial since it involves the usual difficulties in dealing with a fourth order degenerate equation (similar to the thin film equation) together with the coupling with the evolution of the potential ϕ. Then we will consider the sharp interface limit for $\varepsilon \to 0$ and formally derive a free boundary problem in which the stabilizing effect of surface tension is competing with the destabilizing effect of the chemorepulsion mechanism. More precisely, we will see that when $\varepsilon \ll 1$ the dynamic of the cell (represented here by the support $\Sigma(t)$ of ρ) is described by the following Hele-Shaw free boundary problem:

$$\begin{cases} -\Delta q = 0 & \text{in } \Sigma(t), \\ q = \bar{\gamma}\kappa(t) + \beta F(V) & \text{on } \partial\Sigma(t), \\ V = -\nabla q \cdot \mathbf{n} & \text{on } \partial\Sigma(t), \end{cases} \tag{2.3}$$

where $\kappa(t)$ denotes the mean-curvature of the boundary $\partial\Sigma(t)$ (with the convention that the curvature of a sphere is positive) and V denotes its normal outward velocity. Importantly, the function $F : \mathbb{R} \to \mathbb{R}$, whose definition is given in (2.15), will be proved to be a decreasing function of V. As a consequence, the active term $\beta F(V)$ at the boundary has a destabilizing effect which leads to hysteresis phenomena. Indeed, we can rewrite the boundary condition in (2.3) as

$$q - \beta F(-\nabla q \cdot \mathbf{n}) = \bar{\gamma}\kappa(\mathbf{t})$$

which is a (nonlinear) Robin type condition with the "wrong" sign (which might lead to multiple solutions). Note in particular that this condition has the opposite effect of the (linear) Robin condition used in the so-called undercooling Hele-Shaw problem [18, 19, 21, 31, 34].

As mentioned above, System (2.1) is a simple model for cell motility. One of the most remarkable characteristics of eukaryotic cells is their ability to reach and maintain an asymmetric shape spontaneously or in response to external signals. This cellular property, called front-rear polarization, results from symmetry breaking in its internal organization and is necessary for efficient cell migration. In the section of this chapter, we will rigorously establish these properties for the free boundary problem (2.3) in one dimension, proving in particular the existence of multiple traveling wave solutions (thus including non-stationary ones) when the parameter β is large enough.

From a modeling point of view, our system is very simple. We use only two quantities to describe the cell: the phase-field (or order parameter) ρ, describing everything that lies inside the cell (cytoskeleton, solvent, molecular motors...), and the myosin II, a molecular motor that assembles in minifilaments, interacts with actin, behaves as active crosslinkers and generates contractile or dilative stresses in the cytoskeleton network, whose concentration is denoted by ϕ. The main assumptions that lead to (2.1) are the following: (i) the cell velocity, v is given by the local actin flow, (ii) myosin II in the bulk is slowly diffusing, (iii) actin filaments undergo uniform bulk polymerization and depolymerization, (iv) the osmotic pressure involved in the network stress acts to saturate the linear instability causing gel phase separation and to smooth the interface between cytosol-rich and cytosol-poor regions. The underlying processes are: friction of the cytosol on the substrate together with the active character of the myosin II. We refer to Section 2.2 for a detailed presentation of the model with biological motivations.

We briefly introduce the existing literature before stating ours result. The phase-field models have been widely used in the biophysical community to describe cell motility. These models, reviewed in [24, 37], are mostly computational. In [5] a phase-field model, first introduced in [38], was mathematically studied. It consists of a second order parabolic equation for a scalar phase-field function coupled with a vectorial parabolic equation for the actin filament network polarity. The derivation of the sharp interface limit leads to a volume preserving curvature driven motion with an additional nonlinear term due to adhesion to the substrate and protrusion by the cytoskeleton. This sharp interface limit and the limiting model are rigorously studied in one dimension in [4–6]. Numerical simulations allow to observe discontinuity of interface velocities and

hysteresis phenomena. In [4, 6], non-stationary traveling wave solutions are rigorously obtained for the limit problem and the phase-field model. These aforementioned mathematical work deal with second order Allen-Cahn models that lead to mean curvature flow type of free boundary problems. By comparison, we consider here a fourth order Cahn-Hilliard model and derive a Hele-Shaw type free boundary model with surface tension, which is well suited to describe cell motility (see e.g. [37] and references therein) and has the advantage of being volume preserving without the addition of a Lagrange multiplier. However, the analysis of this fourth order degenerate equation is more delicate, even in one dimension. Sharp interface limits for such Cahn-Hilliard equations are formally studied in [23, 33]. The main novelty of our derivation is the role played by the potential ϕ, which leads to the non-linear and destabilizing term $\beta F(V)$ in (2.3). The resulting hysteresis phenomena that we rigorously establish in one dimension is in good agreement with recent models used in the biophysical community [9, 30].

Weak existence in dimension 1

Our first result is concerned with the existence of a weak solution for the coupled system (2.1) in dimension one. To simplify the notations, we take all parameters to be 1, so the system becomes:

$$\begin{cases} \partial_t \rho = \partial_x \left(\rho \, \partial_x \left(-\partial_{xx}\rho + W'(\rho) + \phi \right) \right) & x \in \Omega, \ t > 0 \\ \partial_t \phi = \partial_{xx}\phi - \phi + \rho & x \in \Omega, \ t > 0 \end{cases} \tag{2.4}$$

where Ω is a fixed domain in $\mathbb{R}$ i.e. an open interval of the form $\Omega = (a, b)$ with initial conditions

$$\rho(x, 0) = \rho_{in}(x), \qquad \phi(x, 0) = \phi_{in}(x) \quad \text{for } x \in \Omega, \tag{2.5}$$

and boundary conditions

$$\partial_x \phi_{|\partial\Omega} = 0, \tag{2.6}$$

$$\left(\rho \, \partial_x \left(-\partial_{xx}\rho + W'(\rho) + \phi \right] \right) \big)_{|\partial\Omega} = 0, \tag{2.7}$$

$$\partial_x \rho_{|\partial\Omega} = 0. \tag{2.8}$$

Note that (2.7) is a no-flux boundary condition for ρ, which guarantees that the mass $\int_\Omega \rho \, dx$ is preserved. Since (2.6) holds, the condition (2.7) is equivalent to $\left(\rho \partial_x \left(-\partial_{xx}\rho + W'(\rho) \right) \right)_{|\partial\Omega} = 0$. We will prove the following theorem:

Theorem 2.1.1. *Assume that the potential W is a non-negative function in $C^2(\mathbb{R})$. Then for all $T > 0$ and all non-negative initial data $(\rho_{in}(x), \phi_{in}(x))$ satisfying*

$$\rho_{in} \in H^1(\Omega), \quad W(\rho_{in}) \in L^1(\Omega), \quad \phi_{in} \in L^2(\Omega), \tag{2.9}$$

the system of equations (2.4)-(2.8) has a weak solution $(\rho(x,t), \phi(x,t))$ satisfying

$$\rho \geq 0, \quad \rho \in L^\infty(0, T; H^1(\Omega)) \cap L^2(0, T; H^2(\Omega)), \quad W(\rho) \in L^\infty(0, T; L^1(\Omega)),$$

$$\rho \, \partial_{xxx}\rho \in L^2(\{\rho > 0\}),$$

and

$$\phi \in L^\infty(0, T; L^2(\Omega)) \cap L^2(0, T; H^1(\Omega)).$$

In particular, the first equation in (2.4) is satisfied in the following sense. Let $\Omega_T = \Omega \times [0, T)$ and let $\mathcal{D}(\Omega_T)$ be a set of test functions. Then, $\forall \varphi \in \mathcal{D}(\Omega_T)$,

$$\iint_{\Omega_T} \rho \, \partial_t \varphi \, dx \, dt - \iint_{\{\rho > 0\}} \rho \, \partial_x (-\partial_{xx}\rho + W'(\rho) + \phi) \partial_x \varphi \, dx \, dt = - \int_\Omega \rho_{in}(x) \, \varphi(x, 0) \, dx,$$

where $\{\rho > 0\}$ *indicates the strictly-positive support of* ρ *satisfying the boundary condition* $\partial_x \rho = 0$ *if* $\rho > 0$ *on* $\partial\Omega$ *and the following mass conservation property:*

$$\int_\Omega \rho(x,t)\,dx = \int_\Omega \rho_{in}(x)\,dx \qquad \text{for all } t > 0.$$

The diffusion equation with Neumann boundary conditions for ϕ *is satisfied in the usual weak formulation.*

Note that this type of weak formulation is classical for degenerate fourth order equations such as the thin film equation (see [7, 8]). Since the equation for ρ is degenerate when $\rho = 0$, the first step in the proof of Theorem 2.1.1 is to perform a regularization procedure by introducing a uniformly parabolic equation of order 4 whose solution is ρ^δ where $\delta > 0$ is the regularization parameter. Existence of smooth solutions is well-known for this kind of uniformly parabolic equation. However, because the equation is of order 4, it is a classical fact that the solution might change its sign, even though the initial condition is non-negative. The existence of a solution $(\rho^\delta, \phi^\delta)$ to the coupled system of regularized equations is proved via a fixed point argument on the potential ϕ^δ. The second step consists in passing to the limit $\delta \to 0$. This requires techniques that are classical in the study of the thin film equation, as done in [7]. In particular, an entropy type inequality allows to show that the limit ρ is a non-negative function.

Note that the uniqueness of the solution is a classical open problem for the thin film equation (i.e. when $\phi = 0$ and $W = 0$).

Sharp interface limit in any dimension

Next, we will formally derive the sharp interface limit $\varepsilon \ll 1$ for the system (2.1) in any dimension. Note that if we take $\beta = 0$, the system decouples and we are led to consider the following degenerate Cahn-Hilliard equation (with a given potential):

$$\partial_t \rho^\varepsilon = \operatorname{div}\left(\rho^\varepsilon \nabla\left[\gamma(-\varepsilon\Delta\rho^\varepsilon + \frac{1}{\varepsilon}W'(\rho^\varepsilon) + \phi)\right]\right). \tag{2.10}$$

We recall that for the classical Cahn-Hilliard equation with constant mobility the formal asymptotic limit $\varepsilon \to 0$ was derived by Pego in [33]. The limit leads to phase separations and the free boundary separating the two phases evolves according to a two-phase Mullins-Sekerka type free boundary problem. In the degenerate case that we consider here, a similar formal analysis was performed by Glasner in [23] for non-negative solutions of (2.10) when $\phi = 0$. Importantly, the fact that such a fourth order parabolic equation admits non-negative solutions is due to the degeneracy of the mobility coefficient when $\rho = 0$. In this case, the limit is described by a one-phase Mullins-Sekerka type free boundary problem, also known in two dimensions as Hele-Shaw flow with surface tension.

In this section, we consider the slightly more general system (supplemented with the boundary conditions (2.25), (2.26) and (2.27)):

$$\begin{cases} \partial_t \rho^\varepsilon + \operatorname{div}(\rho^\varepsilon v^\varepsilon) = 0\,, \\ v^\varepsilon = -\nabla\left[\gamma\left(-\varepsilon\Delta\rho^\varepsilon + \frac{1}{\varepsilon}W'(\rho^\varepsilon)\right) + \phi^\varepsilon\right]\,, \\ \partial_t \phi^\varepsilon + \alpha \operatorname{div}(\phi^\varepsilon v^\varepsilon) = \frac{1}{\varepsilon}\left(\eta^2\Delta\phi^\varepsilon + \beta\rho^\varepsilon - \phi^\varepsilon\right)\,, \end{cases} \tag{2.11}$$

where the term $\alpha \operatorname{div}(\phi v)$ (with $\alpha \in [0,1]$) in the last equation accounts for the fact that the myosin II can be actively transported by the local actin flow. The parameter $\eta \geq 0$ allows us to characterize the role plaid by the diffusivity of ϕ in the asymptotic behavior of ρ in Theorem 2.1.2 below. Note that the system (2.1) is a particular case of (2.11) corresponding to $\alpha = 0$ and $\eta = \varepsilon$ and its limit is the object of part (ii) in the following theorem:

Theorem 2.1.2. *Assume that the potential* W *is in* $C^2(\mathbb{R})$ *and satisfies* (2.2). *Formally, the solution* $\rho^\varepsilon(x,t)$ *of the system* (2.11) *converges as* $\varepsilon \to 0$ *to* $\rho^0(t) = \chi_{\Sigma(t)}$ *where the evolution of* $\Sigma(t)$ *is described by the following Hele-Shaw type free boundary problems:*

(i) If $\eta > 0$ is fixed, then the normal velocity V of $\partial\Sigma(t)$ is determined by

$$\begin{cases} -\Delta q = 0 & \text{in } \Sigma(t), \\ q = \bar{\gamma}\kappa(x,t) + \phi^0(x,t) & \text{on } \partial\Sigma(t), \\ V = -\nabla q \cdot n & \text{on } \partial\Sigma(t), \end{cases} \tag{2.12}$$

where $\kappa(x,t)$ denotes the mean-curvature of the boundary $\partial\Sigma(t)$ and for all $t > 0$ the function $\phi^0(\cdot,t)$ is the solution of

$$\phi^0 - \eta^2\Delta\phi^0 = \beta\chi_{\Sigma(t)} \qquad \text{in } \Omega, \tag{2.13}$$

with Neumann boundary conditions on $\partial\Omega$. The constant $\bar{\gamma}$ is given by:

$$\bar{\gamma} = \gamma\sqrt{2}\int_0^1 \sqrt{W(x)}\,dx.$$

(ii) If $\eta = \tau\varepsilon$ for some fixed τ, then the normal velocity V of $\partial\Sigma(t)$ is determined by

$$\begin{cases} -\Delta q = 0 & \text{in } \Sigma(t), \\ q = \bar{\gamma}\kappa(t) + \beta F_\tau((1-\alpha)V) & \text{on } \partial\Sigma(t), \\ V = -\nabla q \cdot n & \text{on } \partial\Sigma(t), \end{cases} \tag{2.14}$$

where the function $F_\tau : \mathbb{R} \to \mathbb{R}$ is defined below (see (2.15)).

The function $F_\tau(V)$ appearing in the limiting equation (2.14) models the effects of the active potential ϕ^ε in the sharp interface limit when $\eta \sim \varepsilon$. Note that in that case, the function ϕ becomes discontinuous across the interface $\partial\Sigma(t)$ and a blow up analysis in the neighborhood of the interface will be necessary. The function F_τ is defined as follows. First, we denote by $\psi(z)$ the unique solution of

$$\psi'(z) = \sqrt{2\,W(\psi(z))}, \qquad \lim_{z\to-\infty}\psi(z) = 0, \qquad \lim_{z\to+\infty}\psi(z) = 1.$$

This function ψ describes the blow-up transition profile for the function ρ^ε, see Section 2.4. Then, for any $V \in \mathbb{R}$, we set

$$F_\tau(V) := \int_{-\infty}^{\infty} \Phi_\tau(V,z)\,\psi'(z)\,dz, \tag{2.15}$$

where $\Phi_\tau(V,z)$ is the unique bounded solution (see Proposition 2.4.2) of

$$\tau^2\Phi'' - V\Phi' - \Phi + \psi = 0.$$

Remarks 2.1.3. *The difference between the asymptotic equations (2.12) and (2.14) shows that the limit $\varepsilon \to 0$ is very sensitive to the particular choice we make for the evolution of the potential ϕ^ε. In both cases, the free boundary condition is of the form $q(x,t) = \bar{\gamma}\kappa(x,t) + h(x,t)$ where h is related to ϕ^ε and ρ^ε in the following way. Formally at least (see Remark 2.4.3), $\phi^\varepsilon\nabla\rho^\varepsilon$ converges as $\varepsilon \to 0$ and in the sense of measure to the vector valued measure*

$$-h(x,t)\,n(x,t)\mathcal{H}^{n-1}|_{\partial\Sigma(t)}.$$

In particular, other models than the ones considered here are possible. For instance, if we assume that ϕ^ε is given for all $t > 0$ by

$$\phi^\varepsilon = \beta\rho^\varepsilon(x,t),$$

then the Dirichlet condition in (2.12) is replaced with the simpler condition:

$$q = \gamma\kappa(t) + \frac{1}{2}\beta,$$

which can be an interesting problem if β is taken to be a function of x and t rather than a constant.

Note that when $\alpha = 1$ or $\beta = 0$, the model (2.14) reduces to the classical Hele-Shaw flow with surface tension. In dimension two, the existence of solutions for this problem was proved by Chen [12] (weak solutions) and by Constantin and Pugh [16] (analytic solutions). The existence of classical solutions is proved by Escher and Simonett [20] for a large class of initial data and in any dimension. Hele-Shaw models with surface tension, coupled to diffusion equations have also been studied in the context of tumor growth models [3, 14]. Finally, we point out that the rigorous derivation of Hele-Shaw free boundary problem from Cahn-Hilliard equation is a notoriously difficult problem. For the uncoupled and non-degenerate problem, the convergence was first proved by Alikakos et al. [1] under the assumption that the limiting problem has a smooth solution. In [13], X. Chen proved the rigorous convergence of the Cahn-Hilliard equation to the varifold solutions of the Hele-Shaw model with weak convergence methdods. Finally, N.Q. Le [29] established new convergence results using the gamma convergence of gradient flows approach introduced by Sandier and Serfaty in [36]. No rigorous results are know in the degenerate case that we are considering here. Note also that the coupling with the function ϕ adds an additional difficulty since the gradient flow structure seems lost in that case.

Properties of the asymptotic models (2.12) and (2.14)

The first system (2.12)-(2.13), which we derive when $\eta = \mathcal{O}(1)$, is closely related to a model for viscous ferrofluids studied by Otto in [32]. It can be written as a gradient flow for an appropriate energy function with respect to the Wasserstein distance over the manifold of characteristic functions with fixed mass. Approximated solutions can thus be constructed via a JKO type time discretization and a conditional existence result is proved in [32]. In this model, the potential ϕ has a destabilizing effect on the Hele-Shaw flow and the dynamics is the result of the competition between the regularizing effect of surface tension and the destabilizing effect of the potential. For small surface tension, fingering instabilities appear and Otto in [32] investigates the asymptotic behavior of approximated solutions of (2.12)-(2.13) when $\bar{\gamma} \ll \eta \ll 1$: The perimeter of $\Sigma(t)$ goes to infinity and the characteristic function $\chi_{\Sigma(t)}$ converges weakly to a function which takes value in $[0, 1]$ and whose dynamics is described by a porous media equation. In that limit, the integrity of the cell is lost, so this is not an appropriate regime in the context of cell motility. However, these fingering instabilities suggest that when $\bar{\gamma} \sim 1$ and β is large enough, the model is well suited to describe the formation of protrusions on the cell's membrane. Further investigation of this model in dimension 2, and in particular the existence of traveling waves solution will be the object of some future work.

We focus now on the second model (2.14), which appears to be new, though it bears some similarities with the model introduced and studied in [4–6, 35] for cell motility. In those papers, a second order mean-curvature flow model is derived, with velocity law given by

$$V = \kappa + G_\beta(V) - \lambda(t) \tag{2.16}$$

for a function G_β which is defined in a similar manner as our F. The model (2.16) is derived as the sharp interface limit of a second order Allen-Cahn equation coupled to a diffusion equation similar to our equation for ϕ. Because such a second order equation does not preserve the volume, the model has to include a Lagrange multiplier $\lambda(t)$. By contrast, the fourth order Cahn-Hilliard equation that constitutes the starting point of our model (as well as the limiting Hele-Shaw flow that we derive) naturally preserves the volume of the cell and does not require the introduction of a Lagrange multiplier. Another significant difference is that the solution of our model (2.4) satisfies $\rho^\varepsilon \geq 0$ - provided the initial data is non-negative - while the solution of the Allen-Cahn equation considered in [4–6, 35] can change sign.

In the asymptotic model (2.16), the velocity $V(x, t)$ must be found at each point $x \in \partial\Sigma(t)$ by solving the algebraic equation (2.16). For some choices of potential W and large enough β, it can be proved that this equation has more than one solution. This leads to hysteresis phenomena (the velocity of the cell at a given time is not uniquely determined by its asymptotic shape) and to

the existence of non-stationary traveling wave like solutions, the existence of which is investigated in [5].

The asymptotic dynamics of our model (2.14) is different and more delicate to characterize than that of the mean-curvature flow (2.16) since the velocity V is determined by a nonlocal (Dirichlet to Neumann type) equation set on $\partial\Sigma(t)$. Indeed, we can understand the model (2.14) by rewriting the equation for $q(x,t)$ as a Robin boundary problem (we take $\alpha = 0$ for simplicity):

$$\begin{cases} -\Delta q = 0 & \text{in } \Sigma(t), \\ q - \beta F_\tau(-\nabla q \cdot \mathbf{n}) = \bar\gamma\kappa(\mathbf{t}) & \text{on } \partial\Sigma(t), \end{cases} \tag{2.17}$$

with $V = -\nabla q \cdot \mathbf{n}$. The analysis of this boundary value problem heavily depends on the behavior (and monotonicity) of the function F_τ. We will prove in particular (see Section 2.5):

Proposition 2.1.4. *The function $V \mapsto F_\tau(V)$ is differentiable monotone decreasing and satisfies*

$$\lim_{V\to+\infty} F_\tau(V) = 0, \qquad \lim_{V\to-\infty} F_\tau(V) = 1.$$

Note that a similar Robin boundary condition, but with $F_\tau(V) = V$ (or more generally with F any *increasing* function), is sometimes used as a stabilizing/regularizing term in Hele-Show flow (the corresponding model is known as Hele-Shaw model with kinetic undercooling - see [18, 19] and the references therein). The effect of F_τ in our case is opposite and thus destabilizing. This "wrong" monotonicity of F_τ leads to some interesting behaviors. In particular, it is easy to check that for a given set $\Sigma(t)$, the function $q(\cdot,t)$, solution of (2.17), is a critical point of the functional

$$\mathcal{F}(q) := \frac{1}{2}\int_{\Sigma(t)} |\nabla q|^2\, dx - \int_{\partial\Sigma(t)} \beta G(\beta^{-1}(q - \bar\gamma\kappa(x,t)))\, dS(x) \tag{2.18}$$

where the function G is a convex function satisfying $G' = -F_\tau^{-1}$. The fact that the functional (2.18) is the difference of two convex functionals suggests that, at least for some values of β, equation (2.17) might have more than one solution, thus leading, as in [5], to some interesting hysteresis phenomena. Intuitively, this is in good agreement with the universal law for cell migration that was highlighted in [30]: for some parameters values, the effect of the potential is high enough to counterbalance the smoothing character of the curvature term and will lead to the polarization of the cell and the existence of persistent trajectories.

In this work we are interested in making this informal discussion rigorous in the one dimensional case. Since there is no mechanism that could split a cell in one dimension, we consider solutions for which $\Sigma(t)$ is an interval $(a(t), b(t))$. Furthermore, it is easy to check that the measure of $\Sigma(t)$ is preserved by (2.14) (this is a consequence of the conservation of mass $\frac{d}{dt}\int \rho^\varepsilon\, dx = 0$). Thus, if we denote $\ell = |\Sigma(t)|$, we get

$$\Sigma(t) = (a(t), b(t)), \qquad b(t) = a(t) + \ell$$

and the normal velocity is given by $-a'(t)$ at the left end boundary point, and by $a'(t)$ at the right end boundary point. We will then prove:

Theorem 2.1.5. *There exists a critical value $\gamma_c := \frac{-1}{2F_\tau'(0)} > 0$ such that*

If $\frac{\beta(1-\alpha)}{\ell} \le \gamma_c$, then the unique solution of (2.14) in dimension 1 is the stationary solution

$$\Sigma(t) = (a(0), b(0))$$

If $\frac{\beta(1-\alpha)}{\ell} > \gamma_c$, then (2.14) has at least two solutions besides the stationary solution (still in dimension 1), which moves with speed $\pm\frac{1}{1-\alpha}c$ for some speed $c > 0$ which depends on the double-well potential W and on the parameter $\frac{\beta(1-\alpha)}{\ell}$.

This theorem proves that, at least in one dimension, our asymptotic model has a non trivial dynamics and exhibits hysteresis phenomena when $\frac{\beta(1-\alpha)}{\ell} > \gamma_c$. Indeed, equation (2.14) does not provide any mechanisms to pick one solution rather than another. Presumably this means that small variations in the function $\rho_{in}^{\varepsilon}(x)$ (which converges to $\chi_{\Sigma(0)}$) could lead to a radically different behavior of the cell (stationary solution v.s. moving traveling wave). Note also that there is nothing that would prevent a solution from changing velocity in a discontinuous way (for example a solution that moves with positive speed could suddenly stop). This indicates an unstable process in which small variation in the media can cause a stationary cell to suddenly start moving, or a moving cell to change direction. Such behaviors are precisely what is observed experimentally.

Finally, we point out that numerical simulations show that non-stationary traveling like solutions exists also for the ε model (2.1) when β is large enough. A rigorous proof of this fact as well as a detailed analysis of the model in 2 dimension will be the object of future work.

Outline

The rest of the chapter is organized as follows: Section 2.2 describes in further details the biological hypothesis that lead to our model. Section 2.3 is devoted to the proof of the existence of solutions in the 1d case (Theorem 2.1.1). In Section 2.4, the sharp interface limit is formally derived (Theorem 2.1.2). The properties of the function F_τ, and in particular Proposition 2.1.4, are established in Section 2.5 and the rigorous analysis of the asymptotic problem in dimension 1 and the proof of Theorem 2.1.5 is given in Section 2.6.

2.2 Biological justification of the model

Cell motility is involved in key physiological processes such as wound healing, morphogenesis, and immunological response. In recent decades, research in cell biology has made spectacular progress, which has identified many of the molecular protagonists involved. In particular, the actin cytoskeleton, composed of actin filaments organized into bundles and networks, has been shown to be an essential element of the motility machinery. Actin filaments continuously polymerize at their "plus" end near the cell membrane and depolymerize at their "minus" end within the cell. This polar behavior can give rise to spontaneous flows. In addition, molecular motors, such as myosin II, assemble into minifilaments, interact with actin, behave as active crosslinking agents and generate contractile or dilative stresses in the network. Finally, this activity in the cytoskeleton occurs continuously thanks to a constant source of energy input, via the hydrolysis of ATP, and it leads to non-equilibrium behavior likely to generate instabilities. The resulting system is intrinsically out of equilibrium, designated as active system. The description of this active system has attracted much attention in the physics community. The desire to construct a minimal model of cellular motility justifies a macroscopic description of the actin cytoskeleton. It has been the focus of active gel theory [25–27], a hydrodynamic approach providing a framework for the quantitative understanding of cellular motility [9].

The motility of eukaryotic cells is closely related to the maintenance of functional asymmetry. This depends on the polymerization and depolymerization of the actin filaments and the active stresses in the actin network. It has been shown that in the presence of significant friction with the solid substrate, the dynamics of the actin gel can be approximated by a two-dimensional flow [9, 27]. Here, to describe the motility of actin-based crawling cells, we consider a two-component two-dimensional fluid bounded by a membrane of arbitrary shape. We focus on the description of cytosol, actin and myosin II.

We use the term cytosol to describe both fluid and gel fractions of the cytoplasm. Indeed, in recent years, it has become clear that the coupling between the cytoskeleton and the cytosol plays an important role in many cellular mechanical phenomena [9, 11, 28]. The result is an interdependent dynamics that we describe now.

Cytosol description

Cytosol mass balance. To develop a phase-field model, we begin by introducing a so-called phase field variable ρ that will describe the cytosol. The phase field variable acts as a marker that will be almost constant (in our case 0 or 1) in the bulk regions, and will smoothly vary between these values in an interfacial region of small thickness.

Recall that here cytosol designates everything that makes up a cell: solvent, actin polymers forming the filaments, actin monomers, nucleus... The conservation of mass is represented by the continuity equation

$$\partial_t \rho + \operatorname{div}(\rho u) = 0 \qquad \text{in } \Omega\,, \tag{2.19}$$

where Ω is a 2D bounded domain, a drop, representing the environment in which the cell evolves (a laboratory e.g.).

We assume that the velocity of the drop is given by the actin flow velocity. Indeed it is well-known that the result of the depolymerization of the actin filaments which is isotropically distributed in the bulk and of the polymerization which occurs at the boundary gives rise to a flow of actin that is directed towards the center in the cell. Hence, in (2.19), the phase field can be thought of as a scalar that is convected by the actin flow u.

Forces on the gel describing the cytosol. Neglecting the dynamics of the actin polarization field, [11], the cytosol can be described as an incompressible isotropic viscous fluid. Since the flows involved in cell motility occur at low Reynolds numbers, we neglect inertia and assume that the cytosol is at mechanical equilibrium. The forces acting on the cytosol are as follows. A force due to stresses in the actin network, the actin filaments-solvent friction and the actin filaments-substrate friction. Neglecting actin filaments-solvent friction force, which is much smaller than the polymer-substrate force, see [11], and also the exchange of momentum between the actin filaments and the solvent, the stress balance on the cytosol reads

$$-\operatorname{div}(\sigma - \Pi\,\mathbb{I}) = -\xi u \qquad \text{in } \Omega\,, \tag{2.20}$$

where ξ is the friction coefficient on the substrate, σ is the Cauchy stress tensor describing the cytosol stress, Π is the osmotic pressure of the cytosol, and $\mathbb{I}$ is the identity tensor.

Remarks 2.2.1. *We note that in equation (2.20) the actin filaments-substrate friction force is written as $-\xi u$, where u is the actin velocity. A more realistic form would be to account for the dependence of the friction force on actin filaments volume fraction. Our choice for such a force in (2.20) corresponds to a linearization and an approximation of the actin filaments volume fraction by a constant value.*

The cytosol stress σ contains passive and active contributions. Indeed, molecular motors are able to transmit stresses. Here, we consider the liquid limit of the gel, valid on large timescales. Within this limit, the passive part of the stress, resulting from the convection of the actin filaments and the remodeling by crosslinking, has the viscous form $\eta\left(\nabla u + \nabla u^T\right)/2$, where η is the viscosity. However, this contribution is known to be very weak, [11]. It does not qualitatively affect the flow and we omit it. Here, in the spirit of [9], we consider the limit when the coefficient of friction ξ is strong and we neglect the viscosity η. The active part, on the other hand, is essential for motility. Since the active stress resulting from the motor activity on the filaments increases with the presence of myosin motors, a simple choice for the network stress is

$$\sigma = -\phi\mathbb{I}\,, \tag{2.21}$$

where ϕ is the myosin concentration. We consider negative values of the activity coefficient as it corresponds to extensile behavior of myosin.

Let us now focus on the description of the osmotic pressure which acts to saturate the linear instability causing gel phase separation and to smooth the interface between cytosol-rich and

cytosol-poor regions. A simple, phenomenological form for Π is

$$\Pi = \gamma \left(-\varepsilon \Delta \rho + \frac{1}{\varepsilon} W'(\rho) \right) , \tag{2.22}$$

where γ is a positive coefficient and W is a double well potential with minima at 1 and 0. Finally, combining equations (2.21) and (2.22) we obtain the equation for ρ

$$\partial_t \rho = \frac{1}{\xi} \mathrm{div} \left(\rho \nabla \left(\gamma \left(-\varepsilon \Delta \rho + \frac{1}{\varepsilon} W'(\rho) \right) + \phi \right) \right) . \tag{2.23}$$

Myosin description

The second module in our model is a convection-reaction-diffusion equation for the myosin concentration ϕ, which relies on several assumptions that we describe now. Myosin motors are known to interact with actin filaments, hence we assume rapid adsorption of myosin on the adhered actin cytoskeleton. Therefore, on the first hand, the effective myosin velocity is given by $v = \alpha u$ where $\alpha > 0$ is the quasi-static fraction of adsorbed molecules convected by the local actin flow u. On the other hand, let us now turn on actin description. Assuming that the diffusion of the free monomers is sufficiently rapid so that we may consider their concentration to be fixed at the cytosol value, we consider that the actin filaments undergo a uniform bulk polymerization with the rate $k_p \rho$. In addition, we assume bulk depolymerization with the rate k_d. Since myosin motors interact with actin filaments, the myosin creation and death rates are related to $k_p \rho$ and k_d.

To describe the random events in the myosin dynamics, we include a diffusion coefficient that is very small. Finally we assume that the actin (and hence also myosin) creation and death rates are very fast in comparison to both the convection and the diffusion rates, meaning that the equation satisfied by the myosin concentration is

$$\partial_t \phi + \alpha \mathrm{div} \left(\phi u \right) = \varepsilon \Delta \phi + \frac{1}{\varepsilon} \left(\beta \rho - \phi \right) \qquad \text{in } \Omega , \tag{2.24}$$

where $\varepsilon > 0$ is a small parameter whose inverse is related to a relaxation time and $\beta > 0$ corresponds to a polymerization rate and where u is given by (2.20). It is to be noticed that for simplicity we only consider one parameter β, the other being fixed to 1, for the myosin creation and death terms.

Boundary conditions

Equations (2.23)-(2.24) form our model for cell motility. They are set in the domain $\Omega \subset \mathbb{R}^2$ and must thus be supplemented with boundary conditions. Because of the divergence form, equation (2.23) preserves the mass $\int_\Omega \rho \, dx$ provided it is supplemented with no-flux boundary conditions

$$\rho \, \partial_{\mathbf{n}} \left(\gamma \left(-\varepsilon \Delta \rho + \frac{1}{\varepsilon} W'(\rho) \right) + \phi \right) = 0 \qquad \text{on } \partial\Omega, \tag{2.25}$$

where $\mathbf{n}$ is the unit normal outwards vector. Moreover, since it is a parabolic equation of order 4, we need one more boundary condition, and we impose the following Neumann boundary conditions:

$$\partial_{\mathbf{n}} \rho = 0 \qquad \text{on } \partial\Omega. \tag{2.26}$$

The equation (2.24) for ϕ is supplemented with Neumann boundary conditions:

$$\partial_{\mathbf{n}} \phi = 0 \qquad \text{on } \partial\Omega. \tag{2.27}$$

2.3 Weak existence of solution in 1D - Proof of Theorem 2.1.1

In this section, we drop the parameters ε, β and γ from our equations to simplify the notations throughout the proof. The system (2.4) becomes:

$$\begin{cases} \partial_t \rho = \partial_x \left(\rho \partial_x \left[-\partial_{xx}\rho + W'(\rho) + \phi \right] \right) & x \in \Omega,\ t > 0 \\ \partial_t \phi = \partial_{xx}\phi - \phi + \rho & x \in \Omega,\ t > 0 \end{cases} \tag{2.28}$$

where Ω is a fixed domain in $\mathbb{R}$ (i.e. open interval of the form $\Omega = (a, b)$) and we recall that W is a non-negative function in $W^{2,\infty}_{loc}$. The system is supplemented with initial and boundary conditions (2.5), (2.6)-(2.8).

Sketch of the proof of Theorem 2.1.1

Since the equation for ρ is degenerate when $\rho = 0$, we perform a classical regularization procedure by introducing the positive mobility coefficient

$$f_{\delta,M}(\rho^\delta) = \min\{M, \delta + |\rho^\delta|\}.$$

Our first task will then be to show that for all $0 < \delta \leq M < \infty$, there exist ρ^δ and ϕ^δ solutions of

$$\begin{cases} \partial_t \rho^\delta = \partial_x \left(f_{\delta,M}(\rho^\delta) \partial_x q^\delta \right) & \text{in } \Omega \times (0,T) \\ q^\delta = -\partial_{xx}\rho^\delta + W'(\rho^\delta) + \phi^\delta & \text{in } \Omega \times (0,T) \\ f_{\delta,M}(\rho^\delta)\partial_x q^\delta = 0 & \text{on } \partial\Omega \times (0,T) \\ \partial_x \rho^\delta(x) = 0 & \text{on } \partial\Omega \times (0,T) \\ \rho(x,0) = \rho_{in}(x) & \text{in } \Omega \end{cases} \tag{2.29}$$

and

$$\begin{cases} \partial_t \phi^\delta = \partial_{xx}\phi^\delta - \phi^\delta + \rho^\delta & \text{in } \Omega \times (0,T) \\ \partial_x \phi^\delta = 0 & \text{on } \partial\Omega \times (0,T) \\ \phi^\delta(x,0) = \phi^\delta_{in}(x) & \text{in } \Omega. \end{cases} \tag{2.30}$$

Note that we have regularized the initial data for the potential ϕ: We define $\phi^\delta_{in} = j_\delta \star \bar{\phi}_{in}$ where j_δ is the usual sequence of mollifiers and $\bar{\phi}_{in}$ is the extension of ϕ_{in} to $\mathbb{R}$ by zero. We then have $\phi^\delta_{in} \in H^1(\Omega)$ for all $\delta > 0$, $\|\phi^\delta_{in}\|_{L^2(\Omega)} \leq \|\phi_{in}\|_{L^2(\Omega)}$ and

$$\phi^\delta_{in} \to \phi_{in} \text{ in } L^2(\Omega) \text{ as } \delta \to 0.$$

We are going to prove the existence of a solution to the coupled system of equations (2.29)-(2.30) by a fixed point argument on the potential ϕ^δ. The proof of Theorem 2.1.1 then consists in passing to the limit $\delta \to 0$. We will prove in particular that $\rho^\delta(x,t)$ converges uniformly to a function $\rho(x,t)$ which satisfies

$$0 \leq \rho(x,t) \leq C_0$$

for some constant C_0 depending on Ω, ρ_{in}, ϕ_{in} and T, but independent of M. By choosing $M \geq C_0$, we will deduce that $f_{\delta,M}(\rho^\delta) \to \rho$ and that ρ satisfies (2.28).

The fixed point argument is relatively classical and uses appropriate energy estimates for equations (2.29) and (2.30) which are detailed below. We note that the regularization of the mobility coefficient in (2.29) makes the equation uniformly parabolic and provides the existence of smooth solutions. However, because the equation is of order 4, it is a classical fact that the solution might take negative values even though we can then prove that the limit ρ is a non-negative function.

2.3.1 A priori estimates

The no-flux boundary condition ensures that smooth solutions to (2.29) satisfy

$$\int_\Omega \rho^\delta(x,t)\,dx = \int_\Omega \rho_{in}(x)\,dx. \tag{2.31}$$

Furthermore, if we define the usual Cahn-Hilliard energy

$$E[\rho^\delta] := \int_\Omega \left(\frac{1}{2}|\partial_x \rho^\delta|^2 + W(\rho^\delta)\right) dx, \tag{2.32}$$

we get (still for smooth solutions):

$$\frac{dE[\rho^\delta(\cdot,t)]}{dt} + \frac{1}{2}\int_\Omega f_{\delta,M}(\rho^\delta)\left|\partial_x[-\partial_{xx}\rho^\delta + W'(\rho^\delta)]\right|^2 dx \le \frac{1}{2}\int_\Omega f_{\delta,M}(\rho^\delta)|\partial_x\phi^\delta|^2\,dx. \tag{2.33}$$

Indeed, multiplying the first equation of (2.29) by $\left[-\partial_{xx}\rho^\delta + W'(\rho^\delta)\right]$, we get

$$\begin{aligned}
\frac{d}{dt}\int_\Omega \left(\frac{1}{2}|\partial_x\rho^\delta|^2 + W(\rho^\delta)\right) dx &= \int_\Omega \left[-\partial_{xx}\rho^\delta + W'(\rho^\delta)\right]\partial_t\rho^\delta\,dx \\
&= -\int_\Omega f_{\delta,M}(\rho^\delta)\,|\partial_x[-\partial_{xx}\rho^\delta + W'(\rho^\delta)]\,|^2\,dx \\
&\quad -\int_\Omega f_{\delta,M}(\rho^\delta)\,\partial_x[-\partial_{xx}\rho^\delta + W'(\rho^\delta)]\,\partial_x\phi^\delta\,dx \\
&\le -\frac{1}{2}\int_\Omega f_{\delta,M}(\rho^\delta)\,|\partial_x[-\partial_{xx}\rho^\delta + W'(\rho^\delta)]\,|^2\,dx \\
&\quad +\frac{1}{2}\int_\Omega f_{\delta,M}(\rho^\delta)\,|\partial_x\phi^\delta|^2\,dx.
\end{aligned}$$

The mass conservation (2.31) and the enregy inequality (2.33), together with classical estimates for the parabolic equation (2.30) play a crucial role in what follows.

2.3.2 Solution to the regularized system for $\delta > 0$: a fixed point argument

As explained above, the first step is to prove the existence of a solution for the regularized system (2.29)-(2.30). More precisely, we will prove:

Proposition 2.3.1. *Assume that ρ_{in} satisfies (2.9) and that $\phi^\delta_{in} \in H^1(\Omega)$. Then, for all $\delta \in (0,M)$, there exists a solution $(\rho^\delta,\phi^\delta) \in (L^\infty(0,T;H^1(\Omega)))^2$ to the coupled system of equations (2.29)-(2.30) which satisfies the a priori estimates (2.31) and (2.33).*

The proof of this result relies on a fixed point argument: Given $\phi \in L^2(0,T;H^1(\Omega))$, we consider the function $\rho \in L^\infty(0,T;H^1(\Omega)) \cap L^2(0,T;H^3(\Omega))$ weak solution to

$$\begin{cases}
\partial_t\rho = \partial_x\left(f_{\delta,M}(\rho)\partial_x\left[-\partial_{xx}\rho + W'(\rho) + \phi\right]\right) & \text{in } \Omega\times(0,T),\\
f_{\delta,M}(\rho)\partial_x\left[-\partial_{xx}\rho + W'(\rho) + \phi\right] = 0 & \text{on } \partial\Omega\times(0,T),\\
\partial_x\rho = 0 & \text{on } \partial\Omega\times(0,T),\\
\rho(x,0) = \rho_{in}(x) & \text{in } \Omega.
\end{cases} \tag{2.34}$$

We then define $\widetilde{\phi}$ the solution of

$$\begin{cases}
\partial_t\widetilde{\phi} = \partial_{xx}\widetilde{\phi} - \widetilde{\phi} + \rho & \text{in } \Omega\times(0,T),\\
\partial_x\widetilde{\phi} = 0 & \text{on } \partial\Omega\times(0,T),\\
\widetilde{\phi}(x,0) = \phi^\delta_{in}(x) & \text{in } \Omega.
\end{cases} \tag{2.35}$$

Introducing the operator

$$\begin{array}{rcl} \mathcal{T} : L^2(0,T;H^1(\Omega)) & \to & L^2(0,T;H^1(\Omega)) \\ \phi & \to & \widetilde{\phi}\,, \end{array} \tag{2.36}$$

we see that any fixed point $\mathcal{T}(\phi) = \phi$ will provide a solution to (2.29)-(2.30).

For a given function $\rho \in L^\infty(0,T;H^1(\Omega))$, the existence of a unique solution $\widetilde{\phi}$ to (2.35) is classical. Moreover $\widetilde{\phi}$ satisfies

$$\frac{d}{dt}\int_\Omega \frac{1}{2}|\widetilde{\phi}|^2\,dx + \int_\Omega |\widetilde{\phi}|^2 + |\partial_x\widetilde{\phi}|^2\,dx = \int_\Omega \rho\,\widetilde{\phi}\,dx, \tag{2.37}$$

and

$$\frac{d}{dt}\int_\Omega \frac{1}{2}|\partial_x\widetilde{\phi}|^2\,dx + \int_\Omega |\partial_x\widetilde{\phi}|^2 + |\partial_{xx}\widetilde{\phi}|^2\,dx = -\int_\Omega \rho\partial_{xx}\widetilde{\phi}\,dx. \tag{2.38}$$

The following result is classical and it justifies the existence of ρ (given the function ϕ) and hence the construction of the operator $\mathcal{T}$.

Proposition 2.3.2. *Under the conditions of Proposition 2.3.1, and for all function $\phi \in L^2(0,T;H^1(\Omega))$, there exists a unique solution*

$$\rho \in L^\infty(0,T;H^1(\Omega)) \cap L^2(0,T;H^3(\Omega))$$

to (2.34) and it satisfies (2.31) and (2.33).

Note that the first boundary condition in (2.34) is satisfied in a weak sense, while the second condition holds in the classical sense.

Proposition 2.3.1 is now a consequence of the following two lemmas.

Lemma 2.3.3. *The operator $\mathcal{T}$ defined by (2.36) is compact in $L^2(0,T,H^1(\Omega))$.*

and

Lemma 2.3.4. *There exists a constant C depending on Ω, ρ_{in}, ϕ_{in}, T and M (but not on δ) such that for all $\phi \in L^2(0,T;H^1(\Omega))$ satisfying $\phi = \sigma\mathcal{T}(\phi)$ for some $\sigma \in [0,1]$, we have*

$$\|\phi\|_{L^2(0,T;H^1(\Omega))} \le C. \tag{2.39}$$

Before proving these two Lemmas, we point out that they imply Proposition 2.3.1.

Proof of Proposition 2.3.1. In view of Lemma 2.3.3 and 2.3.4 we can apply the Leray-Schauder fixed point theorem (see [22]). We deduce that $\mathcal{T}$ has a fixed point in $L^2(0,T,H^1(\Omega))$. This fixed point is a solution to (2.29)-(2.30). □

Remarks 2.3.5. *Note that this fixed point satisfies the bound (2.39) where the constant C does not depend on δ but only of $\|\rho_{in}\|_{L^1(\Omega)}$, $E[\rho_{in}]$. This bound will thus be useful in the next part of the proof when passing to the limit $\delta \to 0$.*

Proof of Lemma 2.3.3. Inequality (2.33) and the definition of $f_{\delta,M}$ imply in particular that

$$\begin{aligned} \sup_{t\in[0,T]} E[\rho(\cdot,t)] &\le E[\rho_{in}] + \frac{1}{2}\int_0^T\int_\Omega f_{\delta,M}(\rho)|\partial_x\phi|^2\,dx\,dt \\ &\le E[\rho_{in}] + \frac{M}{2}\int_0^T\int_\Omega |\partial_x\phi|^2\,dx\,dt \end{aligned}$$

and a classical Poincaré type inequality together with (2.31), implies

$$\|\rho(\cdot,t)\|_{L^2(\Omega)} \le C(\Omega)\left(\int_\Omega \rho(x,t)\,dx + \left(\int_\Omega |\partial_x\rho(x,t)|^2\,dx\right)^{1/2}\right)$$
$$\le C(\Omega)\left(\int_\Omega \rho_{in}(x)\,dx + E[\rho(\cdot,t)]^{1/2}\right).$$

We deduce

$$\|\rho\|^2_{L^\infty(0,T;H^1(\Omega))} \le C(\Omega)\left(\|\rho_{in}\|_{L^1(\Omega)} + E[\rho_{in}] + M\int_0^T\int_\Omega |\partial_x\phi|^2\,dx\,dt\right).$$

This bound, together with the inequality (2.37) yields

$$\frac{d}{dt}\int_\Omega \frac{1}{2}|\widetilde{\phi}|^2\,dx + \frac{1}{2}\int_\Omega |\widetilde{\phi}|^2 + |\partial_x\widetilde{\phi}|^2\,dx \le \int_\Omega |\rho|^2\,dx$$
$$\le C(\Omega,\rho_{in}) + C(\Omega)M\int_0^T\int_\Omega |\partial_x\phi|^2\,dx\,dt,$$

and so

$$\|\widetilde{\phi}\|^2_{L^\infty(0,T,L^2(\Omega))} + \|\widetilde{\phi}\|^2_{L^2(0,T;H^1(\Omega))} \le \|\phi^\delta_{in}\|^2_{L^2(\Omega)}$$
$$+\left(C(\Omega,\rho_{in}) + C(\Omega)M\int_0^T\int_\Omega |\partial_x\phi|^2\,dx\,dt\right)T.$$

Similarly, (2.38) yields

$$\frac{d}{dt}\int_\Omega \frac{1}{2}|\partial_x\widetilde{\phi}|^2\,dx + \frac{1}{2}\int_\Omega |\partial_x\widetilde{\phi}|^2 + |\partial_{xx}\widetilde{\phi}|^2\,dx \le \int_\Omega |\rho|^2\,dx$$
$$\le C(\Omega,\rho_{in}) + C(\Omega)M\int_0^T\int_\Omega |\partial_x\phi|^2\,dx\,dt,$$

and so

$$\sup_{t\in(0,T)}\int_\Omega \frac{1}{2}|\partial_x\widetilde{\phi}|^2\,dx + \frac{1}{2}\int_0^T\int_\Omega |\partial_x\widetilde{\phi}|^2 + |\partial_{xx}\widetilde{\phi}|^2\,dx\,dt$$
$$\le \|\phi^\delta_{in}\|^2_{H^1(\Omega)} + \left(C(\Omega,\rho_{in}) + C(\Omega)M\int_0^T\int_\Omega |\partial_x\phi|^2\,dx\,dt\right)T.$$

We have thus proved that

$$\|\widetilde{\phi}\|^2_{L^2(0,T;H^2(\Omega))} \le \|\phi^\delta_{in}\|^2_{H^1(\Omega)} + \left(C(\Omega,\rho_{in}) + C(\Omega)M\int_0^T\int_\Omega |\partial_x\phi|^2\,dx\,dt\right)T. \tag{2.40}$$

Using now equation (2.35), we also deduce

$$\|\partial_t\widetilde{\phi}\|^2_{L^2(0,T;L^2(\Omega))} \le \|\widetilde{\phi}\|^2_{L^2(0,T,H^2(\Omega))} + \|\rho\|^2_{L^2(0,T;L^2(\Omega))}$$
$$\le C(\phi^\delta_{in}) + \left(C(\Omega,\rho_{in}) + C(\Omega)M\int_0^T\int_\Omega |\partial_x\phi|^2\,dx\,dt\right)T. \tag{2.41}$$

In particular, (2.40) and (2.41) imply that if ϕ belongs to a bounded subset of $L^2(0,T,H^1(\Omega))$ then $\widetilde{\phi}$ is such that

$$\|\widetilde{\phi}\|_{L^2(0,T;H^2(\Omega)} \le C \qquad \text{and} \qquad \|\partial_t\widetilde{\phi}\|_{L^2(0,T;L^2(\Omega))} \le C.$$

By Aubin-Lions lemma, [2], it follows that $\mathcal{T}(\phi) = \widetilde{\phi}$ belongs to a compact subset of $L^2(0,T,H^1(\Omega))$ which completes the proof of Lemma 2.3.3. □

Proof of Lemma 2.3.4. Let $\phi \in L^2(0,T;H^1(\Omega))$ satisfy $\phi = \sigma\mathcal{T}(\phi)$ for some $\sigma \in [0,1]$ and let ρ be the corresponding solution to (2.34). Then the function ϕ satisfies

$$\partial_t \phi = \partial_{xx}\phi - \phi + \sigma\rho \qquad \text{in } \Omega \times (0,T).$$

In particular we have

$$\frac{d}{dt}\int_\Omega \frac{1}{2}|\phi|^2\,dx + \int_\Omega |\phi|^2 + |\partial_x\phi|^2\,dx = \sigma\int_\Omega \rho\phi\,dx,$$

since $\sigma \in [0,1]$ it follows that

$$\frac{d}{dt}\int_\Omega \frac{1}{2}|\phi|^2\,dx + \frac{1}{2}\int_\Omega |\phi|^2 + |\partial_x\phi|^2\,dx \le \int_\Omega \rho^2\,dx.$$

Recalling (2.33) we see that

$$\frac{d}{dt}\int_\Omega \frac{1}{2}|\partial_x\rho|^2 + W(\rho)\,dx \le M\int_\Omega |\partial_x\phi|^2\,dx.$$

Combining the two last inequalities (after multiplying the first one by M), we deduce

$$\begin{aligned}\frac{d}{dt}\int_\Omega \frac{1}{2}|\partial_x\rho|^2 + W(\rho) + 2M|\phi|^2\,dx + M\int_\Omega |\phi|^2 + |\partial_x\phi|^2\,dx \\ \le 4M\int_\Omega \rho^2\,dx \\ \le C(M,\rho_{in})\left(1 + \int_\Omega |\partial_x\rho|^2\,dx\right),\end{aligned}$$

and Gronwall's lemma yields that

$$\sup_{t\in(0,T)}\int_\Omega \frac{1}{2}|\partial_x\rho|^2 + W(\rho) + 2M|\phi|^2\,dx \le Ce^{CT},$$

for some constant C depending on Ω, M, ρ_{in} and $\|\phi_{in}^\delta\|_{L^2(\Omega)}$. Since the H^1 regularization of ϕ_{in} was chosen in order to satisfy $\|\phi_{in}^\delta\|_{L^2(\Omega)} \le \|\phi_{in}\|_{L^2(\Omega)}$, the constant C only depends on Ω, M, ρ_{in} and ϕ_{in}. In particular it is independent of δ.

In turn this gives

$$\int_0^T\int_\Omega |\phi|^2 + |\partial_x\phi|^2\,dx\,dt \le CTe^{CT},$$

for some (other) constant C also depending on Ω, M, ρ_{in} and ϕ_{in}. □

2.3.3 Limit $\delta \to 0$ and weak formulation

We now want to pass to the limit $\delta \to 0$. We proceed as follows:

1. First, using an energy type inequality, we will prove that ρ^δ is bounded in $C^{1/2,1/8}(\Omega\times(0,T))$ and thus converges uniformly (up to a subsequence) to a function $\rho(x,t)$ (and ϕ^δ converges towards ϕ weakly in $L^2(0,T;H^1(\Omega))$;

2. Using an entropy type inequality, we will show that the limit function ρ is non-negative. As a consequence, we will see that it satisfies a L^∞ bound independent of M.

3. Finally, we will pass to the limit in (2.29) and prove that ρ satisfies the limiting equation in a appropriate weak form (the fact that ϕ satisfies the limiting equation is obvious).

A priori bounds and convergence of $(\rho^\delta, \phi^\delta)$. Recalling Remark 2.3.5 we see that the fixed point that we have constructed is such that

$$\|\phi^\delta\|_{L^2(0,T;H^1(\Omega))} \leq C(\Omega, \rho_{in}, \phi_{in}, M, T), \tag{2.42}$$

with the constant independent on δ. Furthermore, integrating (2.33), we find

$$\begin{aligned}
\sup_{t\in(0,T]} E[\rho^\delta(\cdot,t)] + \frac{1}{2}\int_0^T \int_\Omega f_{\delta,M}(\rho^\delta) \left|\partial_x[-\partial_{xx}\rho^\delta + W'(\rho^\delta)]\right|^2 dx\, dt \\
\leq E[\rho_{in}] + \frac{1}{2}\int_0^T \int_\Omega f_{\delta,M}(\rho^\delta) |\partial_x \phi^\delta|^2 \, dx\, dt \\
\leq E[\rho_{in}] + \frac{M}{2}\int_0^T \int_\Omega |\partial_x \phi^\delta|^2 \, dx\, dt.
\end{aligned}$$

Hence using (2.42), we obtain

$$\sup_{t\in(0,T]} E[\rho^\delta(\cdot,t)] + \frac{1}{2}\int_0^T \int_\Omega f_{\delta,M}(\rho^\delta) \left|\partial_x[-\partial_{xx}\rho^\delta + W'(\rho^\delta)]\right|^2 dx\, dt \leq C(\Omega, \rho_{in}, \phi_{in}, M, T), \tag{2.43}$$

with the constant independent on δ. Finally, using (2.31), the definition of E together with Poincaré inequality, inequality (2.43) implies

$$\|\rho^\delta\|^2_{L^\infty(0,T,H^1(\Omega))} \leq C\|\rho_{in}\|^2_{L^1(\Omega)} + \sup_{t\in(0,T]} E[\rho^\delta(\cdot,t)] \leq C(\Omega, \rho_{in}, \phi_{in}, M, T). \tag{2.44}$$

Classical Sobolev embeddings then yield that ρ^δ is Hölder continuous:

$$|\rho^\delta(x,t) - \rho^\delta(y,t)| \leq C\,|x-y|^{1/2}, \qquad \forall (x,y) \in \Omega^2, \ \text{ a.e. } t \in (0,T) \tag{2.45}$$

where C is a constant independent of δ.

We can also check that the flux $f_{\delta,M}(\rho^\delta)\,\partial_x q^\delta$ in Equation (2.29) is bounded in $L^2((0,T)\times\Omega)$. Indeed, we have

$$\begin{aligned}
\int_0^T \int_\Omega f_{\delta,M}(\rho^\delta)\,|\partial_x q^\delta|^2 \, dx\, dt &\leq \int_0^T \int_\Omega f_{\delta,M}(\rho^\delta)\,|\partial_x[\partial_{xx}\rho^\delta - W'(\rho^\delta)]\,|^2 \, dx\, dt \\
&\quad + \int_0^T \int_\Omega f_{\delta,M}(\rho^\delta)\,|\partial_x \phi|^2 \, dx\, dt \\
&\leq \int_0^T \int_\Omega f_{\delta,M}(\rho^\delta)\,|\partial_x[\partial_{xx}\rho^\delta - W'(\rho^\delta)]\,|^2 \, dx\, dt \\
&\quad + M\int_0^T \int_\Omega |\partial_x \phi|^2 \, dx\, dt \\
&\leq C(\Omega, \rho_{in}, \phi_{in}, M, T),
\end{aligned}$$

where we have used (2.42) and (2.43). Consequently, one has

$$\int_0^T \int_\Omega f_{\delta,M}(\rho^\delta)^2 |\partial_x q^\delta|^2 \, dx\, dt \leq M\int_0^T \int_\Omega f_{\delta,M}(\rho^\delta)\,|\partial_x q^\delta|^2 \, dx\, dt \leq C(\Omega, \rho_{in}, \phi_{in}, M, T). \tag{2.46}$$

Classically, the Hölder regularity of ρ^δ with respect to x and the fact that the flux is bounded in L^2 yield some Hölder regularity with respect to t as it is stated in the following lemma, see [7]:

Lemma 2.3.6. *There exists a constant C independent by δ such that*

$$|\rho^\delta(x,t) - \rho^\delta(y,s)| \leq C\left(|x-y|^{1/2} + |t-s|^{1/8}\right),$$

for all $(x,y) \in \Omega^2$ and $(t,s) \in [0,T)^2$.

In particular, the sequence $\{\rho^\delta\}_{\delta>0}$ is uniformly bounded and equi-continuous in $\Omega\times[0,T)$. By the Ascoli-Arzela's Theorem, up to a subsequence, there exists a function ρ such that

$$\rho^\delta \to \rho \quad \text{uniformly in } \Omega\times[0,T) \quad \text{as } \delta\to 0. \tag{2.47}$$

In view of (2.42), we can also choose the subsequence so that

$$\phi^\delta \rightharpoonup \phi \qquad \text{weakly in } L^2(0,T;H^1(\Omega)).$$

Furthermore, passing to the limit in (2.31), (2.42) and (2.43), we get

$$\int_\Omega \rho(x,t)\,dx = \int_\Omega \rho_{in}(x)\,dx, \tag{2.48}$$

$$\|\phi\|_{L^2(0,T;H^1(\Omega))} \le C(\Omega,\rho_{in},\phi_{in},M,T), \tag{2.49}$$

and

$$\sup_{t\in(0,T]} E[\rho(\cdot,t)] + \frac{1}{2}\int_0^T\int_\Omega |k(x,t)|^2\,dx\,dt \le C(\Omega,\rho_{in},\phi_{in},M,T), \tag{2.50}$$

where $k(x,t)$ denotes the weak limit in L^2 of $\sqrt{f_{\delta,M}(\rho^\delta)}\,|\partial_x q^\delta|$ (we have used that the L^2 norm is lower semicontinuous with respect to the weak convergence).

Non-negativity property of the limiting density ρ. We now prove that if the initial condition ρ_{in} is non-negative, then then the limit function ρ is also non-negative:

Proposition 2.3.7 (Non-negativity)**.** *Let ρ^δ be a solution of the regularized equation (2.29) and assume that ρ^δ converges uniformly in x and t to a function ρ. If $\rho_{in}\ge 0$ in Ω, then $\rho(x,t)\ge 0$ for all $(x,t)\in\Omega\times[0,T)$.*

We use here a classical argument first introduced in [7].

Proof. We define the function g_δ by

$$g_\delta(s) = \int_1^s \left(\int_1^r \frac{1}{f_{M,\delta}(\tau)}\,d\tau\right) dr. \tag{2.51}$$

It satisfies in particular $g_\delta \ge 0$ and $g_\delta''(\rho^\delta) = \dfrac{1}{f_{\delta,M}(\rho^\delta)}$. Recalling the boundary condition $f_{\delta,M}(\rho^\delta)\partial_x q^\delta = 0$ on $\partial\Omega\times(0,T)$, with $q^\delta = \partial_{xx}\rho^\delta - W'(\rho^\delta) - \phi$, one has

$$\begin{aligned}
\frac{d}{dt}\int_\Omega g_\delta(\rho^\delta)\,dx = \int_\Omega g_\delta'(\rho^\delta)\partial_t\rho^\delta\,dx &= \int_\Omega g_\delta'(\rho^\delta)\partial_x[f_{\delta,M}(\rho^\delta)\partial_x q^\delta]\,dx\\
&= -\int_\Omega g_\delta''(\rho^\delta) f_{\delta,M}(\rho^\delta)\partial_x\rho^\delta\partial_x q^\delta\,dx\\
&= -\int_\Omega \partial_x\rho^\delta\partial_x q^\delta\,dx.
\end{aligned}$$

Using the definition of q^δ and some integration by parts together with the Neumann boundary condition $\partial_x\rho^\delta = 0$ on $\partial\Omega\times(0,T)$, we get

$$\frac{d}{dt}\int_\Omega g_\delta(\rho^\delta)\,dx = -\int_\Omega |\partial_{xx}\rho^\delta|^2\,dx - \int_\Omega |\partial_x\rho^\delta|^2 W''(\rho^\delta)\,dx - \int_\Omega \partial_x\rho^\delta\partial_x\phi\,dx. \tag{2.52}$$

The last two terms can be bounded as follows (recall that W is in $C^2(\mathbb{R})$ and thus W'' is locally bounded):

$$\left| \int_\Omega |\partial_x \rho^\delta|^2 W''(\rho^\delta)\, dx \right| \leq C(\|\rho^\delta(\cdot,t)\|_{L^\infty(\Omega)}) \int_\Omega |\partial_x \rho^\delta|^2\, dx,$$

$$\left| \int_\Omega \partial_x \rho^\delta \partial_x \phi\, dx \right| \leq \frac{1}{2} \int_\Omega |\partial_x \rho^\delta|^2\, dx + \frac{1}{2} \int_\Omega |\partial_x \phi|^2\, dx.$$

Recalling (2.43), we obtain

$$\frac{d}{dt} \int_\Omega g_\delta(\rho^\delta)\, dx + \int_\Omega |\partial_{xx} \rho^\delta|^2\, dx \leq C(\Omega, \rho_{in}, \phi_{in}, M, T) + \int_\Omega |\partial_x \phi|^2\, dx,$$

and so

$$\sup_{[0,T]} \int_\Omega g_\delta(\rho^\delta)\, dx + \int_0^T \int_\Omega |\partial_{xx} \rho^\delta|^2\, dx\, dt \leq C(\Omega, \rho_{in}, \phi_{in}, M, T) + \int_0^T \int_\Omega |\partial_x \phi|^2\, dx + \int_\Omega g_\delta(\rho_{in})\, dx.$$

Using (2.42) we deduce

$$\sup_{[0,T]} \int_\Omega g_\delta(\rho^\delta)\, dx \leq C(\Omega, \rho_{in}, \phi_{in}, M, T) + \int_\Omega g_\delta(\rho_{in})\, dx. \tag{2.53}$$

Next, we check that the right hand side in (2.53) is bounded: The fact that $f_{\delta,M}(z) \geq \min\{|z|, M\}$ implies that

$$g_\delta(s) \leq \begin{cases} s \ln s - s + 1 & \text{if } 0 \leq s \leq M \\ C(M) s^2 & \text{if } s \geq M \end{cases}$$

In particular, since $\rho_{in} \geq 0$ is such that $\rho_{in} \in L^2(\Omega)$, we deduce

$$\sup_{[0,T]} \int_\Omega g_\delta(\rho^\delta)\, dx \leq C(\Omega, \rho_{in}, \phi_{in}, M, T).$$

We now conclude the proof by a simple contradiction argument: Suppose that there exists (x_0, t_0) such that $\rho(x_0, t_0) = -\eta$ for some $\eta > 0$. The uniform Hölder estimate and the uniform convergence implies that there exists $r > 0$ and $\delta_0 > 0$ such that $\rho^\delta(x, t_0) \leq -\eta/4$ for all $\delta < \delta_0$ and all $x \in B_r(x_0)$. The function g_δ is clearly decreasing for $s < 1$, so this implies

$$g_\delta(-\eta/4) \leq g_\delta(\rho^\delta(x, t_0)) \qquad \text{for all } \delta < \delta_0 \text{ and all } x \in B_r(x_0)$$

and thus

$$g_\delta(-\eta/4)\, |B_r(x_0)| \leq \int_{B_r(x_0)} g_\delta(\rho^\delta(x, t_0))\, dx \leq \int_\Omega g_\delta(\rho^\delta(x, t_0))\, dx \leq C(\Omega, \rho_{in}, \phi_{in}, M, T).$$

However, it is easy to see that $g_\delta(-\eta/4) \to +\infty$ as $\delta \to 0$ (since $\lim_{\delta \to 0} \frac{1}{f_{\delta,M}(\tau)}$ has a non integrable singularity at 0), which leads to a contradiction and completes the proof of the proposition. □

Bound on ρ independent of M. In this section, we show that ρ is bounded in L^∞ independently of M, so that when M is large enough we have $\min\{\rho, M\} = \rho$.

This bound will follow from the energy inequality (2.33) and uses in a crucial way the fact that $\rho \geq 0$. The idea is as follows: We recall that

$$\frac{d}{dt}\int_\Omega \frac{1}{2}|\phi|^2\,dx + \int_\Omega |\phi|^2 + |\partial_x\phi|^2\,dx = \int_\Omega \rho\phi\,dx.$$

The non-negativity of ρ, together with the mass conservation (2.31) and classical Sobolev embeddings imply that the right hand side is bounded by

$$\left|\int_\Omega \rho\phi\,dx\right| \leq \|\phi(\cdot,t)\|_{L^\infty(\Omega)}\int_\Omega \rho\,dx = \|\phi(\cdot,t)\|_{L^\infty(\Omega)}\int_\Omega \rho_{in}\,dx \leq C(\rho_{in})\|\phi(\cdot,t)\|_{H^1(\Omega)}.$$

Consequently, we can obtain a bound on $\|\phi\|_{L^2(0,T;H^1(\Omega))}$ which only depends on ρ_{in}, ϕ_{in} and T. Using this bound in the energy inequality for ρ, we could then deduce a bound on ρ in $L^\infty(0,T;H^1(\Omega))$ which is independent of M. However, we need to be careful with this argument because we cannot pass to the limit in the energy inequality (2.33) (since we only have a weak convergence of $\partial_x\phi^\delta$ in L^2). It is thus not clear that (2.33) holds in the limit $\delta \to 0$.

We will first prove the following result.

Lemma 2.3.8. *Let*

$$Y^\delta(t) = \int_\Omega |\partial_x\phi^\delta|^2\,dx.$$

The following inequalities hold:

$$\int_0^T Y^\delta(t)\,dt \leq \int_0^T\int_\Omega |\phi_{in}|^2\,dx + C\int_0^T\left(\int_\Omega |\rho^\delta(x,t)|\,dx\right)^2 dt, \tag{2.54}$$

and

$$\frac{d}{dt}E[\rho^\delta(\cdot,t)] \leq C\left(1 + E[\rho^\delta(\cdot,t)]^{1/2}\right)Y^\delta(t), \tag{2.55}$$

for a constant C depending only on Ω and $\int_\Omega \rho_{in}\,dx$.

Using this result, a Gronwall type argument will then lead to an appropriate bound on ρ^δ thanks to the following proposition:

Proposition 2.3.9. *There exists a constant C depending only on Ω, $\int_\Omega \rho_{in}\,dx$, $E[\rho_{in}]$, $\|\phi_{in}\|_{L^2}$ and T such that*

$$\sup_{\Omega\times(0,T)} |\rho^\delta(x,t)| \leq C + C\int_0^T\left(\int_\Omega |\rho^\delta(x,t)|\,dx\right)^2 dt.$$

Note that for $\delta > 0$, this proposition does not give any information we did not already have. The important fact is that the upper bound depends on δ only through $\int_\Omega |\rho^\delta|\,dx$. In the limit, using the uniform convergence of ρ^δ, we get a bound on ρ which only depends on $\int_\Omega |\rho|\,dx$. But, as noted above, the non-negativity of ρ and the conservation of mass (2.31) implies that

$$\int_\Omega |\rho|\,dx = \int_\Omega \rho\,dx = \int_\Omega \rho_{in}\,dx.$$

Proposition (2.3.9) therefore implies:

Corollary 2.3.10. *There exists a constant C depending only on Ω, $\int_\Omega \rho_{in}\,dx$, $E[\rho_{in}]$, $\|\phi_{in}\|_{L^2}$ and $T > 0$ such that*

$$0 \leq \rho(x,t) \leq C \qquad \text{in } \Omega\times(0,T).$$

In particular, we can choose $M \geq C$ so that

$$f_{\delta,M}(\rho^\delta) \to \min\{M, \rho(x,t)\} = \rho \qquad \text{uniformly in } \Omega\times(0,T) \text{ when } \delta \to 0.$$

We now turn to the proof of Lemma 2.3.8 and Proposition 2.3.9.

Proof of Lemma 2.3.8. From the energy inequality for ϕ^δ and classical Sobolev embeddings it follows that

$$\begin{aligned}\frac{d}{dt}\int_\Omega \frac{1}{2}|\phi^\delta|^2\,dx + \int_\Omega |\phi^\delta|^2 + |\partial_x\phi^\delta|^2\,dx &= \int_\Omega \rho^\delta\phi^\delta\,dx \\ &\le \sup_{x\in\Omega}|\phi^\delta(x,t)|\int_\Omega |\rho^\delta|\,dx \\ &\le C\left(\int_\Omega |\phi^\delta|^2 + |\partial_x\phi^\delta|^2\,dx\right)^{1/2}\int_\Omega |\rho^\delta|\,dx.\end{aligned}$$

We deduce that

$$\frac{d}{dt}\int_\Omega \frac{1}{2}|\phi^\delta|^2\,dx + \frac{1}{2}\int_\Omega |\phi^\delta|^2 + |\partial_x\phi^\delta|^2\,dx \le C\left(\int_\Omega |\rho^\delta|\,dx\right)^2,$$

hence

$$\int_0^T\int_\Omega |\phi^\delta|^2 + |\partial_x\phi^\delta|^2\,dx\,dt \le \int_\Omega |\phi_{in}|^2\,dx + C\int_0^T\left(\int_\Omega |\rho^\delta|\,dx\right)^2 dt, \tag{2.56}$$

which implies (2.54).

Next, using (2.33), we get

$$\begin{aligned}\frac{d}{dt}E[\rho^\delta(\cdot,t)] &\le \sup_{x\in\Omega} f_{\delta,M}(\rho^\delta)\int_\Omega |\partial_x\phi^\delta|^2\,dx \\ &\le \sup_{x\in\Omega}\left(\delta + |\rho^\delta(x,t)|\right)Y^\delta(t)\end{aligned}$$

and (2.55) follows the following consequence of Poincaré inequality:

$$\begin{aligned}\sup_{x\in\Omega}|\rho^\delta(x,t)| &\le C\|\rho^\delta(\cdot,t)\|_{H^1(\Omega)} \\ &\le C\left(\int_\Omega \rho^\delta(x,t)\,dx + \left(\int_\Omega |\partial_x\rho^\delta|^2\,dx\right)^{1/2}\right) \\ &\le C\left(\int_\Omega \rho_{in}(x)\,dx + E[\rho^\delta(\cdot,t)]^{1/2}\right).\end{aligned} \tag{2.57}$$

□

Proof of Proposition 2.3.9. A Gronwall type argument now yields a bound on $E[\rho^\delta]$. More precisely, we see that the inequality (2.55) implies

$$\frac{d}{dt}\left(1 + E[\rho^\delta(\cdot,t)]\right)^{1/2} \le C\,Y^\delta(t).$$

and so

$$\int_\Omega |\partial_x\rho^\delta(x,t)|^2\,dx \le E[\rho^\delta(\cdot,t)] \le C\left[\int_0^T Y^\delta(s)\,ds + 1\right]^2 \qquad \forall t\in(0,T), \tag{2.58}$$

where the constant C depends only on $\int_\Omega \rho_{in}\,dx, \Omega$ and $E[\rho_{in}]$. Combining inequalities (2.58) and (2.54), and using (2.57), we deduce

$$\sup_{\Omega\times(0,T)}|\rho^\delta(x,t)| \le C + C\int_0^T\left(\int_\Omega |\rho^\delta|\,dx\right)^2 dt,$$

where the constant C depends only on Ω, $\int_\Omega \rho_{in}\,dx$, $E[\rho_{in}]$, $\|\phi_{in}\|_{L^2}$ and T. □

Weak formulation. We now fix $M \geq C$ where C is the constant given by Corollary 2.3.10. We consider a set of test functions $\varphi \in \mathcal{D}(\bar{\Omega} \times [0,T))$. Multiplying the first equation in (2.29) by φ and integrating on Ω_T, we get:

$$\int_0^T \int_\Omega \rho^\delta \partial_t \varphi \, dx \, dt - \int_0^T \int_\Omega f_{\delta,M}(\rho^\delta) \, \partial_x q^\delta \, \partial_x \varphi \, dx \, dt = - \int_\Omega \rho_{in}(x) \, \varphi(x,0) \, dx, \tag{2.59}$$

where we recall that $q^\delta = -\partial_{xx}\rho^\delta + W'(\rho^\delta) + \phi$. We now want to pass to the limit in (2.59). Since $\rho^\delta \to \rho$ uniformly, we have that

$$\int_0^T \int_\Omega \rho^\delta \partial_t \varphi \, dx \, dt \longrightarrow \int_0^T \int_\Omega \rho \, \partial_t \varphi \, dx \, dt, \qquad \forall \varphi \in \mathcal{D}(\Omega_T), \quad \text{as } \delta \to 0. \tag{2.60}$$

Next, recalling (2.46), we see that the function $h^\delta = f_{\delta,M}(\rho^\delta) \, \partial_x q^\delta$ is bounded in $L^2(0,T;L^2(\Omega))$ uniformly with respect to δ. Hence, there exists a function $h \in L^2(0,T;L^2(\Omega))$ such that

$$h^\delta \rightharpoonup h, \qquad \text{weakly in } L^2(0,T;L^2(\Omega)), \quad \text{for } \delta \to 0.$$

This allows us to write the following convergence as $\delta \to 0$

$$\int_0^T \int_\Omega f_{\delta,M}(\rho^\delta) \, \partial_x q^\delta \, \partial_x \varphi \, dx \, dt \longrightarrow \int_0^T \int_\Omega h \, \partial_x \varphi \, dx \, dt, \qquad \text{for all } \varphi \in \mathcal{D}(\Omega_T). \tag{2.61}$$

In order to characterize this function h, we first write, for any $\varphi \in \mathcal{D}(\Omega_T)$:

$$\begin{aligned}
\left| \iint_{\{\rho=0\}} h^\delta \varphi \, dx \, dt \right| &\leq C \left(\iint_{\{\rho=0\}} f_{\delta,M}(\rho^\delta) \, dx \, dt \right)^{1/2} \left(\iint_{\{\rho=0\}} f_{\delta,M}(\rho^\delta) |\partial_x q^\delta|^2 \, dx \, dt \right)^{1/2} \\
&\leq C \left(\iint_{\{\rho=0\}} f_{\delta,M}(\rho^\delta) \, dx \, dt \right)^{1/2} \\
&\longrightarrow C \left(\iint_{\{\rho=0\}} \min\{M, \rho\} \, dx \, dt \right)^{1/2} = 0.
\end{aligned}$$

We deduce that $h = 0$ a.e. in $\{\rho = 0\}$. Next, for $\eta > 0$, we consider the set $\{\rho > \eta\}$. The uniform convergence implies that $\rho^\delta(x,t) > \eta/2$ and so $f_{\delta,M}(\rho^\delta) > \eta/2$ in that set for δ small enough. We deduce

$$\begin{aligned}
\iint_{\{\rho>\eta\}} |\partial_{xxx}\rho^\delta|^2 \, dx \, dt &\leq \frac{2}{\eta} \int_0^T \int_\Omega f_{\delta,M}(\rho^\delta) |\partial_{xxx}\rho^\delta|^2 \, dx \, dt \\
&\leq \frac{2}{\eta} \left(\int_0^T \int_\Omega f_{\delta,M}(\rho^\delta) |\partial_x[-\partial_{xx}\rho^\delta + W'(\rho^\delta)]|^2 \, dx \, dt \right. \\
&\qquad \left. + \int_0^T \int_\Omega f_{\delta,M}(\rho^\delta) |\partial_x W'(\rho^\delta)|^2 \, dx \, dt \right) \\
&\leq \frac{2}{\eta} \left(C + \int_0^T \int_\Omega f_{\delta,M}(\rho^\delta) W''(\rho^\delta)^2 |\partial_x \rho^\delta|^2 \, dx \, dt \right) \\
&\leq \frac{C}{\eta},
\end{aligned}$$

for small δ (where we used (2.43) and Corollary 2.3.10).

In particular

$$\partial_{xxx}\rho^\delta \rightharpoonup \partial_{xxx}\rho \qquad \text{weakly in } L^2(0,T;L^2(\{\rho>\eta\})), \text{ when } \delta\to 0.$$

We deduce (using Corollary 2.3.10) that

$$\begin{aligned} h^\delta &= f_{\delta,M}(\rho^\delta)\,(-\partial_{xxx}\rho^\delta + W''(\rho^\delta)\partial_x\rho^\delta + \partial_x\phi^\delta) \\ &\rightharpoonup \rho\,(-\partial_{xxx}\rho + W''(\rho)\partial_x\rho + \partial_x\phi) \qquad \text{weakly in } L^2(0,T;L^2(\{\rho>\eta\})). \end{aligned}$$

Since this holds for all $\eta>0$, we deduce that $h=\rho\,(-\partial_{xxx}\rho + W''(\rho)\partial_x\rho + \partial_x\phi)$ a.e. in the set $\{\rho>0\}$.

Equation (2.61) thus becomes

$$\int_0^T\int_\Omega f_{\delta,M}(\rho^\delta)\;\partial_x q^\delta\;\partial_x\varphi\,dx\,dt \longrightarrow \iint_{\{\rho>0\}} \rho\,(-\partial_{xxx}\rho + W''(\rho)\partial_x\rho + \partial_x\phi)\partial_x\varphi\,dx\,dt,$$

for all $\varphi\in\mathcal{D}(\Omega_T)$ and the result follows by passing to the limit in (2.59).

2.4 Formal derivation of Sharp Interface Limit - Proof of Theorem 2.1.2

In this section, we give a detailed formal derivation of the asymptotic model describing the evolution of $\rho^0=\lim_{\varepsilon\to 0}\rho^\varepsilon$. We rewrite the system (2.11) as follows:

$$\begin{cases} \varepsilon\partial_t\rho^\varepsilon = \operatorname{div}(\rho^\varepsilon\nabla q^\varepsilon) & \text{in } \Omega\times(0,T),\\ q^\varepsilon = \gamma(-\varepsilon^2\Delta\rho^\varepsilon + W'(\rho^\varepsilon)) + \varepsilon\phi^\varepsilon & \text{in } \Omega\times(0,T),\\ \varepsilon\partial_t\phi^\varepsilon - \alpha\operatorname{div}(\phi^\varepsilon\nabla q^\varepsilon) = \eta^2\Delta\phi^\varepsilon - \phi^\varepsilon + \beta\rho^\varepsilon & \text{in } \Omega\times(0,T), \end{cases} \tag{2.62}$$

together with appropriate boundary conditions on $\partial\Omega$ when either η is a fixed positive parameter, or $\eta=\tau\varepsilon$ for some fixed $\tau\geq 0$. Here the domain Ω is a fixed open subset of $\mathbb{R}^2$.

When $\phi=0$, this is a classical problem (see Pego [33] for the case with constant mobility and Glasner [23] for the degenerate case considered here) and the limit $\varepsilon\to 0$ leads to phase separation. Here, we expect to find, as in [23]:

$$\lim_{\varepsilon\to 0}\rho^\varepsilon(x,t)=\rho^0(x,t)=\chi_{\Sigma(t)}(x),$$

where the set $\Sigma(t)$ describe the inside of the cell and $\Sigma(t)^c$ describes the outside of the cell. When $\phi(x,t)$ is a given function independent of ε, the formal derivation of an asymptotic equation for $\partial\Sigma(t)$ is very similar to [23] and it leads to the following Hele-Shaw free boundary problem with surface tension and active potential:

$$\begin{cases} -\Delta q = 0 & \text{in } \Sigma(t),\\ q = \bar\gamma\kappa(t) + \phi(t,x) & \text{on } \partial\Sigma(t),\\ V = -\nabla q\cdot n & \text{on } \partial\Sigma(t), \end{cases} \tag{2.63}$$

where we recall that $\kappa(t)$ denotes the mean-curvature of the boundary $\partial\Sigma(t)$ and V is the normal velocity of $\partial\Sigma(t)$. This derivation relies on asymptotic expansions and matching asymptotic methods. For the sake of completeness, we will provide all the details below, even though our main contribution is the role played by the coupling with the evolution if ϕ^ε (and leads to the definition of the function $F(V)$ in (2.14)).

2.4.1 Outer Expansions

We first expand ρ^ε, q^ε and ϕ^ε as follows

$$\rho^\varepsilon(x,t) = \rho^0(x,t) + \varepsilon\rho^1(x,t) + \varepsilon^2\rho^2(x,t) + \cdots, \tag{2.64}$$

$$q^\varepsilon(x,t) = q^0(x,t) + \varepsilon q^1(x,t) + \varepsilon^2 q^2(x,t) + \cdots, \tag{2.65}$$

$$\phi^\varepsilon(x,t) = \phi^0(x,t) + \varepsilon\phi^1(x,t) + \varepsilon^2\phi^2(x,t) + \cdots.$$

The function ρ^0 (resp. q^0 and ϕ^0) will describe the asymptotic behavior of ρ^ε (resp. q^ε and ϕ^ε) outside of the small transition layer (of size ε) around the interface $\Gamma(t) = \partial\Sigma(t)$. This expansion is thus usually called the **outer expansion** in the literature. Plugging these expansions into (2.62), we get in particular:

$$\varepsilon\partial_t\rho^0 = \operatorname{div}(\rho^0\nabla q^0) + \varepsilon\operatorname{div}(\rho^1\nabla q^0) + \varepsilon\operatorname{div}(\rho^0\nabla q^1) + \mathcal{O}(\varepsilon^2), \tag{2.66}$$

and

$$\begin{aligned} q^0 + \varepsilon q^1 &= \gamma W'(\rho^0 + \varepsilon\rho^1 + \dots) + \varepsilon\phi^0 + \mathcal{O}(\varepsilon^2), \\ &= \gamma W'(\rho^0) + \varepsilon\gamma W''(\rho^0)\rho^1 + \varepsilon\phi^0 + \mathcal{O}(\varepsilon^2). \end{aligned} \tag{2.67}$$

(we do not worry about the equation for ϕ^ε at this point). Identifying the term of the same order in ε in (2.66), we get:

$$0 = \operatorname{div}(\rho^0\nabla q^0), \tag{2.68}$$

$$\partial_t\rho^0 = \operatorname{div}(\rho^0\nabla q^1) + \operatorname{div}(\rho^1\nabla q^0), \tag{2.69}$$

and doing the same thing with (2.67), we obtain:

$$q^0 = \gamma W'(\rho^0), \tag{2.70}$$

$$q^1 = \gamma W''(\rho^0)\rho^1 + \phi^0. \tag{2.71}$$

2.4.2 Inner Expansions

Since the functions ρ^i and q^i might be discontinuous across the interface $\Gamma(t)$, these equations hold in each phase $\Sigma(t)$ and $\Sigma^c(t)$ and must be supplemented with boundary conditions along $\Gamma(t)$. In order to derive the appropriate boundary conditions, we need to describe the transition layer and use matching asymptotic methods.

This is done by expanding a rescaled version of the solution near a point on $\Gamma(t)$. This is the so-called **inner expansion** which we describe now: We assume that the width of the transition layer is of order ε, and we approximate the interface separating the inside and outside of the cell by the level set

$$\Gamma^\varepsilon(t) = \{x \,|\, \rho^\varepsilon(x,t) = 1/2\}.$$

We fix $t_0 > 0$ and a point $x_0 \in \Gamma^\varepsilon(t_0)$ and we consider $s \mapsto \zeta(s,t)$ a parametrization of $\Gamma^\varepsilon(t)$ near x_0. We denote by z the signed distance from $\Gamma(t) = \partial\Sigma(t)$ ($z > 0$ inside $\Sigma(t)$) and we use (s,z) as an orthogonal local coordinate system in a neighborhood of the interface. For all (x,t) in a small neighborhood of (x_0,t_0), we can write

$$x = X(s,z,t) = \zeta(s,t) + zn(s,t)$$

where $n(s,t)$ is the inward normal unit vector to $\Gamma(t) = \partial\Sigma(t)$ at the point $\zeta(s,t)$ (we recall that the interior of the set $\Sigma(t)$ corresponds to the set $z > 0$). In a small neighborhood of (x_0,t_0), we can invert the change of coordinates $(s,z,t) \mapsto (x,t)$ and we will use the notations:

$$s = S(x,t), \quad z = R(x,t) = \pm d(x,\Gamma(t)).$$

We recall that the distance function satisfies in particular $|\nabla R| = 1$ in the neighborhood of $\Gamma(t)$ where z is well defined and

$$-\Delta R = \kappa \quad \text{on } \Gamma(t) \tag{2.72}$$

where ∇ and Δ denotes the derivative with respect to the variable x and κ is the curvature of Γ (with the convention that it is positive if $\Sigma(t)$ is convex).

In order to describe the transition layer, we rescale the normal variable z by defining the functions $\overline{\rho}^\varepsilon, \overline{q}^\varepsilon$ and $\overline{\phi}^\varepsilon$ so that

$$\rho^\varepsilon(x,t) = \overline{\rho}^\varepsilon(z/\varepsilon, s, t), \quad q^\varepsilon(x,t) = \overline{q}^\varepsilon(z/\varepsilon, s, t), \quad \phi^\varepsilon(x,t) = \overline{\phi}^\varepsilon(z/\varepsilon, s, t).$$

A simple computation then shows that

$$\begin{aligned}
\partial_t \rho^\varepsilon(x,t) &= \left[\frac{1}{\varepsilon} R_t \overline{\rho}^\varepsilon_z + S_t \overline{\rho}^\varepsilon_s + \overline{\rho}^\varepsilon_t\right](z/\varepsilon, s, t),\\
\nabla \rho^\varepsilon(x,t) &= \left[\frac{1}{\varepsilon} \nabla R \overline{\rho}^\varepsilon_z + \nabla S \overline{\rho}^\varepsilon_s\right](z/\varepsilon, s, t),\\
\Delta \rho^\varepsilon(x,t) &= \left[\frac{1}{\varepsilon^2} \overline{\rho}^\varepsilon_{zz} + \frac{1}{\varepsilon} \Delta R \overline{\rho}^\varepsilon_z + |\nabla S|^2 \overline{\rho}^\varepsilon_{ss} + \Delta S \overline{\rho}^\varepsilon_s\right](z/\varepsilon, s, t),
\end{aligned}$$

where we used the fact that $|\nabla R| = 1$ and $\nabla R \cdot \nabla S = 0$. In the new coordinates, the system (2.62) leads in particular to:

$$\begin{cases}
\varepsilon^2\ \overline{\rho}^\varepsilon_z R_t + \varepsilon^3\ (\overline{\rho}^\varepsilon_t + \overline{\rho}^\varepsilon_s S_t) = (\overline{\rho}^\varepsilon \overline{q}^\varepsilon_z)_z + \varepsilon\ \Delta R\ \overline{\rho}^\varepsilon \overline{q}^\varepsilon_z + \varepsilon^2\ [\ \Delta S \overline{\rho}^\varepsilon \overline{q}^\varepsilon_s + |\nabla S|^2\ (\overline{\rho}^\varepsilon \overline{q}^\varepsilon_s)_s\ ],\\
\overline{q}^\varepsilon = -\gamma[\ \overline{\rho}^\varepsilon_{zz} + \varepsilon\ \Delta R \overline{\rho}^\varepsilon_z + \varepsilon^2\ (\Delta S \overline{\rho}^\varepsilon_s + |\nabla S|^2 \overline{\rho}^\varepsilon_{ss})\ ] + \gamma W'(\overline{\rho}^\varepsilon) + \varepsilon\ \overline{\phi}^\varepsilon.
\end{cases} \tag{2.73}$$

Proceeding as with the outer expansion, we expand those functions:

$$\begin{cases}
\overline{\rho}^\varepsilon(z,s,t) = \overline{\rho}^0(z,s,t) + \varepsilon \overline{\rho}^1(z,s,t) + \varepsilon^2 \overline{\rho}^2(z,s,t) + \cdots\\
\overline{q}^\varepsilon(z,s,t) = \overline{q}^0(z,s,t) + \varepsilon \overline{q}^1(z,s,t) + \varepsilon^2 \overline{q}^2(z,s,t) + \cdots\\
\overline{\phi}^\varepsilon(z,s,t) = \overline{\phi}^0(z,s,t) + \varepsilon \overline{\phi}^1(z,s,t) + \varepsilon^2 \overline{\phi}^2(z,s,t) + \cdots
\end{cases} \tag{2.74}$$

and we identify the terms of the same order in ε after plugging these expansions in (2.73).

Terms of order zero: The transition profile $\psi(z)$. After expanding $W'(\overline{\rho}^\varepsilon) = W'(\overline{\rho}^0) + \varepsilon W''(\overline{\rho}^0)\overline{\rho}^1 + \ldots$, the terms of order zero in (2.73) give

$$\begin{cases}
0 = (\overline{\rho}^0 \overline{q}^0_z)_z,\\
\overline{q}^0 = -\gamma \overline{\rho}^0_{zz} + \gamma W'(\overline{\rho}^0).
\end{cases} \tag{2.75}$$

Since we are looking for a positive solution $\overline{\rho}^0 = \overline{\rho}^0(z,s,t)$ joining two states $\rho_\pm(s,t)$ as $z \to \pm\infty$, the first equation implies that $\overline{q}^0$ does not depend on z (we can use (2.70) and the matching conditions (2.92) for q to make this rigorous), and taking the limit $z \to \pm\infty$ in the second equation leads to

$$\overline{q}^0 = \gamma W'(\rho_+) = \gamma W'(\rho_-). \tag{2.76}$$

Now, by multiplying the second equation of (2.75) by ρ^0_z and by integrating in z, we get

$$\frac{\overline{q}^0}{\gamma}\,(\overline{\rho}^0(z) - \rho_-) = -\frac{1}{2}(\overline{\rho}^0_z(z))^2 + W(\overline{\rho}^0(z)) - \gamma W(\rho_-). \tag{2.77}$$

When $z \to +\infty$, we find $\frac{\overline{q}^0}{\gamma}\,(\rho_+ - \rho_-) = W(\rho_+) - \gamma W(\rho_-)$ and so using (2.76), we get that ρ_- and ρ_+ are related by the classical relations

$$\begin{cases}
\dfrac{W(\rho_+) - W(\rho_-)}{\rho_+ - \rho_-} - W'(\rho_+) = 0,\\
\dfrac{W(\rho_+) - W(\rho_-)}{\rho_+ - \rho_-} - W'(\rho_-) = 0.
\end{cases}$$

When W satisfies (2.2), this implies that $\rho_- = 0$ and $\rho_+ = 1$ (and $\overline{q}^0 = 0$ by (2.76)). Equation (2.77) thus becomes

$$(\overline{\rho}^0_z)^2 = 2\,W(\,\overline{\rho}^0\,), \tag{2.78}$$

and so $\overline{\rho}^0(z) = \psi(z)$, where ψ is given by the following lemma:

Lemma 2.4.1. *Assume that the double potential W satisfies (2.2). Then there is a unique profile ψ satisfying*

$$\psi'(z) = \sqrt{2\,W(\,\psi(z)\,)}, \qquad \lim_{z\to-\infty}\psi(z) = 0, \qquad \lim_{z\to+\infty}\psi(z) = 1, \tag{2.79}$$

and such that $\psi(0) = 1/2$. When $W(\rho) = \rho^2(1-\rho)^2$, we get $\psi(z) = \frac{1}{1+e^{-\sqrt{2}z}}$.

Terms of order 1: Solvability condition. Taking the terms of order ε^1 in the system (2.73), we get

$$\begin{cases} 0 = (\psi\overline{q}^1_z)_z, \\ \overline{q}^1 = -\gamma\overline{\rho}^1_{zz} + \gamma\kappa^0\,\psi' + \gamma W''(\psi)\,\overline{\rho}^1 + \overline{\phi}^0, \end{cases} \tag{2.80}$$

where we used (2.72) to approximate $-\Delta R$ by the leading order of the curvature of $\Gamma(t)$ denoted here by κ^0. Assuming that $\overline{q}^1$ is bounded for $z \in \mathbb{R}$ (this will follow from the matching conditions (2.92) once we show that $q^0 = 0$), the first equation in (2.80) implies that $\overline{q}^1$ is independent of z.

The second equation in (2.80) then implies that ρ^1 solves

$$\gamma L_0[\rho^1] := -\gamma\overline{\rho}^1_{zz} + \gamma W''(\psi)\,\overline{\rho}^1 = \overline{q}^1 - \gamma\kappa^0\,\psi' - \overline{\phi}^0. \tag{2.81}$$

To derive a solvability condition for this equation, we first differentiate (2.75) with respect to z to find

$$L_0[\psi'] = W''(\psi)\psi' - \psi''' = 0.$$

Multiplying (2.81) by $\psi'(z)$ and integrating, we deduce

$$\begin{aligned} \int_{-\infty}^{+\infty}\left[\overline{q}^1 - \gamma\kappa^0\,\psi'(z) - \overline{\phi}^0(s,t,z)\right]\psi'(z)\,dz &= \int_{\mathbb{R}} L_0[\rho^1]\psi'(z)\,dz \\ &= \int_{\mathbb{R}} \rho^1 L_0[\psi'](z)\,dz \\ &= 0 \end{aligned}$$

which gives (using (2.79)):

$$\overline{q}^1(s,t) = \bar{\gamma}\kappa_0(s,t) + \int_{-\infty}^{\infty}\overline{\phi}^0(s,t,z)\psi'(z)\,dz, \tag{2.82}$$

where

$$\bar{\gamma} = \gamma\int_{-\infty}^{\infty}|\psi'(z)|^2\,dz = \gamma\sqrt{2}\int_0^1\sqrt{W(x)}\,dx.$$

Terms of order 2. Finally we consider the terms of order ε^2 in (2.73). Since $\overline{q}^0 = 0$ and $\overline{q}^1$ does not depend on z, we find in particular that

$$\psi'(z)V^0 = (\psi\,\overline{q}^2_z)_z, \tag{2.83}$$

where we approximated R_t by the velocity V^0 of the surface Γ (note that $R_t > 0$ if the $\partial\Sigma$ is moving outward, that is if $V > 0$). Integrating with respect to z and using the matching condition at $z \to -\infty$, we deduce

$$\overline{q}^2_z = V^0. \tag{2.84}$$

The function $\overline{\phi}^0$. We finally turn our attention to the function $\overline{\phi}^0$ which appears in the formula (2.82) for $\overline{q}^1$. First, we note that the equation for ϕ^ε in (2.62) yields the following equation for the rescaled function $\overline{\phi}^\varepsilon$:

$$\begin{aligned}\varepsilon^2\overline{\phi}^\varepsilon_z R_t+\varepsilon^3(\overline{\phi}^\varepsilon_t+\overline{\phi}^\varepsilon_s S_t)-\alpha\,[(\overline{\phi}^\varepsilon\overline{q}^\varepsilon_z)_z+\varepsilon^2(\overline{\phi}^\varepsilon\overline{q}^\varepsilon_s)_s|\nabla S|^2+\varepsilon\overline{\phi}^\varepsilon\overline{q}^\varepsilon\Delta R+\varepsilon^2\overline{\phi}^\varepsilon\overline{q}^\varepsilon_s\Delta S]\\ =\eta^2\left(\overline{\phi}^\varepsilon_{zz}+\varepsilon\Delta R\overline{\phi}^\varepsilon_z+\varepsilon^2[\overline{\phi}^\varepsilon_{zz}|\nabla S|^2+\overline{\phi}_s\nabla S]\right)-\varepsilon^2\overline{\phi}^\varepsilon+\varepsilon^2\beta\overline{\rho}^\varepsilon,\end{aligned}\tag{2.85}$$

in which we insert the expansions (2.74).

- **Case 1: When $\eta>0$ is fixed.**

  Since $\overline{q}^0=0$ and $\overline{q}^1$ is constant with respect to z, the terms of order 0 in (2.85) gives

  $$\overline{\phi}^0_{zz}=0$$

  which together with the matching boundary conditions (2.92) will implies that $\overline{\phi}^0$ is independent of z. The term of order 1 then gives

  $$\overline{\phi}^1_{zz}=0$$

  which together with the matching boundary conditions (2.92) will implies that $\overline{\phi}^1$ is linear.

- **Case 2: When $\eta=\tau\varepsilon\ll 1$**

  Since $\overline{q}^0=0$ and $\overline{q}^1$ is constant with respect to z the terms of order ε^0 and ε^1 vanish, so we consider the term of order ε^2 in (2.85) and find:

  $$\overline{\phi}^0_z V^0-\alpha(\overline{\phi}^0\overline{q}^2_z)_z=\tau^2\overline{\phi}^0_{zz}-\overline{\phi}^0+\beta\overline{\rho}^0,$$

  which is equivalent (using (2.84)) to

  $$\tau^2\overline{\phi}^0_{zz}-(1-\alpha)V^0\overline{\phi}^0_z+\beta\overline{\rho}^0-\overline{\phi}^0=0,$$

  where we recall that $\overline{\rho}^0=\psi$. We now use the following result which will be proved later (see Proposition 2.5.1):

  Proposition 2.4.2. *For any $\tau\geq 0$ and for all $V\in\mathbb{R}$, the equation*

  $$\tau^2\Phi''-V\Phi'-\Phi+\psi=0,\tag{2.86}$$

  has a unique (up to translation) bounded solution in $\mathbb{R}$, which we denote $\Phi_\tau(V,z)$.

  We can thus write

  $$\overline{\phi}^0(z,s,t)=\beta\,\Phi_\tau((1-\alpha)V^0(s,t),z),\tag{2.87}$$

  and equation (2.82) now gives

  $$\overline{q}^1(s,t)=\gamma\,\kappa_0(s,t)+\beta\,F_\tau((1-\alpha)V^0(s,t)\,),\tag{2.88}$$

  where the function $F_\tau:\mathbb{R}\to\mathbb{R}$ is defined by

  $$F_\tau(V\,)=\int_{-\infty}^{\infty}\Phi_\tau(V,z)\,\psi'(z)\,dz\qquad\text{for all } V\in\mathbb{R}.\tag{2.89}$$

Remarks 2.4.3. *Equation (2.82) shows that the contribution of the potential ϕ^ε to the free boundary condition is given by*

$$h(s,t) = \int_{-\infty}^{\infty} \overline{\phi}^0(z,s,t)\psi'(z)\,dz$$

which, using our notations yields

$$\begin{aligned} h(s,t) = \lim_{\varepsilon\to 0}\int_{-\infty}^{\infty} \overline{\phi}^\varepsilon(z,s,t)\psi'(z)\,dz &= \lim_{\varepsilon\to 0}\int_{-\infty}^{\infty} \phi^\varepsilon(\varepsilon z,s,t)\psi'(z)\,dz \\ &= \lim_{\varepsilon\to 0}\int_{-\infty}^{\infty} \phi^\varepsilon(z,s,t)\varepsilon^{-1}\psi'(z/\varepsilon)\,dz \\ &= \lim_{\varepsilon\to 0}\int_{-\delta}^{\delta} \phi^\varepsilon(z,s,t)\varepsilon^{-1}\psi'(z/\varepsilon)\,dz \\ &= \lim_{\varepsilon\to 0}\int_{-\delta}^{\delta} \phi^\varepsilon(z,s,t)\partial_z\rho^\varepsilon(s,t,z)\,dz \end{aligned}$$

for any $\delta > 0$. We thus have $\lim_{\varepsilon\to 0}\phi^\varepsilon\partial_z\rho^\varepsilon = h(s,t)\delta(z)$.

In particular, if we take $\phi^\varepsilon(x,t) = \beta(x,t)\rho^\varepsilon(x,t)$ for some smooth function β (instead of the diffusion equation for ϕ^ε), then we get $\overline{\phi}^0(z,s,t) = \beta(\zeta(s,t),t)\psi(z)$ and so

$$\int_{-\infty}^{\infty} \overline{\phi}^0(z)\psi'(z)\,dz = \frac{1}{2}\beta(\zeta(s,t),t)$$

which gives

$$\overline{q}^1(s,t) = \gamma\kappa_0(s,t) + \frac{1}{2}\beta(\zeta(s,t),t) \tag{2.90}$$

2.4.3 Matching boundary conditions and conclusion

We observe that up to now we have two functions: ρ^ε defined away from the interface for which we consider the outer expansion, and $\overline{\rho}^\varepsilon$ defined near the interface for which we consider the inner expansion. The behaviors of these functions are related by the so-called **matching boundary conditions**. These conditions are derived in [10], but we recall the main step of this derivation for the function ρ^ε for the reader's convenience (see also [33]) - the derivation is similar for the functions $\overline{q}$ and $\overline{\phi}$.

We recall that the definition of $\overline{\rho}$ yields:

$$\overline{\rho}^\varepsilon(z,s,t) = \rho^\varepsilon(\zeta(s,t) + \varepsilon z\, n(s,t),t),$$

and a Taylor expansion with respect to ε leads to:

$$\sum_{n=0}^{+\infty}\varepsilon^n\overline{\rho}^n(z,s,t) = \sum_{n=0}^{+\infty}\frac{\varepsilon^n}{n!}\left[\frac{d^n}{d\varepsilon^n}\rho^\varepsilon(\zeta(s,t)+\varepsilon z\, n(s,t),t)\right]_{|\,\varepsilon=0}. \tag{2.91}$$

The matching boundary conditions are obtained by taking the limit $z\to\pm\infty$ and $\varepsilon\to 0$ in the equation (2.91) assuming that $\varepsilon z\to 0$ and $\varepsilon z^2\to 0$. We obtain:

$$\begin{cases} \lim\limits_{z\to\pm\infty}\overline{\rho}^0(z,s,t) = \rho^0(\zeta(s,t)\pm 0,t), \\ \overline{\rho}^1(z,s,t) = \rho^1(\zeta(s,t)\pm 0,t) + z\nabla\rho^0(\zeta(s,t)\pm 0,t)\cdot n \qquad \text{as } z\to\pm\infty \\ \overline{\rho}^2(z,s,t) = \rho^2(\zeta(s,t)\pm 0,t) + z\nabla\rho^1(\zeta(s,t)\pm 0,t)\cdot n \\ \qquad\qquad + \frac{1}{2}z^2 n^T D^2\rho^0(\zeta(s,t)\pm 0,t)\,n \qquad \text{as } z\to\pm\infty. \end{cases} \tag{2.92}$$

The same considerations are valid also for the functions q^ε and $\overline{q}^\varepsilon$ and we impose the same matching conditions on the pressure $\overline{q}^\varepsilon$ for $z\to\pm\infty$ and we get the same formulation of (2.92).

We are now ready to conclude. We recall that $\Gamma(t) = \partial\Sigma$ and we denote by $\rho^0_\pm(x,t)$ the trace of ρ^0 on either side of $\Gamma(t)$. The matching condition of order zero in (2.92) and the fact that $\overline{\rho}^0(z,s,t) = \psi(z)$ then leads to

$$\rho^0_+(x,t) = 1 \text{ on } \Gamma(t), \qquad \rho^0_-(x,t) = 0 \text{ on } \Gamma(t).$$

Furthermore, equations (2.68), (2.70) implies

$$\operatorname{div}(\rho^0 \nabla W'(\rho^0)) = 0,$$

so these boundary conditions lead to

$$\rho^0(x,t) = 1 \text{ in } \Sigma(t), \qquad \rho^0(x,t) = 0 \text{ in } \Sigma(t)^c. \tag{2.93}$$

Since $\overline{q}^0 = 0$, the matching condition of order zero for the pressure leads to $q^0 = 0$. By equation (2.69), since ρ^0 is constant, we then deduce

$$\Delta q^1 = 0 \text{ in } \Sigma(t). \tag{2.94}$$

Since $\overline{q}^1$ is independent from z, the second equation in (2.92) for the pressure leads to

$$q^1(x,t) = \overline{q}^1(s,t) \text{ on } \partial\Sigma(t), \tag{2.95}$$

where $\overline{q}^1$ is given by (2.82). Finally, the third equation in (2.92) for the pressure leads to

$$\lim_{z\to\pm\infty} \overline{q}^2_z(z,s,t) = \nabla q^1(\zeta(s,t) \pm 0, t) \cdot n,$$

and using (2.84) we deduce

$$V^0 = \nabla q^1(\zeta(s,t),t) \cdot n, \tag{2.96}$$

where we remember that $n = n(s,t)$ is the inward normal unit vector to $\Gamma(t)$ at the point $\zeta(s,t)$. Equations (2.93), (2.94), (2.95), (2.96), together with (2.88) fully determine the evolution of $\Sigma(t)$ in the case $\eta = \tau\varepsilon \ll 1$. Note that in that case, the terms of order 0 in the equation for ϕ^ε gives (since $q^0 = 0$)

$$\phi^0 = \beta\rho^0 = \beta\chi_{\Sigma(t)}$$

When $\eta > 0$ is fixed, the term of order 0 in the equation for ϕ^ε gives

$$\phi^0 - \eta^2\Delta\phi^0 = \beta\rho^0 \qquad \text{in } \Omega \setminus \Gamma(t). \tag{2.97}$$

Furthermore, the equations $\overline{\phi}^0_{zz} = 0$ and $\overline{\phi}^1_{zz} = 0$ together with the matching boundary conditions imply that $\phi^0(x,t)$ and $\partial_n\phi^0$ are continuous across the interface $\Gamma(t)$ so that equation (2.97) holds in the whole set Ω.

2.5 Properties of the function F_τ

In this section, we prove Propositions 2.4.2 - which shows in particular that $F_\tau(V)$ is well defined - as well as Proposition 2.1.4.

We recall that $\psi(z)$ denotes the solution of (2.79) and we take $\tau = 1$ for simplicity and we write F instead of F_1 (the result below, and in particular the bounds (2.100) and the limits (2.101) hold for all $\tau > 0$). Proposition 2.4.2 follows from the following result:

Proposition 2.5.1. *The unique bounded solution* Φ *of*

$$\Phi'' - V\Phi' - \Phi + \psi = 0, \tag{2.98}$$

is given by

$$\Phi(V,z) = \int_{\mathbb{R}} G(V, z-s)\psi(s)\,ds, \tag{2.99}$$

where G *is the (Green) function*

$$G(V,z) = \begin{cases} \frac{1}{2\nu} e^{(\mu+\nu)z} & \text{for } z < 0, \\ \frac{1}{2\nu} e^{(\mu-\nu)z} & \text{for } z > 0, \end{cases}$$

with $\mu = \frac{V}{2}$ *and* $\nu = \sqrt{\left(\frac{V}{2}\right)^2 + 1}$. *It satisfies in particular*

$$0 \le \Phi(V,z) \le 1, \qquad \forall z \in \mathbb{R},\ V \in \mathbb{R}. \tag{2.100}$$

The proof of this proposition is straightforward. We note in particular that $\mu + \nu > 0$ and $\mu - \nu < 0$ are the two roots of the characteristic polynomial $r^2 - Vr - 1 = 0$. The inequalities (2.100) follow from (2.98) and the maximum principle, or can be checked directly from the explicit formula (2.99) by using the fact that $0 \le \psi \le 1$ and $G \ge 0$. Indeed,

$$\begin{aligned} 0 \le \Phi(V,z) &\le \frac{1}{2\nu}\int_{-\infty}^{z} e^{-(\nu-\mu)(z-s)}\,ds + \frac{1}{2\nu}\int_{z}^{+\infty} e^{-(\nu+\mu)(s-z)}\,ds \\ &\le \frac{1}{2\nu(\nu-\mu)} + \frac{1}{2\nu(\nu+\mu)} \\ &\le \frac{1}{\nu^2-\mu^2} = 1. \end{aligned}$$

Next, we are interested in the behavior of $\Phi(V,z)$ with respect to V. We start with:

Proposition 2.5.2. *The function* $\Phi(V,z)$ *defined by* (2.99) *satisfies* $0 \le \Phi(V,z) \le 1$ *for all* $z \in \mathbb{R}$ *and*

$$\lim_{V\to+\infty} \Phi(V,z) = 0, \quad \lim_{V\to-\infty} \Phi(V,z) = 1 \qquad \text{for all } z \in \mathbb{R}. \tag{2.101}$$

Proof. We will prove only the second limit (the first one is proved similarly). We note that

$$\nu(V) \sim \frac{1}{2}|V|, \quad \mu(V) = -\frac{1}{2}|V|, \quad \nu + \mu \sim \frac{1}{|V|} \qquad \text{as } V \to -\infty. \tag{2.102}$$

We split the integral in (2.99) in two parts:

$$\Phi(V,z) = \int_{-\infty}^{z} G(V,z-s)\psi(s)\,ds + \int_{z}^{+\infty} G(V,z-s)\psi(s)\,ds.$$

Since $|\psi(s)| \le 1$ for all s, we immediately get:

$$\begin{aligned} \int_{-\infty}^{z} G(V,z-s)\psi(s)\,ds &\le \int_{-\infty}^{z} G(V,z-s)\,ds \\ &= \int_{0}^{+\infty} G(V,s)\,ds \\ &= \frac{1}{2\nu(\nu-\mu)} \sim \frac{2}{|V|(|V|+|V|)}, \end{aligned}$$

which converges to 0 as $V \to -\infty$. For the other piece of the integral, we write

$$\int_z^{+\infty} G(V, z-s)\psi(s)\,ds = \int_z^{+\infty} G(V, z-s)\,ds + \int_z^{+\infty} G(V, z-s)[\psi(s)-1]\,ds,$$

where (using (2.102))

$$\int_z^{+\infty} G(V, z-s)\,ds = \frac{1}{2\nu(\nu+\mu)} \to 1 \text{ as } V \to -\infty,$$

and (using the fact that $|1-\psi(s)| \le e^{-\alpha s}$, see (2.79))

$$\begin{aligned}\left|\int_z^{+\infty} G(V, z-s)[\psi(s)-1]\,ds\right| &\le \int_z^{+\infty} \frac{1}{2\nu} e^{(\mu+\nu)(z-s)} e^{-\alpha s}\,ds \\ &= \int_0^{+\infty} \frac{1}{2\nu} e^{-(\mu+\nu)y} e^{-\alpha(y+z)}\,dy \\ &= e^{-\alpha z}\int_0^{+\infty} \frac{1}{2\nu} e^{-(\mu+\nu+\alpha)y}\,dy \\ &= e^{-\alpha z}\frac{1}{2\nu(\mu+\nu+\alpha)},\end{aligned}$$

which converges to zero as $V \to -\infty$ (using (2.102)). Putting the pieces together, we have thus proved that

$$\lim_{V\to-\infty} \Phi(V, z) = 1 \qquad \text{for all } z \in \mathbb{R}.$$

□

Finally, we recall that $F(V)$ is defined by

$$F(V) = \int_{-\infty}^{+\infty} \Phi(V, z)\psi'(z)\,dz$$

and we turn our attention to the proof of Proposition 2.1.4 which we split into two lemma. First, we have:

Lemma 2.5.3. *The function $V \mapsto F(V)$ is differentiable and satisfies $0 < F(V) < 1$ for all $V \in \mathbb{R}$ and*

$$\lim_{V\to+\infty} F(V) = 0, \quad \lim_{V\to-\infty} F(V) = 1.$$

Proof. The differentiability with respect V follows easily from the explicit formula (2.99) for Φ. Also, since $0 < \Phi(V, z) < 1$ and $\psi'(z) > 0$, we clearly have

$$0 < F(V) = \int_{-\infty}^{+\infty} \Phi(V, z)\psi'(z)\,dz < \int_{-\infty}^{+\infty} \psi'(z)\,dz = 1.$$

Next, we note that

$$\lim_{V\to-\infty} \Phi(V, z)\,\psi'(z) = \psi'(z),$$

for all $z \in \mathbb{R}$ and, using (2.100) and the fact that $\psi'(z) > 0$, we have

$$0 \le \Phi(V, z)\,\psi'(z) \le \psi'(z).$$

Using the Lebesgue dominated convergence theorem and the fact that

$$\int_{-\infty}^{\infty} \psi'(z)\,dz = 1,$$

we deduce

$$\lim_{V\to-\infty} F(V) = 1.$$

The other limit is proved similarly. □

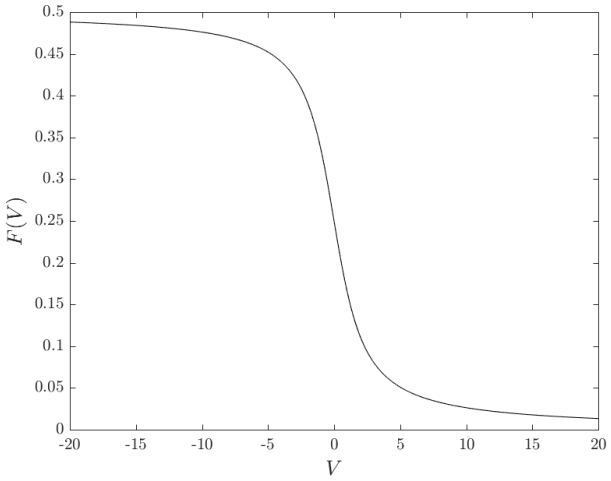

Figure 2.1 – Graphical representation of the function $V \mapsto F(V)$ for $V \in [-20, 20]$ with $W(\rho) = \rho^2(1-\rho^2)$.

Finally, we prove the following Lemma which completes the proof of Proposition 2.1.4:

Lemma 2.5.4. *The function $F(V)$ satisfies $F'(V) < 0$ for all $V \in \mathbb{R}$.*

Proof. This can be proved directly using the explicit formula (2.99) for Φ, or by use of the maximum principle. For example, by differentiating (2.98) with respect to z, we find that the function $\xi(z) = \partial_z \Phi(V, z)$ solves

$$\xi'' - V\xi' - \xi = -\psi'.$$

Since $\psi' \geq 0$, the maximum principle (noting that $\lim_{z\to\pm\infty} \xi = 0$) yields $\partial_z \Phi(V, z) \geq 0$ for all V and z in $\mathbb{R}$. By differentiating (2.98) with respect to V, we then find that the function $\zeta(z) = \partial_V \Phi(V, z)$ satisfies

$$\zeta'' - V\zeta' - \zeta = \partial_z \Phi(V, z) \geq 0, \tag{2.103}$$

and the maximum principle (noting that $\lim_{z\to\pm\infty} \zeta = 0$) implies that $\partial_V \Phi(V, z) \leq 0$ for all V and z in $\mathbb{R}$. It easily follows that $F'(V) \leq 0$.

Alternatively, we note that (2.103) implies

$$\begin{aligned}\partial_V \Phi(V, z) &= -\int_{-\infty}^{+\infty} G(V, z-s)\partial_z \Phi(V, z)\, ds \\ &= -\int_{-\infty}^{+\infty}\int_{-\infty}^{+\infty} G(V, z-s)G(V, s-t)\psi'(t)\, dt\, ds,\end{aligned}$$

and so

$$F'(V) = -\int_{-\infty}^{+\infty}\int_{-\infty}^{+\infty}\int_{-\infty}^{+\infty} G(V, z-s)G(V, s-t)\psi'(t)\psi'(z)\, dt\, ds\, dz,$$

which is negative since every term inside the integral is positive.

□

2.6 The asymptotic model in 1D

In this section, we investigate the properties of the asymptotic problem (2.14) in dimension $n = 1$. This is considerably simpler than the physical case $n = 2$, but we will see that some interesting behavior can already be observed in that case.

As mentioned in the introduction, in dimension 1, there is no mechanism that could split a cell, so we are interested in solutions for which $\Sigma(t)$ is an interval $(a(t), b(t))$. Furthermore, it is easy to check that the measure of $\Sigma(t)$ is preserved by (2.14) (this is a consequence of the conservation of mass $\frac{d}{dt}\int \rho^\varepsilon \, dx = 0$). Thus, if we denote $\ell = |\Sigma(t)|$, we get

$$\Sigma(t) = (a(t), b(t)), \qquad b(t) = a(t) + \ell$$

and the normal velocity is given by $-a'(t)$ at the left end boundary point, and by $a'(t)$ at the right end boundary point.

Since there is no curvature effect in dimension 1, equation (2.63) for $q(x,t)$ reduces to

$$\begin{cases} -\Delta q = 0 & \text{in } \Sigma(t), \\ q = \beta F(-(1-\alpha)\nabla q \cdot n) & \text{on } \partial\Sigma(t). \end{cases}$$

So $q(x,t)$ is a linear function of the form $q(x,t) = s(t)x + C(t)$ satisfying the boundary conditions

$$q(b(t),t) = \beta F(-(1-\alpha)s(t)), \qquad q(a(t),t) = \beta F((1-\alpha)s(t)).$$

We see that this is possible if and only if $s(t)$ is such that

$$s(t)\ell = \beta\Big[F(-(1-\alpha)s(t)) - F((1-\alpha)s(t))\Big]. \tag{2.104}$$

When $\alpha = 1$, this yields a unique solution $s(t) = 0$. Since

$$V(b(t),t) = -V(a(t),t) = -\partial_x q(b(t),t) = -s(t)$$

this correspond to the stationary solution. But for $\alpha \in [0,1)$, (2.104) is equivalent to

$$(1-\alpha)s(t) \in \mathcal{S}_{\frac{\beta(1-\alpha)}{\ell}}, \tag{2.105}$$

where $\mathcal{S}_\gamma$ denotes the set

$$\mathcal{S}_\gamma = \left\{ s \in \mathbb{R} \text{ such that } s = \gamma\big[F(-s) - F(s)\big] \right\}. \tag{2.106}$$

It is clear that we always have $0 \in \mathcal{S}_\gamma$ and so (2.14) has at least one solution (the stationary solution). However, we can prove that when γ is large enough, then the set $\mathcal{S}_\gamma$ includes other values:

Proposition 2.6.1. *There exists a critical $\gamma_c > 0$ such that the following holds*

- *If $\gamma \le \gamma_c$ then $\mathcal{S}_\gamma = \{0\}$.*
- *If $\gamma > \gamma_c$ then $\mathcal{S}_\gamma \supset \{-s(\gamma), 0, s(\gamma)\}$ for some $s(\gamma) > 0$.*

This proposition proves that a bifurcation phenomenon holds: if $\frac{\beta(1-\alpha)}{\ell} \le \gamma_c$ then (2.105) (and thus the asymptotic problem (2.63)) has only one (stationary) solution, but when $\frac{\beta(1-\alpha)}{\ell} \ge \gamma_c$, there are (at least) two additional solutions which are traveling wave like solution moving with constant speed to the left or to the right. We show in Figure 2.2 the graphical representation of the set $\mathcal{S}_\gamma$ defined in (2.106) for $\gamma \in [0, 10]$.

Proof of Proposition 2.6.1. We introduce the function

$$T(s) = F(-s) - F(s).$$

The set $\mathcal{S}_\gamma$ is then the set of solutions $s \in \mathbb{R}$ of the equation

$$\gamma T(s) = s. \tag{2.107}$$

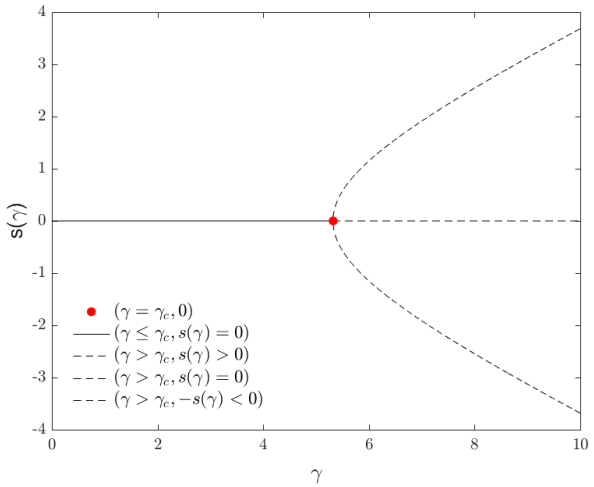

Figure 2.2 – Graphical representation of the points $s = s(\gamma)$ belonging to the set $\mathcal{S}_\gamma$ defined in (2.106) by varying $\gamma \in [0, 10]$. The function $[F(-s) - F(s)]$ was computed numerically. The red dot in the intersection of the graphs represents the (numerical) bifurcation value γ_c. For $\gamma \leq \gamma_c$, there is only one point $s(\gamma) = 0$ in $\mathcal{S}_\gamma$, while for $\gamma > \gamma_c$ there are (at least in the interval $(\gamma_c, 10]$) three points $\{-s(\gamma), 0, s(\gamma)\}$ for some $s(\gamma) > 0$ beloging to $\mathcal{S}_\gamma$. In particular, the (numerical) bifurcaton value is $\gamma_c \simeq 5.3$.

Since T is odd, the non zero solutions come in pairs so we can focus on the positive solutions We note that $T(0) = 0$ and Lemma 2.5.3 implies

$$\lim_{s\to\infty} T(s) = 1. \tag{2.108}$$

To prove Proposition 2.6.1, we can for instance define the map $h(\gamma) = \min_{s>0}(\frac{1}{\gamma}s - T(s))$. It is well defined since $\lim_{s\to\infty} \frac{1}{\gamma}s - T(s) = +\infty$ and the function h is clearly monotone decreasing. Furthermore, if we pick $\bar{s} > 0$ so that $T(\bar{s}) \geq 1/2$ (which we can do thanks to (2.108)), then we have $h(\gamma) \leq 0$ as soon as $\gamma > 2\bar{s}$. We then define

$$\gamma_c = \min\{\gamma \geq 0 \text{ s.t. } h(\gamma) \leq 0\} < \infty,$$

and check that the result holds.

We can in fact be more precise: The monotonicity of F implies that $T(s) > 0$ for $s > 0$ (and $T(s) < 0$ for $s < 0$). The relation (2.107) thus defines a unique $\gamma > 0$ such that $s \in \mathcal{S}_\gamma$ for all $s \neq 0$:

$$\gamma(s) = \frac{s}{T(s)}.$$

This implies in particular that

$$\gamma_c = \lim_{s\to 0} \frac{s}{T(s)} = \frac{1}{T'(0)} = \frac{-1}{2F'(0)} > 0.$$

□

Bibliography

[1] N. D. Alikakos, P. W. Bates, and X. Chen, *Convergence of the Cahn-Hilliard equation to the Hele-Shaw model*, Arch. Rational Mech. Anal., 128 (1994), pp. 165–205.

[2] J.-P. Aubin, *Un théorème de compacité*, C. R. Acad. Sci. Paris, 256 (1963), pp. 5042–5044.

[3] B. V. Bazaliy and A. Friedman, *A free boundary problem for an elliptic-parabolic system: application to a model of tumor growth*, Comm. Partial Differential Equations, 28 (2003), pp. 517–560.

[4] L. Berlyand, M. Potomkin, and V. Rybalko, *Non-uniqueness in a nonlinear sharp interface model of cell motility.* arXiv preprint arXiv:1409.5925v1, 2014.

[5] ——, *Phase-field model of cell motility: traveling waves and sharp interface limit*, C. R. Math. Acad. Sci. Paris, 354 (2016), pp. 986–992.

[6] ——, *Sharp interface limit in a phase field model of cell motility*, Netw. Heterog. Media, 12 (2017), pp. 551–590.

[7] F. Bernis and A. Friedman, *Higher order nonlinear degenerate parabolic equations*, J. Differential Equations, 83 (1990), pp. 179–206.

[8] A. L. Bertozzi and M. Pugh, *The lubrication approximation for thin viscous films: regularity and long-time behavior of weak solutions*, Comm. Pure Appl. Math., 49 (1996), pp. 85–123.

[9] C. Blanch-Mercader and J. Casademunt, *Spontaneous motility of actin lamellar fragments*, Phys. Rev. Lett., 110 (2013), p. 078102.

[10] G. Caginalp and P. C. Fife, *Dynamics of layered interfaces arising from phase boundaries*, SIAM J. Appl. Math., 48 (1988), pp. 506–518.

[11] A. Callan-Jones and R. Voituriez, *Active gel model for amoeboid cell motility*, New J. Phys., 15 (2013), p. 025022.

[12] X. Chen, *The Hele-Shaw problem and area-preserving curve-shortening motions*, Arch. Rational Mech. Anal., 123 (1993), pp. 117–151.

[13] ——, *Global asymptotic limit of solutions of the Cahn-Hilliard equation*, J. Differential Geom., 44 (1996), pp. 262–311.

[14] X. Chen and A. Friedman, *A free boundary problem for an elliptic-hyperbolic system: an application to tumor growth*, SIAM J. Math. Anal., 35 (2003), pp. 974–986.

[15] T. Cieślak, P. Laurençot, and C. Morales-Rodrigo, *Global existence and convergence to steady states in a chemorepulsion system*, in Parabolic and Navier-Stokes equations. Part 1, vol. 81 of Banach Center Publ., Polish Acad. Sci. Inst. Math., Warsaw, 2008, pp. 105–117.

[16] P. Constantin and M. Pugh, *Global solutions for small data to the Hele-Shaw problem*, Nonlinearity, 6 (1993), pp. 393–415.

[17] A. Cucchi, A. Mellet, and N. Meunier, *A Cahn-Hilliard model for cell motility*, SIAM J. Math. Anal., 52 (2020), pp. 3843–3880.

[18] M. C. Dallaston and S. W. McCue, *Bubble extinction in Hele-Shaw flow with surface tension and kinetic undercooling regularization*, Nonlinearity, 26 (2013), pp. 1639–1665.

[19] ——, *Corner and finger formation in Hele-Shaw flow with kinetic undercooling regularisation*, European J. Appl. Math., 25 (2014), pp. 707–727.

[20] J. Escher and G. Simonett, *Classical solutions of multidimensional Hele-Shaw models*, SIAM J. Math. Anal., 28 (1997), pp. 1028–1047.

[21] B. P. J. Gardiner, S. W. McCue, M. C. Dallaston, and T. J. Moroney, *Saffman-Taylor fingers with kinetic undercooling*, Phys. Rev. E, 91 (2015), p. 023016.

[22] D. Gilbarg and N. S. Trudinger, *Elliptic partial differential equations of second order*, Springer-Verlag, Berlin, second ed., 1983.

[23] K. Glasner, *A diffuse interface approach to Hele-Shaw flow*, Nonlinearity, 16 (2003), pp. 49–66.

[24] W. R. Holmes and L. Edelstein-Keshet, *A comparison of computational models for eukaryotic cell shape and motility*, PLoS Comput. Biol., 8 (2012), pp. 1–17.

[25] J.-F. Joanny, F. Jülicher, K. Kruse, and J. Prost, *Hydrodynamic theory for multi-component active polar gels*, New. J. Phys., 422 (2007).

[26] J.-F. Joanny and J. Prost, *Active gels as a description of the actin-myosin cytoskeleton*, HFSP J., 3 (2009), pp. 94–104.

[27] F. Jülicher, K. Kruse, J. Prost, and J.-F. Joanny, *Active behavior of the cytoskeleton*, Phys. Rep., 449 (2007), pp. 3–28.

[28] K. Keren, Z. Pincus, G. M Allen, E. L Barnhart, G. Marriott, A. Mogilner, and J. A Theriot, *Mechanism of shape determination in motile cells*, Nature, 453 (2008), pp. 475–80.

[29] N. Q. Le, *A gamma-convergence approach to the Cahn-Hilliard equation*, Calc. Var. Partial Differential Equations, 32 (2008), pp. 499–522.

[30] P. Maiuri et al., *Actin flows mediate a universal coupling between cell speed and cell persistence*, Cell, 161 (2015), pp. 374–386.

[31] R. H. Nochetto, A. J. Salgado, and S. W. Walker, *A diffuse interface model for electrowetting with moving contact lines*, Math. Models Methods Appl. Sci., 24 (2014), pp. 67–111.

[32] F. Otto, *Dynamics of labyrinthine pattern formation in magnetic fluids: a mean-field theory*, Arch. Rational Mech. Anal., 141 (1998), pp. 63–103.

[33] R. L. Pego, *Front migration in the nonlinear Cahn-Hilliard equation*, Proc. Roy. Soc. London Ser. A, 422 (1989), pp. 261–278.

[34] L. A. Romero, *The Fingering Problem in a Hele-Shaw Cell*, PhD thesis, California Institute of Technology, 1981.

[35] M. S. Mizuhara, L. Berlyand, V. Rybalko, and L. Zhang, *On an evolution equation in a cell motility model*, J. Phys. D: Appl. Phys, 318-319 (2016), pp. 12–25.

[36] E. Sandier and S. Serfaty, *Gamma-convergence of gradient flows with applications to Ginzburg-Landau*, Comm. Pure Appl. Math., 57 (2004), pp. 1627–1672.

[37] F. Ziebert and I. S. Aranson, *Computational approaches to substrate-based cell motility*, Npj Comput. Mater., 2 (2016).

[38] F. Ziebert, S. Swaminathan, and I. Aranson, *Model for self-polarization and motility of keratocyte fragments*, J. R. Soc. Interface, 9 (2011), pp. 1084–1092.

Chapter 3

Traveling Waves in the 2D case

This Chapter refers to the preprint [8] in collaboration with Mellet and Meunier.

3.1 Introduction of the free-boundary model and statement of the results

In this Chapter, we study the existence of Traveling Waves like solution for the following two-dimensional free boundary problem modeling the dynamics of a living cell

$$\begin{cases} \Delta p = 0 & \text{in } \Omega(t), \\ p + \beta f(V) = \gamma\kappa(t) & \text{on } \partial\Omega(t), \\ V = -\nabla p \cdot \mathbf{n} & \text{on } \partial\Omega(t), \\ \Omega(t=0) = \Omega_0. \end{cases} \tag{3.1}$$

Here the set Ω_0 is a bounded domain of $\mathbb{R}^2$, κ represents the mean curvature (positive for a circle) of the evolving free-boundary $\partial\Omega(t)$, $\mathbf{n}$ is the outward-pointing unit normal on $\partial\Omega(t)$, $\gamma \geq 0$ the surface tension is a given constant, $\beta \geq 0$ is a given constant, $f : \mathbb{R} \to \mathbb{R}$ is a given function, and V denotes the normal velocity of the moving free-boundary $\partial\Omega(t)$. In this problem, the domain $\Omega(t)$ represents the space occupied by the cell at time t whose boundary $\partial\Omega(t)$ is unknown and has to be determined together with the unknown function p representing the pressure inside the cell.

The above model comes from the work presented in Chapter **??**, where we study a Cahn-Hilliard model for cell motility and we showed that its formal Sharp Interface Limit leads to free-boundary problem (3.1). As we obtained previously, the function f satisfies the following assumptions

(A1) f is $\mathcal{C}^3(\mathbb{R})$, monotone increasing and odd such that $f(0) = 0$,
(A2) $\lim_{x\to+\infty} f(x) = 1$ and $\lim_{x\to-\infty} f(x) = -1$,
(A3) $f'(0) > 0$, $f''(0) = 0$ and $f'''(0) < 0$,
(A4) $f''(x) \leq 0\ \forall x > 0$ and $f''(x) \geq 0\ \forall x < 0$.

A prototype example of a function f satisfying the previous assumptions is the following

$$f(x) = \tanh(x).$$

The free-boundary problem (3.1) is more complicated than the usual Hele-Shaw problem which corresponds to the case where $\beta = 0$. Indeed, when $\beta \neq 0$ the boundary conditions writes as

$$p = \gamma\kappa(t) - \beta f(-\nabla p \cdot \mathbf{n})$$

which represents a Robin boundary value problem. This represents the originality of our problem, which describes (in some singular limit) the effects of polymerization. Indeed, the term $-\beta f(V)$

can be modelled as a pushing force against the membrane of the cell which generates protrusions responsible of the displacement of the cell [15, 23].

More precisely, unlike in the classical Hele-Shaw equation with surface tension, it is not clear whether the perimeter $\mathcal{P}(\Omega(t))$, defined by $\mathcal{P}(\Omega(t)) = \int_{\partial\Omega(t)} \mathrm{d}\sigma$, is or is not a Lyapunov functional for (3.1). Indeed by using a classical computation done by Otto in [21], we have that

$$\begin{aligned} \frac{\mathrm{d}}{\mathrm{d}t}\mathcal{P}(\Omega(t)) &= \int_{\partial\Omega(t)} \kappa V \,\mathrm{d}\sigma = -\frac{1}{\gamma}\int_{\partial\Omega(t)} P\nabla P\cdot\mathbf{n}\,\mathrm{d}\sigma + \frac{\beta}{\gamma}\int_{\partial\Omega(t)} V f(V)\,\mathrm{d}\sigma \\ &= -\frac{1}{\gamma}\int_{\Omega(t)} |\nabla P|^2\,\mathrm{d}x\,\mathrm{d}y + \frac{\beta}{\gamma}\int_{\partial\Omega(t)} V f(V)\ \mathrm{d}\sigma, \end{aligned} \tag{3.2}$$

where $\mathrm{d}\sigma$ denotes the infinitesimal length element of $\partial\Omega(t)$. By using the assumptions (A1) – (A3) for the function f we have that

$$V f(V) \geq 0.$$

Therefore, the last term in the right-hand side of (3.2) has opposite sign with respect to the first term. We will see later more details on the effect of the term $-\beta f(V)$ but we can see by these calculus that it has a destabilzing effect on the system, while the surface tension term has a stabilizing effect.

A particular case of the boundary condition $(3.1)_2$ with $\beta > 0$ is the so-called undercooling case studied in the work of Dallaston [9] In this case, the function f is a monotone decreasing function of the form $f(x) = -x$ leading to the following boundary condition

$$p = \gamma\kappa(t) + \beta\nabla p\cdot\mathbf{n}.$$

It was proved that the term $\beta\nabla p\cdot\mathbf{n}$ has a stabilizing effect on the problem. Our case differs from this one since f is a monotone increasing function.

We notice also that the model (3.1) is area preserving, thanks to the incompressibility condition. Indeed, we have that

$$\frac{\mathrm{d}}{\mathrm{d}t}|\Omega(t)| = \int_{\partial\Omega(t)} V\,\mathrm{d}\sigma = -\int_{\partial\Omega(t)} \nabla P\cdot\mathbf{n}\,\mathrm{d}\sigma = -\int_{\Omega(t)} \Delta P\,\mathrm{d}x\,\mathrm{d}y = 0. \tag{3.3}$$

Since $f(0) = 0$ the disk B_{R_0} of radius R_0 is the unique stationary solution of the problem (3.1) with

$$p = \gamma/R_0$$

and $|\Omega_0| = |B_{R_0}|$.

In the last section of Chapter 2, we rigorously investigate the properties of the problem (3.1) in the one dimensional case. We proved that it admits Traveling Wave like solutions when the destabilizing term on the boundary condition is strong enough. In particular, we proved the existence of a threshold value $\beta_{\mathrm{th}} > 0$ such that if $\beta \leq \beta_{\mathrm{th}}$ then there exists only one stationary solution and no Traveling Wave, but if $\beta > \beta_{\mathrm{th}}$, there exist (at least) two additional solutions which are Traveling Wave like solutions moving with non-zero constant velocity to the left or to the right.

This Chapter is dedicated to the analysis of the existence of Traveling Wave like solutions of the free boundary problem (3.1) in the two dimensional case.

Before stating our results, we briefly comment the literature on free boundary problems in the physiscs and biophysics domains. Moving boundary problems have raised many interesting and challenging mathematical issues. A well known example is the Stefan problem describing the dynamics of the boundary between ice and water. In the biophysical community, we find a large number of free boundary models to describe tumor and tissue growth, cell motility and other important phenomena. We refer to the works of Shao et al. [22] and the work of Ziebert and Aranson [23] for a review. Most of these models are formulated via a fluid approach with surface tension. Some tumour growth models presented in the work of Friedman et al. [11–13] resemble

to our model (3.1). There is however an important difference: tumor growth naturally involves growth (shrinking) areas while we consider here incompressible solutions. Some cell motility models presented in [2–4, 17, 18] have some similarities with our model. Nevertheless, these are obtained as the limit of an order 2 of Allen-Cahn type equation while we obtain ours as the limit of an order 4 of Cahn-Hilliard type equation. On the other hand, the model studied in [4] involves a nonlinear coupling with a partial differential equation stated in the bulk. Finally, in the work of Günther and Proker [14] travelling wave solutions for a moving boundary problem of Hele-Shaw type has been studied in the case with kinetic undercooling regularization.

A remarkable feature of cell motility is the occurrence of sustained motion in a given direction without exterior impulse. This phenomenon, known as self-polarization, is mathematically described by the existence of traveling wave solutions and thus this study validates the interest of this model to describe cell motility. Traveling wave solutions correspond to a fixed shape domain moving by translation with constant velocity in a given direction, that is

$$\Omega(t) = \Omega_0 + ct\mathbf{u}, \tag{3.4}$$

for some speed c and direction of motion $\mathbf{u}$. In the sequel we refer to (Ω_0, c) as a traveling wave solution of (3.1) if the set $\Omega(t)$ defined by (3.4) is a solution of (3.1). The stationary solution B_{R_0} is a traveling wave solution with zero speed. It is referred to as trivial solution of (3.1). Note that the problem is isotropic so we will always consider $\mathbf{u} = \mathbf{e}_x = (1, 0)$ and $c > 0$.

This Chapter is dedicated to the proof of the following two theorems.

Theorem 3.1.1. *Assume that f satisfies assumptions (A1) – (A4). For all γ, $\beta > 0$, there exists a one parameter family of traveling wave solutions of (3.1) (with $\mathbf{u} = \mathbf{e}_x$) $(\Omega_\lambda, c_\lambda)$ parametrized by $\lambda \in (\frac{\gamma}{\beta f'(0)}, \infty)$ and satisfying:*

(i) $c_\lambda > 0$, Ω_λ is a convex set with $C^{2,1}$ boundary.

(ii) The set Ω_λ is of the form

$$\Omega_\lambda = \{(x, y)\,;\, x_L < x < x_R,\ -h(x) < y < h(x)\}$$

with $x_L < 0 < x_R$ and for some C^3 function h satisfying $h'(0) = 0$.

(iii) At the point $m = (0, h(0)) \in \partial\Omega_\lambda$ the normal vector $\mathbf{n}$ is the vertical vector $(0, 1)$ and the curvature is $\kappa(m) = \lambda/\gamma$.

Property (i) guarantees in particular that we are constructing non-trivial traveling wave solutions (i.e. not stationary solutions). Property (ii) fixes the natural invariance by translation of the model. Property (iii) relates the value of the parameter λ to some geometric property of Ω_λ. It proves that each value of λ yields of different traveling wave and it suggests that increasing values of λ correspond to sets with decreasing volume (something we are not presently able to prove).

While the proof of this theorem is constructive, it does not clearly identify, for a given volume, the critical value of β for which non trivial traveling waves start to exist. Our next theorem will identify this value precisely. Indeed, using a bifurcation argument, we can prove that a branch of traveling solution with non zero speed emerges from the trivial solution B_{R_0} at $\beta = \frac{R_0}{f'(0)}$. This is consistent with the condition $\kappa(m) = \lambda/\gamma > \frac{1}{\beta f'(0)}$ in the theorem above, since $\kappa = \frac{1}{R_0}$ for the disk.

Theorem 3.1.2. *Assume that f satisfies assumptions (A1) – (A4). The problem (3.1) has a branch of traveling wave solutions bifurcating from the radial solution B_{R_0} at $\beta = \frac{R_0}{f'(0)}$, with the bifurcation solution having the following form:*

$$\begin{cases} \beta(s) &= \frac{R_0}{f'(0)} + \alpha s^2 + o(s^2), \\ c(s) &= s + o(s), \end{cases} \tag{3.5}$$

where $\alpha > 0$ and s represents a small parameter. Moreover, the bifurcation appears via a Pitchfork bifurcation.

This theorem shows that at least for some $\beta > \frac{R_0}{f'(0)}$, there exists some traveling wave like solution moving in any direction with positive speed.

The organization of this Chapter is the following. In Section 3.2, we present the biological justification of the problem (3.1). In Section 3.3, we recall some useful basic facts such that the definition of a Traveling Wave like solution to the problem (3.1) and bifurcation's Theory in Banach spaces. The Section 3.4 is devoted to the proof of Theorem 3.1.1 and Section 3.5 to the proof of the Theorem 3.1.2. In Section 3.6 we present a numerical method and we show some particular numerical simulations. Finally, we give some conclusions.

3.2 Biological justification of the model

In the biological physics community, we find a huge number of macroscopic models for cell motility. We refer to the work of Aranson and Ziebert [23] for a review. Most of them are formulated through a fluid approach with surface tension. As far as we know, the works that study some mathematical aspects (bifurcation, Traveling Wave) of models for cell motility and polarization are the works of Beryland et. al. [2–4], the work of Mizuhara et al. [17, 18] and our recent work in collaboration with Meunier and Mellet [7] for free boundary models, and the work of Calvez et. al. [5] and the work of Etchegaray et. al. [10] for cell polarization. The other works are either computational or modeling focused.

In this part we describe the origin of the problem (3.1). On the one hand, it is obtained as a sharp interface limit of a Cahn-Hilliard model to describe the motion of a cell on a two dimansional substrate presented in Chapter **??** and refering to [7]. On the other hand, it is (informally) the first order perturbation of a coupled free boundary model of the type of the model introduced in [16]. Finally, we explain the biophysical meaning of the boundary term $-\beta f(V)$.

Sharp Interface Limit of the phase field model introduced in [7]

In [7], we introduced the following phase-field model to describe the motion of a cell on a two dimensional substrate

$$\begin{cases} \partial_t \rho = \operatorname{div}\left(\rho \nabla\left[\gamma\left(-\varepsilon\Delta\rho + \frac{1}{\varepsilon}W'(\rho)\right) + \phi\right]\right), \\ \partial_t \phi - \varepsilon\Delta\phi = \frac{1}{\varepsilon}\left(\beta\rho - \phi\right), \end{cases} \tag{3.6}$$

with $\varepsilon > 0$, $\gamma > 0$, $\beta \geq 0$ and W a double-well potential satisfying

$$W(0) = W(1) = 0, \quad W(\rho) > 0 \text{ if } \rho \notin \{0, 1\}. \tag{3.7}$$

An example of an admissible double-well potential is $W(\rho) = \rho^2(1-\rho)^2$.

From a modeling point of view, the system (3.6) is very simple. Two quantities are used to describe the cell: the phase field (or order parameter) ρ, describing everything that lies inside the cell (cytoskeleton, solvent, molecular motors...), and the Myosin II, a molecular motor that assembles in minifilaments, interacts with actin, behaves as active crosslinkers and generates contractile or dilative stresses in the cytoskeleton network, whose concentration is denoted by ϕ. The main assumptions that lead to (3.6) are the following: (i) the cell velocity v is given by the local actin flow, (ii) Myosin II in the bulk is slowly diffusing, (iii) actin filaments undergo uniform bulk polymerization and depolymerization, (iv) the osmotic pressure involved in the network stress acts to saturate the linear instability causing gel phase separation and to smooth the interface between cytosol-rich and cytosol-poor regions. The underlying processes is composed by the friction of the cytosol on the substrate together with the active character of the Myosin II.

When $\varepsilon \ll 1$, we showed in [7] that this model is close to the free-boundary problem (3.1) in which the cell is described by a set $\Omega(t)$ (so $\rho^\varepsilon(x,t) \sim \chi_{\Omega(t)}(x)$).

First order perturbation of a coupled free boundary model

Consider the cytoplasm as a confined viscous droplet that is driven on its boundary (i.e., the cell membrane) by an active force induced by the cytoskeleton. Biologically, such a force can be generated either by polymerization of actin against the membrane or by contraction of cortical actomyosin filaments, which adhere to the membrane. Suppose the active force is controlled by a diffusive chemical solute which is advected by the internal cytoplasmic flow. More precisely, consider the following 2D free-boundary problem

$$\Delta p = 0 \qquad \text{in } \Omega(t)\,, \tag{3.8}$$

$$p + \beta f(\nabla\phi \cdot \mathbf{n}) = \gamma\kappa \qquad \text{on } \partial\Omega(t)\,, \tag{3.9}$$

$$V = -\nabla p \cdot \mathbf{n} \qquad \text{on } \partial\Omega(t)\,. \tag{3.10}$$

where ϕ follows an advection-diffusion equation

$$\partial_t\phi + (a-1)\nabla p \cdot \nabla\phi - \Delta\phi = 0 \qquad \text{in } \Omega(t), \tag{3.11}$$

$$\nabla\phi \cdot \mathbf{n} = a\phi\nabla p \cdot \mathbf{n} \qquad \text{on } \partial\Omega(t), \tag{3.12}$$

with $a \in [0, 1)$ being a given constant.

Equation (3.8) states the fluid mass-balance equation (incompressibility condition). The normal force balance on the droplet boundary $\partial\Omega(t)$ is given in (3.9). Note that the Young-Laplace condition is perturbed in this model by an active force, $f(\nabla\phi \cdot \mathbf{n})\mathbf{n}$ which is locally controlled by the normal derivative of the concentration of an internal solute, ϕ. The kinematic condition states that the normal velocity of the sharp interface, V, is given by the normal velocity of the fluid on $\partial\Omega(t)$. In the convection-diffusion dynamics given in (3.11), the total (convective + diffusive) solute flux is $j = (1-a)(-\nabla P)\phi - \nabla\phi$. In (3.12), we impose zero solute flux on the moving boundary, i.e., $j \cdot \mathbf{n} - V\phi = 0$, where we insert the kinematic condition, Eq. (3.10). Simply put, the solute is convected at a slower velocity than that of the fluid. Hence, its concentration decreases (increases) towards an advancing (retracting) front. Note that a similar coupled free boundary model of polarization, migration and deformation of a living cell has recently been introduced in [16].

The problem (3.8) – (3.12) possesses a unique radially symmetric solution of prescribed area and total solute concentration with both $P = P^*$ and $\phi = \phi^*$ being constant.

Consider a small perturbation of ϕ and p around ϕ^* and p^*, that is

$$\phi(t, x, y) = \phi^* + \varepsilon\tilde{\phi}(t, x, y) + \mathcal{O}(\varepsilon^2) \quad \text{and} \quad p(t, x, y) = p^* + \varepsilon\tilde{p}(t, x, y) + \mathcal{O}(\varepsilon^2).$$

In such a case we have

$$\nabla\phi(t, x, y) = \varepsilon\nabla\tilde{\phi}(t, x, y) + \mathcal{O}(\varepsilon^2),$$

and

$$\phi(t, x, y)\nabla p(t, x, y) = \varepsilon\phi^*\nabla\tilde{p}(t, x, y) + \mathcal{O}(\varepsilon^2),$$

hence, at order $\mathcal{O}(\varepsilon)$, the boundary condition (3.12) writes

$$\nabla\tilde{\phi}(t, x, y) \cdot \mathbf{n} = \phi^*\nabla\tilde{p}(t, x, y) \cdot \mathbf{n},$$

which yields the problem (3.1).

Biophysical meaning of the boundary term $-\beta f(V)$

For each $t > 0$, we define the moment $\mathcal{M}_{\Omega(t)}$ of $\Omega(t)$ by

$$\mathcal{M}_{\Omega(t)} = \int_{\Omega(t)} (x, y)\,\mathrm{d}x\,\mathrm{d}y\,,$$

where $z = (x, y)$ is the vector coordinate of a point in $\Omega(t)$. In particular, $\mathcal{M}_{\Omega(t)}$ is a vector containing the x-moment and y-moment.

We define the center of mass $\mathcal{C}_{\Omega(t)}$ by

$$\mathcal{C}_{\Omega(t)} = \frac{\mathcal{M}_{\Omega(t)}}{|\Omega(t)|} = \frac{1}{|\Omega(t)|}\int_{\Omega(t)}(x,y)\,\mathrm{d}x\,\mathrm{d}y = \frac{1}{|\Omega_0|}\int_{\Omega(t)}(x,y)\,\mathrm{d}x\,\mathrm{d}y\,, \tag{3.13}$$

by using the area preservation (3.3).

The velocity $u_{\mathcal{C}}(t)$ of the center of mass of $\Omega(t)$ is given by

$$u_{\mathcal{C}}(t) = \frac{\mathrm{d}}{\mathrm{d}t}\mathcal{C}_{\Omega(t)}. \tag{3.14}$$

From incompressibility $(3.1)_1$ and boundary condition $(3.1)_2$, we deduce that

$$\begin{aligned}
\frac{\mathrm{d}}{\mathrm{d}t}\mathcal{M}_{\Omega(t)} &= \int_{\partial\Omega(t)} zV\,\mathrm{d}\sigma = -\int_{\partial\Omega(t)} z\nabla p\cdot\mathbf{n}\,\mathrm{d}\sigma \\
&= -\int_{\Omega(t)} \mathrm{div}\,(z\nabla p)\,\mathrm{d}x\,\mathrm{d}y = -\int_{\Omega(t)} \nabla p\cdot\nabla z\,\mathrm{d}x\,\mathrm{d}y \\
&= -\int_{\Omega(t)} \mathrm{div}\,(p\nabla z)\,\mathrm{d}x\,\mathrm{d}y = -\int_{\partial\Omega(t)} p\nabla z\cdot\mathbf{n}\,\mathrm{d}\sigma \\
&= -\int_{\partial\Omega(t)} (\gamma\kappa + \beta f(V))\,\nabla z\cdot\mathbf{n}\,\mathrm{d}\sigma\,.
\end{aligned} \tag{3.15}$$

Using that $\nabla z\cdot\mathbf{n}$ is the unit outwards normal vector to $\partial\Omega(t)$ and that

$$\int_{\partial\Omega(t)} \kappa\mathbf{n}\,\mathrm{d}\sigma = \mathbf{0},$$

it follows that

$$u_{\mathcal{C}}(t) = -\frac{\beta}{|\Omega_0|}\int_{\partial\Omega(t)} f(V)\mathbf{n}\,\mathrm{d}\sigma\,. \tag{3.16}$$

We recognize the equation (3.16) as the external force balance equation on the droplet $\Omega(t)$. This justifies our model 3.1 describing the motion of the cell given by the active force $-\beta f(V)$ (representing the activity of the cytoskeleton) which acts by deforming the cell membrane.

3.3 A brief account on some useful facts

In this section we recall some useful facts concerning bifurcation theory in Banach spaces and the definition of a Traveling Wave like solution of the problem (3.1). conditions.

3.3.1 Crandall-Rabinovitz's bifurcation theorem

Let U, V be two real Banach spaces. Our aim will be to analyze the structure of the solution set of the possibly nonlinear operator $\mathcal{F}$ given by

$$\mathcal{F}(\lambda, u) = 0, \quad (\lambda, u) \in \mathbb{R}\times U,$$

where

$$\mathcal{F} : \mathbb{R}\times U \to V$$

is a continuous map. We shall use the Crandall-Rabinovitz's bifurcation theorem to prove the Theorem (3.1.2). For the convenience of the reader, in this section we state the theorem.

Theorem 3.3.1 (Crandall-Rabinovitz's Theorem [6]). *Let U, V be two Banach spaces, W a neighborhood of $(\lambda_0, 0)$ in $\mathbb{R} \times U$ and $\mathcal{F} : W \longrightarrow V$. Suppose that the following properties are satisfied*

1. *$\mathcal{F}(\lambda, 0) = 0$ for all λ in a neighborhood of λ_0;*
2. *The Fréchet partial derivatives $\mathcal{D}_u \mathcal{F}, \mathcal{D}_\lambda \mathcal{F}, \mathcal{D}_{\lambda u} \mathcal{F}$ exist and are continuous;*
3. *$\operatorname{Ker} \mathcal{D}_u \mathcal{F}(\lambda_0, 0)$ is a one dimensional subspace of U spanned by a nonzero vector $u_0 \in U$;*
4. *$\operatorname{Range} \mathcal{D}_u \mathcal{F}(\lambda_0, 0)$ is a closed subspace of V of codimension 1;*
5. *$\mathcal{D}_{\lambda u} \mathcal{F}(\lambda_0, 0)[u_0] \notin \operatorname{Range} \mathcal{D}_u \mathcal{F}(\lambda_0, 0)$.*

If Z is any complement of $\operatorname{Ker} \mathcal{D}_u \mathcal{F}(\lambda_0, 0)$ in U, then, there is a neighborhood N of $(\lambda_0, 0)$ in $\mathbb{R} \times U$, an interval $I = (-\varepsilon, \varepsilon)$ for some $\varepsilon > 0$ and two continuous functions

$$\varphi : (-\varepsilon, \varepsilon) \longrightarrow \mathbb{R}, \quad \psi : (-\varepsilon, \varepsilon) \longrightarrow Z$$

such that $\varphi(0) = \lambda_0$, $\psi(0) = 0$ and

$$\mathcal{F}^{-1}[0] \cap U = \{(\varphi(s), su_0 + s\psi(s)) : |s| < \varepsilon\} \cup \{(\lambda, 0) : (\lambda, 0) \in N\}.$$

If $\mathcal{D}_{uu} \mathcal{F}$ is continuous then the functions φ and ψ are once continuously differentiable.

In Theorem **??**, the point $(\lambda_0, 0) \in \mathbb{R} \times U$ is a bifurcation point of the equation $\mathcal{F}(\lambda, u) = 0$ in the following sense. In a neighborhood of $(\lambda_0, 0)$, the set of solutions of $\mathcal{F}(\lambda, u) = 0$ consists of two curves Γ_1 and Γ_2 which intersect only at the point $(\lambda_0, 0)$, where

$$\Gamma_1 = \{(\lambda, 0) \text{ where } \lambda = \lambda_0\},$$

and Γ_2 is the curve parametrized by

$$\Gamma_2 = \{(\lambda(s), u(s)), \text{ for } |s| \text{ small, and such that } (\lambda(0), u(0)) = (\lambda_0, 0), \text{ with } u'(0) = u_0,\ \lambda'(0) \neq 0\}.$$

3.3.2 Definition of Traveling Wave like solutions of the model

By Traveling Wave like solution of (3.1) we mean a solution of the problem (3.1) which corresponds to a fixed shape domain moving by translation with constant velocity in a given direction, that is

$$\Omega(t) = \Omega_0 + ct\mathbf{u}$$

for some velocity $c \in \mathbb{R}$ and direction of motion $\mathbf{u} \in \mathbb{R}^2$. Without loss of generality, we will assume that $\Omega(t)$ translates along the x-axis with positive velocity, that is $c > 0$ and $\mathbf{u} = \mathbf{e}_x = (1, 0)$. In that case, the boundary velocity given by the condition $(3.1)_1$ writes as

$$V = c(\mathbf{e}_x \cdot \mathbf{n}). \tag{3.17}$$

In this context a Traveling Wave like solution to (3.1) is defined as following.

Definition 3.3.2. *A Traveling Wave like solution to (3.1) is given by a domain $\Omega_0 \in \mathbb{R}^2$, a positive real number c and a function $P(\cdot)$ defined on Ω_0 satisfying*

$$\begin{cases} -\Delta p = 0 & \text{in } \Omega_0, \\ p = \gamma\kappa - \beta f(c\,\mathbf{e}_x \cdot \mathbf{n}) & \text{on } \partial\Omega_0, \\ -\nabla p \cdot \mathbf{n} = c(\mathbf{e}_x \cdot \mathbf{n}) & \text{on } \partial\Omega_0. \end{cases} \tag{3.18}$$

Remarkably, the condition (3.18) mandates that the entire fluid bulk flows at a uniform speed, that is $\nabla p = -(c, 0)$ in Ω_0. More precisely the following result gives the characterization of a Traveling Wave like solution to the problem (3.1).

Proposition 3.3.3. *Any Traveling Wave like solution to (3.1) moving with velocity $c > 0$ in x-direction is given by a domain $\Omega_0 \subset \mathbb{R}^2$ and a real number λ such that the following condition holds*

$$\lambda - cx = \gamma\kappa - \beta f(c(\mathbf{e}_x \cdot \mathbf{n})) \quad \text{on } \partial\Omega_0. \tag{3.19}$$

Proof. We fist note that the first and last equations of (3.18) are equivalent to the existence of a constant λ such that $p(x, y) = \lambda - cx$ in Ω_0. Indeed, the function p has to satisfy

$$\begin{cases} -\Delta p = 0 & \text{in } \Omega_0, \\ -\nabla[p + cx] \cdot \mathbf{n} = \mathbf{0} & \text{on } \partial\Omega_0. \end{cases}$$

and by integration by parts we get that $\int_{\Omega_0} |\nabla(p + cx)|^2 \, \mathrm{d}x \, \mathrm{d}y = 0$. The system (3.18) is thus equivalent to (3.19). □

In this problem, the set Ω_0 and the speed c must be found together. The parameter λ can be seen as a Lagrange multiplier for the volume of Ω_0, but the problem is invariant by translation. Any translation of Ω_0 leads to a solution of (3.19), with the same c but a different value of λ.

3.4 Proof of Theorem 3.1.1

This section is devoted to the proof of Theorem 3.1.1 and give a constructive proof of the existence of traveling wave solutions to (3.1) when β/γ is large enough. This approach can be used to find these traveling wave solution numerically, see Figure 3.1.

Given λ large enough, we look for a set Ω_λ solution of (3.19) in the form:

$$\Omega_\lambda = \{(x, y) \in \mathbb{R}^2 \, ; \, x_L < x < x_R, \; -h(x) < y < h(x)\}. \tag{3.20}$$

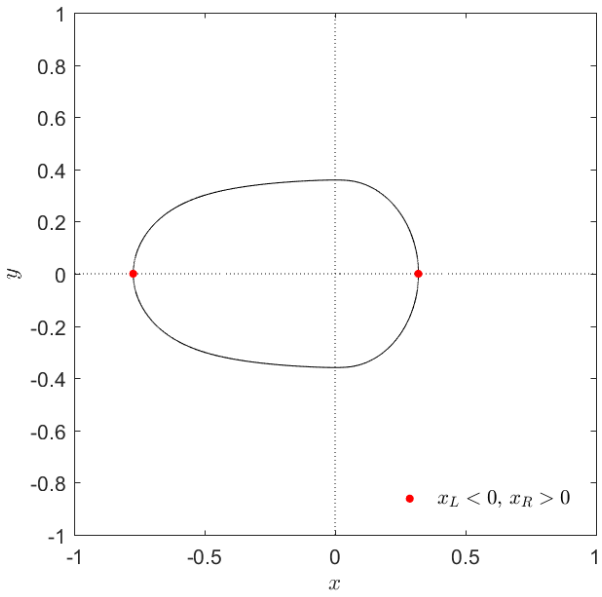

Figure 3.1 – A shape of traveling wave solution Ω_0 defined by (3.20) for $\beta/\lambda = 4$ and $\gamma = 1$. The red dots indicate the point $x_L < 0$ on the left and $x_R > 0$ on the right. The function $h(x)$ is defined for $x \in [x_L, x_R]$ such that conditions (3.21) – (3.22) hold. The graph of h lies on the y-positve part of the plane, while the graph of $-h$ on the y-negative part.

for some function $h(x)$ defined and positive on an interval (x_L, x_R) and satisfying:

$$\begin{cases} h(x_L) = h(x_R) = 0, \\ h'(x_L) = -\infty, \\ h'(x_R) = +\infty. \end{cases} \tag{3.21}$$

We will further fix the invariance by translation in the $\mathbf{e}_x$ direction by requiring that

$$x_L < 0 < x_R, \quad h'(0) = 0. \tag{3.22}$$

Finally, we note that it is enough to prove the result when $\gamma = 1$ up to replacing the coefficients β and λ by β/γ and λ/γ and the function f by $x \mapsto f(\gamma x)$.

Our first task is to write equation (3.19) with (3.20) – (3.21) in term of the function $h(x)$. Note that the boundary conditions (3.21) concern the function h and also its derivative h'. It is natural then to identify a problem for which h' is solution and then find the function h. For this reason, we change variables. We first notice that the tangent vector $\mathbf{t}$, the normal vector $\mathbf{n}$ and the mean-curvature κ are defined by

$$\mathbf{t} = -\frac{(1, h'(x))}{\sqrt{1 + (h'(x))^2}}, \quad \mathbf{n} = \frac{(-h'(x), 1)}{\sqrt{1 + (h'(x))^2}}, \quad \kappa = -\frac{h''(x)}{(1 + (h'(x))^2)^{3/2}}.$$

These quantities can be written easily using the function $Y(x)$ defined by

$$Y(x) = \mathbf{e}_x \cdot \mathbf{n} = \mathbf{n}_x = -\frac{h'(x)}{\sqrt{1 + (h'(x))^2}}. \tag{3.23}$$

In particular, we have

$$\kappa = Y'(x)$$

which is consistent with Frenet's formula $n'_x = -\kappa \mathbf{t}_x$.

Equation (3.19) (with $\gamma = 1$) and condition (3.22) then reduce to the following initial value problem:

$$\begin{cases} Y'(x) = \lambda - cx + \beta f(c\, Y(x))), \quad \text{on } (x_L, x_R), \\ Y(0) = 0. \end{cases} \tag{3.24}$$

while the boundary conditions $(3.21)_{2,3}$ imply

$$Y(x_L) = -1 \quad \text{and} \quad Y(x_R) = +1. \tag{3.25}$$

Finally, we recover the function h inverting (3.23) to find

$$h'(x) = -\frac{Y(x)}{\sqrt{1 - Y^2(x)}}. \tag{3.26}$$

We can thus find h by integrating this relation on (x_L, x) and the boundary condition $(3.21)_1$ requires the function Y to satisfy:

$$\int_{x_L}^{x_R} -\frac{Y(x)}{\sqrt{1 - Y^2(x)}}\, \mathrm{d}x = 0. \tag{3.27}$$

The main result of this section is the following proposition, which implies Theorem 3.1.1:

Proposition 3.4.1. *Given lambda* 0. *For all* β *such that*

$$\beta \lambda f'(0) > 1, \tag{3.28}$$

there exists $c > 0$, x_L *and* x_R *such that the solution* $Y(x)$ *of* (3.24) *satisfies the conditions* (3.25) *and* (3.27).

Proof of Theorem 3.1.1. With $Y(x)$ given by Proposition 3.4.1, we set

$$h(x) = \int_{x_L}^{x} -\frac{Y(x)}{\sqrt{1-Y^2(x)}}\,dx \qquad x \in [x_L, x_R].$$

Condition (3.27) implies that $h(x_L) = h(x_R) = 0$ and we define the set Ω_λ by (3.20). The boundary conditions (3.25) implies that the normal vector is continuous (it achieves the values $(-1, 0)$ and $(1, 0)$ continuously at the extremal points $(x_L, 0)$ and $(x_R, 0)$). This means that $\partial\Omega_\lambda$ is C^1.

Furthermore, we have $\kappa(x) = Y'(x)$ and so Proposition 3.4.6 implies that

$$0 \le \kappa \le \lambda + \beta + c\beta f'(0) \text{ on } \partial\Omega_\lambda$$

which implies that Ω_λ is convex and that $\partial\Omega_\lambda$ is $C^{1,1}$. In turns, (3.24) can be used to show that Y', and therefore κ is Lipschitz continuous so that the boundary $\partial\Omega_\lambda$ is $C^{2,1}$ and satisfies (3.19).

Finally, it is readily seen that $h'(0) = 0$ (since $Y(0) = 0$) and (3.24) implies that the mean-curvature of $\partial\Omega_\lambda$ at the point $(0, h(0))$ is given by $Y'(0) = \lambda$. □

The remainder of this section is devoted to the proof of Proposition 3.4.1. We first find the set of parameters for which the points x_L and x_R satisfying the condition (3.25) exist. In particular, we prove that the existence of x_L depends on λ and β, while for x_R also the parameter c is involved. This is done in Section 3.4.1. The existence of the solution Y is then given by regularity properties of the problem (3.24). We then fix the parameters λ and β such that x_L exists, by considering the solutions of (3.24) for those values of c such that also x_R exists, we will prove, in Section 3.4.2, that there exists a value $c^* > 0$ (depending on λ and β) such that the condition (3.27) is verified.

Remarks 3.4.2. *If we are looking for a traveling wave with $c > 0$, we must have $\lambda \ge 0$. Indeed, if $\lambda < 0$, then $Y'(0) < 0$ and the boundary conditions (3.25) imply that there exists two points $x_1 \in (x_L, 0)$ and $x_2 \in (0, x_R)$ such that $Y(x_1) > 0$, $Y(x_2) < 0$ and $Y'(x_1) = Y'(x_2) = 0$. Equation (3.24) then gives:*

$$cx_1 - \beta f(cY(x_1)) = cx_2 - \beta f(cY(x_2)) = \lambda,$$

which is a contradiction since the first term is negative and the second term is positive.

3.4.1 Proof of Proposition 3.4.1, part I: Existence of x_L and x_R

The first proposition gives the existence of x_L when β is large enough, for a fixed λ, and for all $c > 0$.

Proposition 3.4.3. *Let λ be fixed. Let $\beta > 0$ be such that (3.28) holds. For all $c > 0$, there exists a point $x_L < 0$ such that the solution of (3.24) satisfies $-1 < Y(x) < 0$ for all $x \in (x_L, 0)$ and $Y(x_L) = -1$. Moreover, x_L is such that*

$$-\beta f'(0) < x_L < 0,$$

and we have

$$Y'(x) \ge \frac{1}{\beta f'(0)} \quad \forall x \in [x_L, 0]. \tag{3.29}$$

The concavity of f for $x > 0$, assumption (A4), together with $f(0) = 0$ and the boundednesse character of f imply that the function $c \mapsto \frac{f(c)}{c}$ is monotone decreasing with zero limit when $c \to +\infty$ and with limit $f'(0)$ when $c \to 0$. Therefore, given λ, β satisfying (3.28), there exists a unique $\bar{c} > 0$ such that

$$\frac{f(\bar{c})}{\bar{c}} = \frac{1}{\beta\lambda} < f'(0). \tag{3.30}$$

We prove next.

Proposition 3.4.4. *Let λ be given. Let $\beta > 0$ satisfy (3.28). There exists $c_{\max} > \bar{c}$ such that for all $c \in (0, c_{\max})$, there exists a point $x_R > 0$ such that the solution of (3.24) satisfies $0 < Y(x) < 1$ for all $x \in (0, x_R)$ and $Y(x_R) = 1$. Moreover, x_R is such that*

$$0 < x_R < \frac{\lambda + \beta}{c}, \tag{3.31}$$

and

$$\begin{cases} Y'(x_R) > 0, & \text{if } c < c_{\max}, \\ Y'(x_R) = 0, & \text{if } c = c_{\max}. \end{cases} \tag{3.32}$$

We start with the existence of x_L.

Proof of Proposition 3.4.3. Let

$$x_L = \inf\{a < 0\,;\, Y(x) \in (-1, 0) \text{ for all } x \in (a, 0)\}. \tag{3.33}$$

Since $Y'(0) = \lambda > 0$, we see that $x_L < 0$ and possibly $x_L = -\infty$ if $Y(x) > -1$ for all $x < 0$. We need to show that $x_L > -\infty$ and that $Y(x_L) = -1$.

The convexity of f for $x < 0$, assumption (A4), implies that the function $c \mapsto \frac{f(c)}{c}$ is monotone increasing:

$$f(y) > f'(0)\, y \quad \text{for all } y < 0,$$

hence

$$f(cY(x)) > f'(0)\, cY(x) \quad \text{for all } x \in (x_L, 0).$$

From (3.24) it follows that

$$Y'(x) > \lambda - c\,x + \beta f'(0) cY(x) \quad \text{for all } x \in (x_L, 0). \tag{3.34}$$

Denoting $\mu = c\beta f'(0) > 0$, we rewrite (3.34) as $(e^{-\mu\, x}\, Y(x))' > (\lambda - c\,x) e^{-\mu x}$ and using the condition $Y(0) = 0$ we deduce that

$$Y(x) < \left(\frac{\lambda}{\mu} - \frac{c}{\mu^2}\right)(e^{\mu\, x} - 1) + \frac{c}{\mu}\, x, \quad \text{for all } x \in (x_L, 0). \tag{3.35}$$

Recalling the assumption (3.28) we see that $\frac{\lambda}{\mu} - \frac{c}{\mu^2} > 0$. Since $e^{\mu\, x} - 1 < 0$ for $x < 0$, it follows that

$$Y(x) < \frac{c}{\mu}\, x, \quad \text{for all } x \in (x_L, 0). \tag{3.36}$$

The right-hand side of the previous inequality is monotone decreasing and converges towards $-\infty$ as $x \to -\infty$. Since $Y(x_L) \geq -1$, by definition of x_L, it follows that $x_L > -\infty$ and (3.36) implies that $Y(x_L) < 0$ so that we must have $Y(x_L) = -1$.

To prove (3.29), we note that the function $V(x) = Y'(x)$ solves

$$\begin{cases} V'(x) = -c + c\beta f'(cY(x)) V(x), \\ V(0) = \lambda > 0. \end{cases} \tag{3.37}$$

We thus define

$$x_0 = \inf\left\{x \in [x_L, 0]\,;\, V(y) \geq \frac{1}{\beta f'(0)} \quad \forall y \in [x, 0]\right\}. \tag{3.38}$$

First we see that condition (3.28) implies that $x_0 < 0$. Moreover if $x_0 > x_L$, then we must have

$$V(x_0) = \frac{1}{\beta f'(0)} \quad \text{and} \quad V'(x_0) \geq 0.$$

Recalling that $f'(y) < f'(0)$ for $y < 0$, from (3.37) it follows that

$$V'(x_0) = -c + c\beta f'(cY(x_0)) \frac{1}{\beta f'(0)} < -c + c\beta f'(0) \frac{1}{\beta f'(0)} = 0,$$

hence a contradiction. Consequently $x_0 = x_L$ and (3.29) follows. □

In order to prove Proposition 3.4.4, we first prove the following lemma:

Lemma 3.4.5. *Let $\lambda > 0$ and $\beta > 0$ be given. For any $c > 0$ there exists $0 < \bar{x} < \frac{\lambda+\beta}{c}$ such that the solution $Y(x)$ of (3.24) is increasing on $(0, \bar{x})$ and decreasing on $(\bar{x}, \infty)$. Furthermore, we have*

$$Y(\bar{x}) = \sup_{x\in(0,\infty)} Y(x) \leq \frac{(\lambda+\beta)^2}{2c}. \tag{3.39}$$

Proof of Lemma 3.4.5. Equation (3.24) implies $Y'(0) = \lambda > 0$ and since $f(y) \leq 1$ for all $y \in \mathbb{R}$ it also gives

$$Y'(x) \leq \lambda - cx + \beta \qquad \text{for all } x \in \mathbb{R} \tag{3.40}$$

hence $Y'(x) < 0$ for $x > \frac{\lambda+\beta}{c}$.

Recall that $V(x) = Y'(x)$ solves (3.37). Since $V(0) = \lambda > 0$, $V(x) = Y'(x) < 0$ for $x > \frac{\lambda+\beta}{c}$ and V is a continuous function, there exists a point $\tilde{x} > 0$ such that $V(\tilde{x}) = 0$. Moreover, whenever $V(\tilde{x}) = 0$ we have that $V'(\tilde{x}) = -c < 0$. This implies that V can only change sign once, the existence of $\bar{x}$ follows and $\bar{x} = \tilde{x}$. □

Proof of Proposition 3.4.4. In view of Lemma 3.4.5, x_R exists if and only if $Y(\bar{x}) > 1$ and in such a case we always have

$$x_R < \bar{x}. \tag{3.41}$$

Since this condition is satisfied for small c (see below), we define

$$c_{\max} = \sup\{c_0\,;\, Y(\bar{x}) > 1 \text{ for all } c \in [0, c_0)\}, \tag{3.42}$$

which is finite in view of (3.39). In fact we have $c_{\max} \leq \frac{(\lambda+\beta)^2}{2}$.

We now show that $c_{\max} > \bar{c}$. Define

$$x_R = \sup\{a > 0\,;\, Y(x) \in (0,1) \text{ for all } x \in (0,a)\}, \tag{3.43}$$

with possibly $x_R = +\infty$. Since $Y(0) = 0$ and $Y'(0) = \lambda > 0$, we note that $x_R > 0$. We are going to prove that $x_R < +\infty$ and that $Y(x_R) = 1$. From the concavity of f on $\mathbb{R}_+$, assumption (A4), it follows that

$$f(y) \geq \frac{f(c)}{c} y \qquad \text{for all } 0 \leq y \leq c,$$

and so

$$f(cY(x)) \geq f(c)Y(x) \qquad \forall x \in (0, x_R),$$

which implies

$$Y'(x) > \lambda - c\,x + \beta f(c)\,Y(x) \qquad \text{for all } x \in (0, x_R). \tag{3.44}$$

Denoting $\mu = \beta f(c) > 0$, we rewrite (3.44) as $(e^{-\mu\,x}\,Y(x))' > (\lambda - c\,x)e^{-\mu x}$ and using the condition $Y(0) = 0$ we deduce

$$Y(x) > \left(\frac{\lambda}{\mu} - \frac{c}{\mu^2}\right)(e^{\mu x} - 1) + \frac{c}{\mu} x, \quad \text{for all } x \in (0, x_R]. \tag{3.45}$$

Recalling the definition (3.30) of $\bar{c}$ we notice that $\frac{\lambda}{\mu} - \frac{c}{\mu^2} > 0$ if $c < \bar{c}$, so that the right-hand-side in (3.45) is monotone increasing and converges towards $+\infty$ as $x \to +\infty$. Since $Y(x_R) \leq 1$, by definition of x_R, it follows that $x_R < +\infty$ and (3.45) implies $Y(x_R) > 0$ so that we must have $Y(x_R) = 1$.

Finally, by continuity with respect to c, we notice that when $c = c_{\max}$, we have $Y(\bar{x}) \geq 1$. Moreover, if $Y(\bar{x}) > 1$, then there exists $\delta > 0$ such that $\sup Y > 1$ for $c \in [c_{\max}, c_{\max} + \delta)$ which contradicts the definition of $c_{\max}$. Consequently, $Y(\bar{x}) = 1$ when $c = c_{\max}$ and so $x_R = \bar{x}$ and $Y'(x_R) = 0$. □

Proposition 3.4.6. *Let λ, β and c be such that x_L and x_R (given by Propositions 3.4.3 and 3.4.4) exist. Then $Y(x)$ satisfies*

$$0 \leq Y'(x) \leq \lambda + \beta + c\beta f'(0) \quad \forall x \in (x_L, x_R).$$

Proof. Lemma 3.4.5 and (3.41) implies that $Y'(x) \geq 0$ on $[0, x_R]$. Together with (3.29), this implies that $Y'(x) \geq 0$ on (x_L, x_R). Next, Equation (3.24) implies

$$Y'(x) \leq \lambda - cx_L + \beta$$

and the upper bound follows from Proposition 3.4.3. □

3.4.2 Proof of Proposition 3.4.1, part II: The velocity c

Throughout this section, we fix λ and β such that

$$\beta\lambda f'(0) > 1,$$

and we denote by $Y(x, c)$, $x_L(c)$, $x_R(c)$ the solution of (3.24), (3.25) for all $c \in (0, c_{\max})$. To prove Proposition 3.4.1, it only remains to show that there exists $c \in (0, c_{\max})$ such that (3.27) is satisfied. We thus introduce the function

$$G(c) := \int_{x_L(c)}^{x_R(c)} \frac{Y(x, c)}{\sqrt{1 - Y^2(x, c)}} \, \mathrm{d}x, \tag{3.46}$$

so that Proposition 3.4.1 is a consequence of the following result.

Proposition 3.4.7. *The function $G : [0, c_{\max}) \to \mathbb{R}$ defined by (3.46) is continuous and satisfies*

$$G(0) = 0, \qquad G(c) < 0 \quad \text{for} \quad 0 < c \ll 1,$$

and

$$G(c) \to +\infty, \qquad \text{as} \qquad c \to c_{max}.$$

In particular, there exists $c \in (0, c_{\max})$ such that $G(c) = 0$.

Proof. Continuity of $c \mapsto G(c)$. Differentiating equation (3.24) with respect to c, we find that the function $Z : x \mapsto \partial_c Y(x, c)$ solves

$$\begin{cases} Z'(x) = -x + \beta f'(cY(x))[Y(x) + cZ(x)], & \text{on } (x_L, x_R), \\ Z(0) = 0. \end{cases} \tag{3.47}$$

Moreover using that $0 \leq f'(y) \leq f'(0)$ for all $y \in \mathbb{R}$ and that $|Y| \leq 1$, we deduce that there exists a constant C such that for all $x \in \mathbb{R}$ and for all $c \in (0, c_{max})$

$$|\partial_c Y(x, c)| \leq C.$$

Since $x_L(c)$ and $x_R(c)$ are determined by the conditions

$$Y(x_L, c) = -1 \quad \text{and} \quad Y(x_R, c) = 1.$$

Recalling (3.32) and (3.29) we can apply the Implicit Function Theorem to get that $c \mapsto x_L(c)$ and $c \mapsto x_R(c)$ are continuous Lipschitz functions.

Let c_n be a sequence of positive number such that $c_n \to c > 0$. We fix $\delta > 0$. The continuity of x_L and x_R implies that for large enough n:

$$x_L(c_n) \leq x_L(c) + \delta \leq x_L(c_n) + 2\delta,$$

and

$$x_R(c_n) \geq x_R(c) - \delta \geq x_R(c_n) - 2\delta.$$

Furthermore, since $Y(x, c_n) \to Y(x, c)$ uniformly in $[x_L(c), x_R(c)]$, we have

$$|Y(x, c_n)| \leq 1 - \eta \qquad \text{in } (x_L(c) + \delta, x_R(c) - \delta),$$

for some $\eta > 0$ and n large enough.

We now write

$$\begin{aligned} G(c_n) &= \int_{x_L(c_n)}^{x_R(c_n)} \frac{Y(x, c_n)}{\sqrt{1 - Y^2(x, c_n)}} \, \mathrm{d}x \\ &= \int_{x_L(c_n)+\delta}^{x_R(c_n)-\delta} \frac{Y(x, c_n)}{\sqrt{1 - Y^2(x, c_n)}} \, \mathrm{d}x + \int_{x_L(c_n)}^{x_L(c_n)+\delta} \frac{Y(x, c_n)}{\sqrt{1 - Y^2(x, c_n)}} \, \mathrm{d}x \\ &\quad + \int_{x_R(c_n)-\delta}^{x_R(c_n)} \frac{Y(x, c_n)}{\sqrt{1 - Y^2(x, c_n)}} \, \mathrm{d}x. \end{aligned}$$

The first integral converges to $\int_{x_L(c)+\delta}^{x_R(c)-\delta} \frac{Y(x,c)}{\sqrt{1-Y^2(x,c)}} \, \mathrm{d}x$ when $n \to \infty$. Recalling (3.29) it follows that the second term is bounded by

$$\int_{x_L(c_n)}^{x_L(c_n)+\delta} \frac{2}{\sqrt{1 + Y(x, c_n)}} \, \mathrm{d}x \leq \int_{x_L(c_n)}^{x_L(c_n)+\delta} \frac{2}{\sqrt{C(x - x_L(c_n))}} \, \mathrm{d}x \leq C' \delta^{1/2},$$

where C, C' are positive constants.

Using a similar bound for the third term yields that

$$\lim_{n \to \infty} G(c_n) = \int_{x_L(c)+\delta}^{x_R(c)-\delta} \frac{Y(x, c)}{\sqrt{1 - Y^2(x, c)}} \, \mathrm{d}x + \mathcal{O}(\delta^{1/2}) = G(c) + \mathcal{O}(\delta^{1/2})$$

from which we deduce the continuity of G.

Behavior of G for $c \ll 1$. It is easy to check that

$$Y(x, 0) = \lambda x, \quad x_L(0) = -\frac{1}{\lambda}, \quad x_R(0) = \frac{1}{\lambda},$$

hence

$$G(0) = \int_{-\frac{1}{\lambda}}^{\frac{1}{\lambda}} \frac{\lambda x}{\sqrt{1 - \lambda^2 x^2}} \, \mathrm{d}x = 0. \tag{3.48}$$

To study the behavior of G when $0 < c < \bar{c}$ with $\bar{c}$ given by (3.30), we define the function $H : (-1, 1) \to \mathbb{R}$ by $H(y) = \frac{y}{\sqrt{1-y^2}}$. Using (3.24) we have:

$$\begin{aligned} G(c) = \int_{x_L(c)}^{x_R(c)} H(Y(c, x)) \, \mathrm{d}x &= \frac{1}{\lambda} \int_{x_L(c)}^{x_R(c)} \lambda H(Y(c, x)) \, \mathrm{d}x \\ &= \frac{1}{\lambda} \Bigg[\int_{x_L(c)}^{x_R(c)} \partial_x Y(c, x) H(Y(c, x)) \, \mathrm{d}x \\ &\qquad + \int_{x_L(c)}^{x_R(c)} (cx - \beta f(cY(c, x))) \, H(Y(c, x)) \, \mathrm{d}x \Bigg] \\ &= \frac{1}{\lambda} \int_{x_L(c)}^{x_R(c)} (cx - \beta f(cY(c, x))) \, H(Y(c, x)) \, \mathrm{d}x. \end{aligned}$$

For all $c \in [0, c_{\max})$, we know that

$$\begin{cases} H(Y(c,x)) > 0 & \text{for all } 0 < x < x_R(c), \\ H(Y(c,x)) < 0 & \text{for all } x_L(c) < x < 0. \end{cases} \tag{3.49}$$

We now want to study the sign of the function $cx - \beta f(cY(c,x))$.

Let us consider $0 < x < x_R(c)$. Since

$$f(cY(c,x)) \geq f(c)Y(c,x),$$

by the lower bound (3.45), we have that

$$\begin{aligned} cx - \beta f(cY(c,x)) &\leq cx - \beta f(c)Y(c,x) \\ &\leq cx + \mu \left[-\left(\lambda - \frac{c}{\mu}\right) \frac{e^{\mu x} - 1}{\mu} - \frac{c}{\mu} x \right] = (c - \lambda\mu) \frac{e^{\mu x} - 1}{\mu}, \end{aligned}$$

where $\mu = \beta f(c) > 0$. Since $c - \lambda\mu = c - \lambda\beta f(c) < 0$ for all $c \in [0, \bar{c})$, we deduce that

$$cx - \beta f(cY(c,x)) < 0, \qquad \text{for all } 0 < x < x_R(c). \tag{3.50}$$

Next, we consider $x_L(c) < x < 0$. Since $-1 < Y(x,c) < 0$, we have that

$$f(cY(x,c)) < -f(-c)Y(x,c),$$

and by the upper bound (3.35) it follows that

$$\begin{aligned} cx - \beta f(cY(c,x)) &> cx + \beta f(-c) \left[\left(\lambda - \frac{c}{\mu}\right) \frac{e^{\mu x} - 1}{\mu} + \frac{c}{\mu} x \right] \\ &= \frac{c}{\mu} \left[\mu + \beta f(-c)\right] x + \beta f(-c) \left(\lambda - \frac{c}{\mu}\right) \frac{e^{\mu x} - 1}{\mu}, \end{aligned}$$

where $\mu = c\beta f'(0) > 0$. We deduce

$$cx - \beta f(cY(c,x)) > \frac{1}{f'(0)} \left[cf'(0) + f(-c)\right] x + \frac{-f(-c)}{f'(0)} \left[\lambda\beta f'(0) - 1\right] \frac{1 - e^{\mu x}}{\mu}.$$

Recalling that $x < 0$ and that $cf'(0) + f(-c) > 0$ by the convexity of $f(y)$ for $y < 0$, we see that the first term is negative but it is of order c^2 when $c \ll 1$. The second term is positive since $-f(-c) > 0$, $\lambda\beta f'(0) - 1 > 0$ and $1 - e^{\mu x} > 0$ and of order c. More precisely, we can write:

$$\begin{aligned} cx - \beta f(cY(c,x)) &> \mathcal{O}(c^2|x|) + (c + \mathcal{O}(c^2))) \left[\lambda\beta f'(0) - 1\right] (-x + \mathcal{O}(cx^2)) \\ &> -c \left[\lambda\beta f'(0) - 1\right] x + \mathcal{O}(c^2|x|) + \mathcal{O}(c^2x^2). \end{aligned}$$

Using that $\lambda\beta f'(0) - 1 > 0$, for c small enough, we obtain that

$$cx - \beta f(cY(c,x)) > 0, \qquad \text{for all } x_L(c) < x < 0. \tag{3.51}$$

We can now conclude and give the behavior of G for $c \ll 1$. Inequalities (3.49), (3.50) and (3.51) imply that

$$\begin{cases} \left(cx - \beta f(cY(c,x))\right) H(Y(c,x)) < 0 & \text{for } 0 < x < x_R(c), \\ \left(cx - \beta f(cY(c,x))\right) H(Y(c,x)) < 0 & \text{for } x_L(c) < x < 0, \end{cases} \tag{3.52}$$

as long as $0 < c \ll 1$ and therefore

$$G(c) = \int_{x_L(c)}^{x_R(c)} H(Y(c,x))\,\mathrm{d}x = \frac{1}{\lambda}\int_{x_L(c)}^{x_R(c)} (cx - \beta f(cY(c,x)))\,H(Y(c,x))\,\mathrm{d}x < 0.$$

Behavior of G when $c \to c_{\max}$. In the proof of Proposition 3.4.4 we saw that as $c \to c_{\max}$ we have that

$$Y'(x_R(c)) \to 0.$$

Recalling that $V(x) = Y'(x)$ solves (3.37), for $x \to x_R(c)$ with $c \to c_{\max}$, we deduce that

$$Y(x,c) = 1 - c(x - x_R(c))^2 + \mathcal{O}\left(|x - x_R(c)|^3\right). \tag{3.53}$$

Thus, we get that

$$\begin{aligned} 1 - Y^2(x,c) &= 1 - 1 + 2c(x - x_R(c))^2 + \mathcal{O}\left(|x - x_R(c)|^3\right) \\ &= 2c(x - x_R(c))^2 + \mathcal{O}\left(|x - x_R(c)|^3\right), \end{aligned}$$

leading to

$$\sqrt{1 - Y^2(x,c)} = \sqrt{2c}\,|x - x_R(c)| + \mathcal{O}\left(|x - x_R(c)|^{3/2}\right). \tag{3.54}$$

We notice that for all $\varepsilon > 0$ the function G can be written by

$$\begin{aligned} G(c) &= \int_{x_L(c)}^{x_R(c)} \frac{Y(x,c)}{\sqrt{1 - Y^2(x,c)}}\,\mathrm{d}x \\ &= \int_{x_L(c)}^{x_R(c)-\varepsilon} \frac{Y(x,c)}{\sqrt{1 - Y^2(x,c)}}\,\mathrm{d}x + \int_{x_R(c)-\varepsilon}^{x_R(c)} \frac{Y(x,c)}{\sqrt{1 - Y^2(x,c)}}\,\mathrm{d}x. \end{aligned}$$

The first right hand side is always finite, while the second right hand side by (3.53) and (3.54) for $c \to c_{\max}$ we get that that

$$\int_{x_R(c)-\varepsilon}^{x_R(c)} \frac{Y(x,c)}{\sqrt{1 - Y^2(x,c)}}\,\mathrm{d}x \simeq \int_{x_R(c)-\varepsilon}^{x_R(c)} \frac{1}{\sqrt{2}\,|x - x_R(c)|}\,\mathrm{d}x = +\infty.$$

Therefore, for $c \to c_{\max}$ we get that

$$G(c) \to +\infty \tag{3.55}$$

which completes the proof of Proposition 3.4.7. □

3.5 Proof of Theorem 3.1.2

In this Section we show that a bifurcation of traveling wave solutions from the family of radially symmetric steady states B_{R_0} occurs. This bifurcation is determined by three parameters: the size of the cell R_0, the surface tension γ and the polymerisation strength β which are independent parameters. It is convenient to choose β as the bifurcation parameter in the bifurcation conditions.

Since the disk is a solution of the equation (3.19) with zero bulk velocity $c = 0$, our aim is to seek for other solutions in the form of a perturbation of the disk of radius R_0. We seek for those domain Ω_0 of the form

$$\Omega_0 = \{(r,\theta) \,:\, 0 \le r < R_0 + \rho(\theta) \text{ and } \theta \in [-\pi, +\pi]\}, \tag{3.56}$$

where the function $\rho : \mathbb{R} \to (-R_0, \infty)$ is 2π-periodic and such that

$$\int_{-\pi}^{\pi} (R_0 + \rho(\theta))^2 - R_0^2 \mathrm{d}\theta = 0$$

(this condition guarantee that $|\Omega_0| = |B_{R_0}|$).

Note that the boundary $\partial\Omega_0$ is parametrized by

$$\Big((R_0+\rho(\theta))\cos\theta, (R_0+\rho(\theta))\sin\theta\Big) \quad \text{for } \theta \in [-\pi, +\pi],$$

the normal vector is given by

$$n(\theta) = \frac{1}{((R_0+\rho(\theta))^2+\rho'(\theta)^2)^{1/2}} \begin{pmatrix} (R_0+\rho(\theta))\cos\theta + \rho'(\theta)\sin\theta \\ (R_0+\rho(\theta))\sin\theta - \rho'(\theta)\cos\theta \end{pmatrix},$$

and the mean-curvature by

$$\kappa(\theta) = \frac{(R_0+\rho(\theta))^2 + 2\rho'(\theta)^2 - (R_0+\rho(\theta))\rho''(\theta)}{((R_0+\rho(\theta))^2+\rho'(\theta)^2)^{3/2}}.$$

In such a case equation (3.19) can be rewritten as

$$\gamma\kappa(\theta) - \beta f\left(c\frac{(R_0+\rho(\theta))\cos\theta + \rho'(\theta)\sin\theta}{((R_0+\rho(\theta))^2+\rho'(\theta)^2)^{1/2}}\right) + c(R_0+\rho(\theta))\cos\theta = \lambda, \tag{3.57}$$

for all $\theta \in [-\pi, \pi)$. Therefore, the existence of a boundary $\partial\Omega_0$ solving (3.19) is equivalent to the existence of a function ρ solution of equation (3.57).

The existence of solutions of (3.57) is proved by the following bifurcation theorem:

Theorem 3.5.1. *Assume that f satisfies assumptions (A1) – (A4). There exists an interval $I = (-\varepsilon, +\varepsilon)$ and three C^1 functions $\rho : I \times [-\pi, +\pi] \to \mathbb{R}$, $\beta : I \to \mathbb{R}$ and $c : I \to \mathbb{R}$ such that*

(i) For all $s \in I$, the equation (3.57) has a solution $\rho(s, \theta)$ for all $\theta \in [-\pi, +\pi]$ representing a parametrization of the boundary $\partial\Omega_0$ with $\beta = \beta(s)$ and $c = c(s)$.

(ii) The function $c = c(s)$ is such that $c(s) = s + o(s)$ for all $s \in I$.

(iii) The function $\beta = \beta(s)$ is such that $\beta(0) = \frac{R_0}{f'(0)}$, $\beta'(0) = 0$ and $\beta''(0) > 0$.

Proof of theorem 3.1.2. First, we note that the original problem (3.18) is invariant by translation. Thus, it is natural to eliminate these invariances by looking for solution of (3.57) satisfying the orthogonality conditions $\int_{-\pi}^{\pi} \rho(\theta)\cos\theta \mathrm{d}\theta = 0$ and $\int_{-\pi}^{\pi} \rho(\theta)\sin\theta \mathrm{d}\theta = 0$.

Let the functional spaces

$$X = \mathcal{C}^{2,\alpha}_{\mathrm{per}}(-\pi, \pi) \qquad \text{and} \qquad Y = \mathcal{C}^{0,\alpha}_{\mathrm{per}}(-\pi, \pi).$$

We define the function

$$\mathcal{F} : \mathbb{R} \times X \times \mathbb{R} \times \mathbb{R} \to Y \times \mathbb{R} \times \mathbb{R} \times \mathbb{R}$$

by

$$\begin{aligned} \mathcal{F}(\beta, \rho, c, \lambda) = \Big(&\gamma\kappa(\theta) - \beta f\left(c\frac{(R_0+\rho(\theta))\cos\theta + \rho'(\theta)\sin\theta}{((R_0+\rho(\theta))^2+\rho'(\theta)^2)^{1/2}}\right) \\ &+ c(R_0+\rho(\theta))\cos\theta - \lambda, \\ &\int_{-\pi}^{\pi} (R_0+\rho(\theta))^2 - R_0^2 \mathrm{d}\theta, \int_{-\pi}^{\pi} \rho(\theta)\cos\theta \mathrm{d}\theta, \int_{-\pi}^{\pi} \rho(\theta)\sin\theta \mathrm{d}\theta\Big). \end{aligned} \tag{3.58}$$

The proof of the theorem relies on a series of properties of $\mathcal{F}$ that allow us to apply the (local) bifurcation Theorem 3.3.1.

Lemma 3.5.2. *Assume that f satisfies assumptions (A1) – (A4) and let $\beta_0 = \frac{R_0}{f'(0)}$. Then the functional $\mathcal{F}$ defined by (3.58) has the following properties*

1. $\mathcal{F}(\beta_0, 0, 0, 0) = 0$;
2. $\operatorname{Ker} \partial_{(\rho,c,\lambda)}\mathcal{F}(\beta_0, 0, 0, 0)$ *is a one dimensional subspace of* $\mathbb{R} \times X \times \mathbb{R} \times \mathbb{R}$ *spanned by* $(0, 1, 0)$;
3. $\operatorname{Range} \partial_{(\rho,c,\lambda)}\mathcal{F}(\beta_0, 0, 0, 0)$ *is a closed subspace of* $Y \times \mathbb{R} \times \mathbb{R} \times \mathbb{R}$ *of codimension 1;*
4. $\partial_\beta\, \partial_{(\rho,c,\lambda)}\mathcal{F}(\beta_0, 0, 0, 0)[(0, 1, 0)] \notin \operatorname{Range} \partial_{(\rho,c,\lambda)}\mathcal{F}(\beta_0, 0, 0, 0)$.

Proof of lemma 3.5.2. We first notice that

$$\mathcal{F}(\beta, 0, 0, 0) = (0, 0, 0, 0), \qquad \text{for all } \beta \in \mathbb{R}.$$

Next, we compute $\mathcal{L}_\beta := \partial_{(\rho,c,\lambda)}\mathcal{F}(\beta, 0, 0, 0)$. It is the linear operator

$$\mathcal{L}_\beta : X \times \mathbb{R} \times \mathbb{R} \to Y \times \mathbb{R} \times \mathbb{R} \times \mathbb{R}$$

defined by

$$\mathcal{L}_\beta(\rho, c, \lambda) = \mathcal{F}_\rho(\beta, 0, 0, 0)[\,\rho\,] + \mathcal{F}_c(\beta, 0, 0, 0)\, c + \mathcal{F}_\lambda(\beta, 0, 0, 0)\, \lambda, \tag{3.59}$$

where $\mathcal{F}_\rho(\beta, 0, 0, 0)$ represents the first variation of $\mathcal{F}$ with respect to the function $\rho \in X$ and computed at the point $(\beta, 0, 0, 0) \in \mathbb{R} \times X \times \mathbb{R} \times \mathbb{R}$, and $\mathcal{F}_c(\beta, 0, 0, 0)$, $\mathcal{F}_\lambda(\beta, 0, 0, 0)$ represents the derivatives of $\mathcal{F}$ with respect to $c \in \mathbb{R}$ and $\lambda \in \mathbb{R}$, respectively, and computed in $(\beta, 0, 0, 0)$.

More precisely, for all $(\beta, c, \lambda) \in \mathbb{R} \times \mathbb{R} \times \mathbb{R}$, the linear operator $\mathcal{F}_\rho(\beta, \rho, c, \lambda)$ is defined by

$$\mathcal{F}_\rho(\beta, \rho, c, \lambda)[\eta] = \frac{\mathrm{d}}{\mathrm{d}\varepsilon}\mathcal{F}(\beta, \rho + \varepsilon\eta, c, \lambda)_{|_{\varepsilon=0}}, \quad \text{for } \eta \in X.$$

The parameter ε is a positive real parameter and $\mathrm{d}/\mathrm{d}\varepsilon$ denotes the usual derivative of F with respect to $\varepsilon \in \mathbb{R}$. We observe that the quantity $(\rho + \varepsilon\eta)$ represents the perturbation of ρ of order ε in the direction of the function η. Recalling the definition (3.58) of $\mathcal{F}$, we see that $\mathcal{F}(\beta, \rho + \varepsilon\eta, c, \lambda)$ is given by

$$\begin{aligned}
&\mathcal{F}(\beta, \rho + \varepsilon\eta, c, \lambda) \qquad\qquad (3.60)\\
&= \left(\gamma\, \kappa_{\rho+\varepsilon\eta}(\theta) - \beta f\left(c\frac{(R_0 + \rho(\theta) + \varepsilon\eta(\theta))\cos\theta + (\rho'(\theta) + \varepsilon\eta'(\theta))\sin\theta}{[(R_0 + \rho(\theta) + \varepsilon\eta(\theta))^2 + (\rho'(\theta) + \varepsilon\eta'(\theta))^2]^{1/2}}\right)\right.\\
&+ c\,[R_0 + \rho(\theta) + \varepsilon\eta(\theta)]\cos'(\theta) - \frac{\gamma}{R_0} - \lambda, \int_{-\pi}^{\pi}(R_0 + \rho(\theta) + \varepsilon\eta(\theta))^2 - R_0^2 \mathrm{d}\theta,\\
&\left.\int_{-\pi}^{\pi}[\rho(\theta) + \varepsilon\eta(\theta)]\cos\theta \mathrm{d}\theta, \int_{-\pi}^{\pi}[\rho(\theta) + \varepsilon\eta(\theta)]\sin\theta \mathrm{d}\theta\right),
\end{aligned}$$

where $\kappa_{\rho+\varepsilon\eta}(\theta)$ is the mean-curvature of the perturbed boundary, that is

$$\begin{aligned}
&\kappa_{\rho+\varepsilon\eta}(\theta)\\
= \;& \frac{[R_0 + \rho(\theta) + \varepsilon\eta(\theta)]^2 + 2[\rho'(\theta) + \varepsilon\eta'(\theta)]^2 - [R_0 + \rho(\theta) + \varepsilon\eta(\theta)]\,[\rho''(\theta) + \varepsilon\eta''(\theta)]}{[\,(R_0 + \rho(\theta) + \varepsilon\eta(\theta))^2 + (\rho'(\theta) + \varepsilon\eta'(\theta))^2\,]^{3/2}}.
\end{aligned}$$

We derive the expression (3.60) with respect to ε, we compute it for $\varepsilon = 0$, and we then consider $\rho = 0$, $c = 0$ and $\lambda = 0$. For $\eta = \rho$, we get the following expression

$$\begin{aligned}
&\mathcal{F}_\rho(\beta, 0, 0, 0)[\,\rho\,] \qquad\qquad (3.61)\\
&= \left(-\gamma\,\frac{\rho(\theta) + \rho''(\theta)}{R_0}, \int_{-\pi}^{\pi} 2R_0\rho(\theta)\mathrm{d}\theta, \int_{-\pi}^{\pi}\rho(\theta)\cos\theta\mathrm{d}\theta, \int_{-\pi}^{\pi}\rho(\theta)\sin\theta\mathrm{d}\theta\right).
\end{aligned}$$

The second and the third terms in (3.59) are simpler to compute since c and λ are real quantities. We obtain that

$$\mathcal{F}_c(\beta, 0, 0, 0)\, c = (-c\,\beta f'(0)\cos\theta + c\, R_0\cos\theta, 0, 0, 0)\,, \tag{3.62}$$

and

$$\mathcal{F}_\lambda(\beta,0,0,0)\,\lambda = (-\lambda,0,0,0)\,. \tag{3.63}$$

Finally, the linear operator $\mathcal{L}_\beta$ is given by the sum of the expressions (3.61) – (3.63), that is

$$\begin{aligned}\mathcal{L}_\beta(\rho,c,\lambda) = \Big(&-\gamma\,\frac{\rho(\theta)+\rho''(\theta)}{R_0^2} - c\beta f'(0)\cos\theta + cR_0\cos\theta - \lambda,\\ &2R_0\int_{-\pi}^{\pi}\rho(\theta)\,d\theta, \int_{-\pi}^{\pi}\rho(\theta)\cos\theta\mathrm{d}\theta, \int_{-\pi}^{\pi}\rho(\theta)\sin\theta\mathrm{d}\theta\Big)\,.\end{aligned} \tag{3.64}$$

In the case where $\beta_0 = \frac{R_0}{f'(0)}$, we get that

$$\begin{aligned}&\mathcal{L}_{\beta_0}(\rho,c,\lambda)\\ &= \left(-\gamma\,\frac{\rho(\theta)+\rho''(\theta)}{R_0^2} - \lambda, 2R_0\int_{-\pi}^{\pi}\rho(\theta)\mathrm{d}\theta, \int_{-\pi}^{\pi}\rho(\theta)\cos\theta\mathrm{d}\theta, \int_{-\pi}^{\pi}\rho(\theta)\sin\theta\mathrm{d}\theta\right).\end{aligned}$$

By definition

$$\operatorname{Ker}\mathcal{L}_{\beta_0} = \{(\rho,c,\lambda)\in X\times\mathbb{R}\times\mathbb{R} : \mathcal{L}_{\beta_0}(\rho,c,\lambda) = (0,0,0,0)\in Y\times\mathbb{R}\times\mathbb{R}\times\mathbb{R}\},$$

thus, the elements $\{(\rho,c,\lambda)\}$ belonging to $\operatorname{Ker}\mathcal{L}_{\beta_0}$ are such that

$$-\gamma\frac{\rho(\theta)+\rho''(\theta)}{R_0^2} - \lambda = 0,$$

which is equivalent to

$$\rho''(\theta)+\rho(\theta) = \frac{-R_0^2}{\gamma}\lambda. \tag{3.65}$$

Since the parameter c does not appear in equation (3.65) we deduce that

$$\dim\operatorname{Ker}\mathcal{L}_{\beta_0} \geq 1.$$

We then study the couple (ρ,λ) solving (3.65), which is of the form

$$\rho(\theta) = a\cos\theta + b\sin\theta - \frac{R_0^2}{\gamma}\lambda, \qquad \text{for some } a,b\in\mathbb{R}.$$

By imposing the conditions $\int_{-\pi}^{+\pi}\rho(\theta)\mathrm{d}\theta = 0$, $\int_{-\pi}^{+\pi}\rho(\theta)\cos\theta\mathrm{d}\theta = 0$ and $\int_{-\pi}^{+\pi}\rho(\theta)\sin\theta\mathrm{d}\theta = 0$ we respectively get $\lambda = 0$, $a = 0$ and $b = 0$, hence

$$\operatorname{Ker}\mathcal{L}_{\beta_0} = \{(0,c,0) : c\in\mathbb{R}\} = \operatorname{span}\{(0,1,0)\},$$

and therefore

$$\dim\operatorname{Ker}\mathcal{L}_{\beta_0} = 1.$$

Moreover the range of $\mathcal{L}_{\beta_0}$ consists of all the quadruplets (f,C_1,C_2,C_3) such that $\int_{-\pi}^{\pi}f(\theta)\cos\theta\mathrm{d}\theta = 0$ thus, condition (3) holds.

Lastly, we have prove the transversality condition (4) with respect to the value β_0, that is we have to prove that $(\partial_\beta\mathcal{L}_{\beta_0})(0,1,0)\notin\operatorname{Range}\mathcal{L}_{\beta_0}$. First, we have that

$$(\partial_\beta\mathcal{L}_{\beta_0})(0,1,0) = (-f'(0)\cos\theta,0,0,0).$$

Assume by contradiction that $(\partial_\beta\mathcal{L}_{\beta_0})(0,1,0)\in\operatorname{Range}\mathcal{L}_{\beta_0}$, then we would have that

$$-\gamma\frac{\rho(\theta)+\rho''(\theta)}{R_0^2} - \lambda = f'(0)\cos\theta. \tag{3.66}$$

Multiplying by $\cos\theta$ and integrating on $[-\pi,+\pi]$, it yields that

$$-\gamma\int_{-\pi}^{\pi}\rho(\theta)\cos\theta\mathrm{d}\theta-\gamma\int_{-\pi}^{\pi}\rho''(\theta)\cos\theta\mathrm{d}\theta-\lambda R_0^2\int_{-\pi}^{\pi}\cos\theta\mathrm{d}\theta \tag{3.67}$$
$$=R_0^2f'(0)\int_{-\pi}^{\pi}\cos^2\theta\mathrm{d}\theta.$$

Integrating by parts twice the second term of the left-hand side and using that ρ' is a 2π-period function together with $\int_{-\pi}^{\pi}\rho(\theta)\cos\theta\mathrm{d}\theta=0$, we deduce that

$$\int_{-\pi}^{\pi}\rho''(\theta)\cos\theta\mathrm{d}\theta=\int_{-\pi}^{\pi}\rho'(\theta)\sin\theta\mathrm{d}\theta=-\int_{-\pi}^{\pi}\rho(\theta)\cos\theta\mathrm{d}\theta=0.$$

Then, from equation (3.67) it follows

$$0=R_0^2f'(0)\pi,$$

which represents a contradiction since we have that $f'(0)<0$. □

We can now apply the bifurcation theorem 3.3.1. Let us denote by Z any complement space of $\mathrm{Ker}\,\mathcal{L}_{\beta_0}$, there exists an interval $I=(-\varepsilon,\varepsilon)$ and four $\mathcal{C}^1$ functions $\varphi:I\to\mathbb{R}$, $\psi_1:I\times[-\pi,+\pi]\to Z$, $\psi_2:I\to Z$ and $\psi_3:I\to Z$ such that

$$\mathcal{F}(\varphi(s),\psi_1(s,\theta),\psi_2(s),\psi_3(s))=(0,0,0,0)\quad\text{for all } s\in I,\ \theta\in[-\pi,+\pi], \tag{3.68}$$

and

$$\varphi(0)=\frac{R_0}{f'(0)},\quad \psi_1(0,\theta)=0\text{ for all }\theta\in[-\pi,+\pi],\quad \psi_2(0)=0,\quad \psi_3(0)=0.$$

In particular, the solutions $(\beta,\rho,c,\lambda)=(\beta(s),\rho(s,\theta),c(s),\lambda(s))$ of the equation $\mathcal{F}(\beta,\rho,c,\lambda)=(0,0,0,0)$ are of the form

$$\begin{cases}\beta(s)=\varphi(s), & \rho(s,\theta)=0+s\,\psi_1(s,\theta),\\ c(s)=s+s\,\psi_2(s), & \lambda(s)=0+s\,\psi_3(s)\end{cases} \tag{3.69}$$

and they are such that

$$\begin{cases}\beta(0)=\beta_0=\frac{R_0}{f'(0)},\\ \rho(0,\theta)=0\text{ and }\partial_s\rho(0,\theta)=0,\quad\text{for all }\theta\in(-\pi,+\pi),\\ \partial_\theta\rho(0,\theta)=0\text{ and }\partial_{\theta\theta}\rho(0,\theta)=0,\quad\text{for all }\theta\in(-\pi,+\pi),\\ c(0)=0\text{ and }c'(0)=1,\\ \lambda(0)=0\text{ and }\lambda'(0)=0.\end{cases} \tag{3.70}$$

This achieves the proof of points (i) and (ii) of theorem 3.5.1.

We achieve the proof of lemma 3.5.2 by computing $\beta'(0)$ and $\beta''(0)$.

Lemma 3.5.3. *We have $\beta'(0)=0$.*

Proof of lemma 3.5.3. We differentiate with respect to s the first component of $\mathcal{F}$ and since (3.68) holds for all $s\in I$ we get that

$$\begin{aligned}0=&\gamma\partial_sk(s,\theta)-\beta'(s)f(z(s,\theta))-\beta(s)f'(z(s,\theta))\partial_sz(s,\theta)\\&+c'(s)(R_0+\rho(s,\theta))\cos\theta+c(s)\partial_s\rho(s,\theta)\cos\theta-\lambda'(s),\end{aligned} \tag{3.71}$$

where the functions k and z are defined by

$$k(s,\theta)=\frac{((R_0+\rho)^2+2\partial_\theta\rho^2-(R_0+\rho)\partial_{\theta\theta}\rho)(s,\theta)}{\big(((R_0+\rho)^2+\partial_\theta\rho^2)^{3/2}\big)(s,\theta)}. \tag{3.72}$$

and

$$z(s,\theta) = c(s)\frac{(R_0+\rho(s,\theta))\cos\theta + \partial_\theta\rho(s,\theta)\sin\theta}{(\sqrt{(R_0+\rho(s,\theta))^2+(\partial_\theta\rho(s,\theta))^2})}. \tag{3.73}$$

By using (3.70), we first see that

$$z(0,\theta) = 0 \quad \text{for all } \theta \in [-\pi,+\pi].$$

Since $f(0) = 0$, the coefficient of $\beta'(0)$ vanishes in (3.71) and we do not get any information. Therefore, we differentiate equation (3.71) with respect to s and we get

$$\begin{aligned} 0 =& \gamma\partial_{ss}k(s,\theta) - \beta''(s)f(z(s,\theta)) - 2\beta'(s)f'(z(s,\theta))\partial_s z(s,\theta) \\ &- \beta(s)f'(z(s,\theta))\partial_{ss}z(s,\theta) - \beta(s)f''(z(s,\theta))(\partial_s z(s,\theta))^2 \\ &+ c''(s)(R_0+\rho(s,\theta))\cos\theta + 2c'(s)\partial_s\rho(s,\theta)\cos\theta \\ &+ c(s)\partial_{ss}\rho(s,\theta)\cos\theta - \lambda''(s). \end{aligned} \tag{3.74}$$

Computing (3.74) for $s = 0$, we obtain

$$\begin{aligned} 0 =& \gamma\partial_{ss}k(0,\theta) - 2\beta'(0)f'(0)\partial_s z(0,\theta) - \beta(0)f'(0)\partial_{ss}z(0,\theta) \\ &- \beta(0)f''(0)(\partial_s z(0,\theta))^2 + R_0c''(0)\cos\theta - \lambda''(0). \end{aligned} \tag{3.75}$$

Using (3.73) and (3.70), we deduce that

$$\partial_s z(0,\theta) = \cos\theta, \quad \text{for all } \theta \in [-\pi,+\pi]. \tag{3.76}$$

By multiplying equation (3.74), computed for $s = 0$, by $\cos\theta$, and by integrating on $[-\pi,\pi]$, by using Lemma B.0.2 and since $\beta(0) = -R_0/f'(0)$, we finally obtain

$$\int_{-\pi}^{\pi} (2\beta'(0)f'(0)\cos\theta + \lambda''(0)\,)\cos\theta \mathrm{d}\theta = 0,$$

leading to

$$\beta'(0) = 0.$$

□

Lemma 3.5.4. *We have* $\beta''(0) > 0$.

Proof of lemma 3.5.4. We differentiate (3.74) with respect to s

$$\begin{aligned} 0 =& \gamma\partial_{sss}k(s,\theta) - \beta'''(s)f(z(s,\theta)) - 3\beta''(s)f'(z(s,\theta))\partial_s z(s,\theta) \\ &- \beta'(s)[3f''(z(s,\theta))(\partial_s z(s,\theta))^2 + 3f'(z(s,\theta))\partial_{ss}z(s,\theta)] \\ &- \beta(s)[f'''(z(s,\theta))(\partial_s z(s,\theta))^3 + 3f''(z(s,\theta))\partial_s z(s,\theta)\,\partial_{ss}z(s,\theta) \\ &+ f'(z(s,\theta))\partial_{sss}z(s,\theta)] + c'''(s)(R_0+\rho(s,\theta))\cos\theta \\ &+ 3c''(s)\partial_s\rho(s,\theta)\cos\theta + 3c'(s)\partial_{ss}\rho(s,\theta)\cos\theta \\ &+ c(s)\partial_{sss}\rho(s,\theta)\cos\theta - \lambda'''(s). \end{aligned} \tag{3.77}$$

Multiplying (3.77), computed for $s = 0$, by $\cos\theta$, integrating on $[-\pi,\pi]$, using $\beta(0) = -R_0/f'(0)$, $\beta'(0) = 0$, $z(0,\theta) = 0$, $\partial_s z(0,\theta) = \cos\theta$ for all $\theta \in (-\pi,+\pi)$ and $f(0) = 0$, $f''(0) = 0$, lemma A.0.1 and lemma B.0.2, we obtain

$$\int_{-\pi}^{+\pi} \left(3\beta''(0)f'(0)\cos\theta + R_0\frac{f'''(0)}{f'(0)}\cos^3\theta - 3\partial_{ss}\rho(0,\theta)\cos\theta + \lambda'''(0)\right)\cos\theta \mathrm{d}\theta = 0,$$

leading to

$$-3f'(0)\beta''(0)\int_{-\pi}^{+\pi}\cos^2\theta\mathrm{d}\theta = R_0\frac{f'''(0)}{f'(0)}\int_{-\pi}^{+\pi}\cos^4(\theta)\mathrm{d}\theta - 3\int_{-\pi}^{+\pi}\partial_{ss}\rho(0,\theta)\cos^2(\theta)\mathrm{d}\theta.$$

Using Lemma C.0.3 we deduce that

$$\beta''(0) = -\frac{R_0}{4}\frac{f'''(0)}{(f'(0))^2},$$

hence the result by recalling that $f'''(0) < 0$ by assumption (A3). □

This achieves the proof of lemma 3.5.2. □

3.6 Numerical method via the "shooting method"

In the previous section we showed that the qualitative analysis of the problems (3.24)-(3.25) and (3.26)-(3.27) depends on the parameters λ, β and c (we took the non-restrictive hypothesis that $\gamma = 1$), and we furnished a constructive method for identifying a space of suitable values such that boundary conditions (3.25) and (3.27) are satisfied. This represents the space of values for which a Traveling Wave like solution of the problem (3.1) exists. In this section we introduce a numerical method to solve (3.24)-(3.25) and (3.26)-(3.27) which relies on the same "constructive approach" as the previous section. The general steps of the numerical method are the following:

1. We fix $\lambda > 0$ and we choose β such that the condition (3.28) holds. This ensures the existence of the point x_L. We remark that this condition is independent of the parameter c and the function f is known.

2. We consider a suitable set of values for c for ensuring the existence of the point x_R. Indeed, we showed that there exists a value $c_{\max}$ depending on β and λ such that for $c \in [0, c_{\max})$ the point x_R exists.

3. We define a discretization on the interval $[0, c_{\max})$ and for each value c in the discretized interval we solve numerically the problem (3.24) for β and λ chosen in step 1. The extreme points x_L and x_R are then determined by the use of a "shooting method" that we explain later. We then obtain the numerical solution $(x, c) \longmapsto Y(x, c)$ for $x \in [x_L, x_R]$ and for $c \in [0, c_{\max})$.

4. In order to find the optimal value c^* of c such that the boundary condition (3.27) is satisfied, we follow the analysis previously introduced, that is

$$\text{we find } c^* > 0 \text{ such that } G(c^*) = 0 \text{ where } G(c) = \int_{x_L(c)}^{x_R(c)} \frac{Y(x,c)}{\sqrt{1 - Y^2(x,c)}}\,dx,$$

   where $Y(\cdot, c)$ is the numerical solution obtained in the step 3.

5. We solve the problem (3.24)-(3.25) with $c = c^*$ found in step 4. and β, λ chosen in step 1. We then obtain the related numerical solution $Y = Y(x, c^*)$ and the related extreme points $x_L = x_L(c^*)$ and $x_R = x_R(c^*)$. By solving numerically the equation (3.26), we the find the function h.

This numerical method is then able to compute the quantities related to the Traveling Wave such as its half-positive graph h, its position identified by the points x_L, x_R, and its translation velocity $c = c^*$. The full graph of the related Traveling Wave like solution is then obtained by symmetry of the function h with respect to the x-axes.

We notice that these quantities depend by the choice of the parameters β and λ imposed at step 1. In the following, we will present the numerical method in more details and we will show some numerical simulation for a given choice of the parameters β and λ.

Numerical method for (3.24)-(3.25)

Let β and λ be fixed in step 1 and let c be a value in the interval of $[0, c_{\max})$. We want to solve numerically the following problem

$$\begin{cases} Y'(x) = \lambda - cx - \beta F(cY(x)), & \text{on } (x_L, x_R), \\ Y(0) = 0 \\ Y(x_L) = -1,\ Y(x_R) = +1. \end{cases}$$

We remark that the extreme points x_L and x_R are such that $x_L < 0 < x_R$. Since we have the condition for $x = 0$, the idea is to split the interval (x_L, x_R) into the sub-intervals $(0, x_R)$ and $(0, |x_L|)$ and then use $Y(0) = 0$ as the initial condition. In particular, we consider Y_1 solution of

$$\begin{cases} Y_1'(x) = \lambda - cx - \beta F(cY_1(x)) \text{ on } (0, x_R), \\ Y_1(0) = 0, \end{cases} \tag{3.78}$$

and Y_2 solution of

$$\begin{cases} Y_2'(x) = -\lambda - cx + \beta F(cY_2(x)) \text{ on } (0, |x_L|), \\ Y_2(0) = 0. \end{cases} \tag{3.79}$$

We consider a non-homogeneous discretization on each sub-interval in which we impose a thinner discretization near the right-extreme. This will be useful in the implementation of the "shotting method" which we will explain later. We define a real number $R < x_R$ and we consider N_R points in $[0, R]$ and N_R points in $[R, x_R]$ where R is chosen such that $R \gg (x_R - R)$, that is to be close enough to the point x_R. We then define

$$h_R^1 = \frac{R}{N_R - 1} \quad \text{and} \quad h_R^2 = \frac{x_R - R}{N_R - 1}.$$

We notice that since $R \gg (x_R - R)$, we have that $h_1^R \gg h_2^R$. We proceed with the same approach for the interval $(0, |x_L|)$. We define $L < |x_L|$ such that $L \gg (|x_L| - L)$ and we defineN_L points in $[0, L]$ and N_L points in $[L, |x_L|]$. We then define

$$h_L^1 = \frac{R}{(N_L - 1)} \quad \text{and} \quad h_L^2 = \frac{(|x_L| - L)}{(N_L - 1)},$$

where we have that $h_1^L \gg h_2^L$.

We use an Explicit Euler Method. We denote $Y_1^i = Y_1(x_i)$ and $Y_2^i = Y_2(x_i)$ and the problem (3.78) rewrites by the following numerical rules

$$\begin{cases} Y_1^{i+1} = Y_1^i + h_R(\lambda - cx_i - \beta F(cY_1^i)) \quad \text{for } i = 1, ..., 2N_R \\ Y_1^0 = 0 \end{cases}$$

where $h_R = h_R^1$ for the points in $[0, R]$ and $h_R = h_R^2$ for those in $[R, x_R]$. The problem (3.79) rewrites as follows

$$\begin{cases} Y_2^{i+1} = Y_2^i - h_L(\lambda + cx_i - \beta F(cY_2^i)) \quad \text{for } i = 1, ..., 2N_L \\ Y_2^0 = 0 \end{cases}$$

where $h_L = h_L^1$ for the points in $[0, L]$ and $h_L = h_L^2$ for those in $[L, |x_L|]$.

The numerical solution Y on the joined interval $[x_L, x_R]$ is then obtained by merging Y_1 with the permutation of Y_2, that is

$$Y = [\, Y_2^{2N_L}, Y_2^{2N_L-1}, ..., Y_2^1, Y_2^0, Y_1^0, Y_1^1, ..., Y_1^{2N_R-1}, Y_1^{2N_R}\,]. \tag{3.80}$$

We observe that in (3.80) the quantities $Y_2^{2N_L} = Y_2(x_L)$ and $Y_1^{2N_R}(x_R) = Y_1(x_R)$ are still unknown since the extreme points x_L and x_R are unknown. We solve this problem in the following section.

Determination of the points x_L and x_R via the "shooting method"

We introduce in this section a classical method to determine the points x_L and x_R, the so-called "shooting method". The criteria to choose x_L and x_R will be the boundary conditions $Y(x_L) = -1$ and $Y(x_R) = +1$ (which we have not used yet).

We find $x_R > 0$ such that $Y_1(x_R) = 1$, where Y_1 is solution of the problem (3.78). We proceed by the following iterative procedure:

(I) We define $M > 0$ big enough such that x_R is supposed to belong to the interval $[0, M]$;

(II) At iteration $n = 0$, we solve the problem (3.78) on the interval $[0, M]$ and we define x_R^0 as the point such that $Y_1(x_R^0) = 1$. Since $x_R < M$, the point x_R^0 always exists.

(III) At iteration n, we denote $M^n = (M^{n-1} + x_R^{n-1})/2$ and we find the numerical solution Y_1^n of (3.78) on the interval $[0, M^n]$. If there exists $x > 0$ such that $Y_1^n(x) = +1$, then we define $x_R^n = x$ and we pass to the iteration $n + 1$. Otherwise, we stop the iteration and we define $x_R = x_R^n$.

To compute the numerical solution Y_1^n, we use the non-homogeneous discretization on the interval $[0, M^n]$. This makes more precise the numerical resolution of the equation $Y_1^n(x) = +1$. The condition $Y_1^n(x) = +1$ represents the stop criterion of the iterative procedure and it is implemented numerically by a Bisection Method.

As for the point $x_L < 0$, we use the above procedure (I)-(III) with some light differences. For step (I), we consider $M < 0$ small enough such that $M < x_L$ and for step (II) we solve the problem (3.79) on the interval $[0, |M|]$. In step (III), at each iteration n we define M^n with the same rule where $M^{n-1} < 0$ and $x_L^{n-1} < 0$. We then compute Y_2^n solution of the problem (3.79) on the interval $[0, |M^n|]$ and x_L^n at each iteration n is obtained by solving numerically $Y_2^n(x) = -1$. When the iterative procedure ends, we define $x_L = -|x_L^n|$ where n is the last iteration.

Computation of the velocity $c = c^*$ and function h

We explain in this section the numerical implementation of the step 4. and step 5.. In step 4., we need to compute numerically the quantity $G(c)$. Since G is an integral, we used the Trapeziodal Rule where we used Y as the numerical solution (3.80). We compute the value $c = c^*$ as the positive solution of the equation $G(c) = 0$ implemented via a Bisection Method.

In step 5., we take $c = c^*$ and we solve numerically the following problem

$$\begin{cases} h(x)' = -\dfrac{Y(x)}{\sqrt{1 - Y(x)^2}}, & (x_L, x_R), \\ h(x_L) = 0,\ h(x_R) = 0 \end{cases}$$

where Y is given by (3.80) and x_L and x_R are obtained via the shooting method. We notice that at this point the interval $[x_L, x_R]$ is known and we can solve directly the above problem. We choose to use an Explicit Euler Method with initial condition $h(x_L) = 0$.

We consider N_L, N_R and h_L, h_R as defined previously. We introduce $N = 2N_L + 2N_R$ points in the interval $[x_L, x_R]$ and we define the discretization space δ which is $\delta = h_L$ for those points in

$[x_L, 0]$ and $\delta = h_R$ for those in $[0, x_R]$. We define $h_i = h(x_i)$ and we have the following numerical rule

$$\begin{cases} h_0 = 0, \\ h_i = h_{i-1} - \delta \dfrac{Y_{i-1}}{\sqrt{1-(Y_{i-1})^2}} \quad \text{for } i = 1, .., N-1 \\ h_N = G \end{cases} \tag{3.81}$$

where the value G is the approximation of $G(c^*)$. We then get the numerical solution $h = [h_0, h_1, ..., h_{N-1}, h_N]$ representing the discretized positive half-boundary of the Traveling Wave like solution. The full discretized boundary can be simply obtained by applying a symmetry of h with respect to the x-axis.

3.6.1 Numerical simulations

We showed that for each fixed value of β, λ satisfying (3.28), we have a numerical scheme able to find the velocity and the graph of the related Traveling Wave like solution. We propose here some numerical simulations for a given choice of the parameters β and λ.

Numerical simulations for $\beta = 4$ and $\lambda = 1$

We first consider the function

$$f(x) = \tanh(x),$$

and we choose $\beta = 4$, $\lambda = 1$. The condition (3.28) is satisfied in this case.

For this choice, we get that $c_{\max} \simeq 11$. In Figure 3.2, we show the numerical solution Y of (3.24) for $c = 2$ in Figure 3.2a, $c = 8$ in Figure 3.2b, $c = 12$ in Figure 3.2c and $c = 15$ in Figure 3.2d. We observe that for those values of c strictly smaller then $c_{\max}$ the solution Y reaches the values -1 and $+1$ leading to the existence of both the points $x_L < 0$ and $x_R > 0$. For those values larger that $c_{\max}$, the solution Y reaches the values -1 but it does not reach the value $+1$. This is in agreement with the analysis made in Section 3.4.

We compute then the integral G. We discretize the interval $[0, c_{\max})$ by considering a uniform discretization of width 10^{-3}. In Figure 3.3 we show the numerical integral $G(c)$ for $c \in [0, c_{\max})$. We first notice that for $c = 0$ we get $G(0) = 0$. Then, for $c \ll 1$ we get $G(c) < 0$ and for $c \to c_{\max}$ the integral $G(c)$ assumes positive values. We then observe the existence of a positive point $c = c^*$ such that $G(c^*) = 0$. The numerical value is $c^* \simeq 8.72$ for which $G(c^*)$ is of the order of 10^{-5}.

In Figure 3.4 we plot the graph of the Traveling Wave like solution with velocity $c = c^*$. In particular, in Figure 3.4a we show the solution h of (3.81) with $G = G(c^*)$ computed before. We get $x_L \simeq -0.77$ and $x_R \simeq 0.32$. In Figure 3.4b, we plot the full boundary of the Traveling Wave obtained by symmetry of h with respect to the x-axes.

Conclusions and biological consequences

Spontaneous symmetry breaking is a characteristic of living cells, the model (3.1) introduced in this Chapter allows to describe this biological phenomenon. Indeed, for large enough values of the parameter β, $\beta \geq R_0/f'(0)$, two different behaviors take place: a symmetric cell with a zero velocity or an asymmetric cell with a non zero velocity. From a biological viewpoint this means that the rest state is destabilized through a bifurcation at $\beta = R_0/f'(0)$. In other words, the polarization-translation mode, which breaks the front-symmetry and leads to motility, is unstable for $\beta = R_0/f'(0)$.

As a conclusion, the model presented here is intended to be a highly simplified representation of the biological cell. The analyse performed in this work allows to prove that the models (3.6) and (3.8) – (3.12) are close to an unstable system of equations. The model (3.1) while mathematically unpleasant, describes an important feature of cell motility. Its main interest lies in its relative

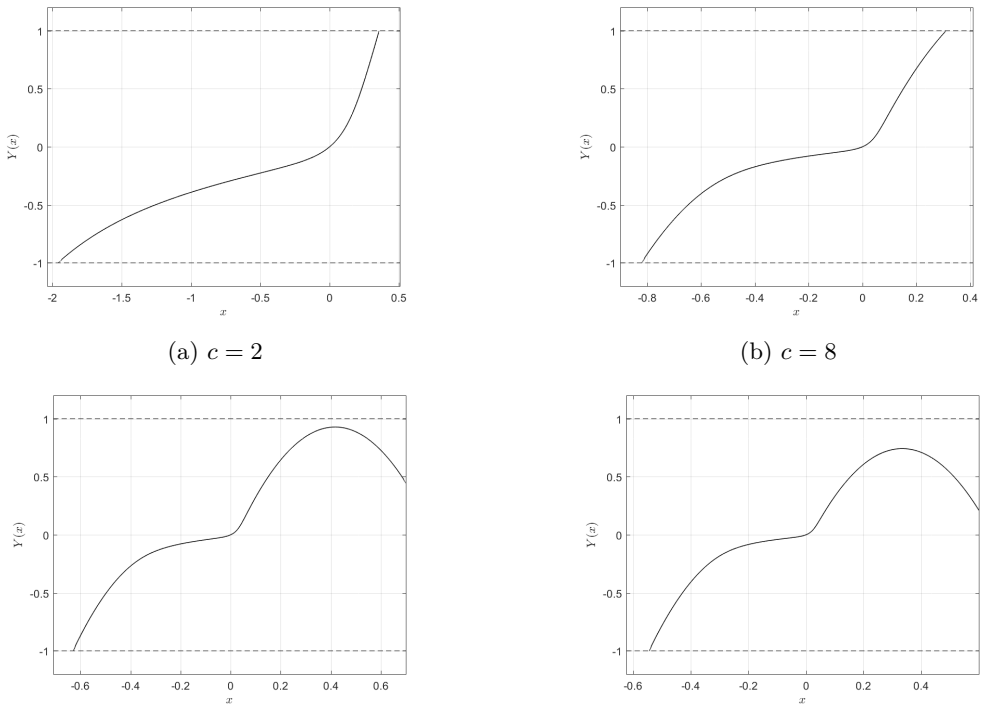

(a) $c = 2$ (b) $c = 8$

(c) $c = 12$ (d) $c = 15$

Figure 3.2 – Numerical solution Y of (3.24) for $\beta = 4$ and $\lambda = 1$ with $c = 2$ in Figure 3.2a, $c = 8$ in Figure 3.2b, $c = 12$ in Figure 3.2c and $c = 15$ in Figure 3.2d.

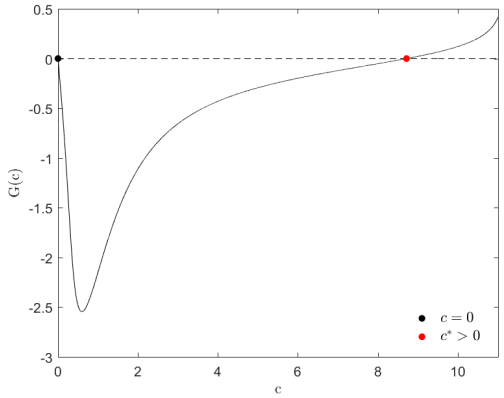

Figure 3.3 – Numerical integral G computed for $c \in [0, c_{\max})$ with $\beta = 4$ and $\lambda = 1$. Numerical value $c^* \simeq 8.72$ and $G(c^*)$ of the order of 10^{-5}.

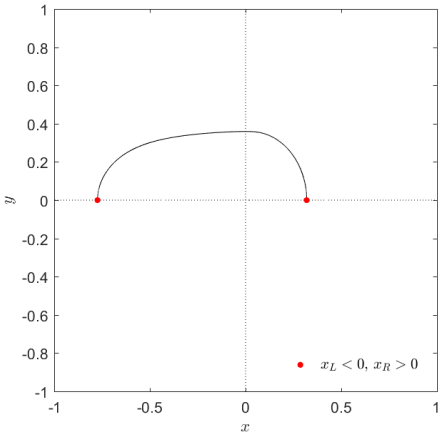

(a) Solution h of (3.81) with $x_L \simeq -0.77$ and $x_R \simeq 0.32$

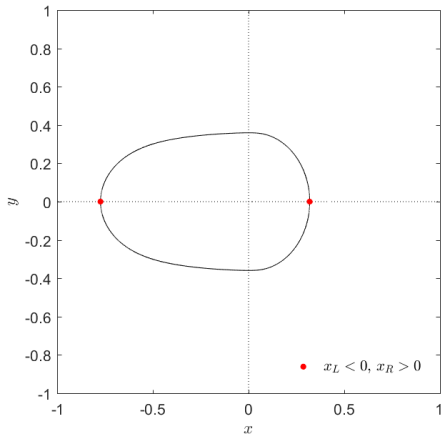

(b) Full graph $[h, -h]$ of the Traveling Wave

Figure 3.4 – In Figure 3.4a the half positive graph of the Traveling Wave and in Figure 3.4b the full graph with $\beta = 4, \lambda = 1$ and $c = c^*$.

simplicity as it is expressed as a single free-boundary model. Since it accurately describes the instability allowing cells to move, a more in-depth mathematical analysis would be interesting and challenging due to the non-conventional boundary condition. We leave the question of the existence of a Lyapunov function for (3.1) as an open question.

Bibliography

[1] L. BERLYAND, J. FUHRMANN, AND V. RYBALKO, *Bifurcation of traveling waves in a Keller-Segel type free boundary model of cell motility*, arXiv preprint arXiv:1705.10352, (2017).

[2] L. BERLYAND AND V. RYBALKO, *Stability of steady states and bifurcation to traveling waves in a free boundary model of cell motility*, Netw. Heterog. Media, 12 (2020).

[3] L. BERLYAND, V. RYBALKO, AND M. POTOMKIN, *Non-uniqueness in a nonlinear sharp interface model of cell motility*, C. R. Math. Acad. Sci. Paris, 354 (2016).

[4] ——, *Sharp interfce limit in a phase fiels model for cell motility*, Netw. Heterog. Media, 12 (2016).

[5] V. CALVEZ, R. J. HAWKINS, N. MEUNIER, AND R. VOITURIEZ, *Analysis of a nonlocal model for spontaneous cell polarization*, SIAM J. Appl. Math., 72 (2012), pp. 594–622.

[6] M. G. CRANDALL AND P. H. RABINOWITZ, *Bifurcation from simple eigenvalues*, J. Functional Analysis, 8 (1971), pp. 321–340.

[7] A. CUCCHI, A. MELLET, AND N. MEUNIER, *A Cahn-Hilliard model for cell motility*, SIAM J. Math. Anal., 52 (2020), pp. 3843–3880.

[8] A. CUCCHI, A. MELLET, AND N. MEUNIER, *Self polarization and traveling wave in a model for cell crawling migration.* preprint, 2021.

[9] M. C. DALLASTON, *Mathematical models of bubble evolution in a Hele-Shaw Cell*, PhD thesis, Queensland University of Technology, 2013.

[10] C. ETCHEGARAY, N. MEUNIER, AND R. VOITURIEZ, *Analysis of a nonlocal and nonlinear Fokker–Planck model for cell crawling migration*, SIAM J. Appl. Math., 77 (2017), pp. 2040–2065.

[11] A. FRIEDMAN, *A hierarchy of cancer models and their mathematical challenges*, Discrete Continuous Dyn. Syst. Ser. B, 4 (2004), p. 147.

[12] A. FRIEDMAN AND B. HU, *Asymptotic stability for a free boundary problem arising in a tumor model*, J. Differential Equations, 227 (2006), pp. 598–639.

[13] A. FRIEDMAN AND F. REITICH, *Symmetry-breaking bifurcation of analytic solutions to free boundary problems: an application to a model of tumor growth*, Trans. AMS, 353 (2001), pp. 1587–1634.

[14] M. GÜNTHER AND G. PROKERT, *On travelling-wave solutions for a moving boundary problem of Hele–Shaw type*, IMA journal of applied mathematics, 74 (2009), pp. 107–127.

[15] K. KEREN, Z. PINCUS, G. M. ALLEN, E. L. BARNHART, G. MARRIOTT, A. MOGILNER, AND J. A. THERIOT, *Mechanism of shape determination in motile cells*, Nature, 453 (2008), pp. 475–480.

[16] I. LAVI, N. MEUNIER, R. VOITURIEZ, AND J. CASADEMUNT, *Motility and morphodynamics of confined cells*, Phys. Rev. E, 101 (2020), p. 022404.

[17] M. S. MIZUHARA, L. BERLYAND, V. RYBALKO, AND L. ZHANG, *On an evolution equation in a cell motility model*, Phys. D, 318 (2016), pp. 12–25.

[18] M. S. MIZUHARA AND P. ZHANG, *Uniqueness and traveling waves in a cell motility model*, arXiv preprint arXiv:1703.00811, (2017).

[19] H. MONOBE AND H. NINOMIYA, *Multiple existence of traveling waves of a free boundary problem describing cell motility*, Discrete Contin. Dyn. Syst. Ser. B, 19 (2014), p. 789.

[20] N. MULLER, M. PIEL, V. CALVEZ, R. VOITURIEZ, J. GONÇALVES-SÁ, C.-L. GUO, X. JIANG, A. MURRAY, AND N. MEUNIER, *A predictive model for yeast cell polarization in pheromone gradients*, PLoS Comput. Biol., 12 (2016), p. e1004795.

[21] F. OTTO, *Dynamics of labyrinthine pattern formation in magnetic fluids: A mean-field theory*, Arch. Rational Mech. and Anal., 141 (1998), pp. 63–103.

[22] D. SHAO, H. LEVINE, AND W.-J. RAPPEL, *Coupling actin flow, adhesion, and morphology in a computational cell motility model*, Proc. Natl. Acad. Sci. U.S.A., 109 (2012), pp. 6851–6856.

[23] F. ZIEBERT AND I. S. ARANSON, *Computational approaches to substrate-based cell motility*, npj Computational Materials, 2 (2016), pp. 1–16.

Chapter 4

Hysteresis in the 2D case

This Chapter refers to an ongoing research representing a third joint work with Mellet and Meunier.

4.1 Introduction and statement of the results

In this Chapter we study the phenomenon of Hysteresis for the two-dimensional free-boundary problem presented in the Chapter 3, which models the dynamics of a living cell:

$$\begin{cases} \Delta p = 0 & \text{in } \Omega(t), \\ p + \beta f(V) = \gamma\kappa(t) & \text{on } \partial\Omega(t), \\ V = -\nabla p \cdot \mathbf{n} & \text{on } \partial\Omega(t), \\ \Omega(t=0) = \Omega_0. \end{cases} \tag{4.1}$$

The domain Ω_0 is a bounded domain of $\mathbb{R}^2$, κ indicates the mean curvature (supposed positive for convex sets) of the evolving free-boundary $\partial\Omega(t)$, $\mathbf{n}$ is the outward-pointing unit normal on $\partial\Omega(t)$, $\gamma \geq 0$ is a given parameters describing the surface tension, $\beta \geq 0$ is a given constant, $f : \mathbb{R} \to \mathbb{R}$ is a given function, and V denotes the normal velocity of the moving free-boundary $\partial\Omega(t)$. In this framework, the moving domain $\Omega(t)$ represents the domain occupied by the cell at time t whose boundary $\partial\Omega(t)$ is unknown and has to be determined together with the unknown function p representing the pressure inside the cell.

The above model comes from the work presented in Chapter 2, where we study a Cahn-Hilliard model for cell motility and we showed that its formal Sharp Interface Limit leads to free-boundary problem (4.1). In this Chapter we will assume f to satisfy the following assumptions:

(A1) f is $\mathcal{C}^3(\mathbb{R})$, monotone increasing and odd such that $f(0) = 0$,

(A2) $\lim_{x\to+\infty} f(x) = 1$ and $\lim_{x\to-\infty} f(x) = -1$,

(A3) $f'(0) > 0$, $f''(0) = 0$ and $f'''(0) < 0$.

We notice that with respect to the Chapter 3 where we studied the existence of Traveling Wave like solution of the model (4.1), here we do not have addition convexity assumption on the function f. A prototype example of a function satisfying the previous assumptions is

$$f(x) = \tanh(x).$$

As we explained in Chapter 3, the originality of the model (4.1) is represented by the boundary condition $(4.1)_2$ describing the effects of polymerization on the motion of the cell: the term $-\beta f(V)$ "pushes" the membrane of the cell and generates protrusions that are responsible of motion [9, 16]. Moreover, using classical computation done by Otto [15] we have that

$$\frac{\mathrm{d}}{\mathrm{d}t}\mathcal{J}(\Omega(t)) = -\frac{1}{\gamma}\int_{\Omega(t)} |\nabla P|^2 \,\mathrm{d}x\,\mathrm{d}y + \frac{\beta}{\gamma}\int_{\partial\Omega(t)} V f(V)\ \mathrm{d}\sigma, \tag{4.2}$$

with $\mathrm{d}\sigma$ the infinitesimal length element of $\partial\Omega(t)$. By assumptions (A1) – (A3), we have that

$$Vf(V) \geq 0,$$

leading to have that the last term in the right-hand side of (4.2) has opposite sign with respect to the first term. Hence, the term $-\beta f(V)$ has a destabilzing effect on the system, while the surface tension term has a stabilizing effect.

Due to the incompressiblity condition, the model (4.1) is area preserving:

$$\frac{\mathrm{d}}{\mathrm{d}t}|\Omega(t)| = -\int_{\Omega(t)} \Delta p \,\mathrm{d}x\,\mathrm{d}y = 0\,,$$

and since $f(0) = 0$, it admits the disk of radius R_0 denoted by B_{R_0} as stationary solution (representing the rest state) with

$$p = \frac{\gamma}{R_0}, \tag{4.3}$$

such that $|B_{R_0}| = |\Omega_0|$.

This Chapter is dedicated to the following question: is the knowledge of the shape of the cell at time t_0 (that is $\Omega(t_0)$) enough to determine $p(t_0)$ and thus characterize the behavior of $\Omega(t)$ for $t \geq t_0$?

To answer this question, we observe that (4.1) implies in particular that the function p solves the following nonlinear Robin boundary value problem:

$$\begin{cases} \Delta p = 0 & \text{in } \Omega, \\ p + \beta f(-\nabla p \cdot \mathbf{n}) = \gamma\kappa, & \text{on } \partial\Omega. \end{cases} \tag{4.4}$$

We will show here that even in the simplest case where $\Omega(t_0)$ is a disk, the equation (4.4) may have more than one solution for some values of β at least. This leads to the answer of the previous question: if we are given only a picture of the cell at a given time t_0, we can not predict its future behavior. Such a phenomenon is called Hysteresis, where future behavior depends not only on the configuration at the time t but also on its history. The Hysteresis in the case of cell motility is in agreement with experimental observations.

In Chapter 2, which refers to our recent work in collaboration with Meunier and Mellet [7], we rigorously analyzed the evolution $\Omega(t)$ solution of the problem (4.1) in the one dimensional case and we showed that it exhibits hysteresis phenomena when the destabilizing term is strong enough. Indeed, by the assumption that the cell does not divide, we considered $\Omega(t)$ as in interval of the form $\Omega(t) = (a(t), b(t))$ and we proved the following theorem:

Theorem 4.1.1 ([7]). *Let us consider an initial set $\Omega(0) = (a(0), b(0))$ with length $\ell = b(0) - a(0)$. For all $\beta > 0$, the set $\Omega(t) = (a(0), b(0))$ is a stationary solution of the problem (4.1). If*

$$\beta > \frac{\ell}{2f'(0)},$$

then (4.1) has at least two other solutions $\Omega_\pm(t)$ moving on the right or on the left with velocity $\pm c \neq 0$, that is

$$\Omega_\pm(t) = (a(0) \pm ct, b(0) \pm ct).$$

This result states in particular that even in the one dimensional case the dynamics of the model is nontrivial.

The aim of this Chapter is to study of the hysteresis phenomenon for the problem (4.1) in the two dimensional case. This Chapter is then dedicated to the proof of the following theorem:

Theorem 4.1.2. *Let the function f to satisfy the assumptions (A1) – (A3) and let us consider $\Omega = B_{R_0}$ the disk of radius R_0 in $\mathbb{R}^2$. Then, there exists an interval $I = (-\varepsilon, \varepsilon)$ and a bifurcation branch $s \in I \mapsto (\beta(s), p(s))$ such that the couple $(\beta, p) = (\beta(s), p(s))$ solves the problem*

$$\begin{cases} \Delta p = 0 & \text{in } B_{R_0}, \\ p + \beta f(-\nabla p \cdot \mathbf{n}) = \dfrac{\gamma}{R_0}, & \text{on } \partial B_{R_0}. \end{cases} \tag{4.5}$$

with

$$p(s, x, y) = \frac{\gamma}{R_0} + \frac{x}{f'(0)} s + o(s), \tag{4.6}$$

and

$$\beta(0) = \frac{R_0}{f'(0)} > 0, \quad \beta'(0) = 0, \quad \beta''(0) > 0. \tag{4.7}$$

The parameter β represents here the bifurcation parameter. This theorem states that for at least some value of $\beta > \frac{R_0}{f'(0)}$ there exist a branch of solutions to the problem (4.5) appearing via a Pitchfork bifurcation.

Since the normal velocity of ∂B_{R_0} is defined by $V = -\nabla p \cdot \mathbf{n}$, we have that the branch $p = p(s)$ defines a branch of boundary velocities given by

$$V = -\frac{\mathbf{e}_x \cdot \mathbf{n}}{f'(0)} s + o(s),$$

which (in first approximation) corresponds to a non-stationary Traveling Wave like solution moving with velocity $\frac{1}{f'(0)} s$ in the direction $\mathbf{e}_x$.

The fact that even when Ω is a disk there is a solution of (4.4) that induces a movement of $\Omega(t)$ in one direction is the illustration of the ability of cells to spontaneously polarize in the absence of any external cue: a perfectly symmetrical cell spontaneously breaks its symmetry, develops a front and a rear (polarization) and begins to move in a given direction, see [4, 8, 14].

The organization of this Chapter is the following. In Section 4.2 we present the biological justification of the problem (4.1). In Section 4.3 we recall some useful basic facts such as the bifurcation's Theory in Banach spaces and the introduction of the Dirichlet-to-Neumann operator. In Section 4.4 we present the main result of this Chapter and it is devoted to the proof of Theorem 4.1.2. Finally, in Section 4.5 we give some conclusions.

4.2 Biological justification of the model

In the biological physics community, we find a huge number of macroscopic models for cell motility. We refer to the work of Aranson and Ziebert [16] for a review. Most of them are formulated through a fluid approach with surface tension. As far as we know, the only works that study some mathematical aspects (bifurcation, Traveling Wave) of models for cell motility and polarization are the works of Beryland et. al. [1–3], the work of Mizuhara et al. [12, 13] and our recent work in collaboration with Meunier and Mellet [7] for free boundary models and the work of Calvez et. al. [4] and the work of Etchegaray et. al. [8] for cell polarization. The other works are either computational or modeling focused.

In this part we describe the origin of the problem (4.1). It is obtained as a Sharp Interface Limit of a Cahn-Hilliard model to describe the motion of a cell on a two dimansional substrate presented in Chapter 2 and refering to the joint work [7]. Finally, by studying the moments of $\Omega(t)$ for the model (4.1), we obtain information on the biophysical meaning of the boundary term $-\beta f(V)$.

Sharp Interface Limit of the phase field model introduced in [7]

In [7], we introduced the following phase-field model to describe the motion of a cell on a two dimensional substrate

$$\begin{cases} \partial_t \rho = \operatorname{div}\left(\rho \nabla\left[\gamma\left(-\varepsilon\Delta\rho + \frac{1}{\varepsilon}W'(\rho)\right) + \phi\right]\right), \\ \partial_t \phi - \varepsilon\Delta\phi = \frac{1}{\varepsilon}\left(\beta\rho - \phi\right), \end{cases} \tag{4.8}$$

with $\varepsilon > 0$, $\gamma > 0$, $\beta \geq 0$ and W a double-well potential satisfying

$$W(0) = W(1) = 0, \quad W(\rho) > 0 \text{ if } \rho \notin \{0, 1\}. \tag{4.9}$$

An example of an admissible double-well potential is $W(\rho) = \rho^2(1-\rho)^2$.

From a modeling point of view, the system (4.8) is very simple. Two quantities are used to describe the cell: the phase field (or order parameter) ρ, describing everything that lies inside the cell (cytoskeleton, solvent, molecular motors...), and the Myosin II, a molecular motor that assembles in minifilaments, interacts with actin, behaves as active crosslinkers and generates contractile or dilative stresses in the cytoskeleton network, whose concentration is denoted by ϕ. The main assumptions that lead to (4.8) are the following: (i) the cell velocity v is given by the local actin flow, (ii) Myosin II in the bulk is slowly diffusing, (iii) actin filaments undergo uniform bulk polymerization and depolymerization, (iv) the osmotic pressure involved in the network stress acts to saturate the linear instability causing gel phase separation and to smooth the interface between cytosol-rich and cytosol-poor regions. The underlying processes is composed by the friction of the cytosol on the substrate together with the active character of the Myosin II.

When $\varepsilon \ll 1$, we showed in [7] that this model is close to the free-boundary problem (4.1) in which the cell is described by a set $\Omega(t)$ (so $\rho^\varepsilon(x,t) \sim \chi_{\Omega(t)}(x)$).

Biophysical meaning of the boundary term $-\beta f(V)$

For each $t > 0$, we define the moment $\mathcal{M}_{\Omega(t)}$ of $\Omega(t)$ by

$$\mathcal{M}_{\Omega(t)} = \int_{\Omega(t)} (x, y)\, \mathrm{d}x\, \mathrm{d}y\,,$$

where $z = (x, y)$ is the vector coordinate of a point in $\Omega(t)$. In particular, $\mathcal{M}_{\Omega(t)}$ is a vector containing the x-moment and y-moment.

We define the center of mass $\mathcal{C}_{\Omega(t)}$ by

$$\mathcal{C}_{\Omega(t)} = \frac{\mathcal{M}_{\Omega(t)}}{|\Omega(t)|} = \frac{1}{|\Omega(t)|}\int_{\Omega(t)} (x, y)\, \mathrm{d}x\, \mathrm{d}y = \frac{1}{|\Omega_0|}\int_{\Omega(t)} (x, y)\, \mathrm{d}x\, \mathrm{d}y\,, \tag{4.10}$$

by using the area preservation.

The velocity $u_{\mathcal{C}}(t)$ of the center of mass of $\Omega(t)$ is given by

$$u_{\mathcal{C}}(t) = \frac{\mathrm{d}}{\mathrm{d}t}\mathcal{C}_{\Omega(t)}. \tag{4.11}$$

From incompressibility $(4.1)_1$ and boundary condition $(4.1)_2$, we deduce that

$$\begin{aligned} \frac{\mathrm{d}}{\mathrm{d}t}\mathcal{M}_{\Omega(t)} &= \int_{\partial\Omega(t)} zV\, \mathrm{d}\sigma = -\int_{\partial\Omega(t)} z\nabla P \cdot \mathbf{n}\, \mathrm{d}\sigma \\ &= -\int_{\Omega(t)} \operatorname{div}\,(z\nabla P)\, \mathrm{d}x\, \mathrm{d}y = -\int_{\Omega(t)} \nabla P \cdot \nabla z\, \mathrm{d}x\, \mathrm{d}y \\ &= -\int_{\Omega(t)} \operatorname{div}\,(P\nabla z)\, \mathrm{d}x\, \mathrm{d}y = -\int_{\partial\Omega(t)} P\nabla z \cdot \mathbf{n}\, \mathrm{d}\sigma \\ &= -\int_{\partial\Omega(t)} (\gamma\kappa + \beta f(V))\, \nabla z \cdot \mathbf{n}\, \mathrm{d}\sigma\,. \end{aligned} \tag{4.12}$$

Using that $\nabla z \cdot \mathbf{n}$ is the unit outwards normal vector to $\partial\Omega(t)$ and that

$$\int_{\partial\Omega(t)} \kappa \mathbf{n}\, d\sigma = \mathbf{0},$$

it follows that

$$u_{\mathcal{C}}(t) = -\frac{\beta}{|\Omega_0|} \int_{\partial\Omega(t)} f(V)\mathbf{n}\, d\sigma\,. \tag{4.13}$$

We recognize that (4.13) represents the external force balance on the droplet $\Omega(t)$. This justifies the model which describes the deformation of the cell membrane under the action of an active force modeled by $-f(V)$ and describing the activity of the cytoskeleton.

4.3 A brief account on some useful facts

In this section we recall some useful facts concerning bifurcation theory in Banach spaces and the introduction of the Dirichlet-to-Neumann operator.

4.3.1 Crandall-Rabinovitz's bifurcation Theorem

Let U, V be two real Banach spaces. Our aim will be to analyze the structure of the solution set of the possibly nonlinear operator $\mathcal{F}$ given by

$$\mathcal{F}(\lambda, u) = 0, \quad (\lambda, u) \in \mathbb{R} \times U,$$

where

$$\mathcal{F} : \mathbb{R} \times U \to V$$

is a continuous map. We shall use the Crandall-Rabinovitz's bifurcation Theorem to prove the Theorem (4.1.2). For the convenience of the reader, in this section we state the theorem.

Theorem 4.3.1 (Crandall-Rabinovitz's Theorem [6])**.** *Let U, V be two Banach spaces, W a neighborhood of $(\lambda_0, 0)$ in $\mathbb{R} \times U$ and $\mathcal{F} : W \longrightarrow V$. Suppose that the following properties are satisfied*

1. *$\mathcal{F}(\lambda, 0) = 0$ for all λ in a neighborhood of λ_0;*
2. *The Fréchet partial derivatives $\mathcal{D}_u\mathcal{F}, \mathcal{D}_\lambda\mathcal{F}, \mathcal{D}_{\lambda u}\mathcal{F}$ exist and are continuous;*
3. *$\operatorname{Ker}\mathcal{D}_u\mathcal{F}(\lambda_0, 0)$ is a one dimensional subspace of U spanned by a nonzero vector $u_0 \in U$;*
4. *$\operatorname{Range}\mathcal{D}_u\mathcal{F}(\lambda_0, 0)$ is a closed subspace of V of codimension 1;*
5. *$\mathcal{D}_{\lambda u}\mathcal{F}(\lambda_0, 0)[u_0] \notin \operatorname{Range}\mathcal{D}_u\mathcal{F}(\lambda_0, 0)$.*

If Z is any complement of $\operatorname{Ker}\mathcal{D}_u\mathcal{F}(\lambda_0, 0)$ in U, then, there is a neighborhood N of $(\lambda_0, 0)$ in $\mathbb{R} \times U$, an interval $I = (-\varepsilon, \varepsilon)$ for some $\varepsilon > 0$ and two continuous functions

$$\varphi : (-\varepsilon, \varepsilon) \longrightarrow \mathbb{R}, \quad \psi : (-\varepsilon, \varepsilon) \longrightarrow Z$$

such that $\varphi(0) = \lambda_0$, $\psi(0) = 0$ and

$$\mathcal{F}^{-1}[0] \cap U = \{(\varphi(s), su_0 + s\psi(s)) : |s| < \varepsilon\} \cup \{(\lambda, 0) : (\lambda, 0) \in N\}.$$

If $\mathcal{D}_{uu}\mathcal{F}$ is continuous then the functions φ and ψ are once continuously differentiable.

In Theorem 4.3.1, the point $(\lambda_0, 0) \in \mathbb{R} \times U$ is a bifurcation point of the equation $\mathcal{F}(\lambda, u) = 0$ in the following sense. In a neighborhood of $(\lambda_0, 0)$, the set of solutions of $\mathcal{F}(\lambda, u) = 0$ consists of two curves Γ_1 and Γ_2 which intersect only at the point $(\lambda_0, 0)$, where

$$\Gamma_1 = \{(\lambda, 0) \text{ where } \lambda = \lambda_0\},$$

and Γ_2 is the curve parametrized by

$$\Gamma_2 = \{(\lambda(s), u(s)), \text{ for } |s| \text{ small, and such that } (\lambda(0), u(0)) = (\lambda_0, 0), \text{ with } u'(0) = u_0,\ \lambda'(0) \neq 0\}.$$

4.3.2 The Dirichlet-to-Neumann operator

Definition 4.3.2. *Let Ω be a smooth enough open set of $\mathbb{R}^2$, the Dirichlet-to-Neumann operator $\mathcal{I}_\Omega$ is defined by*

$$\begin{aligned} \mathcal{I}_\Omega : H^1(\partial\Omega) &\to L^2(\partial\Omega) \\ \varphi &\to \nabla q \cdot \mathbf{n}, \end{aligned}$$

where the function q denotes the harmonic extension of φ to the domain Ω, that is

$$\begin{cases} \Delta q = 0 & \text{in } \Omega, \\ q = \varphi & \text{on } \partial\Omega. \end{cases} \tag{4.14}$$

The name of this operator comes from the fact that it makes the transition between a problem verifying a Dirichlet boundary condition towards a problem with a Neumann boundary condition.

In the case where Ω is the disk of radius R_0, by expanding the function φ in Fourier series, it is possible to define $\mathcal{I}_{R_0} := \mathcal{I}_{B_{R_0}}$ as follows:

Definition 4.3.3. *The Dirichlet-to-Neumann operator $\mathcal{I}_{R_0} : H^1(\mathbb{R}/2\pi\mathbb{Z}) \to L^2(\mathbb{R}/2\pi\mathbb{Z})$ is defined by*

$$\mathcal{I}_{R_0}(\varphi)(\theta) = \sum_{n=1}^{\infty} nR_0^n \left(a_n \cos(n\theta) + b_n \sin(n\theta)\right),$$

for $\varphi(\theta) = a_0 + \sum_{n=1}^{\infty} R_0^n \left(a_n \cos(n\theta) + b_n \sin(n\theta)\right)$.

This definition comes from the fact that harmonic functions q on B_{R_0} write in polar coordinate for $(r, \theta) \in [0, R_0] \times \mathbb{R}/2\pi\mathbb{Z}$ as

$$q(r, \theta) = \sum_{n \geq 0} \left(a_n \cos(n\theta) r^n + b_n \sin(n\theta) r^n\right),$$

when we discarded solutions that diverge at $r = 0$, and then

$$\nabla q(R_0, \theta) \cdot \mathbf{n} = (\partial_r q)(R_0, \theta) = \sum_{n \geq 0} nR_0^{n-1} \left(a_n \cos(n\theta) + b_n \sin(n\theta)\right).$$

For simplicity, in the sequel the operator $\mathcal{I}_{R_0}$ will be denoted by $\mathcal{I}$. This latter definition is useful for the following fact

Lemma 4.3.4. *The operator $\mathcal{I}_{R_0}$ has eigenvalues $n \in \mathbb{N} \setminus \{0\}$. Furthermore* $\operatorname{Ker}(-\mathcal{I} + nI_d) = \operatorname{span}\{\cos(n\theta)\}$ *which then have dimension* 1*, for all $n \in \mathbb{N} \setminus \{0\}$.*

4.3.3 Remarks on the elliptic problem (4.4)

Since f is a nonlinear function, the natural functional space for the problem (4.4) is $H^{\frac{5}{2}}(\Omega)$. Indeed in such a case, the trace of p on $\partial\Omega$ belongs to $H^2(\partial\Omega)$ and $\nabla p \cdot \mathbf{n}$ belongs to $H^1(\partial\Omega)$ hence in $L^\infty(\partial\Omega)$ which allows us to define $f(-\nabla p \cdot \mathbf{n})$. In the case where f admits a continuous reciprocal function f^{-1}, we can transform the problem (4.4) into

$$\begin{cases} \Delta P = 0 & \text{in } \Omega, \\ \nabla P \cdot \mathbf{n} = f^{-1}\left(\frac{P}{\beta}\right) & \text{on } \partial\Omega. \end{cases} \tag{4.15}$$

By multiplying the equation $(4.15)_1$ by p and by integrating by parts we obtain

$$\int_\Omega |\nabla P|^2 \, \mathrm{d}x \, \mathrm{d}y = \int_{\partial\Omega} P f^{-1}\left(\frac{P}{\beta}\right) \mathrm{d}\sigma. \tag{4.16}$$

Recalling that f satisfies assumptions (A1) – (A3), we deduce that

$$xf^{-1}(x) \geq 0 \qquad \forall x \in \mathbb{R}.$$

Therefore there is no obstruction for this compatibility condition (4.16) to be satisfied for a non zero function P. Moreover the problem (4.15) has the following energy functional

$$\mathcal{J}(P) = \frac{1}{2}\int_\Omega |\nabla P|^2 \,\mathrm{d}x\,\mathrm{d}y - \int_{\partial\Omega} G(P)\,\mathrm{d}\sigma, \tag{4.17}$$

where G is a primitive function of $g(x) = xf^{-1}(x/\beta)$, that is $G'(x) = g(x)$. In fact, critical points of (4.17) in $H^1(\Omega)$ are solutions of the problem (4.15) in the weak sense. In the case where f^{-1} is increasing on $\mathbb{R}_+$ it is possible to prove that the problem (4.15) admits a unique positive solution, see [5]. This is not the case here since according to the hypotheses (A1) – (A3), f^{-1} is decreasing on $\mathbb{R}_+$.

4.4 Proof of the Theorem 4.1.2

In this section we present the proof of the Theorem 4.1.2. In the first part, we show that the problem (4.5) is equivalent to a particular boundary equation. Then, we will show that the boundary equation satisfies the Crandall-Rinovitch's Theorem 4.3.1 leading to the appearance of a local bifurcation. This leads then to a local bifurcation for the original problem (4.5).

4.4.1 Reduction of the problem to a boundary equation

In this section we reduce the problem (4.5) to a boundary equation of the form

$$\mathcal{F}(\lambda, u) = 0, \tag{4.18}$$

where $\lambda \in \mathbb{R}$, u represents a function defined in ∂B_{R_0} and the maps $u \to \mathcal{F}(\lambda, u)$ is an operator mapping some neighborhood of the origin of U into V (for each fixed λ), where the spaces U and V are specified in the following.

We consider solutions of (4.5) such that they are symmetric with respect to the y-axis. In this framework, we define the spaces U and V as follows

$$U = \left\{ u(\theta) = \sum_{n=1}^{\infty} a_n R_0^n \cos(n\theta) \;:\; \sum_{n=1}^{\infty} n^2 R_0^{2n} |a_n|^2 < \infty \right\},$$

and

$$V = \left\{ u(\theta) = \sum_{n=1}^{\infty} a_n R_0^n \cos(n\theta)\,; \sum_{n=1}^{\infty} R_0^{2n} |a_n|^2 < \infty \right\}.$$

These spaces are the closure for the H^1 and L^2-norm, respectively, of the set of smooth functions of θ that are 2π-periodic, even and with mean zero on the interval $[-\pi, \pi)$. The spaces U and V are naturally equipped with the norms

$$\|u\|_U = \sum_{n=1}^{\infty} n^2 R_0^{2n} |a_n|^2 \qquad \|u\|_V = \sum_{n=1}^{\infty} R_0^{2n} |a_n|^2.$$

We then define the operator $\mathcal{F}$ as follows

$$\begin{aligned} \mathcal{F}: \quad & \mathbb{R} \times U \quad \to V, \\ & (\lambda, u) \quad \mapsto \mathcal{F}(\lambda, u) = -\mathcal{I}(u) + \lambda f^{-1}(u), \end{aligned} \tag{4.19}$$

where $\mathcal{I} = \mathcal{I}_{R_0}$ is the Dirichlet-to-Neumann operator introduced in the definition 4.3.3 and the function f satisfies the assumptions (A1) – (A3).

We note that the problem (4.18) has a lot of invariances. In particular, for any solution u of (4.18), the translation (which corresponds to a rotation in the original problem (4.5)) $u(\cdot + \alpha)$ is also a solution for any α.

We first notice that the equation (4.18) is well defined. Indeed, we have the following lemma:

Lemma 4.4.1. *Let $\lambda \in \mathbb{R}$. Then, for any λ there exists a neighborhood $W \subset \mathbb{R} \times U$ of the point $(\lambda, 0) \in \mathbb{R} \times U$ such that $\mathcal{F}$ maps W into V.*

Proof. Recalling the definition 4.3.3 of $\mathcal{I}$, we see that cosinus modes are stables by $\mathcal{I}$. Moreover since $H^1 \subset L^\infty$ in the one dimensional case, we can assume that $-1/2 < u < 1/2$ in that neighborhood so that $f^{-1}(u)$ is well-defined and bounded. □

In the following, we show the importance of the equation $\mathcal{F}(\lambda, u) = 0$.

Proposition 4.4.2. *Assume that $\beta \neq 0$. The problem (4.5) is equivalent to the problem $\mathcal{F}(\lambda, u) = 0$ where $u = (p - \frac{\gamma}{R_0})/\beta$ and $\lambda = R_0/\beta$.*

Proof. Let p be a solution to (4.5). First, we write the harmonic function p in polar coordinate

$$p(r, \theta) = a_0 + \sum_{n=1}^{\infty} r^n \left(a_n \cos(n\theta) + b_n \sin(n\theta)\right).$$

We notice that we can directly determine the coefficient a_0. Indeed, on ∂B_{R_0} we have that

$$p(R_0, \theta) = a_0 + \sum_{n=1}^{\infty} R_0^n \left(a_n \cos(n\theta) + b_n \sin(n\theta)\right),$$

$$(\nabla p \cdot \mathbf{n})(R_0, \theta) = \sum_{n=1}^{\infty} n R_0^{n-1} \left(a_n \cos(n\theta) + b_n \sin(n\theta)\right)$$

and for all $\theta \in [0, 2\pi)$ the boundary condition in equation (4.5) reduces to

$$\begin{aligned} &a_0 + \sum_{n=1}^{\infty} R_0^n \left(a_n \cos(n\theta) + b_n \sin(n\theta)\right) \\ &+\beta f\left(-\sum_{n=1}^{\infty} n R_0^{n-1} \left(a_n \cos(n\theta) + b_n \sin(n\theta)\right)\right) = \frac{\gamma}{R_0}. \end{aligned}$$

In particular, for $\theta = 0$ we get that

$$a_0 + \sum_{n=1}^{\infty} R_0^n a_n + \beta f\left(-\sum_{n=1}^{\infty} n R_0^{n-1} a_n\right) = \frac{\gamma}{R_0}$$

and for $\theta = \pi$ we obtain that

$$a_0 - \sum_{n=1}^{\infty} R_0^n a_n + \beta f\left(\sum_{n=1}^{\infty} n R_0^{n-1} a_n\right) = \frac{\gamma}{R_0}.$$

Summing the two previous equations and using the assumptions (A1) – (A3) made on f, $f(v) = -f(-v)$ for all $v \in \mathbb{R}$, it follows that

$$a_0 = \frac{\gamma}{R_0}.$$

Let us now define the function $\psi : [0, 2\pi) \to \mathbb{R}$ by

$$\psi(\theta) := p(R_0, \theta) - \frac{\gamma}{R_0} = \sum_{n=1}^{\infty} R_0^n \left(a_n \cos(n\theta) + b_n \sin(n\theta)\right). \tag{4.20}$$

Recalling the definition 4.3.3 of the Dirichlet-to-Neumann operator, we can rewrite the boundary condition in equation (4.5) as

$$\psi(\theta) + \beta f\left(-R_0^{-1}\mathcal{I}[\psi](\theta)\right) = 0, \tag{4.21}$$

and since f is odd, this leads to the following equation

$$f^{-1}\left(\frac{\psi(\theta)}{\beta}\right) = \frac{\beta}{R_0}\mathcal{I}\left(\frac{\psi(\theta)}{\beta}\right). \tag{4.22}$$

Performing the changing of variables

$$u = \beta^{-1}\psi, \quad \lambda = \beta^{-1}R_0 \quad \text{and} \quad g(s) = f^{-1}(s), \tag{4.23}$$

we finally obtain the equation (4.18).

Let $u \in U$ be a solution of the equation $\mathcal{F}(\lambda, u) = 0$, that is

$$\lambda f^{-1}(u) = \mathcal{I}(u).$$

Since $\lambda \neq 0$, we have that

$$u = f\left(\frac{\mathcal{I}(u)}{\lambda}\right).$$

Let us define the function $\tilde{p} = -\beta u + \frac{\gamma}{R_0}$. Since $-\beta\mathcal{I}(u) = \mathcal{I}(\tilde{p})$, it follows that

$$\tilde{p} = \frac{\gamma}{R_0} - \beta f\left(-\frac{\mathcal{I}(\tilde{p})}{\beta\lambda}\right).$$

Let us consider now the elliptic problem

$$\begin{cases} \Delta p = 0 & \text{in } B_{R_0}, \\ p = \tilde{p} & \text{on } \partial B_{R_0}. \end{cases}$$

We get that

$$\mathcal{I}(\tilde{p}) = -\nabla p \cdot \mathbf{n} \qquad \text{on } \partial B_{R_0}.$$

This leads to have that p is a solution of the problem (4.5) with $\beta = R_0/\lambda$. □

4.4.2 Local bifurcation

We recall that we are considering $\Omega = B_{R_0}$ as a disk of radius R_0. In this part, we will prove the following result:

Theorem 4.4.3. *Let the function f to satisfy the assumptions (A1) – (A3). For all $n \in \mathbb{N}$ there exists an interval $I = (-\varepsilon, \varepsilon)$ and a bifurcation branch $s \in I \mapsto (\beta_n(s), p_n(s)) \in \mathbb{R} \times X$ such that for all $s \in I$ the couple $(\beta, p) = (\beta_n(s), p_n(s))$ is solution of the problem (4.5) with (in polar coordinates)*

$$p_n(s, r, \theta) = \frac{\gamma}{R_0} + \frac{R_0}{nf'(0)}\frac{r^n}{R_0^n}\cos(n\theta)s + o(s). \tag{4.24}$$

and

$$\beta_n(0) = \frac{R_0}{nf'(0)}, \quad \beta_n'(0) = 0, \quad \beta_n''(0) > 0 \quad \text{for all } n \in \mathbb{N}. \tag{4.25}$$

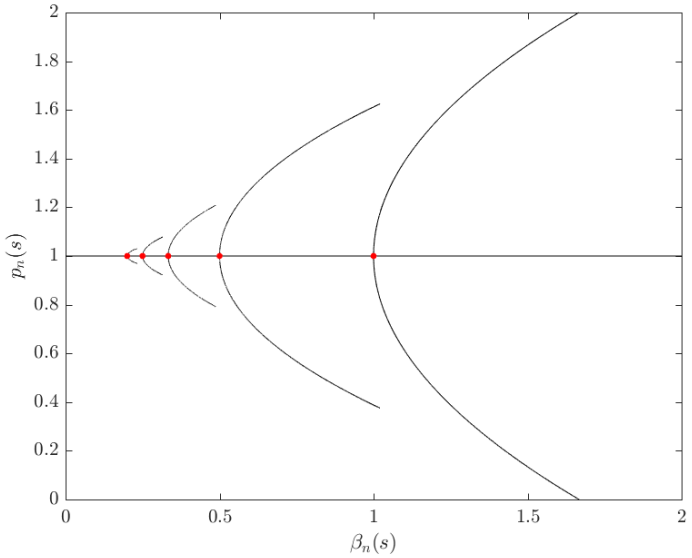

Figure 4.1 – Plot of the solution $s \in I \mapsto (\beta_n(s), p_n(s))$ of the problem (4.5) for $I = [-5, +5]$. We consider here $\gamma = 1$ and $R_0 = 1$. For all $s \in I$, the line $(\beta_n(s), \gamma/R_0)$ is the stationary solution and each curve represents the set of solutions $(\beta_n(s), p_n(s))$ for each $n \in \{1, 2, 3, 4, 5\}$. Starting from the right, the first curve is for $n = 1$ and the last curve for $n = 5$. The red dots indicates the bifucation points $\beta_n(0)$, for each $n \in \{1, 2, 3, 4, 5\}$.

This Theorem 4.4.3 represents a more general case where the Theorem 4.1.2 which corresponds to the bifurcation for $n = 1$.

The Theorem 4.4.3 states that there exists a countable number of bifurcation branches which are solutions of the problem (4.5). For all $n \in \mathbb{N}$, the value $\beta_n(0)$ represents the bifurcation point: for all $\beta > \beta_n(0)$ the problem (4.5) admits more than one solution. This implies also the non-uniqueness of the boundary velocity V obtained by computing $V = -\nabla p \cdot \mathbf{n}$.

The proof of Theorem 4.4.3 is divided into two sections. First, we use the reduction of the elliptic problem (4.5) as the nonlocal boundary equation defined by (4.18) and we prove that it satisfies the assumptions of the local bifurcation Crandall-Robinovitch's Theorem. This leads to the local existence of a bifurcation branch solution to the boundary equation. Then, we can back to the original problem and thanks to the Proposition (4.4.2), we will show that there exists a bifurcation brunch of solution to the problem (4.5). We will show finally that this bifurcation appears through a supercritical Pitchfork bifurcation.

Local bifurcation for the boundary equation (4.18)

We recall that $g'(0) = 1/f'(0)$ where $f'(0) > 0$. Therefore, we have that $g'(0) \neq 0$ and we can define the real numbers

$$\lambda_n := \frac{n}{g'(0)}. \tag{4.26}$$

We start by proving the following Proposition:

Proposition 4.4.4. *For all $n \in \mathbb{N}$, the operator $\mathcal{F}$ defined as in (4.19) where the function f satisfies the assumptions (A1) – (A3) has the following properties:*

1. $\mathcal{F}(\lambda_n, 0) = 0$;
2. $\operatorname{Ker} \mathcal{D}_u \mathcal{F}(\lambda_n, 0)$ *is a one dimensional subspace of* $\mathbb{R} \times U$ *spanned by* $u_0 = \cos(n\theta)$;

3. Range $\mathcal{D}_u\,\mathcal{F}(\lambda_n, 0)$ *is a closed subspace of* V *of codimension 1;*
4. $\mathcal{D}_{\lambda u}\,\mathcal{F}(\lambda_n, 0)[u_0] \notin \text{Range}\,\mathcal{D}_u\,\mathcal{F}(\lambda_n, 0)$.

Proof. First, by recalling the assumptions (A1) – (A3) made on f and the definitions 4.23 and 4.19 of g and $\mathcal{F}$, we note that

$$\mathcal{F}(\lambda, 0) = 0 \quad \text{for all } \lambda \in \mathbb{R}.$$

The Fréchet derivative $\mathcal{D}_u\mathcal{F}$ of the operator $\mathcal{F}$ is given by

$$\mathcal{D}_u\mathcal{F}(\lambda, u)[w] = -\mathcal{I}[w] + \lambda g'(u)w.$$

The kernel of the operator $\mathcal{D}_u\mathcal{F}(\lambda, 0)$ is the set of solutions $v \in U$ to the following equation

$$-\mathcal{I}[v] + \lambda g'(0)v = 0.$$

Thanks to the Lemma 4.3.4, the solutions of this equation are the eigenfunctions $v_n \in \text{span}\{\cos(n\theta)\}$ such that for all $\theta \in [0, 2\pi)$ it holds that

$$(n - \lambda g'(0))v_n = 0.$$

A non-zero solution to this latter equation exists if and only if $\lambda = \lambda_n$ where λ_n given by (4.26). Therefore, the operator $\mathcal{D}_u\mathcal{F}(\lambda, 0)$ is not an isomorphism whenever λ equals one of the λ_n and the second result of the proposition follows.

Let $v \in V$. Then $v = \sum_{p=1}^{\infty} \alpha_p \cos(p\theta)$ and

$$\begin{aligned}\mathcal{D}_u\mathcal{F}(\lambda_n, 0)[v] &= -(n - \lambda_n g'(0))\alpha_n \cos(n\theta) - \sum_{\substack{p=1 \\ p\neq n}}^{\infty} (p - \lambda_n g'(0))\alpha_p \cos(p\theta) \\ &= -\sum_{\substack{p=1 \\ p\neq n}}^{\infty} (p - \lambda_n g'(0))\alpha_p \cos(p\theta),\end{aligned}$$

where we used the definition (4.26) of λ_n. Therefore, the space V can be written as

$$V = \text{ Ker } D_u\mathcal{F}(u, \lambda_n) \bigoplus \text{ Range } D_u\mathcal{F}(u, \lambda_n)$$

and the third property of the proposition follows.

Let us now prove the last result. We see that

$$\mathcal{D}_{\lambda u}\mathcal{F}(\lambda_n, 0)[v] = g(0)v.$$

We proceed by contradiction. We suppose that there exists a function $w_n = \alpha_n \cos(n\theta)$ with $\alpha_n \neq 0$ such that $\mathcal{D}_{\lambda u}\mathcal{F}(\lambda_n, 0)[w_n] \in \text{Range}\,\mathcal{D}_u\mathcal{F}(\lambda_n, 0)$. This means that there exists $v = \sum_0^{\infty} \beta_k \cos(k\theta)$ belonging to V such that

$$-\mathcal{I}(w_n) + \lambda_n g'(0)w_n = g'(0)v. \tag{4.27}$$

Multiplying this equality by $\cos(n\theta)$ and integrating on $[-\pi, +\pi]$, we obtain

$$\alpha_n \int_{-\pi}^{+\pi} [-n + \lambda_n g'(0)] \cos^2(n\theta)\, d\theta = \beta_n \int_{-\pi}^{+\pi} g'(0) \cos^2(n\theta)\, d\theta.$$

which could be possible if and only if

$$\alpha_n\,(-n + \lambda_n g'(0)) = \beta_n g'(0), \quad \text{for all } n \in \mathbb{N}.$$

Since $\lambda_n = n/g'(0)$ and $g'(0) \neq 0$ it follows that $\beta_n = 0$. Similarly, multiplying (4.27) by $\cos(k\theta)$ and integrating on $[-\pi, +\pi]$ we obtain that $\beta_k = 0$ for all $k \neq n$. Therefore, we find a contradiction and the last result of the proposition is proved. □

The Proposition 4.4.4 states that the operator $\mathcal{F}$ defined by (4.19) satisfies the Crandall-Robinovitch's Theorem. Therefore we can have the following properties. For each $n \in \mathbb{N}$, let Z_n be any complement of $\mathcal{D}_u\mathcal{F}(\lambda_n, 0)$ in V. Then, there is a neighborhood N_n of $(\lambda_n, 0)$ in $\mathbb{R} \times U$, an interval $I_n = (-\varepsilon_n, \varepsilon_n)$ and two C^1 functions $\psi_{1,n} : I_n \to \mathbb{R}$ and $\psi_{2,n} : I_n \times [-\pi, +\pi] \to Z_n$ such that

$$\mathcal{F}^{-1}(0) \cap N_n = \{(\psi_{1,n}(s), s\cos(n\theta) + s\psi_{2,n}(s,\theta)),\ s \in I_n\} \cup \{(\lambda_n, 0) :\ (\lambda_n, 0) \in N_n\}$$

and

$$\psi_{1,n}(0) = \lambda_n, \quad \psi_{2,n}(0,\theta) = 0 \text{ for all } \theta \in [-\pi, +\pi].$$

In particular, we get that the solutions $(\lambda, u) = (\lambda(s), u(s,\theta))$ for all $s \in I_n$ and $\theta \in [-\pi, +\pi]$ of the equation $\mathcal{F}(\lambda, u) = 0$ are of the form

$$\lambda(s) = \psi_{1,n}(s), \qquad u(s,\theta) = s\cos(n\theta) + s\psi_{2,n}(s,\theta), \tag{4.28}$$

such that

$$\lambda(0) = \lambda_n, \quad u(0,\theta) = 0 \text{ for all } \theta \in [-\pi, +\pi]. \tag{4.29}$$

Local bifurcation for the problem (4.21)

We return now to the variables of the original problem (4.21). We previously defined that $\lambda = R_0/\beta$ and $u = \psi/\beta$ where the function $\psi = \psi(\theta)$ is defined by (4.20). By equations (4.28)-(4.29), we get that for all $n \in \mathbb{N}$ there exists an interval $I = (-\varepsilon, +\varepsilon)$ and two continuous function $\beta_n : I \to \mathbb{R}$ and $\psi_n(\cdot,\theta) : I \times [-\pi, +\pi] \to Z_n$ such that

$$\psi_n(s,\theta) + \beta_n(s) f\left(-R_0^{-1}\mathcal{I}[\psi_n](s,\theta)\right) = 0, \quad \text{for all } s \in I, \theta \in [-\pi, +\pi]. \tag{4.30}$$

In particular, the solutions $(\beta, \psi) = (\beta(s), \psi(s,\theta))$ for all $s \in I$ and $\theta \in [-\pi, +\pi]$ are of the form

$$\beta_n(s) = \frac{R_0}{\lambda_n(s)}, \quad \psi_n(s,\theta) = \beta_n(s)u(s,\theta), \tag{4.31}$$

and they are such that

$$\beta_n(0) = \frac{R_0}{\lambda_n} = \frac{g'(0)R_0}{n} > 0, \quad \psi_n(0,\theta) = u(0,\theta) = 0 \text{ for all } \theta \in [-\pi, +\pi]. \tag{4.32}$$

We observe moreover that for all $n \in \mathbb{N}$ the function $\psi_n(s,\theta)$ satisfies

$$\partial_s\psi_n(0,\theta) = \beta_n(0)\partial_s u(0,\theta) = \frac{R_0}{nf'(0)}\cos(n\theta)$$

and for small $s \in I$ we can write that

$$\psi_n(s,\theta) = \frac{R_0}{nf'(0)}\cos(n\theta)s + o(s)$$

which corresponds to have that

$$p_n(s,r,\theta) = \frac{\gamma}{R_0} + \frac{R_0}{nf'(0)}\frac{r^n}{R_0^n}\cos(n\theta)s + o(s). \tag{4.33}$$

In conclusion, we proved that for all $n \in \mathbb{N}$ there exist an interval $I = (-\varepsilon, +\varepsilon)$ and a branch $(\beta_n(s), p_n(s))$ defined for $s \in I$ such that it is solution of the problem (4.5) where $\beta_n(s)$ and $p_n(s)$ are given by the first equation in (4.31) and by the equation (4.33), respectively.

So far we have proved that for all $n \in \mathbb{N}$ a bifurcation of solutions for the equation (4.18) appears at each point $(\lambda_n, 0)$ leading to the existence of a bifurcation branch of solutions for the equation (4.5) occurring at each point $(\beta_n, 0)$. In the following, we characterize qualitatively this phenomenon by proving qualitative properties of the function $\lambda_n(s)$, and thus for $\beta_n(s)$.

Lemma 4.4.5. *Let $\mathcal{F}$ be defined as in (4.19) with f satisfying (A1) – (A3) and the functions $\lambda : I_n \to \mathbb{R}$, $u : I_n \times [-\pi, +\pi] \to Z_n$ given by (4.28) such that (4.29) hold. Then, we have $\lambda_n'(0) = 0$ and $\lambda_n''(0) > 0$. In particular, at the point $(\lambda_n, 0)$ a Pitchfork bifurcation appears.*

Proof. We consider the equation $\mathcal{F}(\lambda_n(s), u(s,\theta)) = 0$ and we compute its first derivative with respect to $s \in I$. It leads to the following equality

$$\begin{aligned} 0 = &- \mathcal{I}(\partial_{ss} u(s,\theta)) + \lambda_n''(s) g(u(s,\theta)) + 2\lambda_n'(s) g'(u(s,\theta)) \partial_s u(s,\theta) \\ &+ \lambda_n(s) g''(u(s,\theta)) \partial_s u(s,\theta)^2 + \lambda_n(s) g'(u(s,\theta)) \partial_{ss} u(s,\theta). \end{aligned} \tag{4.34}$$

By (4.29), we have that $\lambda_n(0) = \lambda_n$, $u(0,\theta) = 0$, $\partial_s u(0,\theta) = w_n(\theta)$ for all $\theta \in [-\pi, +\pi]$. Therefore, by computing the equation (4.34) for $s = 0$ and since $g(0) = 0, g''(0) = 0$ we get that

$$0 = -\mathcal{I}(\partial_{ss} u(0,\theta)) + 2\lambda_n'(0) g'(0) w_n(\theta) + \lambda_n g'(0) \partial_{ss} u(0,\theta).$$

By multiplying for w_n and by integrating on $[-\pi, +\pi]$, we get that

$$\int_{-\pi}^{+\pi} \left[\mathcal{I}(\partial_{ss} u(0,\theta)) - \lambda_n g'(0) \partial_{ss} u(0,\theta)\right] w_n(\theta) \mathrm{d}\theta = 2\lambda_n'(0) g'(0) \int_{-\pi}^{+\pi} w_n^2(\theta) \mathrm{d}\theta.$$

Since $w_n = \cos(n\theta)$, if we integrate by parts two times the above equality is true if and only if we have that

$$\lambda_n'(0) = 0, \tag{4.35}$$

and the first result of the Lemma is proved.

By computing the derivative of (4.34) with respect to s, we get the following equation

$$\begin{aligned} 0 = &- \mathcal{I}(\partial_{sss} u(s,\theta)) + \lambda_n'''(s) g(u(s,\theta)) \\ &+ 3[\, \lambda_n''(s) g'(u(s,\theta)) \partial_s u(s,\theta) + \lambda_n'(s) g''(u(s,\theta)) \partial_s u(s,\theta)^2 \\ &+ \lambda_n'(s) g'(u(s,\theta)) \partial_{ss} u(s,\theta)\,] \\ &+ \lambda_n(s) g'''(u(s,\theta)) \partial_s u(s,\theta)^3 + \lambda_n(s) g''(u(s,\theta)) u(s,\theta) \partial_{ss} u(s,\theta) \\ &+ \lambda_n(s) g'(u(s,\theta)) \partial_{sss} u(s,\theta). \end{aligned} \tag{4.36}$$

By (4.29), we have that $\lambda_n(0) = \lambda_n$, $u(0,\theta) = 0$, $\partial_s u(0,\theta) = w_n(\theta)$ for all $\theta \in [-\pi, +\pi]$. Therefore, by computing the equation (4.36) for $s = 0$ and since $g(0) = 0$, $g''(0) = 0$ and $\lambda'(0) = 0$ we get that

$$\mathcal{I}(\partial_{sss} u(0,\theta)) - \lambda_n(0) g'(0) \partial_{sss} u(0,\theta) = 3\lambda_n''(0) g'(0) w_n(\theta) + \lambda_n g'''(0) w_n(\theta)^3.$$

By multiplying for w_n and by integrating on $[-\pi, +\pi]$, we obtain the following equality

$$\begin{aligned} &\int_{-\pi}^{+\pi} \left[\mathcal{I}(\partial_{sss} u(0,\theta)) - \lambda_n g'(0) \partial_{sss} u(0,\theta)\right] w_n(\theta) \mathrm{d}\theta \\ = &\int_{-\pi}^{+\pi} \left[3\lambda_n''(0) g'(0) w_n(\theta)^2 + \lambda_n g'''(0) w_n^4(\theta)\right] \mathrm{d}\theta. \end{aligned}$$

We observe that the right-hand side term is zero and we then get

$$\lambda_n''(0) = -\frac{\lambda_n g'''(0) \int_{-\pi}^{+\pi} w_n^4(\theta) \mathrm{d}\theta}{3g'(0) \int_{-\pi}^{+\pi} w_n^2(\theta) \mathrm{d}\theta}.$$

Since the quantity $g'''(0) = f''''(0)/f'(0)^2 < 0$, we finally get that

$$\lambda_n''(0) < 0, \tag{4.37}$$

and the second result of the Lemma is proved.

In conclusion, the equality (4.35) and the inequality (4.37) allow us to say that the bifurcation branch has a stationary point at $(\lambda_n, 0)$ and it has a left-orientated convexity. Therefore, at the point $(\lambda_n, 0)$ a Pitchfork bifurcation appears. □

By returning to the original variables, we have that

$$\beta_n(s) = \frac{R_0}{\lambda_n(s)}.$$

By using (4.35) we deduce that

$$\beta_n'(0) = -\frac{R_0}{\lambda_n^2(0)}\lambda_n'(0) = 0,$$

and by using (4.35) and (4.37) it follows that

$$\beta_n''(0) = 2\frac{R_0}{\lambda_n^3(0)}\lambda_n'(0)^2 - \frac{R}{\lambda_n^2(0)}\lambda_n''(0) = -\frac{R}{\lambda_n^2(0)}\lambda_n''(0) > 0.$$

4.5 Conclusion and biological consequences

We first give some results concerning the free-boundary problem (4.1).

Proposition 4.5.1. *Let $\mathcal{F}$ be defined as in (4.19) with f satisfying (A1) – (A3). At $\beta = \beta_n(0) = \frac{R_0}{nf'(0)}$, the function defined by (4.24) generates the following normal velocity*

$$V = V(\theta) = -\left(\nabla p_n \cdot \mathbf{n}\right)(R_0, \theta) = -\frac{1}{f'(0)}\cos(n\theta)s + o(s), \qquad \text{for all } \theta \in [-\pi, +\pi].$$

Moreover, the instantaneous velocity V_{cm} of the center of mass of B_{R_0} has a nonzero value for $\beta > \beta_1 = R_0/f'(0)$.

Proof. In polar coordinates we have

$$(\nabla p_n \cdot \mathbf{n})(r, \theta) = \partial_r p_n(r, \theta) = \frac{1}{f'(0)}\frac{r^{n-1}}{R_0^{n-1}}\cos(n\theta) + o(s),$$

which implies that

$$V(\theta) = (-\nabla p_n \cdot \mathbf{n})(R_0, \theta) = -\frac{1}{f'(0)}\cos(n\theta)s + o(s),$$

and the first result is proved.

The center of mass $\mathcal{C}_{B_{R_0}(t)} = \frac{1}{\pi^2}\left(\int_{B_{R_0}(t)} x\,\mathrm{d}x, \int_{B_{R_0}(t)} y\,\mathrm{d}x\right)$ of B_{R_0} has the instantaneous velocity

$$\begin{aligned}\frac{\mathrm{d}}{\mathrm{d}t}\pi^2\mathcal{C}_{B_{R_0}(0)} &= \left(\int_{\partial B_{R_0}(0)} xV\,\mathrm{d}\sigma, \int_{\partial B_{R_0}(0)} yV\,\mathrm{d}\sigma\right) \\ &= -\frac{s}{f'(0)}\left(\int_{-\pi}^{+\pi}\cos(\theta)\cos(n\theta)\mathrm{d}\theta, \int_{-\pi}^{+\pi}\sin(\theta)\cos(n\theta)\mathrm{d}\theta\right).\end{aligned}$$

These integrals have the following values:

$$\int_{-\pi}^{+\pi}\cos(\theta)\cos(n\theta)\mathrm{d}\theta = \begin{cases}\pi & \text{for } n = 1\\ 0 & \text{for } n \geq 2\end{cases}$$

and

$$\int_{-\pi}^{+\pi}\sin(\theta)\cos(n\theta)\mathrm{d}\theta = 0, \qquad \text{for all } n \in \mathbb{N}.$$

Therefore, the center of mass $\mathcal{C}_{B_{R_0}(t)}$ has non-zero instantaneous velocity only for modes $n = 1$. □

In conclusion, the domain B_{R_0} moves along the x-direction with a non-zero instantaneous velocity which appears for those values $\beta > \beta_1 = R_0/f'(0)$. We observe that the critical value β_1 is the same critical value obtained in the 1D analysis condced in our recent work [7]: $\beta > \frac{\ell}{2f'(0)}$ with $\ell = 2R$ the diameter of the cell.

Spontaneous symmetry breaking is a characteristic of living cells and the model (4.1) introduced in this work allows to describe this biological phenomenon. Indeed for large enough value of the parameter β, that is $\beta > R_0/f'(0)$, two different behaviors take place: a symmetric cell with a zero velocity or an asymmetric cell with a non-zero velocity. From a biological viewpoint this means that the rest state (4.3) is destabilized through a bifurcation at $\beta = R_0/f'(0)$. In other words, the polarization-translation mode, which breaks the front-symmetry and leads to motility, is unstable for $\beta = R_0/f'(0)$. This is in good agreement with the linear stability analysis performed in [10], where the authors proved that the rest state for their equations is linearly instable as soon as $a\chi \geq R_0/f'(0)$. Both results are in good agreement by recalling that the a parameter comes from the derivative of $f(ax)$.

We note that when $\beta > \frac{R_0}{f'(0)}$ the model (4.1) does not allow to select one solution over another. Remembering that (4.1) is only asymptotically close to the phase-field original model [7] or that (4.1) is a first order perturbation of the coupled free-boundary model introduced in [10], for these latter models, this means that small variations in the initial condition can lead to a radically different behavior of the cell (stationary solution v.s. moving traveling wave).

Moreover, there is nothing that would prevent a solution from changing velocity in a discontinuous way (for example a solution that moves with positive speed could suddenly stop). This indicate an unstable process in which small variation in the media can cause a stationary cell to suddenly start moving, a phenomena referred to as self-polarization. Such behaviors are precisely what is observed experimentally.

In conclusion, the model presented here is intended to be a highly simplified representation of the biological cell. The analyse performed in this work allows to prove that the models in [7] and [10] are close to an unstable system of equations. The model (4.1) while mathematically unpleasant, describes an important feature of cell motility. Its main interest lies in its relative simplicity as it is expressed as a single free-boundary model. Since it accurately describes the instability allowing cells to move, a more in-depth mathematical analysis would be interesting and challenging due to the non-conventional boundary condition. We leave the question of the existence of a Lyapunov function for (4.1) as an open question.

Bibliography

[1] L. BERLYAND AND V. RYBALKO, *Stability of steady states and bifurcation to traveling waves in a free boundary model of cell motility*, Netw. Heterog. Media, 12 (2020).

[2] L. BERLYAND, V. RYBALKO, AND M. POTOMKIN, *Non-uniqueness in a nonlinear sharp interface model of cell motility*, C. R. Math. Acad. Sci. Paris, 354 (2016).

[3] ——, *Sharp interfce limit in a phase fiels model for cell motility*, Netw. Heterog. Media, 12 (2016).

[4] V. CALVEZ, R. J. HAWKINS, N. MEUNIER, AND R. VOITURIEZ, *Analysis of a nonlocal model for spontaneous cell polarization*, SIAM J. Appl. Math., 72 (2012), pp. 594–622.

[5] D. S. COHEN, *Generalized radiation cooling of a convex solid*, Journal of Mathematical Analysis and Applications, 35 (1971), pp. 503–511.

[6] M. G. CRANDALL AND P. H. RABINOWITZ, *Bifurcation from simple eigenvalues*, J. Functional Analysis, 8 (1971), pp. 321–340.

[7] A. CUCCHI, A. MELLET, AND N. MEUNIER, *A Cahn–Hilliard model for cell motility*, SIAM J. Math. Anal., 52 (2020), pp. 3843–3880.

[8] C. ETCHEGARAY, N. MEUNIER, AND R. VOITURIEZ, *Analysis of a nonlocal and nonlinear Fokker–Planck model for cell crawling migration*, SIAM J. Appl. Math., 77 (2017), pp. 2040–2065.

[9] K. KEREN, Z. PINCUS, G. M. ALLEN, E. L. BARNHART, G. MARRIOTT, A. MOGILNER, AND J. A. THERIOT, *Mechanism of shape determination in motile cells*, Nature, 453 (2008), pp. 475–480.

[10] I. LAVI, N. MEUNIER, R. VOITURIEZ, AND J. CASADEMUNT, *Motility and morphodynamics of confined cells*, Phys. Rev. E, 101 (2020), p. 022404.

[11] I. LAVI, N. MEUNIER, R. VOITURIEZ, AND J. CASADEMUNT, *Motility and morphodynamics of confined cells*, Phys. Rev. E., 101 (2020), p. 022404.

[12] M. S. MIZUHARA, L. BERLYAND, V. RYBALKO, AND L. ZHANG, *On an evolution equation in a cell motility model*, Phys. D, 318 (2016), pp. 12–25.

[13] M. S. MIZUHARA AND P. ZHANG, *Uniqueness and traveling waves in a cell motility model*, arXiv preprint arXiv:1703.00811, (2017).

[14] N. MULLER, M. PIEL, V. CALVEZ, R. VOITURIEZ, J. GONÇALVES-SÁ, C.-L. GUO, X. JIANG, A. MURRAY, AND N. MEUNIER, *A predictive model for yeast cell polarization in pheromone gradients*, PLoS Comput. Biol., 12 (2016), p. e1004795.

[15] F. OTTO, *Dynamics of labyrinthine pattern formation in magnetic fluids: A mean-field theory*, Arch. Rational Mech. and Anal., 141 (1998), pp. 63–103.

[16] F. ZIEBERT AND I. S. ARANSON, *Computational approaches to substrate-based cell motility*, npj Computational Materials, 2 (2016), pp. 1–16.

Chapter 5

Cell migration in complex environments

This Chapter refers to the proceedings [4] in collaboration with Etchegaray, Meunier, Navoret and Sabbagh.

Introduction

Cell migration plays a central role in a wide variety of biological phenomena. In the immune system, leukocytes migrate into areas of injury where they mediate the immune response [5]. Migration of fibroblasts and vascular endothelial cells is crucial for wound healing [18]. In metastasis state, tumor cells migrate from the initial tumor mass into the circulatory system and then leave and migrate into other sites [1, 12]. Finally, cell migration is significant in many technological applications, such as tissue engineering, since it plays an important role in colonization of biomaterials scaffolding.

A striking feature of animal cells is their ability to polarize in response to environmental cues. This asymmetry is fundamental to the structure and function of most cell types. Front-rear polarization, characterized by the establishment of cell protrusive polarity and directed migration, is controlled by intrinsic cell properties but also by extracellular cues such as biochemical and physical cues. We will focus here on the impact of biochemical and mechanical cues for cell crawling on a substrate. The starting point is to enrich the stochastic model introduced in [6], which describes cell crawling on an homogeneous substrate in the absence of any biochemical cues, to account for biochemical and mechanical cues. We first study the 1D case in the presence of a constant gradient of attractive signal in the medium, and we show that it captures different cell behaviours, namely a transition between migration dominated by the cell's internal activity and migration dominated by the external signal. More precisely, if the cell sensitivity to the signal is weak then the cell does not always follow the signal and it can go in another direction. On the contrary the cell follows the signal if its sensitivity to the signal is high. We proceed by investigating numerically the additional role of physical constraints composed by an homogeneous distribution of topographical obstacles. This is done by considering the cell as a rigid disk in the spirit of [10] and by using a specific numerical method, introduced in [13, 17], to solve the problem of the contact with obstacles. We start by considering the case of a Brownian particle and we study the effect of the obstacles and then the effect of an external constant force on the particle dynamics. Successively, we take into account the cell internal activity. We observe the existence of a velocity value that the cell can not exceed even if the directional force intensity increases. We find that this threshold value depends on the number of obstacles. It is to be noticed that such a result was already observed in [2] for the case of a tracer particle that moves in a geometrically confined lattice system populated by bath particles moving randomly. We believe that this study could help to better understand some aspects of cell motility in tissues.

The chapter is presented as follows. In Section 5.1 we describe the stochastic model we will consider to describe cell crawling over a flat substrate in the presence of a constant gradient of external signal. In Section 5.1.1, we study in the one dimensional case the stochastic model presented in the previous section and we show some numerical simulations. Finally in Section 5.2, we consider the two dimensional case and we enrich the stochastic model to account for the presence of topographical obstacles and we show finally some numerical simulations.

5.1 A 2D stochastic model for cell crawling under constant gradient in signal

A discrete stochastic jump process

In this section, we enrich the model introduced in [8] that describes the cell crawling over a flat surface in the absence of external cue. We extend the model to take into account the effect of a constant gradient of attractive signal on the dynamics.

In the absence of external cue, cell crawling consists of four main steps which are schematized in Figure 5.1. At first, the cell extends protrusions in its direction of motion that adhere to the substrate and de-adhere at the cell rear. We distinguish two types of cell protrusion: lamellipodia that are wide and flat, and filopodia that are finger-like extensions. Finally, contractile forces generate at the rear of the cell pull the whole cell body forward.

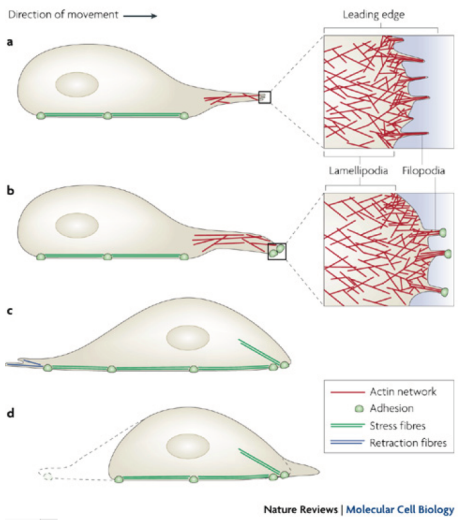

Figure 5.1 – A scheme representing the process of cell motion diveded into three steps: (a) the creation of protrusions, (b)-(c) the adhesion of the cell front and the dehadesion of the cell rear, (d) contraction forces to pull the cell body forward. Image from [15].

We first recall the model introduced and studied in [6, 8, 9]. The cell is considered as a point, and the apparition/retraction of filopodial extensions are associated to forces acting on the cell dynamics. A schematized description is presented in Figure 5.2. Let N_t be the number of filopodia adhering on the substrate at time t, and denote by $\vec{V}_t$ and $(\vec{F}_i)_{i=1,\dots,N_t}$ respectively the cell velocity and the filopodial forces exerted by the filopodia at time t. Each filopodial force $\vec{F}_i$ is assumed to be unitary and constant in time. Denoting by $\theta_i = \arg(\vec{F}_i)$, $\theta_t = \arg(\vec{V}_t)$ and $v_t = ||\vec{V}_t||$, the force and the velocity can be written in polar coordinates as $\vec{F}_i = (\cos\theta_i, \sin\theta_i)$ and $\vec{V}_t = (v_t, \theta_t)$. The cell motion with velocity $\vec{V}_t$ on the substrate leads to the appearance of a friction force which writes $\vec{f} = -\gamma\vec{V}_t$, where the parameter γ denotes the global friction substrate coefficient. Since

the crawling of a cell on an adhesive substrate occurs at very small scales, the inertia is negligible for this system.

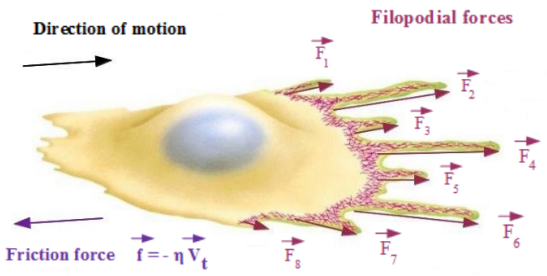

Figure 5.2 – A scheme of a cell which moves by crawling on the substrate. The forces $\vec{F_i}$ rapresent the filopodial forces pointing at the direction of motion which give rise to the cell velocity $\vec{V_t}$. The force $\vec{f}$ rapresents the friction force where η is a friction coefficient. In the model, the friction coefficient is denoted by the paramater γ. Image from [14].

Therefore by the force balance principle, the sum of the filopodial forces $(\vec{F_i})_{i=1,\dots,N_t}$ and the friction $\vec{f}$ cancels leading to

$$\gamma \vec{V_t} = \sum_{i=1}^{N_t} (\cos\theta_i, \sin\theta_i). \tag{5.1}$$

Each filopodium is identified by the quantitative parameter $\theta \in [0, 2\pi)$ which indicates its orientation and one can introduce the Dirac measure δ_θ which characterizes each filopodium. In this framework, the set of all filopodial forces are described by the finite point measure ν_t defined by

$$\nu_t = \sum_{i=1}^{N_t} \delta_{\theta_i}.$$

For any measurable function f on $[0, 2\pi)$, the measure ν_t is such that $\langle \nu_t, f \rangle := \sum_{i=1}^{N_t} f(\theta_i)$ and $N_t = \langle \nu_t, 1 \rangle$ corresponds to the filopodia population size. With this notation, Equation (5.1) translates into

$$\gamma \vec{V_t} = \big(\langle \nu_t, \cos \rangle, \langle \nu_t, \sin \rangle \big). \tag{5.2}$$

The Equation (5.2) represents the discrete model for computing the velocity $\vec{V_t}$ which is entirely described by the measure-valued jump process $(\nu_t)_t$. The events that rule the protrusion activity are the following:

- **Creation of filopodia**: new filopodia form with rate $c(\theta; \vec{V_t})$, so that they form uniformly for a null velocity, and preferentially in the direction of motion when the velocity increases. This allows to model cell polarization. More precisely, the creation rate of filopodia is proportional to the probability density of a circular normal distribution centered in the direction of motion.
- **Individual death**: each filopodium may disappear with rate d.
- **Individual reproduction**: each filopodium is able to induce the formation of a new protrusion having the same orientation or a slightly modified orientation with reproduction rate r. In this latter case, the orientation of the new filopodium is chosen following a probability distribution $g(\cdot, \theta_i)$ assumed centered in the "parent's" orientation θ_i with constant variance.

The environment affects the cell migration either mechanically (i.e. rigidity and adhesiveness of the substrate, presence of obstacles,...) or chemically due to the presence of some molecular species which attract or repulse it. In both cases, the cell feels its outer environment by using molecular receptors located at its membrane and at protrusion tips. We consider now the situation where a constant gradient in attractive signal is present in the environment. We assume that the external signal causes the cell to polarize towards its source by inducing a constant bias in the protrusions activity. We enrich the model previously described by considering that the signal interferes with the creation of the protrusions and by taking into account the direction of the signal. Let θ_g be the angle pointing to the direction of the constant gradient of signal. A simple choice is to assume that the creation rate is a convex interpolation between the direction of cell motion θ_t and the direction of the signal θ_g:

$$c(\theta; \vec{V}_t, \theta_g) = c^* \left[(1-h) \frac{e^{\kappa(v_t)\cos(\theta-\theta_t)}}{2\pi I_0(\kappa(v_t))} + h \frac{e^{\beta\cos(\theta-\theta_g)}}{2\pi I_0(\kappa_2)} \right], \tag{5.3}$$

where $v_t = \|\vec{V}_t\|$, $\kappa(v_t) = \alpha v_t$ with $\alpha \geq 0$ representing the cell capacity to polarize i.e. to create protrusions in the direction of movement, the parameter $\beta \geq 0$ represents the cell sensitivity to the signal, I_0 denotes the 0-order modified Bessel function of first kind and $h \in [0,1]$ is a real number. We remark that for $h = 0$ we obtain the creation rate of the model of migration without signal introduced in [8]. It can be shown that these rates define a well-posed Markovian Jump process with values in the space of finite point measures on $[0, 2\pi)$ (see [7, 8, 11]).

A continuous stochastic model

As it was done in the absence of external signal [6, 8], by using a rescaling procedure, by accelerating the dynamics and by considering infinitesimal filopodial forces, it is possible to derive a continuous model from the discrete one presented in the previous section. In particular, it is possible to obtain the following Stochastic Differential Equation for the cell velocity $\vec{V}_t$:

$$d\vec{V}_t = \left[\frac{c}{\gamma} ((1-h)\tanh(\alpha v_t)\, \vec{e}_{\theta_t} + h \tanh(\beta)\, \vec{e}_{\theta_g}) - \lambda \vec{V}_t \right] \mathrm{d}t + \frac{\sigma}{\gamma}\, \mathrm{d}\vec{W}_t, \tag{5.4}$$

for $0 < t \leq T$ with $T < +\infty$. In Equation (5.4) $\lambda > 0$ is related to the lifetime of filopodia, $\sigma > 0$ quantifies the intensity of the noise, $\vec{e}_{\theta_t} = \vec{V}_t / v_t$ denotes the direction of the cell motion, $\vec{e}_{\theta_g}$ denotes the direction of the constant gradient of signal, and $(\vec{W}_t)_{t\geq 0}$ represents a given 2d standard Brownian motion. This equation has to be supplemented by a random initial velocity $\vec{V}_0$. We remark that when $h = 0$ we get

$$d\vec{V}_t = \left[\frac{c}{\gamma} \tanh(\alpha v_t) \vec{e}_{\theta_t} - \lambda \vec{V}_t \right] \mathrm{d}t + \frac{\sigma}{\gamma} \mathrm{d}\vec{W}_t. \tag{5.5}$$

Equation (5.5) was introduced in [7] as the continuous model to describe the cell crawling in the absence of signal. The first term in the right-hand side represents the capacity of the cell to polarize and to generate driving forces in the direction of motion. The second term accounts for a death term that originates in the discrete model from either protrusions retraction or the formation of protrusions in a direction antagonist to motion. Finally, the last term represents the stochastic fluctuations of the cell dynamics. When $\alpha = 0$, the model describes the dynamics of a passive particle moving by a damped Brownian motion. Whereas if $\alpha > 0$, the model takes into account the additional term related to the intracellular dynamics, namely the dynamics of the actin cytoskeleton and the capacity to polarize.

In the following section, we consider the one dimensional case and we study the different behaviors arising from the competition of the two phenomena, polarization vs external signal, when varying both parameters α and β.

5.1.1 The 1D case of the continous stocastic model

In this section we study equation (5.4) in dimension one. We follow the lines of [8] in which equation (5.5) was studied in dimension one. The direction of the signal $\vec{e}_{\theta_g}$ becomes $+1$ if the signal is located on the positive side of the real line and -1 if it is located on the negative side. More precisely, we reach the following equation

$$\mathrm{d}V_t = \left[\frac{c}{\gamma}(1-h)\tanh(\alpha V_t) \pm h\frac{c}{\gamma}\tanh(\beta) - \lambda V_t\right]\mathrm{d}t + \frac{\sigma}{\gamma}\mathrm{d}W_t, \tag{5.6}$$

for $0 < t \leq T$. In this framework, the cell velocity V_t is a stochastic process taking values in $\mathbb{R}$ and W_t is the standard 1D-Brownian motion. In the first part of this section, we follow the lines of [8] and we recall how one can find the stationary distribution of V_t solving (5.6). In the second part we present the results of some numerical simulations.

Let $p_s(V,t)$ be the probability distribution of V_t. By Ito's formula, the density $p_s(V,t)$ solves the following Fokker-Planck partial differential equation

$$\partial_t\, p_s(V,t) = -\partial_V\left[f^{\pm}(V)\, p_s(V,t)\right] + \frac{\sigma^2}{2\gamma^2}\,\partial_V^2 p_s(V,t),$$

where

$$f^{\pm}(V) := \frac{c}{\gamma}(1-h)\tanh(\alpha V) \pm h\frac{c}{\gamma}\tanh(\beta) - \lambda V.$$

The stationary distribution $p_s(V)$ then satisfies the following equation

$$-\partial_V\left[f^{\pm}(V)\, p_s(V)\right] + \frac{\sigma^2}{2\gamma^2}\,\partial_V^2 p_s(V) = 0.$$

Integrating twice with respect to V, we get the explicit formulation for $p_s(V)$:

$$p_s(V) = \mathcal{N}\, e^{-W^{\pm}(V)}, \tag{5.7}$$

where $\mathcal{N}$ is a normalization constant and

$$W^{\pm}(V) := -\frac{2\gamma^2}{\sigma^2}\left((1-h)\frac{c}{2\alpha\gamma}\ln(\cosh(\alpha V)) \pm h\frac{c}{\gamma}\tanh(\beta)V - \frac{\lambda}{2}V^2\right). \tag{5.8}$$

In order to study the different behaviours of the stationary velocity by varying the parameters α and β, one can look for the values of V that minimize the function $W^{\pm}$. Indeed by equation (5.7), the minima points of $W^{\pm}$ are also the maxima points of the stationary distribution p_s, and thus they represent the velocities which have the greatest probability to occur. In the following we consider the case for which the signal is on the negative side of the real line, and thus we analyze the function W^{-}.

Figure 5.3 shows the graph of the function W^{-} for $\beta = 0.1$ with $\alpha = 0.1$ (Figure 5.3a) and $\alpha = 10$ (Figure 5.3b). One can notice that for $\alpha = 0.1$ the function W^{-} has only one global minimum realized by $V \sim 0$. Instead, for $\alpha = 10$ there exist two minima points $V_1 < 0 < V_2$ for which W^{-} has a global minimum in V_1 and a local minimum in V_2. Therefore by considering $\beta = 0.1$, for $\alpha = 0.1$ the most probable velocity is $V \sim 0$ and the cell moves as a Brownian motion, whereas for $\alpha = 10$ there are two most probable velocities $V_1 < 0$ and $V_2 > 0$ but for which $W^{-}(V_1) < W^{-}(V_2)$ and the cell moves with higher probability towards the signal.

Figure 5.4 shows the case for $\beta = 1$ with $\alpha = 0.1$ (Figure 5.4a) and $\alpha = 10$ (Figure 5.4b). One can notice that the function W^{-} has one global minimum for both $\alpha = 0.1$ and $\alpha = 10$ realized respectively by $V_3 < 0$ and $V_4 < 0$ for which $V_3 < V_4$. This means that if $\beta = 1$ the cell moves towards the signal for both the values $\alpha = 0.1$ and $\alpha = 10$. In Figure 5.5 we show the graph of W^{-} with the same value $\beta = 1$ but for $\alpha = 100$. One can notice that in this case W^{-} has a global minimum for $V_5 < 0$ and a local minimum for $V_6 > 0$ such that $W^{-}(V_5) \ll W^{-}(V_6)$. Even if α is much more larger then the cases presented in Figure 5.4, the signal is strong enough to be picked up by the cell which then moves towards the signal.

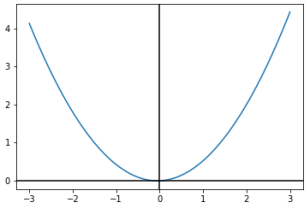

(a) $\alpha = 0.1$

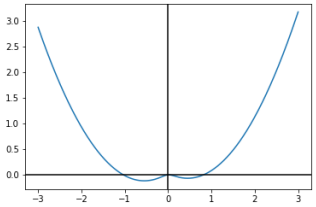

(b) $\alpha = 10$

Figure 5.3 – Graph of the potential W^- defined by (5.8) for $h = 0.5$, $\lambda = 1$, $\gamma = c = \sigma = 1$, $\beta = 0.1$, $\alpha = 0.1$ (5.3a) and $\alpha = 10$ (5.3b).

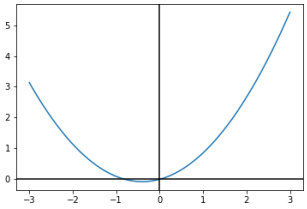

(a) $\alpha = 0.1$

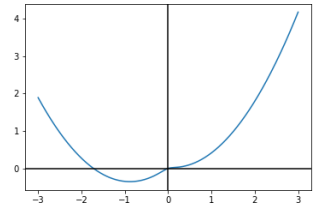

(b) $\alpha = 10$

Figure 5.4 – Graph of the potential W^- defined by (5.8) for $h = 0.5$, $\lambda = 1$, $\gamma = c = \sigma = 1$, $\beta = 1$, $\alpha = 0.1$ (5.4a) and $\alpha = 10$ (5.4b).

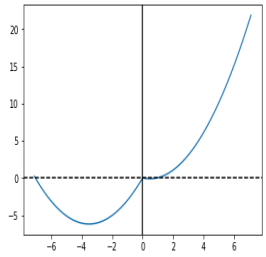

Figure 5.5 – Graph of the potential W^- defined by (5.8) $h = 0.5$, $\lambda = 1$, $\gamma = c = \sigma = 1$, $\beta = 1$ and $\alpha = 100$.

5.1.2 Numerical simulations of the 1D case

In this section we present some numerical simulations of equation (5.6). We consider $h = 0.5$, $\lambda = 1$, $\gamma = c = \sigma = 1$ and the signal located in the negative side. We set $T = 1000$ and let $dt = 0.01$ be the time-step in the time interval $[0, 1000]$, and let $I = T/dt = 10000$ be the number of time iterations in $[0, 1000]$. For $n = 0, ..., I-1$ let $V^n = V(t^n)$ be the velocity at time $t^n := n \times dt$. We consider the initial condition $V^0 = 0$ and we compute the velocity V^{n+1} by using Euler-Maruyama method as follows:

$$V^{n+1} = V^n + \left[\frac{c}{2\gamma}\tanh(\alpha V^n) \pm \frac{c}{2\gamma}\tanh(\beta) - \lambda V^n\right]dt + \frac{\sigma}{\gamma}dW_n. \tag{5.9}$$

Figures 5.6a and 5.6b show respectively the velocity histogram and the cell trajectory for $\beta = 0.1$ and $\alpha = 0.1$. We notice that the most probable velocity is around zero and that the cell moves as a Brownian particle. This is in agreement with the graph of W^- presented in Figure 5.3a.

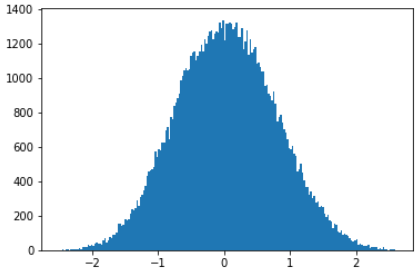

(a) Velocity histogram for $\alpha = 0.1$

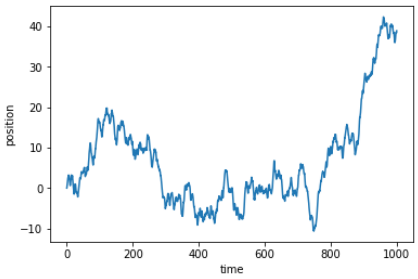

(b) Trajectory for $\alpha = 0.1$

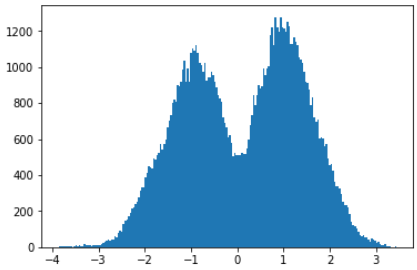

(c) Velocity histogram for $\alpha = 10$

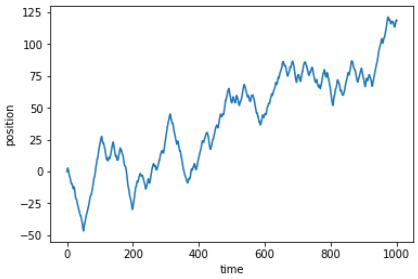

(d) Trajectory for $\alpha = 10$

Figure 5.6 – Histogram for the velocity V solution of Equation (5.6) (5.6a,5.6c) and cell trajectory (5.6b,5.6d) for $h = 0.5$, $\lambda = 1$, $\gamma = c = \sigma = 1$, $\beta = 0.1$, $\alpha = 0.1$ (5.6a,5.6b) and $\alpha = 10$ (5.6c,5.6d).

Figures 5.6c and 5.6d show respectively the velocity histogram and the cell trajectory for $\beta = 0.1$ and $\alpha = 10$. We notice that there exist two most probable velocities, one strictly positive and the other strictly negative. We observe then that the cell moves with non-zero mean velocity by showing more persistence in the trajectory with respect to the Figure 5.6b.

Figures 5.7a and 5.7b show respectively the velocity histogram and the cell trajectory for $\beta = 1$ and $\alpha = 0.1$. The velocity histogram has a single peak shifted towards the direction of the signal and the cell trajectory show a strong persistence in the direction of the signal. This is in agreement with the graph of W^- presented in Figure 5.4a.

Figures 5.7c and 5.7d show respectively the velocity histogram and the cell trajectory for $\beta = 1$ and $\alpha = 10$. We observe that the velocity histogram does not have a unimodal shape but its larger peak is in the direction of motion. In addition, the cell trajectory has the same qualitative behavior as the one presented in Figure 5.7b.

Therefore, it seems that the cell may not follow the signal and go into the wrong direction if β is small and α is big, whereas when β is big the cell follows the signal if α is small and it may escape if α is big.

5.2 The effect of topographical obstacles in a 2D framework

In this section, we study numerically the behavior of an active particle, with the previously described dynamics, in an environment containing obstacles and chemoattractants. In our framework, we consider one single moving particle in an environment containing a uniform distribution of fixed circular obstacles, where a constant gradient in signal induces a directional bias in its displacement.

We consider N uniformly distributed circular obstacles, each of center $q_i \in \mathbb{R}^2$ and radius $r_O > 0$. We also assume the cell to be a disk of center $X = X_t \in \mathbb{R}^2$ and radius $r > 0$. Let $T < +\infty$ and $t \in [0, T]$. As in the previous section, we denote by $\vec{V}_t \in \mathbb{R}^2$ the particle velocity at time t. In the absence of obstacles, the velocity $\vec{V}_t$ is solution of Equation (5.4). To deal with the presence of obstacles, that equation is complemented with a non-overlapping constraint. In

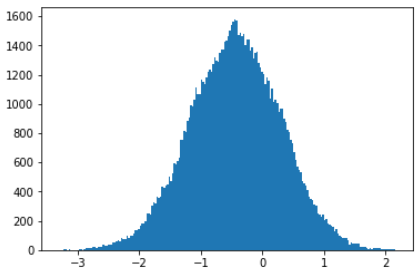

(a) Velocity Histogram for $\alpha = 0.1$

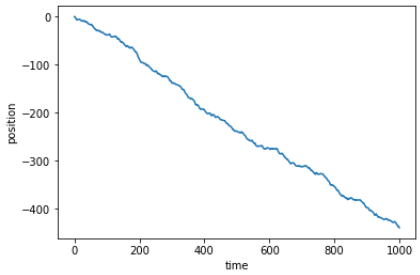

(b) Trajectory for $\alpha = 0.1$

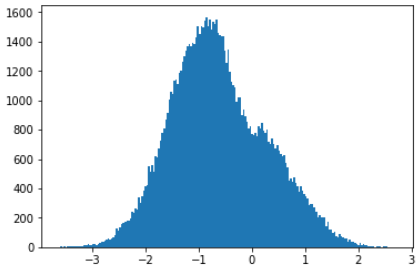

(c) Velocity Histogram for $\alpha = 10$

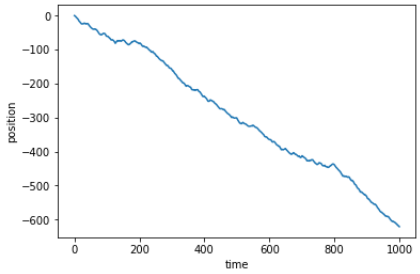

(d) Trajectory for $\alpha = 10$

Figure 5.7 – Histogram for the velocity V solution of Equation (5.6) (5.7a,5.7c) and cell trajectory (5.7b,5.7d) for $h = 0.5$, $\lambda = 1$, $\gamma = c = \sigma = 1$, $\beta = 0.1$, $\alpha = 0.1$ (5.7a,5.7b) and $\alpha = 10$ (5.7c,5.7d).

particular, we use the method introduced in [13, 17] which was developed for the case of a set of N moving particles. In the following, we give the main ideas of this framework and its numerical treatment. Finally, we show some numerical simulations.

5.2.1 Contact algorithm

In this section we recall the contact algorithm presented in [13], that is meant to deal with the non-overlapping constraint. In the following we indicate by $V = V_t = \vec{V_t}$ the particle velocity and we use the notations of [13]. In particular, V is called spontaneous velocity, since it is the natural velocity which describes the particle's free motion. Now, when the particle "meets" an obstacle, its velocity does need to be modified by the contact algorithm in order to avoid the overlapping situation. This defines a (unique) new velocity $\mathcal{V}$ which will be called actual velocity. This method is based on a projection of the spontaneous velocities onto a set of admissible velocities.

Let $\overline{q} = (X, q_1, \dots, q_N) \in \mathbb{R}^{2(N+1)}$ be the vector of positions and for $i = 1, ..., N$ let $D_i(\overline{q}) := ||q_i - X|| - r_O - r$ be the signed distance between the obstacle i and the particle. We require $\overline{q}$ to belong to the set of feasible configuration Q defined by

$$Q = \{\overline{q} \in \mathbb{R}^{2(N+1)},\ D_i(\overline{q}) \geq 0\ \ \forall i = 1, ..., N\}.$$

The contact between the particle and an obstacle occurs when $D_i(\overline{q}) = 0$ for some $i = 1, ..., N$. In that case the velocity V needs to be modified in order to satisfy the non-overlapping constraint. One can introduce the set $\mathcal{C}_{\overline{q}}$ defined by

$$\begin{cases} \mathcal{C}_{\overline{q}} = \{v \in \mathbb{R}^2 : \text{ if } D_i(\overline{q}) = 0, \text{ then } G_i(\overline{q}) \cdot v \geq 0, \text{ for all } i = 1, ..., N\}, \\ G_i(\overline{q}) = e_i(\overline{q}) = \dfrac{X - q_i}{||X - q_i||} \in \mathbb{R}^2. \end{cases}$$

The quantity $G_i(\overline{q})$ indicates the normalized vector starting from q_i and pointing to X. If we denote by s the straight line passing through X and orthogonal to $G_i(\overline{q})$, the condition $G_i(\overline{q}) \cdot v \geq 0$

imposes that the particle's velocity v must belong to the semi-space identified by the line s which does not contain the vector $G_i(\overline{q})$. Thus, the condition $G_i(\overline{q}) \cdot v \geq 0$ gives the admissible velocities v for which the non-overlapping constraint is verified. The actual velocity $\mathcal{V} \in \mathcal{C}_{\overline{q}}$ is defined as the admissible velocity which is the closest to V in the least square sense. Let P: $\mathbb{R}^2 \to \mathcal{C}_{\overline{q}}$ be the projection operator of the spontaneous velocity space onto the admissible velocity space. Then $\mathcal{V}$ is solution of the following problem

$$\mathcal{V}_t = \mathrm{P}_{\mathcal{C}_{\overline{q}}}(V_t), \quad \text{for all } t \in (0, T]. \tag{5.10}$$

For the mathematical properties of the contact algorithm expressed by Equation (5.10), we refer to [13, 17]. In the following, we recall the numeral method for solving Equation (5.10) introduced in [13].

Numerical scheme introduced in [13]

In this section, we recall the numerical scheme introduced in [13] to simulate the dynamics of a particle in interaction with topographical obstacles. In particular, in [13] it is shown that the approximation of $\mathcal{V}$ is also the solution of a minimization problem reformulated in a saddle-point form, whose resolution can be done by the Uzawa algorithm (see also [16]).

For fixed $T < +\infty$, we consider $[0, T]$ as the time interval. Let $I \in \mathbb{N}^*$ and $\delta := T/I$. We denote by $\{t^n := n\delta\}$ for $n = 1, ..., I$ the time discretization. Let $V^n := V_{t^n}$ and $\mathcal{V}^n := \mathcal{V}_{t^n}$. The quantity V^n is then obtained by the following rule

$$\begin{cases} \mathcal{V}^n = \mathrm{P}_{\mathcal{C}^\delta_{\overline{q}^n}}(V^n), \\ \mathcal{C}^\delta_{\overline{q}} = \{v \in \mathbb{R}^2,\ D_i(\overline{q}) + \delta\, G_i(\overline{q}) \cdot v \geq 0 \text{ for all } i = 1, ..., N\}. \end{cases} \tag{5.11}$$

The definition of $\mathcal{C}^\delta_{\overline{q}}$ is based on a first order approximation, in terms of velocity, of the non-overlapping constraint expressed in $\mathcal{C}_{\overline{q}}$. Let $U := V^n$, $\mathcal{U} := \mathcal{V}^n$, and $\mathcal{C}_{\overline{q}} := \mathcal{C}^\delta_{\overline{q}}$. Let the functional J defined by $J(v) := ||v - U||^2$. The actual velocity $\mathcal{U}$ is solution of the following minimization problem under constraints

$$\begin{cases} \mathcal{U} \in \mathcal{C}_{\overline{q}}, \\ J(\mathcal{U}) = \min\limits_{v \in \mathcal{C}_{\overline{q}}} J(v). \end{cases} \tag{5.12}$$

Let $B : \mathbb{R}^2 \to \mathbb{R}^N$ be the operator defined by

$$Bv := (B_1 v, ..., B_N v) \ \text{ where } \ B_i v := -\delta\, G_i(\overline{q}) \cdot v.$$

The set of constraints $\mathcal{C}_{\overline{q}}$ rewrites as follows

$$\mathcal{C}_{\overline{q}} = \{v \in \mathbb{R}^2 : Bv \leq D\}, \ \text{ where } D = D(\overline{q}) = (D_i(\overline{q}))_{i=1,...,N} \in \mathbb{R}^N.$$

Let C be the cone $\mathbb{R}^N_+$ and let $\mathcal{L} : \mathbb{R}^2 \times C \to \mathbb{R}$ be the Lagrangian associated to (5.12) defined by

$$\mathcal{L}(v, \mu) = J(v) + \mu \cdot (Bv - D).$$

Consider the following saddle-point problem

$$\begin{cases} (\mathcal{U}, \lambda) \in \mathbb{R}^2 \times C, \\ \mathcal{L}(\mathcal{U}, \mu) \leq \mathcal{L}(\mathcal{U}, \lambda) \leq \mathcal{L}(v, \lambda) \ \ \forall v \in \mathbb{R}^2, \forall \mu \in C. \end{cases} \tag{5.13}$$

One can remark that for the problem (5.13), the couple solution $(\mathcal{U}, \lambda)$ is such that $\mathcal{U}$ realizes the minimum of $\mathcal{L}$ among the velocities $v \in \mathbb{R}^2$ and λ realizes the maximum of $\mathcal{L}$ among the lagrangian multipliers $\mu \in C$. On can have the following properties.

Proposition 5.2.1 ([13]). *If the couple* $(\mathcal{U}, \lambda)$ *is solution of (5.13), then* $\mathcal{U}$ *is solution of (5.12).*

Proposition 5.2.2 ([13]). *The couple* $(\mathcal{U}, \lambda)$ *is solution of (5.13) if and only if the couple* $(\mathcal{U}, \lambda)$ *is solution of (5.14) defined by*

$$\begin{cases} \mathcal{U} + B^t\lambda = U, \\ B\mathcal{U} \leq D, \\ \lambda \cdot (B\mathcal{U} - D) = 0. \end{cases} \tag{5.14}$$

The interest is then to solve (5.14) numerically. To this aim, a possible choice is to use the Uzawa algorithm which generates two sequences (v_k, μ_k) according to the following rule

$$\begin{cases} \rho > 0, \quad \mu_0 \in C, \\ v_k = U - B^t\mu_{k-1}, \\ \mu_k = \Pi_+(\mu_{k-1} + \rho\,[Bv_k - D]), \end{cases} \tag{5.15}$$

where Π_+ is the euclidean projection onto the cone C and ρ is a fixed parameters. The algorithm can be shown to converge as soon as $0 < \rho < 2/||B||^2$ see e.g. [3]. Under this hypothesis, one can get that μ_k converges to some λ and v_k converges to $\mathcal{U}$ such that the couple $(\mathcal{U}, \lambda)$ is solution of (5.14).

5.3 Numerical simulations in a 2D framework

We present in this section some numerical simulations. We describe the geometry we use and a method for building the uniform distribution of obstacles and then we show some numerical results. We use in particular the following numerical method. We set $T = 50$ and let $dt = 0.05$ be the time-step in the time interval $[0, 50]$, and let $I = T/dt = 2000$ be the number of time iterations in $[0, 50]$. For $n = 0, ..., I-1$ let $V^n \in \mathbb{R}^2$ be the spontaneous velocity and $\mathcal{V}^n \in \mathbb{R}^2$ be the actual velocity at time $t^n = n \times dt$. We then write $V^n = (u^n, v^n)$ and $\mathcal{V}^n = (z^n, w^n)$ and we consider random initial conditions V^0 and $\mathcal{V}^0$. We first compute the velocity V^{n+1} by using the Euler-Maruyama Method for the Equation (5.4):

$$\begin{cases} u^{n+1} = z^n + \dfrac{c}{\gamma}\left[(1-h)\tanh(\alpha||\mathcal{V}^n||)\, e^x_{\theta_n} + h\tanh(\beta)\, e^x_{\theta_g} - \lambda z^n\right] dt + \dfrac{\sigma}{\gamma} dW^x_n, \\ v^{n+1} = w^n + \dfrac{c}{\gamma}\left[(1-h)\tanh(\alpha||\mathcal{V}^n||)\, e^y_{\theta_n} + h\tanh(\beta)\, e^y_{\theta_g} - \lambda w^n\right] dt + \dfrac{\sigma}{\gamma} dW^y_n, \end{cases}$$

where $\vec{e}_{\theta_n} = (e^x_{\theta_n}, e^y_{\theta_n})$ is the direction of the motion at time t^n, $\vec{e}_{\theta_g} = (e^x_{\theta_g}, e^y_{\theta_g})$ is the direction of the constant gradient of the signal and $dW_n = (dW^x_n, dW^y_x)$ indicates the 2D-Brownian motion at time t^n. Successively, we compute the velocity $\mathcal{V}^{n+1}$ by using the Uzawa algorithm described in (5.15). In particular, at step $k+1$ of the Uzawa algorithm we compute

$$\begin{cases} z^{n+1}_{k+1} = u^{n+1} - (\mu_k \cdot \mathbf{e}_1)\, dt, \\ w^{n+1}_{k+1} = v^{n+1} - (\mu_k \cdot \mathbf{e}_2)\, dt, \\ \mu_{k+1} = \Pi_+(\mu_k - \rho[\,(z^{n+1}_{k+1}\mathbf{e}_1 + w^{n+1}_{k+1}\mathbf{e}_2)\, dt - \mathbf{G}\,]) \end{cases}$$

with initial condition $\mu_0 = 0$ and $\rho > 0$, where $\mathbf{e}_1, \mathbf{e}_2 \in \mathbb{R}^N$ indicate respectively the normalized distance between the center of the particle and the centers of the obstacles along the x-axis and the y-axis and the vector $\mathbf{G} \in \mathbb{R}^N$ indicates the signed distance between the particle and the obstacles.

In the following, we simulate different cases. First, we investigate the effect of obstacles on the dynamics of a Brownian particle that may be damped by a friction term. Then, we additionally

consider a constant directional force and its effect on the dynamics. Finally, we consider the full dynamics as described in Equation (5.4), that accounts for cell dynamics. In particular, it provides some intrinsic persistence in the displacement, and we investigate its interaction with both the obstacles and the constant force. We remark that the constant force can describe the presence of a constant gradient in chemical signal in the environment of the particle.

Geometry and obstacles distribution

We start by describing the geometry of the domain and the obstacles distribution. We consider a domain $\Omega = [0, L] \times [0, H]$, for some $L, H > 0$ and an uniform obstacles distribution which depends on the dimensions of Ω. Let r_O and r be the obstacles radius and the cell radius respectively, and let N be the total number of obstacles in Ω. N is computed by the following rule. Let $\varepsilon > 0$ be a geometry parameter to assure the particle to pass between two obstacles and let $d = 2r_O + 2r + 2\varepsilon$ be the minimal distance between two obstacles to ensure the passage of the particle. Let N_1 and N_2 be the number of obstacles along the horizontal and vertical directions respectively, defined by

$$N_1 = \left[\frac{L}{d}\right] \text{ and } N_2 = \left[\frac{H}{d}\right],$$

where $[\,\cdot\,]$ indicates the integer part function. The total number of obstacles in the domain Ω is then

$$N = N_1 \times N_2.$$

We decide to fix the parameter $\varepsilon = 0.01$ and to consider $r = mr_O$ for some $m > 0$. In Figure 5.8 we show two examples of the geometry for a particular choice of the parameters.

In the following, we consider the domain $\Omega = [0, 2] \times [0, 2]$ for which we impose periodic boundary conditions on the particle's displacement. We consider different numbers of obstacles N by varying the obstacles radius r_O.

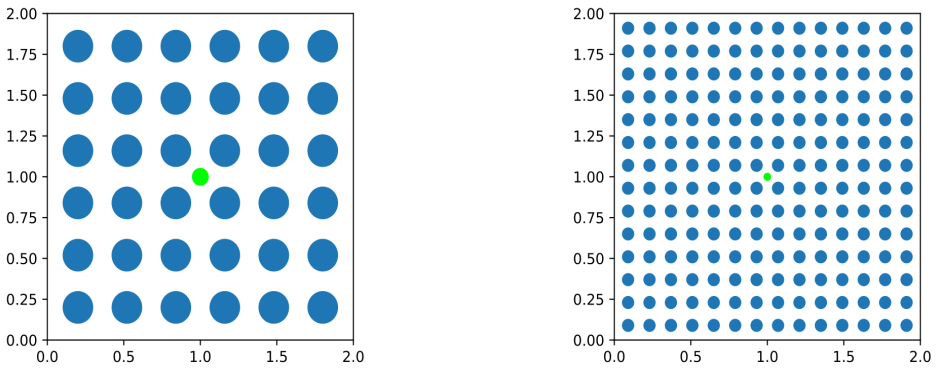

(a) $N = 36$ (b) $N = 900$

Figure 5.8 – Domain $\Omega = [0, 2] \times [0, 2]$. Obstacles in blue, cell initial position in green. For case (a): $\varepsilon = 0.01$, $r_O = 0.1$, $r = r_O/2 = 0.05$. For case (b): $\varepsilon = 0.01$, $r_O = 0.04$, $r = r_O/2 = 0.02$.

5.3.1 Effect of obstacles on the dynamics of a Brownian particle

In this section, we consider the case of a particle moving according to a damped Brownian motion. In particular, we set $\alpha = 0, \beta = 0, \sigma = 1$ and we investigate the particle's dynamics for different values of $\lambda > 0$ and different numbers of obstacles.

In Figure 5.9, we show the one and two dimensional velocity histograms for $N = 36$ obstacles (Figures 5.9a-5.9c), and for $N = 900$ obstacles in (Figures 5.9d-5.9f). We first notice that the one dimensional velocity histograms are symmetric. This is due to the fact that there is not any bias in the particle's dynamics, and the obstacles are uniformly distributed in the domain. By analysing the two dimensional velocity histograms, we notice that the presence of obstacles does have an effect on the direction of the velocity. For $N = 36$, they show different shapes depending on the value of lambda. For $\lambda = 0$, the histogram has a squared shape, while it becomes more circular for larger values of λ. This shows that when the dynamics is weakly damped, the obstacles act on the directionality of the particle by preventing displacements in other directions than along the x and y axis. For $N = 900$, the 2D histograms have the same squared shape, but as λ increases, this shape becomes more smooth. In particular, we see that as the number of obstacles increases, the squared shape of the velocity histogram becomes more squared.

In Figure 5.10, we show two trajectories for $N = 900$ obstacles with $\lambda = 0$ (Figure 5.10a) and $\lambda = 3$ (Figure 5.10b). We notice that for $\lambda = 0$ we observe directional displacement in the particle's trajectory, which covers all the domain. For $\lambda = 3$, we observe a more compact trajectory, which mainly covers the upper-right part of the domain. This shows how the persistence induced by the obstacles is stronger for $\lambda = 0$ than for $\lambda = 3$.

$N = 36$

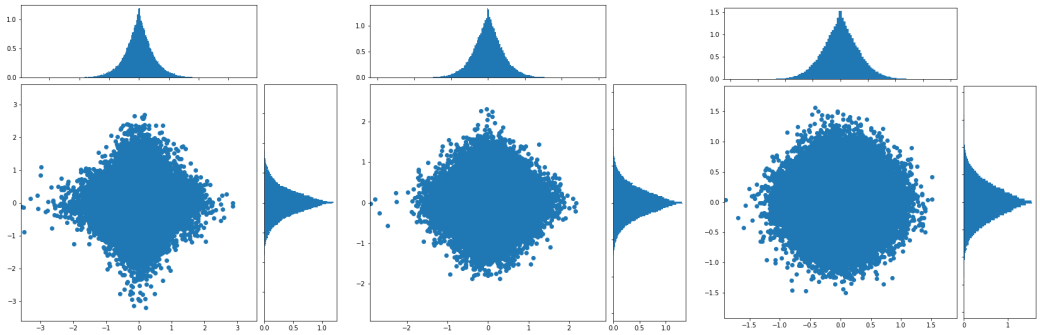

(a) $\lambda = 0$ (b) $\lambda = 1$ (c) $\lambda = 3$

$N = 900$

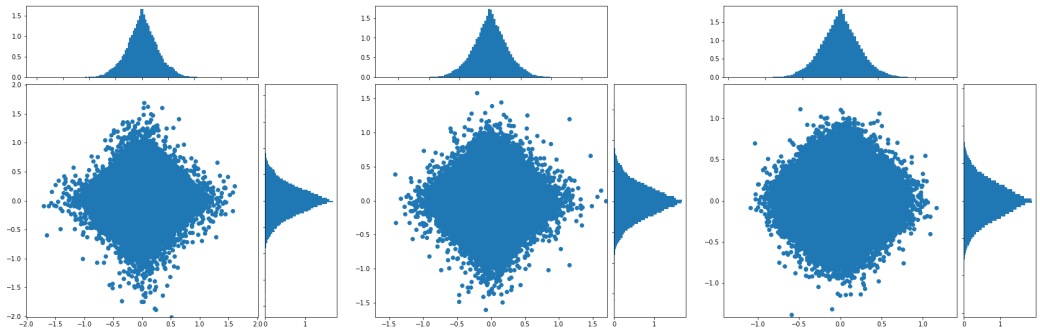

(d) $\lambda = 0$ (e) $\lambda = 1$ (f) $\lambda = 3$

Figure 5.9 – One and two dimensional velocity histograms for $N = 36$ obstacles (5.9a-5.9c) and for $N = 900$ obstacles (5.9d-5.9f). Parameters: $\alpha = 0$, $\beta = 0$, $\sigma = 1$, $\lambda = 0$ (5.9a) and (5.9d), $\lambda = 1$ (5.9b) and (5.9e), $\lambda = 3$ (5.9c) and (5.9f).

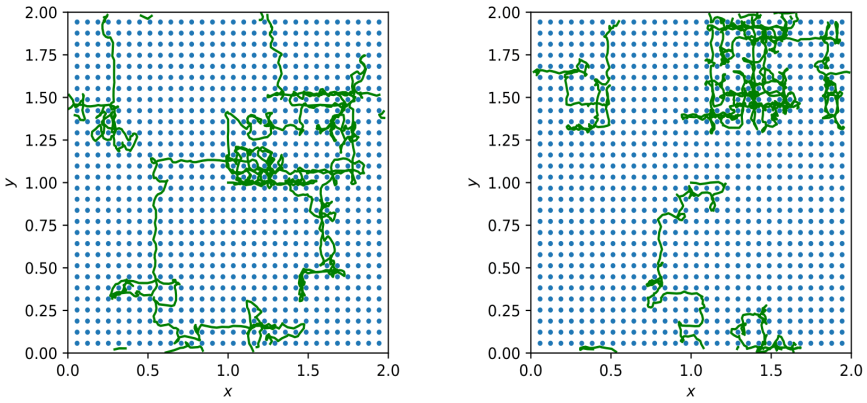

(a) $\lambda = 0$ (b) $\lambda = 3$

Figure 5.10 – Particle's trajectories for $N = 900$ obstacles. Paramters: $\alpha = 0$, $\beta = 0$, $\sigma = 1$, $\lambda = 0$ (5.10a) and $\lambda = 3$ (5.10b).

5.3.2 Effect of a constant force on the dynamics of a Brownian particle

In this section, we study the effect of a constant directional force on a Brownian particle. In particular, we set $\alpha = 0$, $\lambda = 1$, $\sigma = 0.2$ and then we consider a normalized force $F = (2 \times 2/5, 1.5 \times 2/5)$. The parameter β describes the intensity of the effect of the force F on the particle's dynamics. We investigate the interplay between the force and the obstacles by varying β and the number of obstacles N.

Figure 5.11 shows the mean velocity modulus as a function of different values of β, for different numbers of obstacles. Since Equation (5.4) involves only $\tanh(\beta)$, we take $\beta \in [0, 10]$, as larger values do not change the dynamics. The mean velocity was obtained by simulating the model among $M = 100$ simulations. Figure 5.11 shows that the mean velocity modulus curve has a non-strictly-monotone behaviour with respect to β, for any number of obstacles. This is explained by the presence of the obstacles. For small values of β, the curve is monotonic-increasing when β increases. But when β is large enough, the curve reaches an horizontal asymptote. This is due to the fact that when the force intensity is strong enough, the particle gets stuck between the obstacles. We notice also that the mean velocity modulus decreases as the number of obstacles N increases. This shows how obstacles make the environment congested and prevent the particle's motion.

In Figure 5.12, we show the one and two dimensional velocity histograms for $N = 900$ obstacles with $\beta = 0.5$ (Figure 5.12a), $\beta = 2$ (Figure 5.12b) and $\beta = 6$ (Figure 5.12c). We first notice that the one dimensional histograms for x-component and y-component of the velocity show an asymmetry towards positive values, which is due to the bias induced by the force F. Since the x-component of the force is greater than its y-component, the asymmetry is stronger in the x-component of the velocity than in its y-component. For $\beta = 0.5$, the asymmetry is very weak and it becomes stronger as β increases. By analysing the two dimensional velocity histograms, we notice that the presence of the force makes the velocity distribution more concentrated toward the half-upper-right side of the domain. For $\beta = 0.5$, this effect is weak but remarkable. As β increases the effect becomes stronger and more remarkable. Figure 5.13 shows two particle's trajectories for $N = 900$ obstacles, for $\beta = 0.5$ (Figure 5.13a) and $\beta = 6$ (Figure 5.13a). We first notice that for both the cases, the particle's trajectory covers all the domain. For $\beta = 6$, the trajectory direction points toward the upper-right side of the domain, while for $\beta = 0.5$ the trajectory direction changes more frequently. This is due due to the fact that as β increases, the intensity of the effect of the force on the particle's dynamics becomes stronger.

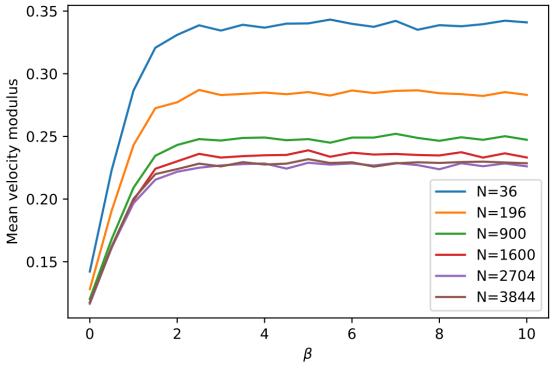

Figure 5.11 – Mean velocity modulus among $M = 100$ simulations. We set $\alpha = 0$, $\lambda = 1$, $\sigma = 0.2$ and we simulated for 20 values of $\beta \in [0, 10]$. Numbers of obstacles considered: $36, 196, 900, 1600, 2704, 3844$.

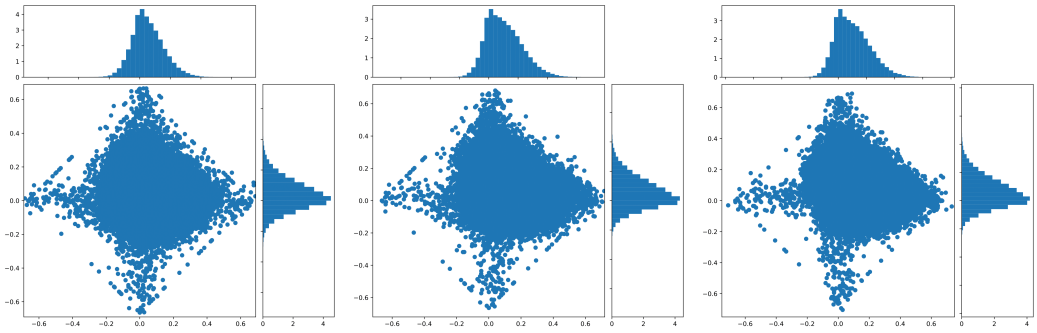

(a) $\beta = 0.5$ (b) $\beta = 2$ (c) $\beta = 6$

Figure 5.12 – One and two dimensional velocity histograms for $N = 900$ obstacles. Parameters: $\alpha = 0$, $\lambda = 1$, $\sigma = 0.2$, $\beta = 0.5$ (5.12a), $\beta = 2$ (5.12b), $\beta = 6$ (5.12c).

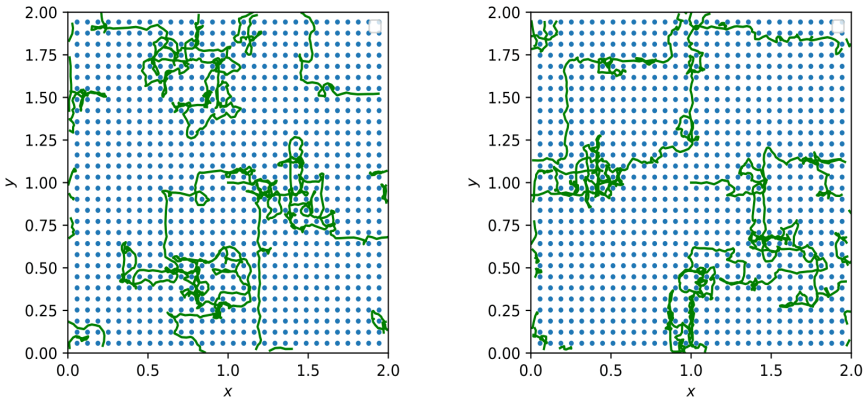

(a) $\beta = 0.5$ (b) $\beta = 6$

Figure 5.13 – Particle's trajectories for $N = 900$ obstacles. Parameters: $\alpha = 0$, $\lambda = 1$, $\sigma = 0.2$, $\beta = 0.5$ (5.13a) and $\beta = 6$ (5.13b).

5.3.3 Dynamics of an active particle with cellular dynamics

In this section, we study the effect of a constant directional force on an active particle for which the velocity is solution of equation (5.4) and mimics the dynamics of a cell. In particular, we set $\lambda = 1$, $\sigma = 0.2$ and we take the same force F as previously, namely $F = (2 \times 2/5, 1.5 \times 2/5)$. We perform similar numerical experiments as the ones done in the previous section, but now we consider $\alpha > 0$. The parameter α appears in the dynamics in (5.4) through the term $\tanh(\alpha v)$, where v indicates the norm of the velocity. To investigate the competition between the two parameters α and β, we focus on large values of α. In particular, in the following we consider $\alpha = 30$ and we let vary $\beta \in [0, 10]$.

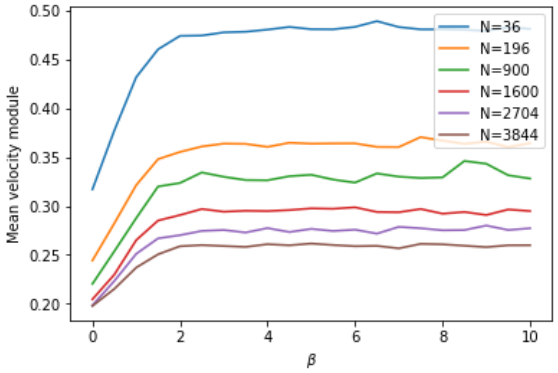

Figure 5.14 – Mean velocity modulus among $M = 100$ simulations. We set $\alpha = 30$, $\lambda = 1$, $\sigma = 0.2$ and we simulated for 20 values of $\beta \in [0, 10]$. Numbers of obstacles considered: $36, 196, 900, 1600, 2704, 3844$.

Figure 5.14 shows the mean velocity modulus as a function of different values of β and for different numbers of obstacles, by setting $\alpha = 30$. In comparison with Figure 5.11, we notice that the qualitative behaviour of the mean velocity modulus does not change. We remark only that in Figure 5.14 the mean velocity modulus assumes smaller values with respect to the results presents in Figure 5.11.

In Figure 5.15, we show the one and two dimensional velocity histograms for $N = 900$ obstacles with $\beta = 0.5$ (Figure 5.15a), $\beta = 2$ (Figure 5.15b) and $\beta = 6$ (Figure 5.15c). We first notice that the one dimensional histograms for x-component and y-component of the velocity show a shift towards positive values, which is due to the bias induced by the force F. In comparison with the histograms in Figure 5.12, this asymmetry is less strong for both the x-component and the y-component. This is due to the fact that the internal dynamics intensity may play against the effect of the force. By analysing the two dimensional velocity histograms, we notice that in comparison with Figure 5.12, the velocity distribution is less squared and more concentrated in other other parts of the domain with respect to the half-upper-right side. For $\beta = 0.5$, this behaviour is more remarkable. As β increases, the velocity distribution becomes more concentrated towards parts of the domain different from the half-upper-right side. This is due to the fact that the force intensity is less efficient on the particle's dynamics because now the particle feels also its own internal dynamics. Figure 5.16 shows two particle's trajectories for $N = 900$ obstacles, for $\beta = 0.5$ (Figure 5.16a) and $\beta = 6$ (Figure 5.16b). We notice that for $\beta = 0.5$, the particle's trajectories mainly covers the upper part of the domain. For $\beta = 6$, we can recognize some persistence directions in agreement with the direction of the force, but they are also very perturbed. Indeed, since $\alpha > 0$ and big enough, the particle's dynamics feels the competition between the force intensity and its own internal dynamics. For this reason, the particle may cover different directions with respect to that induced by the constant force. This is in agreement with the velocity histogram in Figure (5.15c).

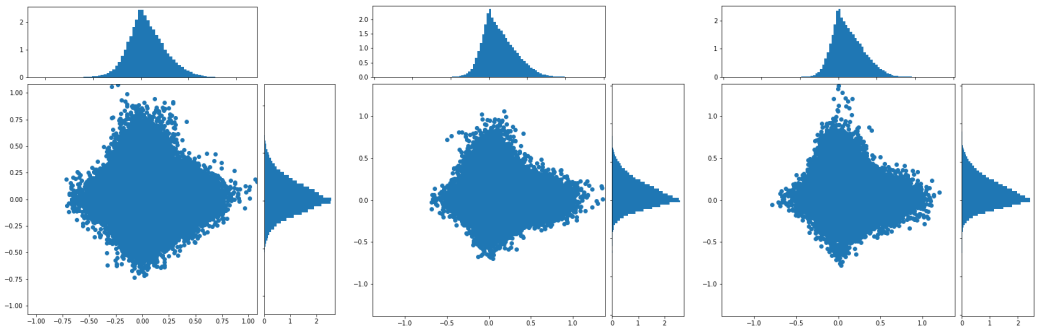

(a) $\beta = 0.5$ (b) $\beta = 2$ (c) $\beta = 6$

Figure 5.15 – One and two dimensional velocity histograms for $N = 900$ obstacles. Parameters: $\alpha = 30$, $\lambda = 1$, $\sigma = 0.2$, $\beta = 0.5$ (5.15a), $\beta = 2$ (5.15b), $\beta = 6$ (5.15c).

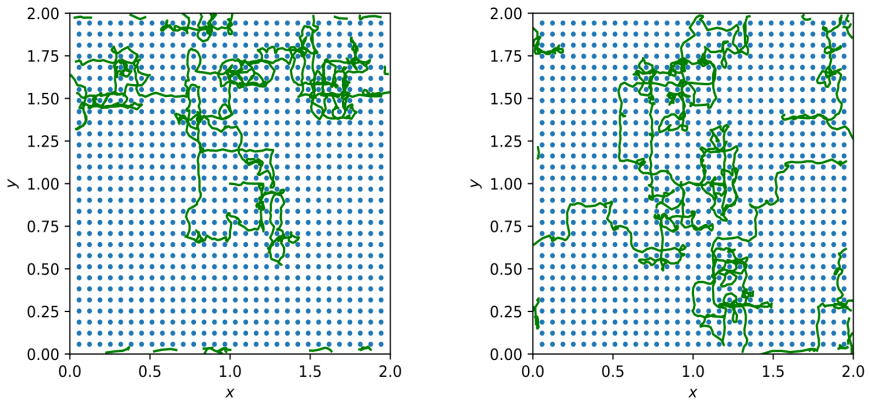

(a) $\beta = 0.5$ (b) $\beta = 6$

Figure 5.16 – Particle's trajectories for $N = 900$ obstacles. Parameters: $\alpha = 30$, $\lambda = 1$, $\sigma = 0.2$, $\beta = 0.5$ (5.16a) and $\beta = 6$ (5.16b).

5.4 Conclusions

In this chapter, we studied the effects of some particular biochemical and mechanical cues on cell migration. In the first part, we introduced a two dimensional continuous stochastic model to describe the effects of biochemical cues on cell migration. This continuous model relies on biological assumptions. More precisely we considered the dynamics of a cell in the presence of a constant gradient of attractive signal. With this model we wanted to study the competition between the internal cell's dynamics and the intensity of the signal. In the one dimensional case, we obtained an explicit formulation of the stationary velocity distribution. We noticed that when the signal intensity is weak, the cell moves according to its internal dynamics. If instead the signal intensity is strong enough, the cell follows the signal.

In the second part, we numerically investigated the combined effects of obstacles and of a constant directional force on the cell's dynamics for a cell described as an active particle. We first considered a damped Brownian particle in a crowded environment and without external signal. For this case, by analysing the two dimensional velocity histograms, we noticed that the presence of obstacles has an effect on the directionality of the particle, which becomes stronger as the number of obstacles increases and as the damped effect decreases. Then, we studied the additional effect of a constant directional force. We noticed that the mean velocity modulus increases as the

force intensity increases until it reaches a limit value. Moreover, we saw that the mean velocity modulus decreases as the number of obstacles increases, but this does not change its qualitative behaviour. We analysed also the two dimensional velocity histograms. We first noticed that the one dimensional histograms show an asymmetry towards positive values which becomes more evident as the force intensity increases. Furthermore, the two dimensional velocity distribution seems to be more concentrated in the direction of the external constant force. This behaviour becomes more remarkable as the force intensity increases. Finally, we considered an active particle whose dynamics is also characterized by an internal dynamics in a crowded environment and with an external constant force. We noticed that the mean velocity modulus does not change qualitatively with respect to the previous case. As for the two dimensional histograms, we noticed that the velocity distribution is not only concentrated in the direction of the external constant force, but also in other regions of the domain. This different behavior is due to the presence of the internal dynamics.

We can thus observe that the presence of the obstacles has an effect on the directional behavior of the particle's dynamics. Indeed, the presence of the obstacles enforces the particle to move towards particular regions of the domain. The presence of an external constant force enforces the particle to move in the direction of the force. Furthermore, the internal dynamics enforces the persistence induced by the presence of the obstacles as well as the by external constant force.

Bibliography

[1] O. Barreiro, P. Martín, F. Sánchez-Madrid, and R. González-Amaro, *Molecular cues guiding inflammatory responses*, Cardiovascular Research, 86 (2010), pp. 174–182.

[2] O. Bénichou, P. Illien, G. Oshanin, A. Sarracino, and R. Voituriez, *Nonlinear response and emerging nonequilibrium microstructures for biased diffusion in confined crowded environments*, Phys. Rev. E, 93 (2016), p. 032128.

[3] P. Ciarlet, *Introduction à l'analyse numérique matricielle et à l'optimisation*, Masson, (Paris, 1990).

[4] A. Cucchi, C. Etchegaray, N. Meunier, L. Navoret, and L. Sabbagh, *Cell migration in complex environments: chemotaxis and topographical obstacles*, ESAIM: Proceedings and Surveys, 67 (2020), pp. 191–209.

[5] P. N. Devreotes and S. H. Zigmond, *Chemotaxis in Eukaryotic cells: A focus on leukocytes and dictyostelium*, Annual Review of Cell Biology, 4 (1988), pp. 649–686. PMID: 2848555.

[6] C. Etchegaray, *Mathematical and numerical modelling of cell migration*, thesis, Université Paris-Saclay, 2016.

[7] C. Etchegaray and N. Meunier, *Crawling migration under chemical signalling: A stochastic model*, Mathematical Methods in the Applied Sciences, 41 (2018), pp. 8799–8815.

[8] C. Etchegaray and N. Meunier, *A stochastic model for protrusion activity*, ESAIM: Proceedings, 62 (2018), pp. 56–67.

[9] C. Etchegaray, N. Meunier, and R. Voituriez, *A 2D deterministic model for single-cell crawling, a minimal multiscale approach*, submitted for publication, pp. 1385–405.

[10] ——, *Analysis of a nonlocal and nonlinear Fokker-Planck model for cell crawling migration*, SIAM Journal on Applied Mathematics, 77 (2017), pp. 2040–2065.

[11] N. Fournier and S. Meleard, *A microscopic probabilistic description of a locally regulated population and macroscopic approximations*, Annals of Applied Probability, 14 (2004).

[12] C. GRABHER, A. CLIFFE, K. MIURA, J. HAYFLICK, R. PEPPERKOK, P. RØRTH, AND J. WITTBRODT, *Birth and life of tissue macrophages and their migration in embryogenesis and inflammation in medaka*, Journal of leukocyte biology, 81 (2007), pp. 263–71.

[13] A. LEFEBVRE, *Numerical modelling of fluid/particle flows*, theses, Université Paris Sud - Paris XI, 2007.

[14] A. LODISH AND S. ZIPURSKY, *Molecular cell biology*, Biochemestry and Molecular Biology Education, 29 (2001), pp. 126–33.

[15] P. K. MATTILA AND P. LAPPALAINEN, *Filopodia: molecular architecture and cellular functions*, Nature reviews Molecular cell biology, 9 (2008), pp. 446–454.

[16] B. MAURY, *A time-stepping scheme for inelastic collisions*, Numerische Mathematik, 102 (2006), pp. 649–679.

[17] B. MAURY AND J. VENEL, *A discrete contact model for crowd motion*, ESAIM: Mathematical Modelling and Numerical Analysis, 45 (2011), pp. 145–168.

[18] S. MCDOUGALL, J. DALLON, J. SHERRATT, AND P. MAINI, *Fibroblast migration and collagen deposition during dermal wound healing: Mathematical modelling and clinical implications*, Philosophical transactions. Series A, Mathematical, physical, and engineering sciences, 364 (2006), pp. 1385–405.

Chapter 6

Conclusions and perspectives

Cell migration is a highly complex phenomenon: it is the result of many interactions between biological components living inside the cell and it occurs through different time and space scales. Cell migration is still not fully understood. It takes place in some of the most important biological processes and thus the development of biological, physical and mathematical models describing this phenomenon plays an essential role. An overview of the biological background and mathematical existing models is presented in Chapter 1 representing the Introduction of the Thesis. In this Thesis, we considered the particular case of cell migration by crawling and we developed two different modeling approaches. In the first one, we consider the cell as a moving domain with deformable shape whose motion is stimulated by its internal dynamics. For this case, the derivation of a particular free-boundary model and its analysis in the one and two dimensional cases are presented in Chapter 2, Chapter 3 and Chapter 4. The second approach consist in modeling the cell as an active particle whose motion is stimulated by both the internal dynamics and the external environment. For this case, presentation and the numerical simulations of the a particular stochastic model are presented in Chapter 5.

Chapter 2 is dedicated to the study of a phase-field model for cell migration by crawling and to the derivation of its sharp interface limit. Our phase-field model is represented by a Cahn-Hilliard type equation describing the evolution of the phase-field function coupled with a convection-reaction-diffusion equation describing the active internal dynamics of the cell. We studied its sharp interface limit and we proved that the model converges formally to a Hele-Shaw free-boundary problem including a surface tension and an additional boundary term depending on the boundary velocity. It is known that the surface tension has a stabilizing effect for the problem, while the velocity-dependent term has a destabilizing effect on the free boundary. The mathematical and numerical properties of the problem strongly depend by this term. We conduced a rigorous analysis in the one dimensional case and we showed that the model has a non-trivial dynamics and exhibits hysteresis phenomena. In particular, we proved that there exists a critical value such that if the intensity of the destabilizing term is less than this value then only the stationary solution exists, otherwise there exist other two moving solutions, one with positive velocity and the other one with negative velocity. Moreover, there is nothing assuring that one solution moves with the same sign of the velocity: for example a solution that moves with positive velocity could suddenly stop.

Chapter 3 and Chapter 4 are dedicated to the study of the limiting free-boundary problem in the two dimensional case. In Chapter 3 we study the existence of traveling wave solutions of the problem. A traveling wave solution corresponds to a fixed shape domain which moves by translation with constant velocity in a given direction. Since the problem is isotropic, we analyze the case where the domain translates along the x-axis with positive velocity. First, we prove the existence of traveling wave solutions for big enough value of the intensity of the destabilizing term. While this result is constructive, it does not clearly identify the critical value for which non trivial traveling waves start to exist. By a bifurcation argument we are able to precise this critical

value. Indeed, we prove that a local branch of traveling solution with non zero speed emerges from the trivial solution (the disk) at a critical value well precised. Therefore, if the intensity of the destabilizing term is strong enough, two different behaviors take place: a trivial traveling wave solution with a zero velocity corresponding to a cell of symmetric form, or a non-trivial traveling wave corresponding to an asymmetric cell moving with non-zero velocity. This free-boundary model while mathematically unpleasant, describes an important feature of cell motility, that is the self-polarization observed for migrating cells.

In Chapter 4 we study the Hysteresis phenomenon for our free-boundary problem. We analyzed the following question: is the knowledge of the shape of the domain at a given time t_0 is enough to characterize the behavior of the domain for times $t > t_0$? We proved that even in the simplest case where the domain at time $t = 0$ is a disk, the problem admits more than one solution for $t > t_0$ when the destabilizing term is strong enough. Via a bifurcation argument, we proved that there exists a (local) branch of solutions of the problem when the destabilizing term is strong enough. Therefore, the answer of the above question is no, and Hysteresis phenomenon takes place for our free-boundary model.

Chapter 5 is dedicated to the study of the effects of a complex external environment on the cell migration in a two dimensional framework. We considered here the cell as an active particle and we analyzed the competition of three quantities: the internal active dynamics of the cell, the action of a constant spatial gradient of attracting signal and the presence of circular non-moving obstacles. We considered an existing continuous stochastic model describing the cell motion via its protrusion and we added the effect of the signal and the presence of the obstacles. In the one dimensional case, if the signal intensity is weak the cell moves according to its internal dynamics, but when the signal intensity is strong enough the cell follows the signal. In this case we do not consider the obstacles. In the two dimensional case, we investigated numerically the combined effect of internal activity, attracting signal and obstacles. We consider two different cases. First, we analyzed the interaction of the signal with the presence of the obstacles. We found numerically the existence of a velocity value depending on the number of obstacles that the cell can not exceed, even if the force intensity increases. Moreover, the velocity histogram seems to be more concentrated in the direction of the force and this behavior becomes more remarkable as the force intensity increases. Then, we introduced also the effect of the active internal dynamics. We numerically found that there still exists a (different) velocity value that the cell cannot exceed. In addition, the velocity histogram is not only concentrated in the direction of the force, but also in other regions of the domain. This different behavior is due to the presence of the internal dynamics.

For the study presented in Chapter 5, further analysis can be done. First, a different choice of the obstacles shape can be studied such as obstacles of squared shape as well as obstacles of non-convex shape. This could lead to interesting effects on the directionality of the motion. Second, one can consider a non-homogeneous distribution of obstacles inside the domain in order to induce a particular direction of motion. Finally, a time-dependent attracting signal can be considered.

Appendix A

Computation of $\partial_s k$, $\partial_{ss} k$ and $\partial_{sss} k$

We recall that $\rho = \rho(s,\theta)$ and $k(s,\theta)$ are defined by (3.69), (3.70) and (3.72) for $s \in I$ and $\theta \in [-\pi, +\pi]$.

Lemma A.0.1. *The following equalities hold:*

$$\int_{-\pi}^{\pi} \partial_s k(0,\theta)\cos\theta \mathrm{d}\theta = 0, \int_{-\pi}^{\pi} \partial_{ss} k(0,\theta)\cos\theta \mathrm{d}\theta = 0 \text{ and } \int_{-\pi}^{\pi} \partial_{sss} k(0,\theta)\cos\theta \mathrm{d}\theta = 0.$$

Proof. We define the functions

$$\begin{aligned} N(s,\theta) &= ((R_0+\rho)^2 + 2\partial_\theta\rho^2 - (R_0+\rho)\partial_{\theta\theta}\rho)(s,\theta) \\ D(s,\theta) &= \big(((R_0+\rho)^2 + \partial_\theta\rho^2)^{3/2}\big)(s,\theta) \end{aligned}$$

so that

$$k(s,\theta) = \frac{N(s,\theta)}{D(s,\theta)} \quad \text{and} \quad \partial_s k(s,\theta) = \left(\frac{(\partial_s N)D - N(\partial_s D)}{D^2}\right)(s,\theta) \tag{A.1}$$

with

$$\begin{aligned} (\partial_s N)(s,\theta) &= (2(R_0+\rho)\partial_s\rho + 4\partial_\theta\rho\,\partial_{s\theta}\rho - R_0\partial_{s\theta\theta}\rho - \partial_s\rho\,\partial_{\theta\theta}\rho - \rho\,\partial_{s\theta\theta}\rho)(s,\theta), \\ (\partial_s D)(s,\theta) &= (3(\partial_\theta\rho\,\partial_{s\theta}\rho + (R_0+\rho)\partial_s\rho)\sqrt{(R_0+\rho)^2 + (\partial_\theta\rho)^2}\,)(s,\theta). \end{aligned}$$

We see that

$$R_0^2\partial_s k(0,\theta) = -\partial_{s\theta\theta}\rho(0,\theta),$$

hence the first equality $\int_{-\pi}^{\pi} \partial_s k(0,\theta)\cos\theta \mathrm{d}\theta = 0$ follows by integrating by parts and by using $\partial_s\rho(0,\theta) = 0$.

We then define

$$n(s,\theta) = ((\partial_s N)D - N(\partial_s D))(s,\theta) \quad \text{and} \quad d(s,\theta) = D^2(s,\theta),$$

so that

$$\partial_{ss} k(s,\theta) = \left(\frac{(\partial_s n)d - n(\partial_s d)}{d^2}\right)(s,\theta), \tag{A.2}$$

where

$$(\partial_s n)(s,\theta) = ((\partial_{ss} N)D - N(\partial_{ss} D))(s,\theta) \quad \text{and} \quad (\partial_s d)(s,\theta) = (2D\partial_s D)(s,\theta),$$

with

$$\begin{aligned} (\partial_{ss} N)(s,\theta) =& (2\partial_s\rho^2 + (2R_0 + 2\rho - \partial_{\theta\theta}\rho)\partial_{ss}\rho + 4(\partial_{s\theta}\rho)^2 \\ &+ 4\partial_\theta\rho\,\partial_{ss\theta}\rho - R_0\partial_{ss\theta\theta}\rho - 2\partial_s\rho\partial_{s\theta\theta}\rho - \rho\partial_{ss\theta\theta}\rho)(s,\theta), \end{aligned}$$

and

$$(\partial_{ss} D)(s,\theta) = \big(3((R_0+\rho)^2+(\partial_\theta\rho)^2)^{-1/2}((R_0+\rho)\partial_s\rho+\partial_\theta\rho\partial_{s\theta}\rho)^2 \\ + 3\sqrt{(R_0+\rho)^2+(\partial_\theta\rho)^2}((\partial_s\rho)^2+(R_0+\rho)\partial_{ss}\rho+(\partial_{s\theta}\rho)^2+\partial_\theta\rho\partial_{ss\theta}\rho)\big)(s,\theta).$$

We see that

$$\partial_{ss} N(0,\theta) = (2R_0 - \partial_{\theta\theta}\rho(0,\theta))\,\partial_{ss}\rho(0,\theta) + 4\,(\partial_{s\theta}\rho(0,\theta))^2 - R_0\partial_{ss\theta\theta}\rho(0,\theta),$$

and

$$\partial_{ss} D(0,\theta) = 3R_0\left(R_0\partial_{ss}\rho(0,\theta) + (\partial_{s\theta}\rho(0,\theta))^2\right),$$

hence

$$\begin{aligned}\partial_s n(0,\theta) &= -R_0^4\partial_{ss}\rho(0,\theta) + 2R_0^3\partial_{\theta\theta}\rho(0,\theta)\partial_{ss}\rho(0,\theta) + R_0^3\,(\partial_{s\theta}\rho(0,\theta))^2 \\ &\quad -R_0^4\partial_{ss\theta\theta}\rho(0,\theta) + 3R_0^2\partial_{\theta\theta}\rho(0,\theta)\,(\partial_{s\theta}\rho(0,\theta))^2,\end{aligned}$$

and

$$\partial_s d(0,\theta) = 0.$$

Consequently we obtain

$$\begin{aligned}R_0^2\partial_{ss}k(0,\theta) &= -\partial_{ss}\rho(0,\theta) + 2\frac{1}{R_0}\partial_{\theta\theta}\rho(0,\theta)\partial_{ss}\rho(0,\theta) + \frac{1}{R_0}\,(\partial_{s\theta}\rho(0,\theta))^2 \\ &\quad -\partial_{ss\theta\theta}\rho(0,\theta) + \frac{3}{R_0^2}\partial_{\theta\theta}\rho(0,\theta)\,(\partial_{s\theta}\rho(0,\theta))^2.\end{aligned} \tag{A.3}$$

Now we use that $\int_{-\pi}^{\pi}\partial_{\theta\theta}\rho(0,\theta)\partial_{ss}\rho(0,\theta)\cos\theta\mathrm{d}\theta = 0$, $\int_{-\pi}^{\pi}(\partial_{s\theta}\rho(0,\theta))^2\cos\theta\mathrm{d}\theta = 0$, $\int_{-\pi}^{\pi}\partial_{\theta\theta}\rho(0,\theta)\,(\partial_{s\theta}\rho(0,\theta))^2\cos\theta\mathrm{d}\theta = 0$ together with $\int_{-\pi}^{\pi}\partial_{ss\theta\theta}\rho(0,\theta)\cos\theta\mathrm{d}\theta = -\int_{-\pi}^{\pi}\partial_{ss}\rho(0,\theta)\cos\theta\mathrm{d}\theta$ to obtain the second equality $\int_{-\pi}^{\pi}\partial_{ss}k(0,\theta)\cos\theta\mathrm{d}\theta = 0$.

Similarly, we define

$$a(s,\theta) = ((\partial_s n)d - n(\partial_s d))(s,\theta) \quad \text{and} \quad b(s,\theta) = d^2(s,\theta),$$

and we have that

$$\partial_{sss}k(s,\theta) = \left(\frac{(\partial_s a)b - a(\partial_s b)}{b^2}\right)(s,\theta), \tag{A.4}$$

where

$$(\partial_s a)(s,\theta) = ((\partial_{ss}n)d - n(\partial_{ss}d))(s,\theta) \quad \text{and} \quad (\partial_s b)(s,\theta) = 2(d\,\partial_s d)(s,\theta),$$

with

$$\begin{aligned}(\partial_{ss}n)(s,\theta) &= ((\partial_{sss}N)D - N(\partial_{sss}D) + (\partial_{ss}N)\partial_s D - (\partial_s N)(\partial_{ss}D))(s,\theta), \\ (\partial_{ss}d)(s,\theta) &= 2((\partial_s D)^2 + D\,\partial_{ss}D)(s,\theta)\end{aligned}$$

in which

$$\begin{aligned}(\partial_{sss}N)(s,\theta) &= (6\partial_s\rho\,\partial_{ss}\rho + (2R_0+2\rho-\partial_{\theta\theta}\rho)\partial_{sss}\rho + 12\partial_{s\theta}\rho\,\partial_{ss\theta}\rho \\ &\quad + 4\partial_\theta\rho\partial_{sss\theta}\rho - (R_0+\rho)\partial_{sss\theta\theta}\rho - 3\partial_{ss}\rho\partial_{s\theta\theta}\rho - 3\partial_s\rho\partial_{ss\theta\theta}\rho)(s,\theta)\end{aligned}$$

and

$$\begin{aligned}(\partial_{sss}D)(s,\theta) &= -3((R_0+\rho)^2+(\partial_\theta\rho)^2)^{-3/2}((R_0+\rho)\partial_s\rho+\partial_\theta\rho\partial_{s\theta}\rho)^3 \\ &\quad + 9((R_0+\rho)^2+(\partial_\theta\rho)^2)^{-1/2}((R_0+\rho)\partial_s\rho+\partial_\theta\rho\partial_{s\theta}\rho)(\partial_\theta\rho\partial_{ss\theta}\rho+(\partial_s\rho)^2) \\ &\quad + 9((R_0+\rho)^2+(\partial_\theta\rho)^2)^{-1/2}((R_0+\rho)\partial_s\rho+\partial_\theta\rho\partial_{s\theta}\rho)\left((R_0+\rho)\partial_{ss}\rho+(\partial_{s\theta}\rho)^2\right) \\ &\quad + 3\sqrt{(R_0+\rho)^2+(\partial_\theta\rho)^2}(3\partial_s\rho\partial_{ss}\rho+(R_0+\rho)\partial_{sss}\rho) \\ &\quad + 3\sqrt{(R_0+\rho)^2+(\partial_\theta\rho)^2}(3\partial_{s\theta}\rho\partial_{ss\theta}\rho+\partial_\theta\rho\partial_{sss\theta}\rho)(s,\theta).\end{aligned}$$

Using that $\partial_s \rho(0,\theta) = 0$ and $\partial_\theta \rho(0,\theta) = 0$, we see that

$$\begin{aligned}\partial_{sss} N(0,\theta) &= (2R_0 - \partial_{\theta\theta}\rho(0,\theta))\,\partial_{sss}\rho(0,\theta) + 12\partial_{s\theta}\rho(0,\theta)\partial_{ss\theta}\rho(0,\theta) \\ &\quad -R_0\partial_{sss\theta\theta}\rho(0,\theta) - 3\partial_{ss}\rho(0,\theta)\partial_{s\theta\theta}\rho(0,\theta),\end{aligned}$$

and

$$\partial_{sss} D(0,\theta) = 3R_0^2\partial_{sss}\rho(0,\theta) + 9R_0\partial_{s\theta}\rho(0,\theta)\partial_{ss\theta}\rho(0,\theta).$$

Since $\partial_s D(0,\theta) = 0$, $\partial_s d(0,\theta) = 0$, $\partial_s b(0,\theta) = 0$, we deduce that

$$R_0^{12}\partial_{sss}k(0,\theta) = \partial_s a(0,\theta) = R_0^6\partial_{ss}n(0,\theta) - R_0^3 n(0,\theta)\partial_{ss}D(0,\theta).$$

We first compute

$$\begin{aligned}\int_{-\pi}^{\pi}\partial_{ss}n(0,\theta)\cos\theta\mathrm{d}\theta &= R_0^3\int_{-\pi}^{\pi}\partial_{sss}N(0,\theta)\cos\theta\mathrm{d}\theta \\ &\quad -\int_{-\pi}^{\pi}N(0,\theta)\partial_{sss}D(0,\theta)\cos\theta\mathrm{d}\theta \\ &\quad -\int_{-\pi}^{\pi}\partial_s N(0,\theta)\partial_{ss}D(0,\theta)\cos\theta\mathrm{d}\theta.\end{aligned}$$

We see that $\int_{-\pi}^{\pi}\partial_s N(0,\theta)\partial_{ss}D(0,\theta)\cos\theta\mathrm{d}\theta = 0$ and

$$\int_{-\pi}^{\pi}N(0,\theta)\partial_{sss}D(0,\theta)\cos\theta\mathrm{d}\theta = 3R_0^4\int_{-\pi}^{\pi}\partial_{sss}\rho(0,\theta)\cos\theta\mathrm{d}\theta.$$

Furthermore, we also have

$$\int_{-\pi}^{\pi}\partial_{sss}N(0,\theta)\cos\theta\mathrm{d}\theta = 3R_0\int_{-\pi}^{\pi}\partial_{sss}\rho(0,\theta)\mathrm{d}\theta,$$

hence

$$\int_{-\pi}^{\pi}\partial_{ss}n(0,\theta)\cos\theta\mathrm{d}\theta = 0.$$

Finally we also have

$$\int_{-\pi}^{\pi}n(0,\theta)\partial_{ss}D(0,\theta)\cos\theta\mathrm{d}\theta = 0,$$

hence we deduce the third equality $\int_{-\pi}^{\pi}\partial_{sss}k(0,\theta)\cos\theta\mathrm{d}\theta = 0$. □

Appendix B

Computation of $\partial_s z$, $\partial_{ss} z$ and $\partial_{sss} z$

We recall that $\rho = \rho(s,\theta)$ and $z(s,\theta)$ are defined by (3.69), (3.70) and (3.73) for $s \in I$ and $\theta \in [-\pi, +\pi]$. We define the functions

$$\mathcal{N}(s,\theta) = (R_0 + \rho(s,\theta))\cos\theta + \partial_\theta \rho(s,\theta)\sin\theta$$
$$\mathcal{D}(s,\theta) = \sqrt{(R_0 + \rho(s,\theta))^2 + (\partial_\theta \rho(s,\theta))^2},$$

so that

$$z(s,\theta) = c(s)\frac{\mathcal{N}(s,\theta)}{\mathcal{D}(s,\theta)} \quad \text{and} \quad \partial_s z(s,\theta) = c'(s)\frac{\mathcal{N}(s,\theta)}{\mathcal{D}(s,\theta)} + c(s)\frac{\nu(s,\theta)}{\delta(s,\theta)},. \tag{B.1}$$

where

$$\nu(s,\theta) = ((\partial_s \mathcal{N})D - \mathcal{N}(\partial_s \mathcal{D}))(s,\theta) \quad \text{and} \quad \delta(s,\theta) = \mathcal{D}^2(s,\theta).$$

Since $c(0) = 0$ and $c'(0) = 1$, we obtain the expression of $\partial_s z(s,\theta)$.

Lemma B.0.1. *For all $\theta \in [-\pi, \pi]$ we have $\partial_s z(0,\theta) = \cos\theta$.*

Moreover we can continue the calculations to deduce the following result.

Lemma B.0.2. *The following equalities hold:*

$$\int_{-\pi}^{\pi} \partial_{ss} z(0,\theta)\cos\theta \mathrm{d}\theta = \pi c''(0), \text{ and } \int_{-\pi}^{\pi} \partial_{sss} k(0,\theta)\cos\theta \mathrm{d}\theta = \pi c'''(0).$$

Proof. First we see that

$$\partial_s \mathcal{N}(s,\theta) = \partial_s \rho(s,\theta)\cos\theta + \partial_{s\theta}\rho(s,\theta)\sin\theta,$$

and

$$\partial_s \mathcal{D}(s,\theta) = \frac{(R_0 + \rho(s,\theta))\partial_s \rho(s,\theta) + \partial_\theta \rho(s,\theta)\partial_{s\theta}\rho(s,\theta)}{\sqrt{(R_0 + \rho(s,\theta))^2 + \partial_\theta \rho(s,\theta)^2}}$$

Differentiating (B.1) with respect to s we obtain

$$\partial_{ss} z(s,\theta) = c''(s)\frac{\mathcal{N}(s,\theta)}{\mathcal{D}(s,\theta)} + 2c'(s)\frac{\nu(s,\theta)}{\delta(s,\theta)} + c(s)\frac{h(s,\theta)}{g(s,\theta)}, \tag{B.2}$$

where

$$h(s,\theta) = ((\partial_s \nu)\delta - \nu(\partial_s \delta))(s,\theta) \quad \text{and} \quad g(s,\theta) = \delta^2(s,\theta)$$

with

$$(\partial_s \nu)(s,\theta) = ((\partial_{ss}\mathcal{N})\mathcal{D} - \mathcal{N}(\partial_{ss} D))(s,\theta) \quad \text{and} \quad (\partial_s \delta)(s,\theta) = (2\mathcal{D}\partial_s D)(s,\theta).$$

Recalling that $c(0) = 0$ and $c'(0) = 1$, we deduce that

$$\partial_{ss} z(0,\theta) = c''(0)\frac{\mathcal{N}(0,\theta)}{\mathcal{D}(0,\theta)} + 2\frac{\nu(0,\theta)}{\delta(0,\theta)}.$$

Using the previous computations, it follows that $\mathcal{N}(0,\theta) = R_0\cos\theta$, $\mathcal{D}(0,\theta) = R_0$, $\partial_s\mathcal{N}(0,\theta) = \partial_{s\theta}\rho(0,\theta)\sin\theta$, $\partial_s\mathcal{D}(0,\theta) = 0$, hence $\nu(0,\theta) = R_0\partial_{s\theta}\rho(0,\theta)\sin\theta$ and $\delta(0,\theta) = R_0^2$. Consequently the first equality $\int_{-\pi}^{\pi}\partial_{ss} z(0,\theta)\cos\theta \mathrm{d}\theta = \pi c''(0)$ follows by integrating by parts (B.2), taken in $s = 0$, and using (3.70).

To prove the second equality we must go one step further. We first see that

$$(\partial_{ss}\mathcal{N})(s,\theta) = \partial_{ss}\rho(s,\theta)\cos\theta + \partial_{ss\theta}\rho(s,\theta)\sin\theta,$$

and

$$\begin{aligned}&(\partial_{ss}\mathcal{D})(s,\theta) = \\ &-((R_0+\rho)^2 + (\partial_\theta\rho)^2)^{3/2}((R_0+\rho)\partial_s\rho + \partial_\theta\rho\partial_{s\theta}\rho)((R_0+\rho)\partial_s\rho + \partial_\theta\rho\partial_{s\theta}\rho)\\ &+((R_0+\rho)^2 + (\partial_\theta\rho)^2)^{-1/2}(R_0\partial_{ss}\rho + (\partial_s\rho)^2 + \rho\partial_{ss}\rho + (\partial_{s\theta}\rho)^2 + \partial_\theta\rho\partial_{ss\theta}\rho)(s,\theta).\end{aligned}$$

Using (3.70), we obtain

$$\partial_{ss}\mathcal{N}(0,\theta) = \partial_{ss}\rho(0,\theta)\cos\theta + \partial_{ss\theta}\rho(0,\theta)\sin\theta$$

and

$$\partial_{ss}\mathcal{D}(0,\theta) = \frac{1}{R_0}\left(R_0\partial_{ss}\rho(0,\theta) + (\partial_{s\theta}\rho(0,\theta))^2\right).$$

Hence $g(0,\theta) = R_0^4$ and we see that $h(0,\theta) = R_0^2\left(R_0\partial_{ss\theta}\rho(0,\theta)\sin\theta - (\partial_{s\theta}\rho(0,\theta))^2\cos\theta\right)$.

Differentiating (B.2) with respect to s we have

$$\partial_{sss} z(s,\theta) = c'''(s)\frac{\mathcal{N}(s,\theta)}{\mathcal{D}(s,\theta)} + 3\,c''(s)\frac{\nu(s,\theta)}{\delta(s,\theta)} + 3\,c'(s)\frac{h(s,\theta)}{g(s,\theta)} + c(s)\,\partial_s\left(\frac{h(s,\theta)}{g(s,\theta)}\right). \tag{B.3}$$

Since $c(0) = 0$ and $c'(0) = 1$, we obtain

$$\partial_{sss} z(0,\theta) = c'''(0)\frac{\mathcal{N}(0,\theta)}{\mathcal{D}(0,\theta)} + 3\,c''(0)\frac{\nu(0,\theta)}{\delta(0,\theta)} + 3\frac{h(0,\theta)}{g(0,\theta)}.$$

First we see that

$$R_0\int_{-\pi}^{\pi}\frac{\nu(0,\theta)}{\delta(0,\theta)}\cos\theta \mathrm{d}\theta = \frac{1}{2}\int_{-\pi}^{\pi}\partial_{s\theta}\rho(0,\theta)\sin 2\theta \mathrm{d}\theta = 0.$$

Similarly, we have

$$R_0^2\int_{-\pi}^{\pi}\frac{h(0,\theta)}{g(0,\theta)}\cos\theta \mathrm{d}\theta = \int_{-\pi}^{\pi}\left(\frac{R_0}{2}\partial_{ss\theta}\rho(0,\theta)\sin 2\theta - (\partial_{s\theta}\rho(0,\theta))^2\cos^2\theta\right)\mathrm{d}\theta.$$

Furthermore integrating by parts and using that $\partial_s\rho(0,\theta) = 0$ we deduce that

$$R_0^2\int_{-\pi}^{\pi}\frac{h(0,\theta)}{g(0,\theta)}\cos\theta \mathrm{d}\theta = -R_0\int_{-\pi}^{\pi}\partial_{ss}\rho(0,\theta)\cos 2\theta \mathrm{d}\theta.$$

We now prove the following result which will achieve the proof of the second equality $\int_{-\pi}^{\pi}\partial_{sss} z(0,\theta)\cos\theta \mathrm{d}\theta = \pi c'''(0)$.

Lemma B.0.3. *It holds that*

$$\int_{-\pi}^{\pi}\partial_{ss}\rho(0,\theta)\cos 2\theta \mathrm{d}\theta = 0.$$

Proof of Lemma C.0.1. Recalling (3.75) and using that $\beta'(0) = 0$ and $f''(0) = 0$, we have

$$0 = \gamma \partial_{ss} k(0,\theta) - \beta(0) f'(0) \partial_{ss} z(0,\theta) + R_0 c''(0) \cos\theta - \lambda''(0). \tag{B.4}$$

Multiplying (C.1) by $\cos 2\theta$, using the expression of $\partial_{ss} z(0,\theta)$ and integrating on $[-\pi, \pi]$ we first see that $\int_{-\pi}^{\pi} \partial_{ss} z(0,\theta) \cos 2\theta \mathrm{d}\theta = 0$, hence

$$\int_{-\pi}^{\pi} \partial_{ss} k(0,\theta) \cos 2\theta \mathrm{d}\theta = 0.$$

Furthermore using the expression (A.3) of $\partial_{ss} k(0,\theta)$ and integrating on $[-\pi, \pi]$ we see that

$$R_0^2 \int_{-\pi}^{\pi} \partial_{ss} k(0,\theta) \cos 2\theta \mathrm{d}\theta = 3 \int_{-\pi}^{\pi} \partial_{ss} \rho(0,\theta) \cos 2\theta \mathrm{d}\theta.$$

□

□

Appendix C

Useful computations

Lemma C.0.1. *It holds that*

$$\int_{-\pi}^{\pi} \partial_{ss}\rho(0,\theta)\cos 2\theta \mathrm{d}\theta = 0.$$

Proof of Lemma C.0.1. Recalling (3.75) and using that $\beta'(0) = 0$ and $f''(0) = 0$, we have

$$0 = \gamma\partial_{ss}k(0,\theta) - \beta(0)f'(0)\partial_{ss}z(0,\theta) + R_0 c''(0)\cos\theta - \lambda''(0). \tag{C.1}$$

Multiplying (C.1) by $\cos 2\theta$, using the expression of $\partial_{ss}z(0,\theta)$ and integrating on $[-\pi,\pi]$ we first see that $\int_{-\pi}^{\pi} \partial_{ss}z(0,\theta)\cos 2\theta \mathrm{d}\theta = 0$, hence

$$\int_{-\pi}^{\pi} \partial_{ss}k(0,\theta)\cos 2\theta \mathrm{d}\theta = 0.$$

Furthermore using the expression (A.3) of $\partial_{ss}k(0,\theta)$ and integrating on $[-\pi,\pi]$ we see that

$$R_0^2 \int_{-\pi}^{\pi} \partial_{ss}k(0,\theta)\cos 2\theta \mathrm{d}\theta = 3\int_{-\pi}^{\pi} \partial_{ss}\rho(0,\theta)\cos 2\theta \mathrm{d}\theta.$$

□

Lemma C.0.2. *It holds that*

$$\int_{-\pi}^{\pi} \partial_{ss}\rho(0,\theta)\mathrm{d}\theta = 0.$$

Proof of Lemma C.0.2. Recalling (3.58), it follows that

$$\int_{-\pi}^{\pi} \big((R_0+\rho(\theta))^2 - R_0^2\big)\mathrm{d}\theta = 0.$$

Differentiating twice this equality with respect to s we obtain

$$\int_{-\pi}^{\pi} \big(R_0\partial_{ss}\rho(s,\theta) + (\partial_s\rho(s,\theta))^2 + \rho(s,\theta)\partial_{ss}\rho(s,\theta)\big)\mathrm{d}\theta = 0.$$

Taking it in $s = 0$ and using that $\rho(0,\theta) = 0$ together with $\partial_s\rho(0,\theta) = 0$ we obtain the result. □

From Lemma C.0.1 and Lemma C.0.2, we deduce that

Lemma C.0.3. *It holds that*

$$\int_{-\pi}^{\pi} \partial_{ss}\rho(0,\theta)\cos^2\theta \mathrm{d}\theta = 0.$$